Spaceborne monitoring of the recent contribution of glaciers from the Andes to water resources and sea level rise

Inés Dussaillant

Université Fédérale
Toulouse Midi-Pyrénées

THÈSE

En vue de l'obtention du

DOCTORAT DE L'UNIVERSITÉ DE TOULOUSE

Délivré par l'Université Toulouse 3 - Paul Sabatier

Présentée et soutenue par

Inés DUSSAILLANT

Le 11 octobre 2019

Contribution récente des glaciers des Andes à la ressource en eau et à la hausse du niveau marin. Apport des observations satellitaires

---

Ecole doctorale : **SDU2E - Sciences de l'Univers, de l'Environnement et de l'Espace**

Spécialité : **Océan, Atmosphère, Climat**

Unité de recherche :
LEGOS - Laboratoire d'Etudes en Géophysique et Océanographie Spatiale

Thèse dirigée par
Etienne BERTHIER et Vincent FAVIER

Jury

M. Christophe KINNARD, Rapporteur
M. Daniel FARINOTTI, Rapporteur
Mme Dana FLORICIOIU, Examinatrice
M. Vincent JOMELLI, Examinateur
M. Etienne BERTHIER, Directeur de thèse
M. Vincent FAVIER, Co-directeur de thèse

In every walk with Nature one receives far more than he seeks
–John Muir

Acknowledgements

It was walking through this exact glacial landscape when I decided to study glaciers and pursue my career as a glaciologist. So, first of all, I have to thank Nature and this particular moment for providing me the clarity needed to take an important decision.

I happened to end in France doing the project that I most dreamt of: measure the recent evolution of Andean glaciers (including the glaciers in the picture!). For this opportunity and for believing in me, I thank Etienne Berthier, my thesis Director. A Director of excellence. Always available, always honest with his constructive critics and emphasising on RIGOR!. It was a privilege to work at his side and to learn the ways of science from his good example, in line with my own principles. The best way of thanking him is to be able to pass forward all the knowledge he gave to me! That is my goal and he is the example to follow.

For being welcomed at the birthplace of glaciology in France (IGE) I thank Vincent Favier, my Co-director. His never-ending ideas where always motivating, it was only a pity to have a deadline to finish my contract!

Only a good leader knows how to choose and build a good team: I am proud to have formed part of the ASTERIX family during this last three years. I thank Fanny for her never-ending will to help and to be available for everything. Full of positive energy and motivation for science and mountains, she became an inspiring friend. Romain came later bringing the dynamism of the ASTERIX team to its tipping point. Thanks to him -also and inspiring friend and colleague- for all his help, all his patient explanations and for his infinite kindness.

I thank Simon and Gino for their useful and insightful comments and advices during the development

of my thesis. And Antoine, for his important contribution on the Tropics. I also thank my colleagues from Argentina Mariano, Pierre y Lucas, that always received me with the arms wide open. Salud! for all the good –and bad- experiences in the field, the asados and the scientific discussions. And for more to come!. Also thanks to Hernan, Lidia, Laura, Pepe, Ricardo, Cristi and the un-nameable amount of friends and colleagues from Mendoza.

For all the "PhD moments", all those tears spread, the hugs, and then the laughs out loud when we where supposed to be quiet, I thank Violaine! Our office was full of good energy -and full of plants- It was a pleasure to share it with her and share this bitter-sweet-process together. Thanks to all the team of PhD's and Post-Docs in LEGOS and more; my good friend Marina (the unidentified poet), Cesar (in his deep heart he knows he is a climber), Joaquin, Antoine, Fifi, Marine, Zaida, Audrey, Manon, Lise, Alice, Simon, Carlos y Cami. And from IGE, all the good friends and master fellows that continued in science Gabi (amigas desde la Patagonia hasta siempre!), Marion (very important at the end, she knows why), Maria, Lucas and Marion, Jay, and el chilenito Claudio! Thank also to all the people behind this two laboratories, helping science to move forward: the Directors -Alex and Pierre-, the beautiful and efficient secretaries -Agathe, Nadine, Martine and Brigitte-, the informatics and all the permanent researchers that create this motivating environments. A special thanks to the members of the ECHOS team -Frederique, Sarah, Alejandro, Denis, Sylvain, Alexei- for the glacio-coffees shared and the smiles crossing corridors.

From the rest of the Toulousain world I thank Thomas who was always there with his bike, was it for a good climb or just a talk. Harold and Cony arrived in the most important moment to remind me the taste of my longed Chile. But the most special embrace goes to my best yoga teacher and friend from the heart Gerda and the always smiling and caring Marcos. Mamita y Papito -and Luna of course-, the closest to a family I had in France. They showed me the secrets of Ariège on top of skis, with climbing shoes or without them. Their kindness and care kept me going through the most difficult parts of this journey. Thanks to la Payasita Caro, my deep friend and coach -of body and soul-, even from far away she managed to make me laugh and sweat (and allowed my ass not to go square while writing this thesis). Thanks also to Chris, for sharing this short moment of life with me.

My real family from far away stayed always a strong support. Thanks to my sisters, nephews and nieces, for their loving messages. But specially to my parents, if it wasn't for their effort, I would never had the chance to be -here, in this moment- and become the glaciologist I dreamed of while walking over my glaciers.

Chaltu may Ñuque Mapu

Résumé

Les glaciers Andins présentent des taux de recul parmi les plus important au monde, et contribuent à la hausse du niveau des mers. Ils constituent aussi des ressources en eau vitales pour les vastes zones semi-arides le long de la Cordillère des Andes (10°N-56°S), en alimentant les rivières lors des sécheresses. En dépit du retrait des glaciers Andins, les mesures directes des fluctuations glaciaires sont éparses, de court terme, incomplètes, et ne permettent donc pas une estimation précise de la perte de glace récente à l'échelle de la chaîne entière. Décrire quantitativement cette perte à différentes échelles spatio-temporelle est cruciale afin de mieux anticiper les impacts écologiques, économiques et sociaux.
Premièrement, nous avons évalué la performance d'une méthode visant à calculer les changements de masse des glaciers Andins. Cette méthode utilise les séries temporelles des modèles numériques de terrain (DEM) produit par des images stéréoscopiques Advanced Spaceborn Thermal Emission and Reflection Radiometer (ASTER). Sur la zone de validation de la méthode, le Champ de Glace Nord de Patagonie (NPI), nous avons observé un bilan de masse fortement négatif de -1.06 ± 0.14 m w.e. a^{-1} pour la période 2000-2012. Ces résultats sont cohérent avec les estimations faites précédemment, mais aussi avec une seconde estimation (-1.02 ± 0.21 m w.e. a^{-1}) obtenue indépendamment par différentiation de DEMs de meilleur résolution, Shuttle Radar Topography Mission (SRTM) et Satellite pour l'Observation de la Terre 5 (SPOT5). Ce travail nous a permis de (*i*) valider la méthode appelée « ASTER monitoring Ice towards eXtinction » (ASTERIX) sur la totalité des Andes, (*ii*) confirmer l'absence de pénétration du signal radar SRTM dans la bande C sur la neige du NPI (sauf pour une petite région au dessus de 2900 m a.s.l) avec des effets négligeables sur le bilan de masse du NPI; et enfin (*iii*) fournir la base de travail pour une analyse des variations du bilan de masse du NPI durant différentes sous périodes entre 1975 et 2016, grâce à des DEMs supplémentaires.
Ensuite, nous avons généré plus de 30000 DEMs ASTER afin de calculer la perte de l'intégralité des glaciers Andins, et ce pour les deux dernières décennies. La perte de masse à l'échelle des Andes s'élève ainsi à -22.9 ± 5.9 Gt yr^{-1} (-0.72 ± 0.22 m w.e. a^{-1}) pour la période d'étude entière, ou -26.0 ± 6.0 Gt a^{-1} en incluant les pertes subaquatiques. Toutes les régions affichent une diminution du volume de glace. Les taux les plus négatifs sont observés dans les Andes Patagoniennes (-0.78 ± 0.25 m w.e. a^{-1}) et dans les Andes Tropicales (-0.42 ± 0.24 m w.e. a^{-1}). Les pertes sont modérées dans les régions intermédiaires des Andes Arides (-0.28 ± 0.18 m w.e. a^{-1}). Pour la première fois à l'échelle des Andes, une tendance inter-décennale de la perte volumique a été mise en évidence. Les taux d'amincissement des glaciers tropicaux et ceux situé sous 45°S sont négatifs et stables sur la période considérée. Cependant, alors que les glaciers des Andes arides sont proche de l'équilibre dans les années 2000, leur taux d'amincissement augmentent drastiquement à partir de 2010, coïncident ainsi avec une période de sécheresse intense depuis 2010. L'étude des contributions des pertes de masse décennales des glaciers aux débits des rivières révèle que la fonte de ces glaciers a en partie aidé à minimiser les impacts négatifs de cette sécheresse dans les Andes arides.
Les résultats obtenus au cours de cette thèse apportent une meilleure compréhension des pertes récentes des glaciers Andins, localement et régionalement. Nous avons fourni un jeu de donnée multi-décennale de haute résolution, qui sera utile pour contraindre la diversité des estimations existantes de perte volumique récente à l'échelle des Andes. Ce travail constitue une base solide dans la poursuite des efforts de calibrations des modèles hydrologiques et glaciologiques, nécessaire et cruciale pour projeter le futurs des glaciers et le devenir des ressources en eau dans les Andes.

Abstract

Andean glaciers are amongst the fastest shrinking and the largest contributors to sea level rise in the world. They also represent crucial water resources in the vast semi-arid portions of this large Andes Cordillera (10°N-56°S), sustaining river runoff during dry periods and buffering the effects of droughts. Despite the widespread shrinkage of these glaciers, direct measurement of glacier fluctuations in the Andes are sparse, short-termed and in many cases incomplete, preventing the accurate quantification of recent ice loss for the entire mountain range. Comprehensively quantifying the magnitude of this loss at different special scales is crucial to better constrain future economical, ecological and social impacts. First, we evaluated the performance of a methodology to calculate glacier mass changes on Andean glaciers using time series of digital elevation models (DEMs) derived from Advanced Spaceborne Thermal Emission and Reflection Radiometer (ASTER) stereo images. Over our validation zone, the Northern Patagonian Icefield, we found strongly negative icefield-wide mass balance rates of -1.06 ± 0.14 m w.e. yr^{-1} for the period 2000-2012, in good agreement with estimates from earlier studies and with a second independent estimate (-1.02 ± 0.21 m w.e. yr^{-1}) obtained by differencing the better resolved Shuttle Radar Topography Mission (SRTM) DEM with a Satellite pour l'Observation de la Terre 5 (SPOT5) DEM. Importantly, this work permitted us to (i) validate "ASTER monitoring Ice towards eXtinction" (ASTERIX) method over the Andes; (ii) confirm the lack of penetration of the C-band SRTM radar signal into the NPI snow and firn except for a small high altitude region (above 2900 m a.s.l.) with negligible effects on NPI-wide mass balance; and (iii) provide the basis for an analysis of NPI mass balance changes during different sub-periods between 1975 and 2016 using additional DEMs.
Then, we processed more than 30000 ASTER DEMs to calculate the integrated volume of ice lost by Andean glaciers during the past two decades. Andes-wide mass loss amounts to -22.9 ± 5.9 Gt yr^{-1} (-0.72 ± 0.22 m w.e. yr^{-1}) for the entire period (or -26.0 ± 6.0 Gt yr-1 including subaqueous losses). All regions show consistent glacier wastage, with the most negative mass balance rates in the Patagonian Andes (-0.78 ± 0.25 m w.e. yr^{-1}) and Tropical Andes (-0.42 ± 0.24 m w.e. yr^{-1}). Relatively moderate loss (-0.28 ± 0.18 m w.e. yr^{-1}) is measured in the intermediate regions of the Dry Andes. The inter-decadal patterns of glacier mass loss is an important contribution of this work, observed for the first time at an Andes-wide scale. We observe steady thinning rates in the Tropics and south of 45°S. Conversely, glaciers from the Dry Andes were stable during the 2000s, shifting to drastic thinning rates during the 2010s, coinciding with conditions of sustained drought since 2010. The evaluation of the imbalanced glacier contribution to river discharge during these two decades revealed that glaciers partially helped to mitigate the negative impacts of this sustained drought in the Dry Andes.
The results obtained in this thesis contribute to the understanding of recent Andean glacier evolution at a local, regional and Andes-wide scale. We provide a high-quality, multi-decadal dataset that will be useful to constrain the diversity of present 21^{th} century Andes-wide mass loss estimates, in the pursuit of the good calibration of glaciological and hydrological models intended to project future glacier changes and to improve water resource management in the Andes.

Introduction

What can glaciers tell us?

As part of the global cryosphere, mountain glaciers and icefields outside the large ice sheets of Greenland and Antarctica are important components of the climatic system, interacting directly with the atmosphere and contributing to the hydrosphere. The interest on mountain glacier is threefold: First they are important indicators of climate change: glacier changes are the result of an integrated response to climate, and so, past and present glacier fluctuations can be used as valuable proxies of past glacier fluctuations and improve the prediction the future climate scenarios (Oerlemans, 2001). Secondly, they are crucial water resources with the capacity to store fresh water in winter and then release it back when its most needed, during the summer months and enhanced periods of drought, providing water over the driest regions of the world (e.g. Pritchard, 2019). Finally, all mountain glaciers currently represent a total volume of 158 ± 41 x 10^3 km^3 of ice, if all this ice melts, it is equivalent to 0.32 ± 0.08 m of sea level change (Farinotti et al., 2019). The correct quantification of the pace at which these glaciers are shrinking is also important to constrain ongoing and future sea level rise (SLR) and predict its impacts.

The ongoing global glacier retreat has been documented by local ground observations, remote sensing and modelling techniques, but there is still no consensus between the different global and regional glacier volume change estimates. There is a strong need to constrain regional glacier changes and to fill the existing gap between the observations, which show strong glacier retreat, and the understanding of the drivers of these changes. Since the pioneering work from Meier (1984), many studies have tried to assess the global glacier contribution to SLR, and the relative contribution of each mountain glacierized region outside the ice sheets. The last assessment by Zemp et al. (2019), suggests that glacier mass loss may be larger than previously reported, with glaciers contributing 25 to 30% of the observed SLR for the period 2006-2016.

The recent progress in global glacier models has helped to understand the processes responsible for these glacier changes and predict future glacier evolution (e.g. Huss and Hock, 2015; Marzeion et al., 2012, 2014) which is still one of the major uncertainties in SLR projections (Church et al., 2013). This models have also been linked with hydrological models to assess the global impact of glacier changes over water resources (e.g. Huss and Hock, 2018; Kaser et al., 2010). These results have also helped to improve the understanding of the role of glaciers in the hydrological cycle, agreeing that regions with dry climates depend strongly on glacier melt to sustain populations living downstream (Pritchard, 2019).

Despite the advances in modelling approaches, the quality and quantity of observations used to calibrate them will determine their capacity to predict future changes (assuming that models are well representing glacier physical processes). The heterogeneity of techniques existing to measure glacier changes, the different time periods considered and the wide divergence that still exist on volume change estimates in some glacierized regions of the world, illustrates the need to reach consensus to be able to make a reliable diagnosis and prediction of both regional and global glacier changes and its impacts. Regarding this, some glacierized regions of the world have been better surveyed with direct observation than others. In this context, the Andes have received relatively little attention, and this lack of solid observational data has hindered the implementation of glacier models at the Andes-wide scale, which still show large uncertainties in this region (e.g. Huss and Hock, 2018; Marzeion et al., 2012).

What can Andes glaciers tell us?

Glaciers in the Andes mountain range located in South America (from 10°N to 56°S) play a major hydrological role. North of 40°S, glaciers are key for water resources, sustaining river discharge during dry periods when their enhanced melt can compensate the water deficit due to reduced rain and snowfall (e.g. Condom et al., 2012; Gascoin et al., 2011; Huss and Hock, 2018; Kaser et al., 2010; Soruco et al., 2015). Further south, between 40°S and 55°S, the large Patagonian icefields are the largest mountain glacier contributors to eustatic sea level rise per unit area, accounting for around 7-15% of the global glacier mass loss (Abdel Jaber et al., 2018; Malz et al., 2018; Rignot et al., 2003; Willis et al., 2012a,b) . These glaciers stand as an essential indicator of climate change along a globally unique latitudinal transect of the Southern Hemisphere. Glaciological measurements are scarce mainly because these glaciers are difficult to access and studies using remote sensing data are still very limited in regions outside from the large Patagonian icefields. Additionally, there is still no consensus on the magnitude of the icefields mass loss and their contribution to SLR.

Andes-wide glacier changes estimation also vary greatly, first because of the interpolation of scarce glaciological and geodetic data (Cogley, 2009; Gardner et al., 2013; Marzeion et al., 2015; Mernild and Wilson, 2016; Reager et al., 2016; Zemp et al., 2019, 2015) and secondly because of the heterogeneity of the methods used and time periods considered. This lack of consensus translates in highly divergent modelled predictions of glacier change and contribution to river discharge in the Andes. Until now, the regional estimates from Gardner et al., (2013) has been preferred to calibrate glaciological models in the Andes (e.g. Huss and Hock, 2015, 2018) even though they consider a short period from 2003 to 2009, because they provide a reconciled estimate (i.e. considering the different methodologies). However, this is not true for the Andean region, where the lack of data obliges them to rely only on the Gravimetry technique.

At present, the heterogeneity and divergence of Andes-wide glacier volume change estimates reveals the need for consensus. An integrated and spatially resolved estimate of recent Andes glacier changes in the Andes, spanning for a sufficiently long time period and covering multiple time periods, is needed to (i) understand Andean glacier responses to climate change, (ii) constrain global SLR contribution and (iii) calibrate models projecting Andean glacier changes and their impact on hydrology.

Organization of the manuscript

In this context, the goal of this PhD work is to estimate the glacier changes of the Andes Cordillera from satellite data. Glacier volume change and mass balance rates will be estimated at a local, regional and Andes-wide scale by means of the geodetic method: Differencing of multi-temporal digital elevation models (DEMs). Throughout this work we make use of diverse Andes elevation data derived from: (i) Advanced Spaceborne Thermal Emission and Reflection Radiometer (ASTER) DEMs from 2000 to 2018; (ii) the Shuttle Radar Topography Mission (SRTM) DEM from February 2000; and (iii) Satellite pour l'observation de la Terre (SPOT) DEMs from missions 5-HRS, 6 and 7 acquired in 2005, 2012 and 2016. And (iv) Chilean cartography (Instituto Geografico militar, IGM) that will allow extending the temporal frame of the study as far back as 1975.

The manuscript is organized in four main chapters. **Chapter 1** reviews the current state of the art in the knowledge of Andean climate and glaciers. At the end of this chapter, the main research questions addressed in this work are defined. **Chapter 2** is based on a published article and presents the validation of our methodology over the NPI. **Chapter 3** is the cornerstone of this PhD work and present the geodetic estimation of Andes-wide mass loss. This chapter is based on an accepted article and also provides details of ongoing unpublished work on the estimation of frontal ablation. **Chapter 4** presents ongoing unpublished work analysing sub-periods NPI mass balance changes between 1975 and 2016 using additional elevation data. We finish with a short conclusion summarizing the main results of this work, ongoing collaborations and future possible research directions.

Introduction

Que nous apprennent les glaciers?

En tant qu'objet naturel de la cryosphère, les glaciers de montagne et les calottes glaciaires (en dehors des calottes continentales que sont le Groenland et de l'Antarctique) sont des composants majeurs du système climatique, en interaction directe avec l'atmosphère et l'hydrosphère. L'intérêt des glaciers de montagne est triple. Premièrement ils sont d'excellents indicateurs du changement climatique. En effet les forçages climatiques sont responsables des variations glaciaires, et donc les fluctuations glaciaires passées et présentes peuvent être utilisées comme proxy pour prédire les scénarios climatiques futures (Oerlemans, 2001). Deuxièmement, les glaciers constituent des ressources en eau cruciales et jouent le rôle de château d'eau en stockant l'eau sous forme solide en hiver, puis en la relâchant lors des périodes de fonte, procurant ainsi de l'eau pour les régions les plus arides du globe, au moment le plus opportun (e.g. Pritchard, 2019). Enfin, les glaciers de montagne présents sur la planète représentent un volume de glace de 158 ± 41 x 10^3 km^3 qui, si ce volume venait à fondre entièrement, est équivalent à une hausse du niveau de la mer de 0.32 ± 0.08 m (Farinotti et al., 2019). Connaître précisément le rythme auquel ces glaciers s'amenuisent est par conséquent important pour contraindre la hausse du niveau des mer et anticiper ses impacts.

Le retrait des glaciers dans le monde a été documenté par des mesures locales de terrain, par télédétection et modélisation, mais il n'y a toujours pas de consensus entre les différentes estimation régionale et globale des variations de volumes. Il est donc nécessaire de contraindre les estimations régionales et de faire le lien entre les observations, qui témoignent d'un fort retrait glaciaire, et les facteurs conduisant à ces changements. Depuis le travail pionnier de Meier (1984), de nombreuses études ont essayer de traduire les pertes globales des glaciers en hausse du niveau des mers, ainsi que la contribution individuelle et relative des glaciers de montagne en dehors des calottes continentales. Les dernières évaluations en date ont revu à la hausse les pertes de masse des glaciers de montagne précédemment estimée, avec une contribution à la SLR de 25 à 30% pour la période 2006-2016 (Zemp et al., 2019).

Les progrès récents effectués dans la modélisation globale des glaciers a permis de mieux appréhender les processus responsable de ces changements et de prédire leur évolution future (e.g. Huss and Hock, 2015; Marzeion et al., 2012, 2014) Cependant, les incertitudes associées à ces prédictions constituent encore une source d'erreur majeur dans les projections de la hausse du niveau des mers (Church et al., 2013). Ces modèles glaciologiques ont aussi été couplé avec des modèles hydrologiques afin d'évaluer l'impact global des changements glaciaires sur les ressources en eau (e.g. Huss and Hock, 2018; Kaser et al., 2010). Ces résultats ont aussi permis de comprendre le rôle des glaciers dans le cycle hydrologique, confirmant le fait que les régions au climat aride dépendent étroitement de la fonte des glaces afin de répondre aux besoins en eaux des populations en aval (Pritchard, 2019).

Malgré ces progrès dans le domaine de la modélisation, ce sont la quantité et qualité des observations permettant de calibrer les modèles qui déterminera leur capacité à prédire les changement futurs (à condition toutefois que les processus physiques de ces modèles soit correctement représenté). L'hétérogénéité des techniques existantes pour mesurer les changements glaciaires, les différentes échelles de temps considérées et la divergence actuelle des estimations de changement volumique de certaines régions englacées du globe, illustrent le besoin de converger vers un diagnostic fiable et unique pour les

changement régionaux et globaux. En regard à cela, certaines régions englacées ont été mieux documentées que d'autres grâce à la réalisation d'observations directes. Ainsi les Andes ont reçu relativement peu d'attention, ce qui entraîne un manque d'observations directes et rend difficile l'implémentation des modèles à l'échelle des Andes. De ce fait, les processus régissant le comportement des glaciers de cette région, ainsi que les conséquences hydrologique associées, sont encore sujets à de large incertitudes (e.g. Huss and Hock, 2018; Marzeion et al., 2012).

Que nous apprennent les glaciers des Andes?

Les glaciers de la Cordillère des Andes en Amérique du Sud (de 10°N à 56°S) jouent un rôle hydrologique majeur. Au nord du parallèle 40°S, les glaciers sont cruciaux pour les ressources en eau. Ils contribuent significativement aux débits des rivières pendant les périodes sèches quand l'eau de fonte peut compenser le déficit d'eau due au très faibles précipitations liquides et solides (e.g. Condom et al., 2012; Gascoin et al., 2011; Huss and Hock, 2018; Kaser et al., 2010; Soruco et al., 2015). Plus au sud, entre 40°S et 55°S, les vastes champs de glace patagons sont les glaciers apportant la plus grande contribution à la hausse eustatique du niveau des mers par unité de surface, comptant pour environ 7-15% des pertes de masse glaciaires globales (Abdel Jaber et al., 2018; Malz et al., 2018; Rignot et al., 2003; Willis et al., 2012a,b) . Ces glaciers sont les indicateurs climatiques d'une bande latitudinale unique en hémisphère sud. Les mesures glaciologiques dans les Andes sont rares due aux conditions d'accès difficile et les études géodésiques reste très limitées en dehors des grands champs de glace. De plus, il n'y a toujours pas de consensus sur la magnitude de ces changements de masses et leur contribution à la hausse du niveau marin.

L'estimation des changements des glaciers Andins est entachée d'une forte disparité. La première cause est due à l'interpolation d'un nombre limité de données glaciologiques et géodésiques (Cogley, 2009; Gardner et al., 2013; Marzeion et al., 2015; Mernild and Wilson, 2016; Reager et al., 2016; Zemp et al., 2019, 2015) , la seconde est l'hétérogénéité des périodes d'étude et des méthodes utilisées. Ce manque de cohérence se traduit par une divergence importante dans les projections de l'évolution glaciaire et la contribution aux débits des cours d'eau Andins. Jusqu'à maintenant, l'estimation régionale de Gardner et al., (2013) a été préféré pour calibrer les modèles glaciologiques dans les Andes (e.g. Huss and Hock, 2015, 2018) bien qu'ils considèrent une courte période de 2003 à 2009, parce qu'ils fournissent une estimation réconciliée (i.e. considérant les différentes méthodes). Cependant, ce n'est pas vrai pour l'intégralité des Andes, où le manque de données les a forcé à s'appuyer sur une seule technique.

Actuellement, une estimation complète des changements glaciaires récent dans les Andes, cohérente, et distribué spatialement reste nécessaire afin de, (i) comprendre la réponse des glaciers Andins face au changement climatique, (ii) contraindre les contributions à la hausse du niveau des mers, (iii) calibrer les modèles projetant le futur des glaciers Andins et leur impact sur l'hydrologie.

Organisation du manuscrit

L'objectif de ce travail doctoral est d'estimé les changements glaciaires le long de la Cordillère des Andes à partir des données satellites. Les changements volumiques et les bilans de masse seront estimés à une échelle locale, régionale et pour la globalité des Andes. Ceci reposera sur la méthode géodésique en différenciant des Modèles de Terrain Numérique (Digital Elevation Models, DEMs). A travers ce travail nous avons utilisé différentes données topographiques dans les Andes à partir de: (i) Advanced Spaceborne Thermal Emission and Reflection Radiometer (ASTER) DEMs de 2000 à 2018, (ii) the Shuttle Radar Topography Mission (SRTM) DEM depuis fevrier 2000, et (iii) Satellite pour l'Observation de la Terre (SPOT) DEMs des missions 5-HRS, 6 et 7 acquises en 2005, 2012 et 2016. Enfin, (iv), la Cartographie Chilienne (Instituto Geografico Militar, IGM) qui permet d'étendre temporellement cette étude jusqu'à l'année 1975.

Ce manuscrit s'organise en quatre chapitres. Le **Chapitre 1** synthétise l'état de l'art sur le climat et

les glaciers andins. A la fin de ce chapitre les principales questions scientifiques seront posées. Le **Chapitre** 2 est basé sur un article publié et présente la validation de notre méthode sur le Champ de Glace Nord en Patagonie (North Patagonian Icefield, NPI). Le **Chapitre** 3 est le cœur de cette thèse et présente l'estimation géodésique des pertes de masse à l'échelle des Andes. Ce chapitre est basé sur un article accepté et fournit aussi les détails d'un travail en cours et non publié sur l'estimation de l'ablation frontale. Le **Chapitre** 4 présente un travail en cours et non publié qui analyse pour différentes sous périodes les changements de bilans de masse du NPI entre 1975 et 2016. Nous finirons ce manuscrit avec une conclusion résumant les résultats principaux de ce travail, les collaborations en cours et les futures directions de recherche.

Contents

Chapter 1

Andean Glaciers and climate

1.1 Characteristics of the Andes mountain range

1.1.1 Geographical situation

The Andes are the longest continental mountain range of the world running across the west coast of South America over more than 7000 km from Colombia (10°N) up to the Southern-most region of Tierra del Fuego (56°S) at the Austral end of Chile and Argentina (Figure 1.1). Along the tropical and subtropical portion of the Andes average elevation exceeds 4000 m a.s.l. containing the highest peak of America, the Aconcagua (32°S) at 6980 m a.s.l. and the world's highest volcano, the Ojos del Salado (27°S) at 6890 m a.s.l. South of 35°S average heights decrease to about 1500 m a.s.l. but still containing many peaks above 3000 m a.s.l. In contrast with their longitude, the Andes stay a relatively narrow range with typical widths of 200 km and a maximum of 700 km in the subtropical region, where they split into two mountain ranges surrounding the South American Altiplano. This high elevation plateau presents average elevations of 4000 m a.s.l. and is exceeded only by the Tibetan Plateau on surface and altitude. Large rivers drain from the Andes to the Atlantic Ocean, the largest being the Amazon river with a length of 7000 km, followed by the Parana (4900 km). Towards the western slopes of the Andes, rivers reach the Pacific Ocean coasts fast, with the largest river (rio Loa) extending only 440 km.

There is still no consensus on the delimitation and naming of Andean regions. As they cross along seven South American countries, generally political boundaries are referred to for simplification. For scientific aims, a wide range of possibilities have been proposed, varying greatly depending on the focus of the research topic. In this manuscript I define a set of seven sub-regions according to latitude and prevailing climatic conditions and based on previous regional glaciological subdivisions (Masiokas et al., 2009; Rabatel et al., 2013a; Sagredo and Lowell, 2012). The Tropical Andes corresponds to the region North of 20°S containing the Inner and the Outer Tropics. The Dry Andes, between 17°S and 37°S encloses the Desert and Central Andes. Further South, the Patagonian Andes are divided between North Patagonia, South Patagonia which contains the two major Andean icefields: the Northern Patagonian Icefield (NPI) and the Southern Patagonian Icefield (SPI) and finally The Fueguian Andes to the South of The Magellan Strait (Figure 1.1).

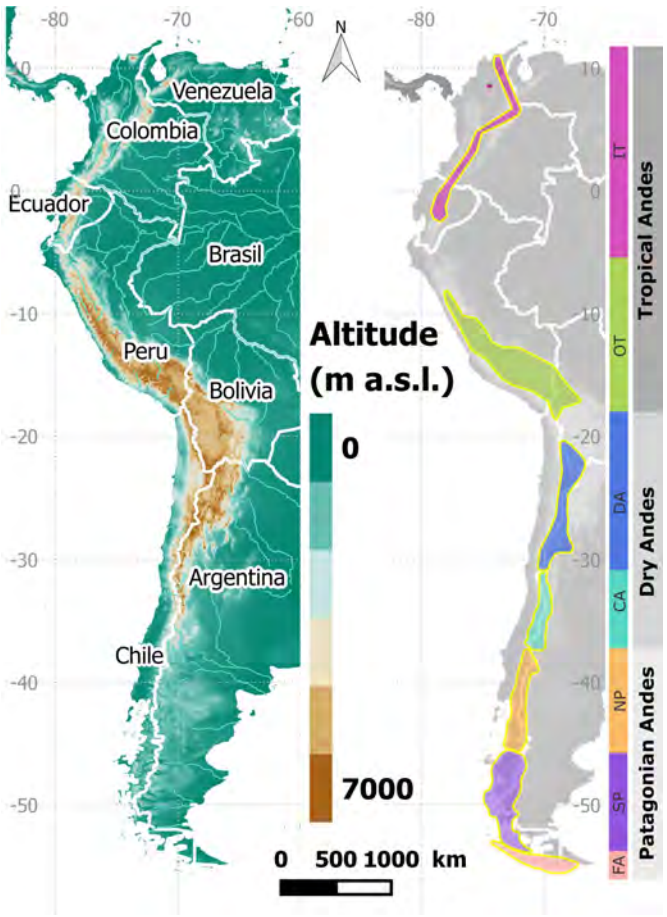

Figure 1.1: Elevation range of the Andes Cordillera (from SRTM 4.1 data resampled at 500 m) and the definition of Glacio-climatological regions used through the manuscript. IT (Inner Tropics) and OT (Outer Tropics) correspond to the Tropical Andes; DA (Desert Andes) and CA (Central Andes) to the Dry Andes; and NP (North Patagonia), SP (South Patagonia) and FA (Fuaguian Andes) to the Patagonian Andes.

1.1.2 Climatic diversity

Consistent with its latitudinal extension and altitude, the Andes exhibit heterogeneous climate settings with Tropical, Subtropical and Extratropical features. In the Tropical (10°N-17°S) and Subtropical regions (17°S-37°S) large scale circulation is characterized by the Inter-Tropical Convergence Zone (ITCZ) and the Trade winds blowing from the East while westerly winds blowing from the Pacific Ocean dominate circulation in the Extratropical region (south of 35°S). Mean annual temperature is mostly controlled by latitude and elevation with a 0 isotherm that stays close to 4000 m a.s.l. at the tropical and subtropical latitudes dropping to 500 m a.s.l. at the southern tip of the continent (Garreaud, 2009; Sagredo and Lowell, 2012). The transport of moisture towards the Andes is mostly determined by the tropospheric low-level flow represented in Figure 1.2 (Garreaud, 2009). The height and continuity of the mountain range disrupts tropospheric circulations resulting in contrasted climate conditions all along the eastern and western sides of the Cordillera (Figure 1.3).

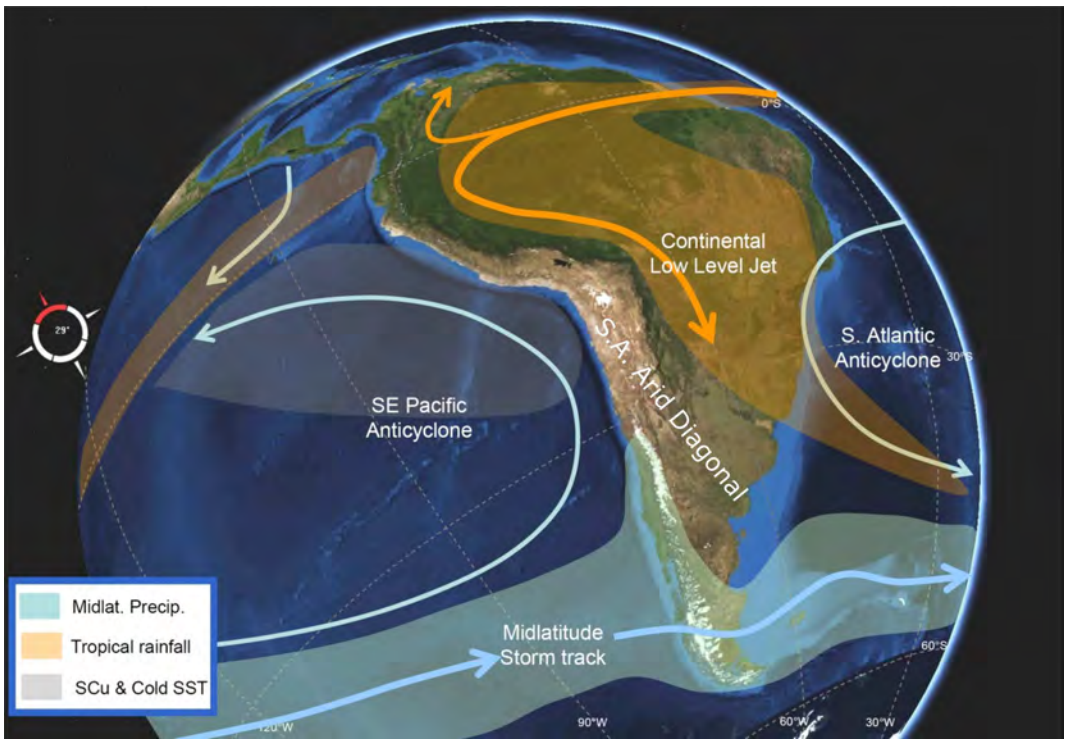

Figure 1.2: Low level tropospheric flow (below 1500 m a.s.l.) around the Andes Cordillera. The main processes responsible for moisture transport towards the Andes and the relative precipitation areas are shown. In the Tropical Andes, trade winds blow moisture from the Amazon basin and the westerly winds blow moisture from the Pacific ocean at extratropical latitudes. The Dry South American Diagonal is clearly visualized between these two major circulations. Major climate features like the South East pacific Anticyclone and cold sea surface temperatures across the Pacific coast are also shown. Figure from Garreaud (2009)

Regional precipitation regimes

The Tropical Andes can be divided into two climatic zones, delineated by the seasonal migration of the ITCZ. The Inner Tropics (North of 5°S), present constant temperature an humidity conditions with precipitations occurring all year long. The Outer Tropics (5°S-17°S) is characterized by alternating dry season and wet seasons, with the corresponding seasonality on specific humidity, cloud cover and precipitation (Rabatel et al., 2013a).

From Tropical to subtropical latitudes, wet conditions prevail along the Eastern slopes of the Andes resulting from the constant easterly flow bringing moisture from the Amazon basin (Garreaud et al., 2003). The Tropical Andes receive most precipitations from deep convective storms that develop over the high altitude mountain range, enhancing orographic precipitation that can reach up to 6000 mm/yr at the eastern Ecuatorian Andes (Garreaud, 2009; Vuille et al., 2000a,b). Contrasting arid and cold conditions prevail along the western slopes descending to the Pacific Ocean. This gradient reverses south of 35°S were the area of low precipitations shifts to the East of the mountain range in the Patagonian steppes of Argentina, thus creating the South American Arid Diagonal that crosses the Andes between 19-23°S (Messerli et al., 1998). The Desert Andes, located at the north of this Arid Diagonal, present mean annual precipitations decreasing from 400 mm at 18° to less than 100 mm at 23°S. The gentle descent of air (subsidence), enhanced by the upwelling of cold water along the Pacific coast at this latitude, maintains the subtropical anticyclone over the South East Pacific, resulting in arid and stable conditions all year long (Houston and Hartley, 2003; Rutllant et al., 2003). The South American Altiplano, also in the Desert Andes, exhibits its own climate conditions. It remains extremely dry during most of the year excepting the austral summer (November-March, a period named the South American Monsoon) when intense convective storms developing in the Amazonian basin bring significant precipitations (Zhou and Lau, 1998). The east-west precipitation contrast is high at this latitude, with the dry Atacama Desert in the West and the Chaco wetlands in the East, also influenced by the Monsoon summer rainstorms.

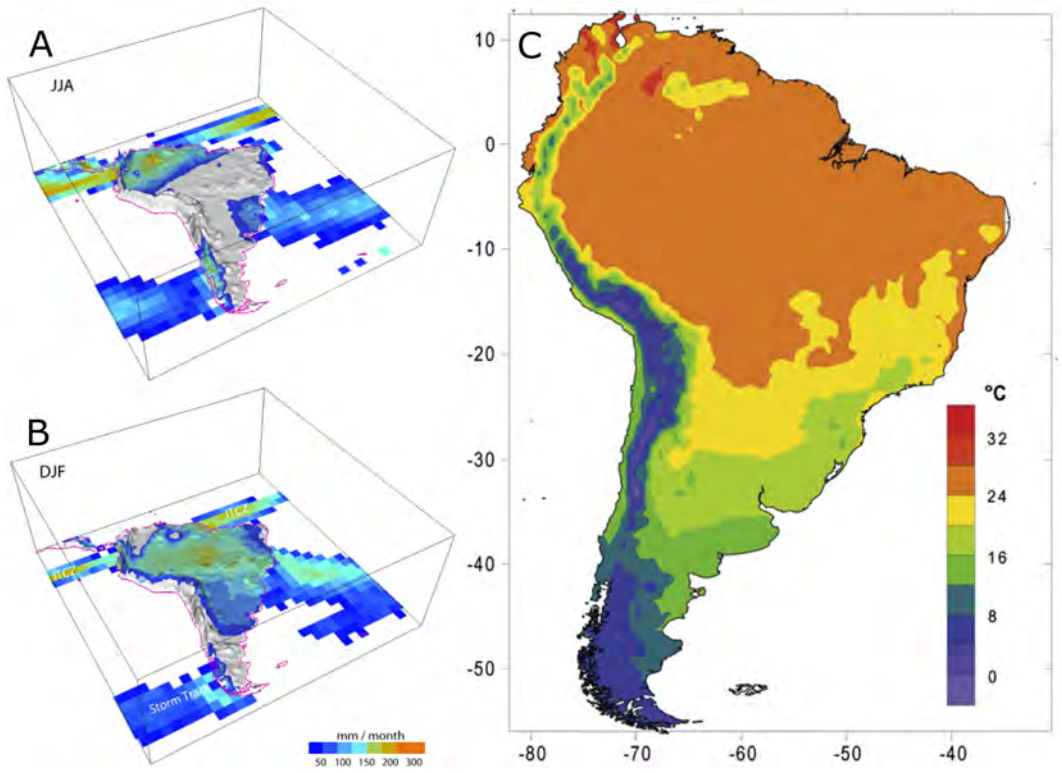

Figure 1.3: Long term mean precipitation and temperature over South America. (A) Mean precipitation for Austral winter (June-July-August) and (B) summer (December-January-February). Figure from Garreaud et al 2009. (C) Mean annual temperature from the high resolution data set for surface climate model (New et al., 2002). Figure from Sagredo and Lowell (2012).

South of 21°, precipitations are produced mostly by the passage of extratropical frontal systems (Garreaud, 2009; Garreaud et al., 2009). The Central Andes are characterized by a Mediterranean climate with dry summers and cold winters. This is the result of the north to south displacement of the South East Pacific Anticyclone, inhibiting precipitation in summer and allowing the passage of westerlies and frontal precipitation in winter (Rutllant et al., 2003). Total annual precipitation ranges from 500 mm around 31°S to 2500 mm at 36°S (Pellicciotti et al., 2014). Further South in the Patagonian Andes the latitude band of maximum precipitation coincides with the location of the storm track, 45°S-55°S in summer and 35°S-45°S in winter. Precipitation maxima occur at the western slopes enhanced by moisture uplift by the orographic effect of the Andes. Deep rainforest and large icefields are characteristic of this wet region in the Chilean Patagonia. Extreme precipitation gradients are found here, with totals exceeding 7000-8000 mm at the SPI and little moisture is left when the air masses cross toward Argentina (Lenaerts et al., 2014; Smith and Evans, 2007; Villalba et al., 2003).

Inter-annual and inter-decadal climate variability

Three large scale modes are responsible for natural climate variability in South America, modulating temperature and precipitation in the Andes at interannual and interdecadal time scales (Figure 1.4 Garreaud et al., 2009). Over Tropical and Subtropical Andes, climate variability is mostly dominated by the El Niño Southern Oscillation (ENSO) and the Pacific Decadal Oscillation (PDO) while further South is regulated by the Southern Annular Mode (SAM) (also known as the Antarctic oscillation, AAO).

ENSO is a coupled ocean-atmosphere phenomenon regulated mostly by the equatorial Pacific mean surface temperature. It is characterized by irregular fluctuations between a warm phase (El Niño) and a cold phase (La Niña) with a periodicity of 2 to 7 years (DIAZ, 1992). There is general agreement that rainfall and temperature anomalies associated to ENSO are the major source of inter-annual variability over South America (Francou et al., 2004; Garreaud, 2009; Vuille et al., 2000a,b). Overall, El Niño episodes are characterized with below average precipitation over the Tropics, above average rainfall over Subtropical South America and generalized warmer than normal air temperatures. Opposite

anomalies are observed during La Niña event, with cold and wet conditions in the Tropical region and a contrasting cold and dry Subtropical Andes. This contrasted tendencies have shown evident effects over snow pack and streamflow (e.g. Masiokas et al., 2010) and glacier mass balance (e.g. Francou et al., 2004) in the Tropical and Dry Andes regions.

The PDO is responsible for inter-decadal changes in South American climate, characterized by a periodicity of 20 to 30 years (Mantua and Hare, 2002). PDO related precipitation and temperature anomalies are similar in spatial structure to ENSO (i.e. they present an ENSO Like pattern) but their effect is less intense (Garreaud et al., 2009). Previous studies have shown El Niño (La Niña) rainfall anomalies to be stronger during the warm (cold) phases of PDO (Andreoli and Kayano, 2005). The PDO effect on glaciers is also similar to that of ENSO. A climatic shift from a cold to a warm PDO phase has been observed after 1976/77 where El Niño events have become more frequent and intense compared to previous decades, with clear impacts on natural systems and water resources (Garreaud et al., 2009; Mantua and Hare, 2002).

The SAM is the leading pattern of interannual variability over the southern tip of South America (Garreaud et al., 2009; Gillett et al., 2006). It is characterized by pressure anomalies of one sign centered on the Antarctic and anomalies of opposite sign on a circumpolar band at about 40°-50°S (Thompson and Wallace, 2000). The positive phase of SAM is associated with a strengthening and poleward shift of the westerlies, enhancing dry conditions and warm air temperatures across Patagonia and contrasted cold-wet conditions in Antarctica. The SAM has shown a marked trend towards its positive phase during the last decades, increasing the temperatures in southern South America (Thompson and Solomon, 2002; Villalba et al., 2012). However, the effect of SAM over Andes glaciers is still poorly known.

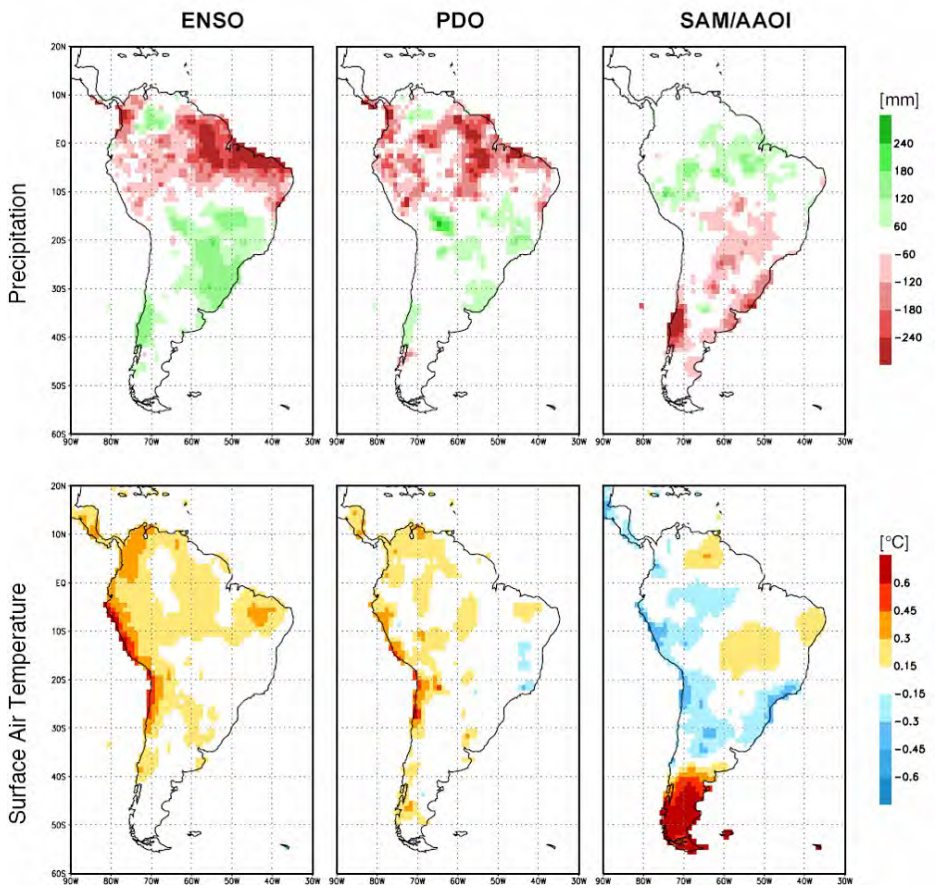

Figure 1.4: Annual mean precipitation and surface air temperature fields regressed upon ENSO Index, PDO Index and SAM or AAO Index. The value of the regression coefficient β indicates the local anomalies in the field (in physical units: mm or °C) associated with a unit anomaly of the index. This figure helps visualizing the similar spatial structure of the ENSO-related and PDO-related and anomalies, the reduced amplitude of PDO compared with ENSO, and the influence of SAM over the Southernmost latitudes. Figure from Garreaud et al. (2009)

1.2 Andes Glaciers

1.2.1 Glacier inventories

The wide variety of topographic and climatic conditions described above, result in a large diversity of ice masses along the Andes Cordillera. The magnitude and spatio-temporal distribution of precipitation and temperatures will determine the possibility of glaciers to exist in some locations and not others. Before studying glaciers, we need to know where they are located and how large they are, this is represented in glacier inventories. The interest on knowing where Andean glaciers are is quite recent compared to the rich glaciological legacy existing for example, in the European Alps. The first photographs and historical maps of glaciers were produced by the first explorers of the Andes at the beginning of the 20th century (e.g. Dr. Federico Reichert, Padre Alberto de Agostini) and the first known inventory of Andes glaciers was published only in 1956 by Louis Lliboutry, the French researcher, pioneer in South American glaciology, and was restricted to glaciers located in the Chilean Andes (Lliboutry, 1956).

In recent decades, with the birth and development of satellite remote sensing techniques, more precise and standardized glacier outlines have been produced from optical satellite images, permitting to map glaciers at a global scale with high precision. Semi-automatic methods based on the differential reflectance of snow and ice on the visible and the shortwave infrared bands permit to distinguish ice and snow from other surfaces (Paul et al., 2015). However, this methodology is far from being exact and posterior manual editions are usually recommended by the Global Land and Ice Measurements from Space (GLIMS) initiative (Racoviteanu et al., 2009). In general, errors due to the interpretation of glacierized surfaces from satellite scenes are around 5% for exposed ice and up to 30% for debris covered glaciers (Paul et al., 2013).

Geographical institutions in most South American Andean countries have produced independent, high quality and multi-temporal glacier inventories for all glaciers within their territories. However, combining these revised inventories to obtain an inventory at the entire Andes scale is not straightforward: (i) there is no methodological homogeneity in the way these inventories were created. (ii) They are temporally heterogeneous, representing glacier extents for a wide range of dates. (iii) The data is not always freely accessible. To my knowledge only Peru (www.ana.gob.pe), Argentina (www.glaciaresargentinos.gob.ar) and Chile (www.dga.cl) allow free access to complete glacier inventories. And finally, (iv) political issues between countries have induced unrealistic glacier outline interpretations. For example, glaciers at the border between Chile and Argentina are defined with the political limits rather than the real glaciological limits, and there are still conflict zones involving glaciers like in the SPI, where the limit zone is not demarcated and mapping is restricted (e.g. Chilean-Argentinian Treaty, 1998). This denotes the strong need for South American countries to joins efforts in the homogenization of glacier inventories, where politics need to be set aside in the favour of science.

Until now, the only complete and homogeneous glacier inventory covering the entire Andes range is the Randolph Glacier Inventory (RGI, Pfeffer et al., 2014). RGI, currently on its 6th version, is a global inventory of glacier outlines covering all 19 glacierized regions of the world, supplemental to the GLIMS dataset and intended to support glacier research and monitoring worldwide. The Andes are contained within two regions, RGI region 16, corresponding to Low Latitudes, where more than 99% of the glacierized area of this region is concentrated in the Tropical Andes; and RGI region 17, corresponding to the Southern Andes. Outlines represent ice extents of years from 2000 to 2003. Its quality is good enough for regional studies and it has been widely used before for Andes-wide glacier change estimations (Braun et al., 2019) and for glaciological and hydrological modelling (e.g. Huss and Hock, 2018; Marzeion et al., 2015). Large Icefields and some individual glaciers have been updated with high quality independent outlines; however, there is no doubt that many zones could still be improved, especially small mountain glaciers and snow patches are incorrectly mapped in the current RGI v6.0.

1.2.2 Spatial distribution of Andes glaciers and their characteristics

The RGI glacier inventory gives insight in the spatial distribution of Andean glaciers, which is strongly linked with altitude and the varying climate contexts. Glaciers cover a wide range of altitudes from the highest peaks and volcanoes above 5000 m a.s.l. in the Tropical and Subtropical Andes to sea level in Patagonia and Tierra del Fuego (Figure 1.5). From the Desert Andes to the South, the glaciers mean altitude starts descending progressively until altitudes bellow the 500 m a.s.l. at the southern edge of the continent. Largest glaciers are found at the lowest altitudes in the Patagonian Andes, more particularly in the large NPI, SPI and Cordillera de Darwin Icefields (Figure 1.5).

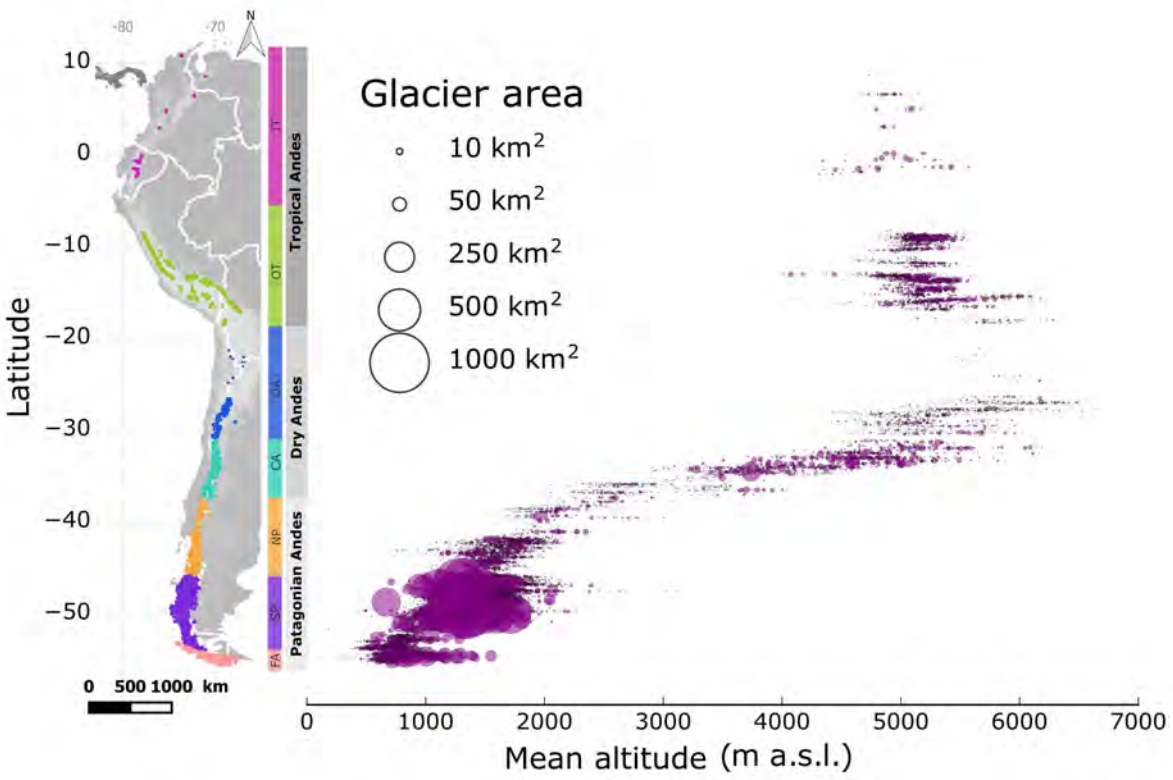

Figure 1.5: Latitudinal and regional distribution of Andean glaciers as a function of the mean altitude. Glacier surface area is depicted with the size of the circles.

1.2.3 Sensitivity to climate and seasonal cycle

Regional climates play an important role in modulating glacier response to climate variability (Fujita, 2008; Oerlemans and Reichert, 2000; Rupper and Roe, 2008; Sagredo et al., 2014). Understanding the sensitivity of a glacier is key for the interpretation of past, present and future glacier fluctuations.

In the Andes, the wide variety of climatic conditions result in a large quantity and diversity of ice masses (Clapperton, 1983; Garreaud et al., 2009; Sagredo and Lowell, 2012), resulting in important variability in glacier sensitivities, particularly to air temperature, to the total amount of precipitation received and to its seasonality. Glacier sensitivity is usually defined as the change in mass balance induced by a 1°C change in temperature or a 10% change in precipitation. In general, the sensitivity to temperature and precipitation changes increase dramatically with the amount of annual precipitation (Cogley et al., 2011). For this reason, glaciers located in maritime climates (Patagonian Andes) or tropical climates (Tropical Andes) presenting high rates of mass turnover, are usually more sensitive to climate changes (Meier, 1984; Oerlemans and Reichert, 2000).

Glaciers receiving precipitation during the summer months (i.e. summer accumulation type glaciers) are more sensitive to warming than those receiving precipitation only during the winter months (i.e. winter accumulation type glaciers). For summer accumulation type glaciers warming (i) prolongs the

duration of the melting period, (ii) causes a significant decrease in summer snow accumulation, because precipitations fall as rain in a warmer environment, and additionally (iii) decreases the glacier surface albedo enhancing the absorption of solar radiation and therefore melt (Fujita, 2008). In opposition, for winter accumulation type glaciers, warming only prolongs the melting period without changing snowfall in summer. Sensitivity of these glaciers is mostly controlled by the duration of the ablation season and the differences between melting and sublimation rates (Kaser, 2001).

Tropical (Low Latitude) glaciers are amongst the most sensitive glaciers of the world (Kaser, 2001). The great majority of low latitude glaciers are located in the Andes mountains. In the Inner Tropics, glaciers are summer type: the continuous humid conditions and stable temperatures causes accumulation and ablation to occur simultaneously all year, during summer and winter (Figure 1.6, Kaser and Georges, 1999; Rabatel et al., 2013a). Interannual mass balance variability is mainly controlled by the air temperature, which determines the snowline altitude, as observed in the vertical mass balance profiles for this region (Figure 1.6, Kaser and Georges, 1999; Francou et al., 2004; Kaser, 2001). Glaciers in the inner tropics are highly sensitive to warming, but seasonal snowfall also plays an important role controlling the surface albedo that will determine the intensity and duration of the melt season, particularly during the period when solar radiation is strong (Rabatel et al., 2013a).

Glaciers in the Outer Tropics are winter accumulation type glaciers: the tropical conditions in winter causes ablation and accumulation to occur simultaneously, but in summer the dry subtropical conditions makes accumulation almost inexistent and most of the ablation occurs by sublimation (Wagnon et al., 1999) (Figure 1.6). These glaciers are mainly sensitive to the seasonal distribution of precipitation but also to the total amount (Favier et al., 2004; Francou et al., 2003; Wagnon et al., 2001). Inter-annual mass balance variability depends mostly on the beginning of the wet season, with any delay causing very negative mass balances due to reduced snow accumulation, low albedo and large ablation rates (e.g. during El Niño events, Rabatel et al., 2013a; Wagnon et al., 2001).

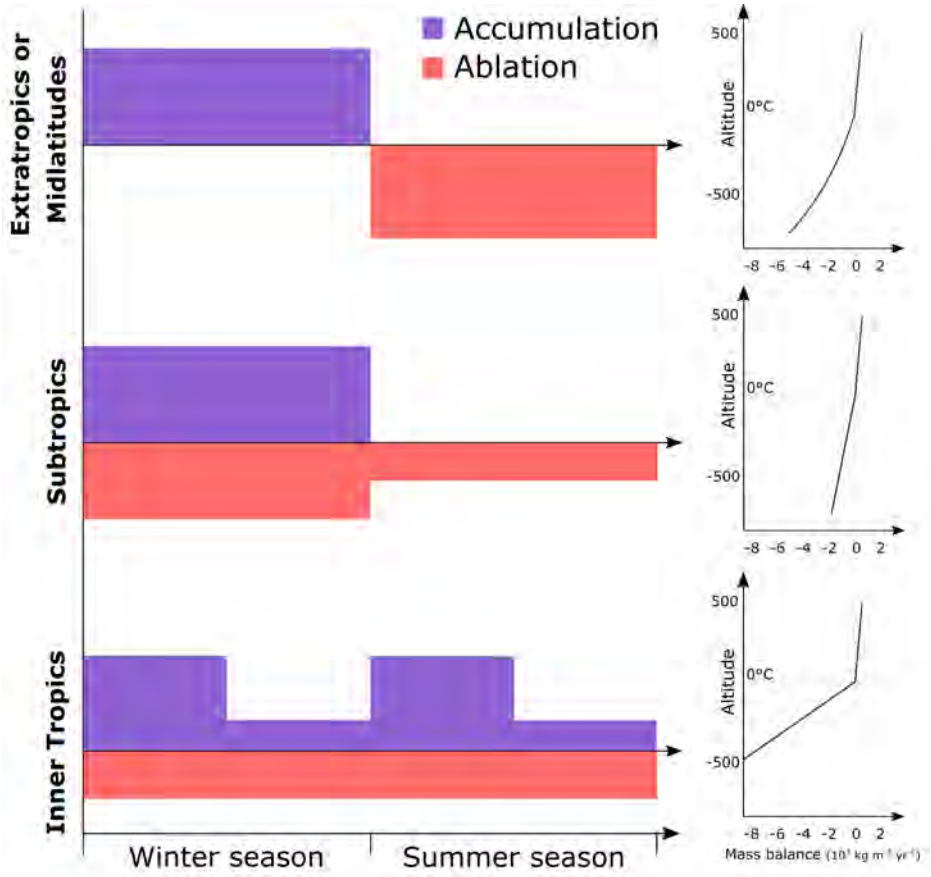

Figure 1.6: Schematic comparison of Inner Tropical, Subtropical and Extratropical-Midlatitude glacier mass balance regimes and their corresponding modelled vertical mass balance profiles. Note that at the x-axis changes in mass balance are in respect to the mass balance at the 0°C level. Figure modified from Kaser and Georges (1999)

In the extremely dry Desert Andes (Subtropics) glacier accumulation is sparse, coming from occasional precipitations, and almost all ablation result from sublimation (Ginot et al., 2006; MacDonell et al., 2013; Gascoin et al., 2013). Most of these high altitude glaciers are located above the 0°C isotherm and are rarely exposed to melting temperatures (Sagredo and Lowell, 2012). They are strongly sensitive to changes in air humidity, which controls the amount of precipitation but more importantly, affects the balance between melt and sublimation (Kaser, 2001; Rabatel et al., 2011).

In Southern regions at midlatitudes (Central Andes to Patagonia), accumulation occurs during winter and ablation during summer (Figure 1.6), with the exception of maritime glaciers located close to the South Pacific coast in Patagonia and Tierra del Fuego, which receive precipitations all year long. Sublimation is still important in the Central Andes but becomes almost negligible in the Southernmost regions where melt dominates. Continental glaciers in this regions, are sensitive to the amount of precipitations, while the effect of temperature is only significant during summer months, because it favours melt and increases the duration of the ablation season (Oerlemans and Reichert, 2000). Maritime glaciers are more sensitive to temperature changes, and their mean annual temperature is strongly dependent on the sea surface temperature (Kerr and Sugden, 1994). Warming in maritime glaciers induces high melt rates at the glacier tongue and increases the altitude of the 0°C isotherm, reducing significantly the fraction of precipitation falling as snow (Oerlemans and Reichert, 2000).

The glacier equilibrium line altitude (ELA), is also used as a proxy for sensitivity of glaciers to their climate. The ELA is the altitude at which the glacier surface mass balance is equal to 0, with accumulation occurring above and ablation below. It can be approximated by the annual maximum altitude of the snowline (Rabatel et al., 2005). The ELA is also sensitive to climate conditions, and directly affects glacier mass balance by affecting the surface ratio between the accumulation and the ablation zones.

ELA changes are strongly tied to the dominant ablation process. In regions where melt is dominant, the ELA is more sensitive to air temperature, while in sublimation dominant regions, the ELA is more sensitive to precipitation (Rupper and Roe, 2008). In the Andes, the ELA sensitivity to temperature reveals variations between 140 to 230 m for every 1°C in temperature change, with the Inner Tropics being the most sensitive region (larger melt rates) and the Desert Andes the less sensitive (larger sublimation rates)(Sagredo et al., 2014). Similarly, the ELA was shown to be more sensitive to precipitation in the Desert Andes (dry climate), than over regions like the Inner Tropics and Patagonia, presenting humid climates and frequent cloud cover (Sagredo et al., 2014).

Hydrological context and contribution to streamflow

The seasonal fluctuations of glaciers are very important for hydrology as they can significantly modify the quantity and timing of streamflow even in catchments where the ice cover is relatively low (Radić and Hock, 2014). There are still considerable ambiguities with respect to the definition of glacier runoff, and therefore, no consensus on the way to quantify it. The runoff originating at the glacier terminus has different origins, it may come from the melt of ice, snow or firn, but it may also come from rain on the glacier or melting from the snow located outside the glacier, and is also affected by processes like evaporation, sublimation and refreezing of liquid water. Different concepts generally used in literature vary essentially on those that include or not the snow accumulation and the water coming from the glacier that has not been generated from melt (Radić and Hock, 2014).

Glacier runoff can be considered as a function of annual or multiannual glacier volume changes, and can be directly linked to glacier-wide mass balance measurements (see section 1.3). In this case, glaciers runoff is considered as an 'excess discharge' of water originating from the glacier volume changes during a particular period (Lambrecht and Mayer, 2009; Pritchard, 2019), and directly represents the imbalanced condition of the glacier. This concept assumes that glaciers produce runoff only when they are losing mass (they are imbalanced), and their contribution is zero when they are in balance or present positive volume changes. Thus, this so-called imbalanced glacier contribution to runoff stands as a direct measure of the perennial changes in glacier water storage and represents an important measure of the sustainability of glaciers as future water resources. In this thesis work, I will estimate the decadal imbalance glacier contribution of glaciers over seven important Andean river basins during the last two decades, and how the interdecadal variability of glacier contribution is linked with climate. This volumetric approach, however, is not very useful for hydrologists because in fact glaciers influence streamflow on a seasonal scale, even when they are in balance with their climates (Huss, 2011; Kaser et al., 2010; Radić and Hock, 2014). In winter accumulation regimes, when the accumulation period is different form the ablation period, there is a delay between the moment (winter) when water is stored on the glacier, and the moment (summer) when melt water is produced (Figure 1.7A). This is called the seasonally delayed runoff and plays an important role sustaining river flows during the dry season or during periods of extreme drought, compensating for otherwise reduced flows, specially when rivers are located in arid and semiarid regions (Huss and Hock, 2018; Kaser et al., 2010; Radić and Hock, 2014).

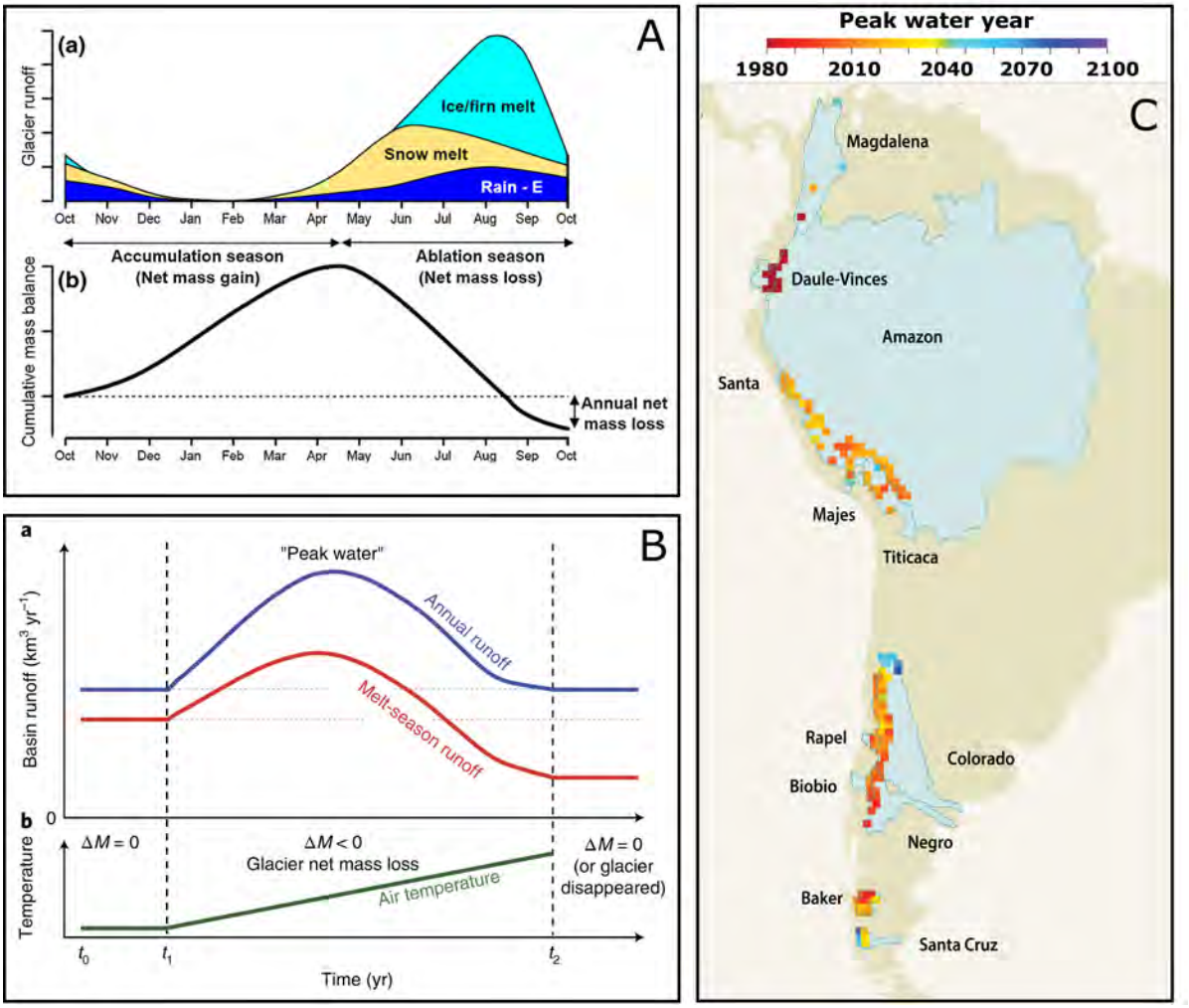

Figure 1.7: Panel A: (a) Schematic seasonal variation of total runoff and its components, E is evaporation. (b) Cumulative glacier mass balance in specific units (m w.e. yr-1) showing a year with negative mass balance. Figure from Radić and Hock (2014). **Panel B:** Schematic illustration of the changes in runoff from glacierized basin in response to continuous atmospheric warming. Figure from Huss and Hock (2018). **Panel C:** Peak water in all the glacierized macroscale drainage basins. Figure from Schoolmeester et al. (2018), data from Huss and Hock (2018).

Several studies have attempted to document the glacio-hydrology in the Andes, with a concentrated attention on the most vulnerable zones, the Tropical Andes and some selected catchments at the arid and semiarid regions of Chile and Argentina. In a global scale study, Kaser et al. (2010) used a monthly glacier melt model comparing glacial melt inputs with precipitation patterns to assess the effect of glaciers on seasonal water resources in glacierized basins around the world. For the Andes, they studied only the Santa river basin in Peru, where climate is arid and maximum ablation rates are synchronized with the dry season. Seasonally delayed glacier contribution in the Santa basin showed to reach a maximum (January) of 71% of the total runoff at the glacier front (Kaser et al., 2010). Similar contributions were found by other modelling approaches, showing that almost 38% of the Santa total annual flow comes from melting glaciers (Buytaert et al., 2017; Condom et al., 2012; Vergara et al., 2007). Similar results where also found in Bolivia (Soruco et al., 2015). Buytaert et al. (2017) coupled the model from Kaser et al. (2010) with a regional water balance model of the Tropical Andes and high resolution spatial data on water use along the watershed. They found a large seasonal variation in the contribution of glacial melt and persistent strong glacier contributions on all arid and semiarid Pacific basins and on those located in the Altiplano of South Peru and Bolivia. Glacier contribution to streamflow is maximum at glacier front and decreases downstream, consequently the glacier contributions calculated in the above mentioned studies are valid only for a specific location in the basin.

In the Desert and Central Andes of Chile, glacier contribution to river discharge is also considerable, reaching maximum values of 50% and 58% of the total runoff at the outlet of Glaciar Bello and Universidad during enhanced periods of drought (Ayala et al., 2016; Bravo et al., 2017), and up to 47% at the outlet of Juncal Norte in the late ablation season (Ragettli and Pellicciotti, 2012). Mean annual glacier contributions can reach up to 23% in basins with less than 11% glacier coverage (Gascoin et al., 2011). This estimates are however, not free of uncertainties, most of them regarding the non consideration of the sublimation fluxes, known to be important in the arid and semiarid regions (e.g. Wagnon et al., 2001), groundwater contribution to streamflow during the dry season, which has been suggested to be considerable in semiarid basins (e.g. Rodriguez et al., 2016). In many cases the lack of reliable and continuous streamflow data and regional glacier change assessments in this vulnerable regions do not allow to perform regional estimates of glacier contribution to streamflow.

Concerning the future of glacier meltwater availability in the Andes, in an assessment of the hydrological consequences of glacier decline around the world, Huss and Hock (2018) project the largest summer month reductions in glacier runoff over Central Asia and the Andes for the end of the century. Noticeably, they are also the two regions of the world where more than 50% of the total basin runoff comes from snow and ice (Huss et al., 2017). Glacier in the Andes have experienced continuous retreat during the last decades (Casassa et al., 2007; Pellicciotti et al., 2014; Rabatel et al., 2013a). When a glacier is in balance with its climate, its annual contribution to streamflow stays constant through time, but when a glacier is exposed to a warming climate, it retreats and water is released from its long-term storage (i.e. glacier imbalance contribution). As a consequence, glacier runoff is expected to increase until reaching a maximum 'peak water' beyond which runoff starts to gradually decrease, because the reduced glacier volume cannot support high melt rates anymore (Figure 1.7B, Huss and Hock, 2018). If temperatures continue to increase, the glacier will end up disappearing. If the glacier reaches a new equilibrium with a decreased volume, the water released during the melt season is expected to decrease bellow the initial value when the glacier was larger (as expressed by the red line in figure 1.7). Most of the Andes basins dominated by small glaciers have already reached the peak water or it is expected to occur within the next decades (Figure 1.7C, Gascoin et al., 2011; Bravo et al., 2017; Huss and Hock, 2018; Vuille et al., 2018).

Because they hold large populations that are dependent on meltwater during summer, the Tropical and the Dry Andes regions are the most threatened by the projected glacier changes, specially during enhanced periods of droughts. The intense negative effects of an uncommonly long period of drought in the Central Andes have already been documented. This so called "mega-drought" has also been readily observed in terms of decreased streamflow, rainfall, snow accumulation and vegetation productivity, among other indicators (Garreaud et al., 2017; Rivera et al., 2017). The influence of this mega-drought on glacier changes in the Dry Andes is an important aspect that will be considered in this work. The high impacts on water resources are expected to affect socioeconomic activities such as agriculture and hydropower, which are in many cases the principal economic activities of many Andean countries (Bradley et al., 2006; Buytaert et al., 2017; Vuille et al., 2018). The United Nations Educational, Scientific and Cultural Organization (UNESCO) recently evaluated water risk in the Andes considering different indicators and the population growth expected for 2020 (Figure 1.8, Schoolmeester et al., 2018), it is interesting to see that the regions with high risk coincide with the regions where glacier melt help sustain streamflow during the dry seasons. This stresses the need to constrain glacier changes in this regions and start thinking about mitigation policies.

Figure 1.8: Population and water risk in Andean countries. Population estimates for 2020 by administrative unit (city, town). Water risk includes 12 global indicators: Baseline water stress, Inter-annual variability, Seasonal variability, Flood occurrence, Drought severity, Upstream storage, Groundwater stress, Return flow ratio, Upstream protected land, Media coverage, Access to water and Threatened amphibians. Figure from Schoolmeester et al. (2018)

1.3 What is the glacier mass balance?

1.3.1 Glacier mass balance as an indicator of glacier health

Glacier are recognized as sensitive indicators of climate changes (Oerlemans, 2001). Glacier surface area and length fluctuations have been used historically as observations of glacier evolution in the Andes (e.g. Aniya et al., 1997; Aniya and Enomoto, 1986). However, these variables are indirect climatic indicators as they result from a combination of both climatic forcing and glacier dynamics, which is unique to every glacier and is determined by its slope, exposition, the state of the glacier surface (ice or debris covered) and the type of glacier front (if its terminates on land, a lake or the ocean).

Glacier mass balance is a measure of the evolution of the quantity of snow and ice that is stored in the glacier, directly linked to variations in accumulation (precipitation) and ablation cycles (temperature and energy fluxes) (Cuffey and Paterson, 2010). Mass balance annual series and the spatial distribution of these changes with altitude allow to detect changes in climate (Oerlemans, 2001). In this sense, an unhealthy glacier is not in equilibrium with its climate, presenting sustained (year to year) negative mass changes that can ultimately lead to its disappearance.

In simple terms, the mass balance ($\dot{b}$) at a specific point of a glacier is defined as the difference between the accumulation and the ablation (Cuffey and Paterson, 2010).

$$\dot{b} = accumulation - ablation \tag{1.1}$$

Where mass gains may come from multiple sources such as snowfall, avalanches, wind snow distribution or refreezing of the liquid water infiltrating the glacier. Ablation is governed by different processes including melt of snow and ice, sublimation of snow and ice and losses due to the rupture of icebergs or seracs at the glacier front, depending if the glacier ends in a water body or not.

The glacier-wide surface mass balance ($\dot{B}$) is obtained by integrating the specific mass balance ($\dot{b}$) on the entire glacier area (A) (Cuffey and Paterson, 2010):

$$\dot{B} = \frac{1}{A} \int_A \dot{b} dA \tag{1.2}$$

Note that glacier-wide surface mass balance ($\dot{B}$) is not equal to the total glacier-wide mass balance ($\triangle M$). Most direct observations neglect internal and subglacial mass balance changes, usually accepted to be an order of magnitude less than surface fluxes. Glacier-wide surface mass balance estimate ($\dot{B}$), also omits frontal ablation, that corresponds to the sum of the mass loss by calving, subaerial frontal melting and sublimation above the water line, and subaqueous frontal melting below the water line (Cogley et al., 2011). Mass losses by frontal ablation (specially calving) can be significant and even dominant on glaciers that end on water bodies (Sakakibara and Sugiyama, 2014; Truffer and Motyka, 2016) like many glaciers in the Patagonian Andes that finish in lakes or the ocean (Warren and Aniya, 1999). Over these glaciers, the glacier-wide mass balance ($\triangle M$) need to account for frontal ablation (A_f) and is expressed as:

$$\triangle M = \dot{B} + A_f \tag{1.3}$$

Or it can be simplified as a function of calving (D) when subaerial frontal melting, sublimation and subaqueous frontal melting are negligible.

$$\triangle M = \dot{B} + D \tag{1.4}$$

As a convention, mass balance is measured at the end of the ablation season of the hydrological year (end of spring, generally March-April in the Southern Hemisphere (Masiokas et al., 2016; Rabatel et al., 2013a). It is generally expressed as a surface unit in the form of meter water equivalent per year (m w.e. yr^{-1}). Figure 1.9 represents the evolution of the specific mass balance through the hydrological year for the different areas of a glacier (Cuffey and Paterson, 2010). The accumulation zone is characterized by a positive mass balance, conversely in the ablation zone the mass balance is negative. These two zones are divided by a line where the annual mass balance is equal to zero (i.e. accumulation equals ablation), also defined as the equilibrium line. The ELA may vary from year to year determining the accumulation area ratio (AAR), or the ratio between the accumulation areas and ablation areas of the glacier .

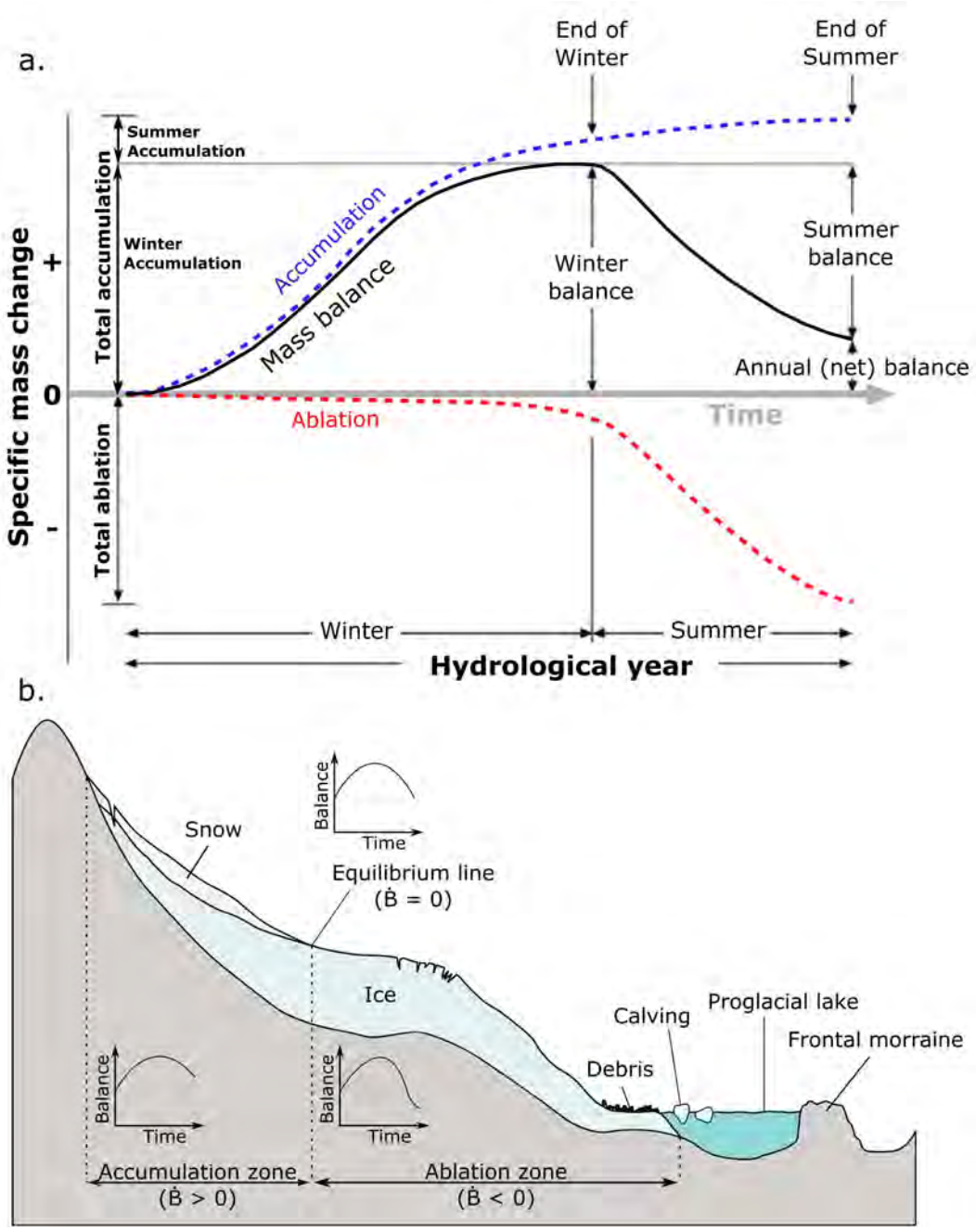

Figure 1.9: (a) Definition of the principal mass balance terms and their evolution throughout the hydrological year. Figure adapted from Cuffey and Paterson (2010). **(b) Schematic representation of a mountain glacier.** $\dot{B}$ **correspond to the annual mass balance.** Glaciers terminating on lakes or the ocean are frequent in the Patagonian Andes, where calving plays an important role on the ablation process. Figure adapted from Gardelle et al. (2012).

1.3.2 How to measure glacier mass balance?

Glaciological Method

The glaciological method, also referred as the direct method, consists on in situ measurements of annual or sub-annual accumulated snow and surface wastage (i.e. ablation) at a series of points distributed along the glacier surface (Cogley et al., 2011). It is a measure of the surface mass balance ($\dot{B}$) of a glacier. Local mass balance at the end of the accumulation season is estimated by snow probe measurements along the glacier surface (Figure 1.10b), together with density measurements at snow pits. During the ablation season, the emergence of long stakes installed the previous year allows determining the layer of snow or ice that has been lost (Figure 1.10a). Stakes in the accumulation zone are better installed at the end of winter at the snow level and emergence measured during the next summer, permitting to differentiate snow losses from ice losses. In the ablation zone, stakes are generally installed during

the end of summer and measured one year later. The annual glacier-wide surface mass balance is then obtained by extrapolation of the point measurements over a larger area such as an elevation band or the entire glacier. A discussion on the different techniques of surface mass balance measurements is available in Fountain et al. (1999). If measurements are performed repeatedly and during an extended period of time, the glaciological method will provide crucial information about the temporal variability of glacier mass balance. However, for practical reasons, only small and accessible glaciers can be monitored with this method, and the extrapolation to larger regions is challenging as the observed changes are not necessarily representative of the regional glacier mass changes.

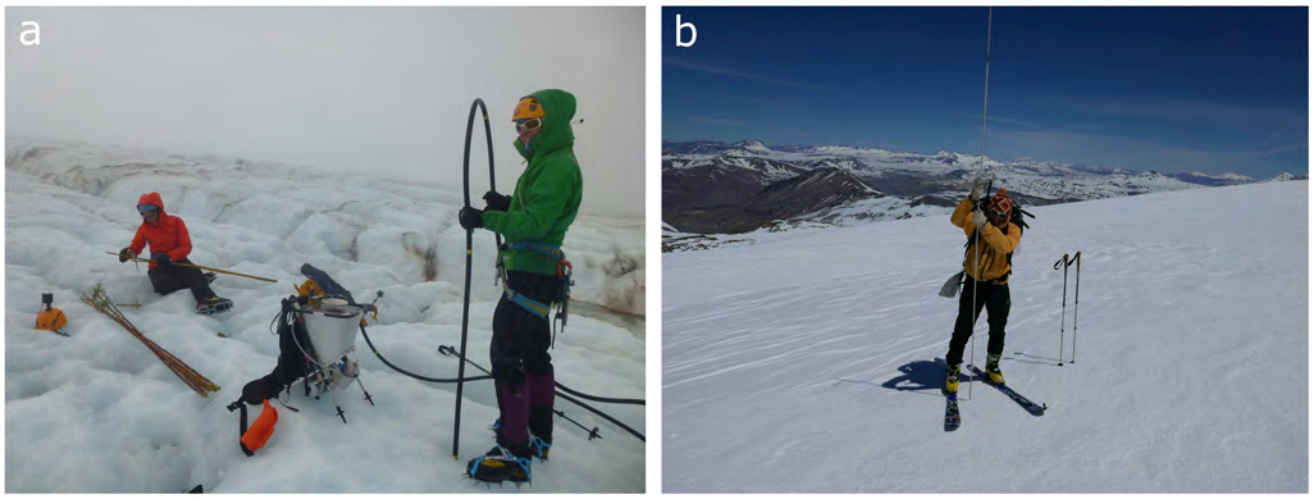

Figure 1.10: Examples of glaciological measurements performed during this PhD work on the Argentinian Andes as a collaboration with the Argentinian glaciology institute (IANIGLA). (a) Installation of 6 m bamboo stakes at the ablation area of Alerce glacier (Monte Tronador, North Patagonia) in spring using a water vapour perforator. (b) Winter snow probing at the accumulation area of Aguas Negras glacier (Desert Andes).

The uncertainties of the glaciological method lie mostly on the problems of sampling: (i) the use of a limited number of point measurements, which are not necessarily able to capture the spatial variability of surface mass balances along the glacier. (ii) The difficulties to measure certain zones of the glacier like steep slopes or crevassed zones. And (iii) the errors on every specific measure. Therefore, glacier-wide mass balance estimations by the glaciological method can be biased and need to be calibrated with the other methodologies. Total uncertainties on the annual glaciological mas balance lie between 0.2 and 0.4 m w.e. yr^{-1} (e.g. Sicart et al., 2007; Thibert et al., 2008; Zemp et al., 2013). Geodetic measurements are usually preferred for calibration (Thibert and Vincent, 2009; Zemp et al., 2013).

The hydrological method

The hydrological method allows to measure the glacier-wide mass balance ($\dot{B}$) by measuring the fluxes of water coming in and out of the glacier. It compares the mass gains by precipitation (P) on top of the glacier to the losses by melt, measured as the water runoff (Q) at the glacier front, and the losses by evaporation and sublimation of snow and ice (E).

$$\dot{B} = P - Q - E \tag{1.5}$$

The uncertainties of this methodology are therefore linked to the ability to measure the different components. Over Zongo glacier in Bolivia, Sicart et al. (2007) showed that the hydrological method underestimates the glacier-wide mass balance by 0.6 m w.e. yr^{-1} with respect to the glaciological method. This inaccuracy is attributed mostly to the difficulties in measuring the high spatial variability of precipitations in mountainous regions, especially due to the lack of measurements at high altitude. But also on the capacity to model meltwater discharge and energy fluxes on the entire glacier basin (e.g. Sicart et al., 2011).

The gravimetric method

The Gravity Recovery and Climate Experiment (GRACE) mission consists in two twin satellites flying 220 km apart over the same orbit. The continuous monitoring of the distance between these two satellites permits to determine the spatial variations of the Earth surface gravity fields at a monthly scale. Changes in the Earth gravity fields can result from numerous processes of mass changes in the oceans, like redistribution of mass through oceanic circulation, or in the in the Earth interior, like tectonic uplift, erosion, changes in surface and subsurface hydrology and also the mass losses or gains over glacierized surfaces. The largest limitation of this methodology is the difficulty to differentiate the signal corresponding to each one of these components. In order to isolate the signal associated with glacier changes, corrections considering the hydrological redistribution of water in the earth surface and subsurface and the glacial isostatic adjustment need to be taken into account. The global mass balance estimation will therefore be dependent on the ability to model the hydrological and isostatic signal, which can lead to large uncertainties (e.g. Wouters et al., 2019; Jacob et al., 2012).

Particularly in the Andes, the reduced spatial resolution of GRACE (at best 1° by 1° latitude longitude) makes the separation of the glacier signal from the hydrologic signal extremely difficult, especially in the Tropical and Dry Andes regions, where glaciers are small and discontinuously distributed. In Patagonia, the glacier signal is clearer, because the glacierized surface is larger, but the influence of isostatic adjustment is strong (Dietrich et al., 2010; Ivins et al., 2011; Richter et al., 2016) contributing to large uncertainties also in this region.

The geodetic Method

The Geodetic Method (volumetric method, photogrammetric method) permits to calculate the total volume changes of a glacier during a specific time period by comparing repeated surveys of its surface topography. This is the methodology that will be used in this thesis to calculate Andean glacier mass balance. I provide here a brief description of the general aspects of the geodetic methodology. Further details and methodological adaptations will be provided in the next chapters. The geodetic method needs at least two, or more, different topographic maps or digital elevation models (DEMs) of the glacier surface obtained at different times. To insure a reliable volume change estimation, a relatively complete coverage of the entire glacier surface is a key aspect of the input DEMs, as high biases may arise if only a fraction of the glacier is surveyed (e.g. only the glacier tongue, Berthier et al., 2010). The precision of the results is also a function of the time separation between DEMs, where time periods larger than 5 or 10 years are usually preferred to minimize uncertainties. After differencing both topographies, the resulting elevation changes are integrated over the entire glacier area to obtain the total glacier volume change. Volume change ($\triangle V$ in m^3) derived by differencing DEMs is expressed as (Zemp et al., 2013):

$$\triangle V = r^2 \sum_{k=1}^{k} \triangle h_k \tag{1.6}$$

Where k is the number of pixels covering the glacier area, r is the pixel size (in m), and ($\triangle h_k$) is the elevation change at the individual pixel (in m). Volume is then converted to geodetic mass balance ($\dot{M}$) using a density conversion factor ($f_{\triangle V}$, in kg m^{-3}):

$$\dot{M} = \triangle V \times f_{\triangle V} \tag{1.7}$$

There is still no agreement on $f_{\triangle V}$, a first possibility is to apply the density of ice 900 kg m^{-3} to the entire glacier surface assuming that the density profiles in the accumulation zone remain unchanged and that all losses and gains correspond to ice (e.g. Arendt et al., 2002). This is true for the ablation area, but this assumption may not apply over the accumulation area. For this reason, other authors prefer to use a differential conversion factor for the accumulation zone (above the ELA) using an approximated

density of 650 kg m^{-3} for firn (Hagg et al., 2004). Huss (2013) showed that under some hypothesis, the volume to mass conversion can be approximated by a constant value of 850 ± 60 kg m^{-3} for geodetic measurement performed for periods larger than 3 years. In this work, all volume to mass conversions will use this density conversion factor.

The uncertainties of the geodetic method depend mostly on the precision of the DEM and the error inherent to the volume to mass conversion. Consequently, the characteristics of the input data and the technique selected to elaborate the DEMs will determine to a great extent the final accuracy of the method. Four different techniques are usually used to produce DEMs over glacierized regions.

- **Aerial photographs:** This pioneering technique is based on the principle of image stereoscopy. The topography is reconstructed by measuring the distortion between two images acquired over the same terrain with different viewing directions. The identification of homologous points can be performed either manually or by automatic correlation, in both cases the quality of the correlation depend directly on the contrast of the images. The first photographs over glacierized regions go back to the beginning of the 20th century (1950s for the Andes). Due to the optical nature of the images, larger errors are expected over the glacier accumulation zones, where the high albedo of the snow surface causes images to oversaturate, preventing image correlation. Cloud cover on the images is also a source of error, as clouds do not represent the surface of the terrain. Recent studies have automatized this technique in order to obtain many digital elevation models over glaciers with a high level of statistical accuracy (Belart et al., 2019; Papasodoro et al., 2015).
- **Satellite optical imagery:** Same as described above, except the stereoscopic pair of images are captured from satellite optical sensors in the visible and infrared wavelengths. The larger distance of the satellite to the surface of the Earth permits to obtain images covering much larger glacierized surfaces than aerial photographs. Toutin (2001) summarizes the different techniques to build DEMs from satellite images and their applicability to different sensors. At present, automated tools designed for processing stereo images captured from satellites, like the Ames Stereo Pipeline (ASP, Shean et al., 2016) from the National American Space Agency (NASA) or MicMac (Rupnik et al., 2017) are freely available for public use with specifications for a wide range of different sensors. In this work I will exploit DEMs obtained from the ASTER, SPOT5, SPOT6 and SPOT7 satellite sensors, but other such as Pleiades, KH9-Hexagon are also widely used to measure glacier changes.
- **RADAR interferometry:** InSAR (Interferometric Synthetic Aperture radar) is used for mapping the scattering properties of the earth surface. Radar images taken from slightly different point of view allow the construction of digital elevation models of meter-scale accuracy (Bürgmann et al., 2000). The InSAR microwave operative frequencies permits the signal to travel through the atmosphere and therefore to operate during night and day and even across clouds, contrarily to optical systems, which are passive sensors. The scattering coefficient of the earth surface received by the radar, will depend on the polarization of the radar wave, the roughness of the surface and the dielectric constant of the material at the earth surface layers. The latter is a measure of the permittivity of the earth surface to the radar signal and depends directly on its water content. The dryer the surface the deeper the radar signal will penetrate in the ground (Jaber et al., 2016; Rignot et al., 2001). This property is fundamental for glaciers, because the penetration of the radar signal will be more or less important depending on the state of the snow/ice cover (if it is dry or wet), and the scattering signal received will not necessarily represent the superficial layer. Radar signal penetration is the largest source of uncertainties for InSAR derived DEMs (e.g. SRTM, TanDEM-X) over glacierized regions (Berthier et al., 2016; Dehecq et al., 2016; Rignot et al., 2001). In this work the radar SRTM C-band DEM will be exploited to measure glacier changes along the Andes, and several works using TerraSAR-X Digital Elevation Measurement (TanDEM-X) will be referred further along the manuscript.
- **Airborne or satellite altimetry:** This technique consist in measuring the travel time of an impulse signal emitted to the earth surface by a satellite or airborne altimeter and then reflected back to the same sensor. The distance from the surface to the satellite or plane can be deter-

mined. Altimeters can be laser (LIDAR, LIght Detecting and RAnging) or RADAR depending on the wavelength of operation. Elevation data is provided as a limited number of altimetry profiles along surface. Thus, for application on glacierized topographies, this technique is better adapted for large glaciers permitting to obtain good measurements of the accumulation zone. ICESat (Ice, Cloud, and land Elevation Satellite) and CryoSat-2 missions have been widely used to measure changes in the large ice sheets of Antarctica and Greenland (e.g. Helm et al., 2014; Pritchard et al., 2012). For mountain glaciers the technique was expected not to work as well, but it has recently been shown to be relevant in mountain glaciers of High Mountain Asia (HMA) (Kääb et al., 2012).

Over recent years, the geodetic method using spaceborne derived DEMs has become a popular tool to measure recent glacier changes, permitting to cover large glacierized regions with high accuracy, and helping to improve previous estimates. For example, recent geodetic estimates in HMA demonstrate glacier losses to be smaller than what was previously considered as a reference by the last IPCC assessment (Brun et al., 2017). The recent advances on the processing of historical airborne images have permitted to produce considerably more accurate topographic maps than what was possible before. The exploitation of this earlier datasets permits to extend glacier changes observations further back in time. As stated before, geodetic estimates are also important references to test and correct the cumulative mass balances obtained by the glaciological method (e.g. Andreassen et al., 2016; Thibert and Vincent, 2009; Zemp et al., 2013) which can sometimes be strongly biased by sampling problems. However, attention must be taken, as both methods measure different quantities: the geodetic method integrates the subaerial part of frontal ablation. In calving glaciers, where frontal ablation is not a negligible part of the mass loss (Truffer and Motyka, 2016), large discrepancies can be observed between the surface mass balance measured by the glaciological method and the geodetic mass balance.

1.3.3 Model based mass balance estimations

Glacier mass changes can also be simulated and projected by surface mass balance models of diverse complexity. The purpose of glacier mass balance modelling is to relate glacier mass balance changes with climatic conditions, to predict how glaciers will respond to possible climate changes (Oerlemans, 2001). This approach directly models the evolution of glacier surface mass balance in time by simulating melt and accumulation at the glacier surface, using climate data as input forcing (Oerlemans, 2001). Melt is commonly modelled by positive degree day models (DDM), which are based on an empirical relationship between the ablation of snow and ice and the sum of positive daily temperatures (Cuffey and Paterson, 2010). These models are calibrated using in situ and geodetic mass balance observations and have shown to efficiently simulate glacier melt (Hock, 2003). However, the extrapolation to larger regions is challenging as these models are not physically based (Réveillet et al., 2017).

During the last years, mass balance models have been exploited to simulate global glacier mass loss and project the consequent contribution to sea level rise (e.g. Huss and Hock, 2015; Kaser et al., 2010; Marzeion et al., 2015). This works still hold large uncertainties related mostly with the scarcity of accurate calibration data, the complexity of modelling climatic conditions in mountainous terrains, and the intrinsic uncertainty of future climate scenarios (Huss and Hock, 2015). The emergence of large scale data sets of global glacier inventories (Pfeffer et al., 2014), global ice thickness estimation (Farinotti et al., 2019; Huss and Farinotti, 2012) and global glacier mass loss estimations (Gardner et al., 2013) have allowed for more sophisticated models to be developed in recent years, where complex processes like frontal ablation are now accounted for (Huss and Hock, 2015).

One of the largest gaps for these modelling approaches is the lack of fully constrained global glacier mass loss estimations for model calibration. In many regions of the world, including the Andes, there is still no consensus between the different methodologies.

1.4 Present knowledge in Andes glacier evolution

In the context of recent glacier changes, some regions of the Earth have been documented much more extensively than other. Regions like Europe and North America present well established data collection

projects allowing for abundant long-term observations. Similarly, the Arctic and Antarctic regions have been extensively monitored due to their global relevance. In recent years, High Mountain Asia glacier changes have shown a large growing interest due to their importance for water resources. The Andes mountain range has received slightly less attention from the glaciological community.

In recent years, together with the accession and development of the satellite era, investigations in the Andes have been increasing fast. However most of the interest is still concentrated over the Patagonian Icefields, which contain the largest glacierized surfaces in the Andes. Tropical glaciers have also been the target of many studies, mainly because of their high sensitivity to climate variability, that makes them interesting subjects to understand glacier-climate interactions (e.g. Francou et al., 2003, 2004; Favier et al., 2004; Wagnon et al., 2001). More recently, the importance of glaciers as water resources has been stressed over dry Andean glaciers (e.g. Burger et al., 2018; Buytaert et al., 2017; Vuille et al., 2018; Bravo et al., 2017) and their capacities to act as buffers reducing the impact of the frequent and intense droughts (Garreaud et al., 2017). Figure 1.12 summarize all available mass balance estimates for local glaciers or glacierized region in the Andes. In general the surveyed ice surfaces are small, with the only exception of geodetic studies in Patagonia (Annex 1, Tables A1 and A2). The location of these surveyed glaciers (or specific glacierized regions) and the corresponding methodologies used are displayed in Figure 1.11.

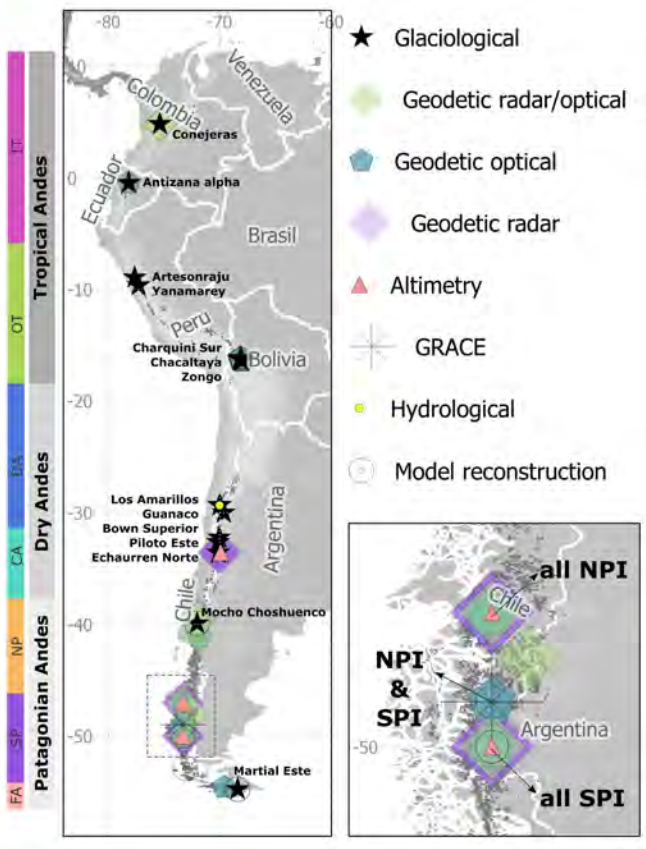

Figure 1.11: Distribution of study sites with published mass balance observations along the Andes with their respective methodologies. For more information on area surveyed, dates and refferences, please refer to Annex 1, Tables A1 and A2. The lower panel presents the independent studies over the entire NPI and SPI (symbols centred on the Icefields) or containing the two (symbols centred between the two icefields). The names of the glaciers monitored by the glaciological method are specified in the figure.

1.4.1 Glacier change observations from in situ measurements and aerial photographs

There are very few long-term direct glacier mass balance observations in the Andes. The first reason for this lack of in situ observations is because most South American countries do not have national glacier monitoring programs and they rely mostly on international cooperation. Until recently Chile was the

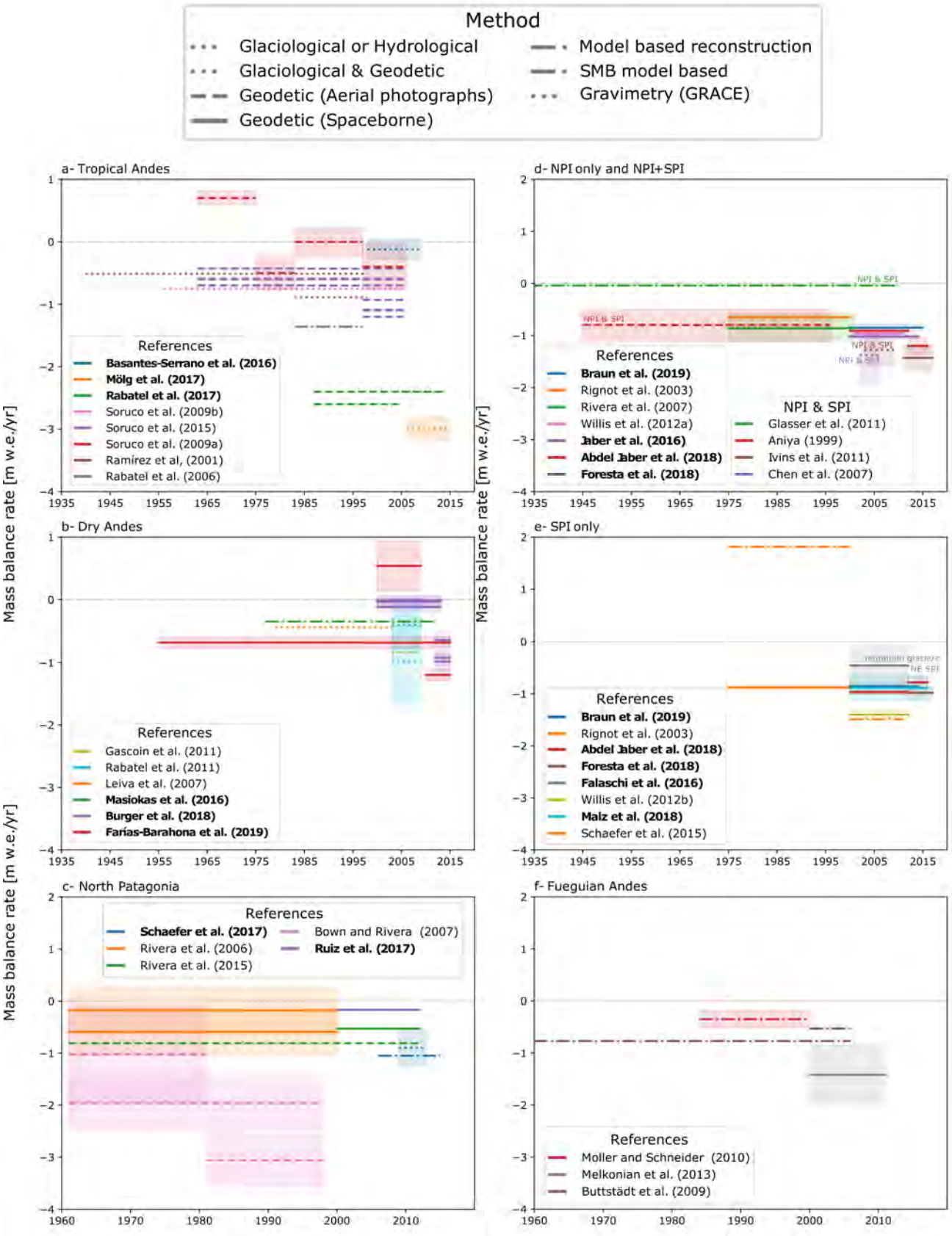

Figure 1.12: Summary of the published mass balance estimates for local glaciers and specific glacierized regions obtained by diverse methodologies. In bold, studies published during the development of this PhD work (2016 onwards). For more details please refer to Annex 1, Tables A1 and A2

only exception, but now also Argentina presents its own national monitoring program after the promulgation of the 'Law for the Protection of Glaciers' in 2010. This PhD work stands as a collaboration

between France and the Argentinian institution in charge of this monitoring (Argentinian Institute of Snow, Glacier and Environmental Sciences, IANIGLA). I thus participated to the mass balance data collection for four glaciers (spring, 2017 and winter, 2018). In the Tropical Andes, observations have been initiated during the 1990s and 2000s thanks to international projects. The close collaboration of the French National Research Institute for Development (IRD) has promoted glacier mass balance monitoring in Bolivia since 1991, Ecuador since 1994 and glaciers in Peru and Colombia in 2003 and 2006 (Rabatel et al., 2013a) and still helps reinforcing the autonomy of national institutes.

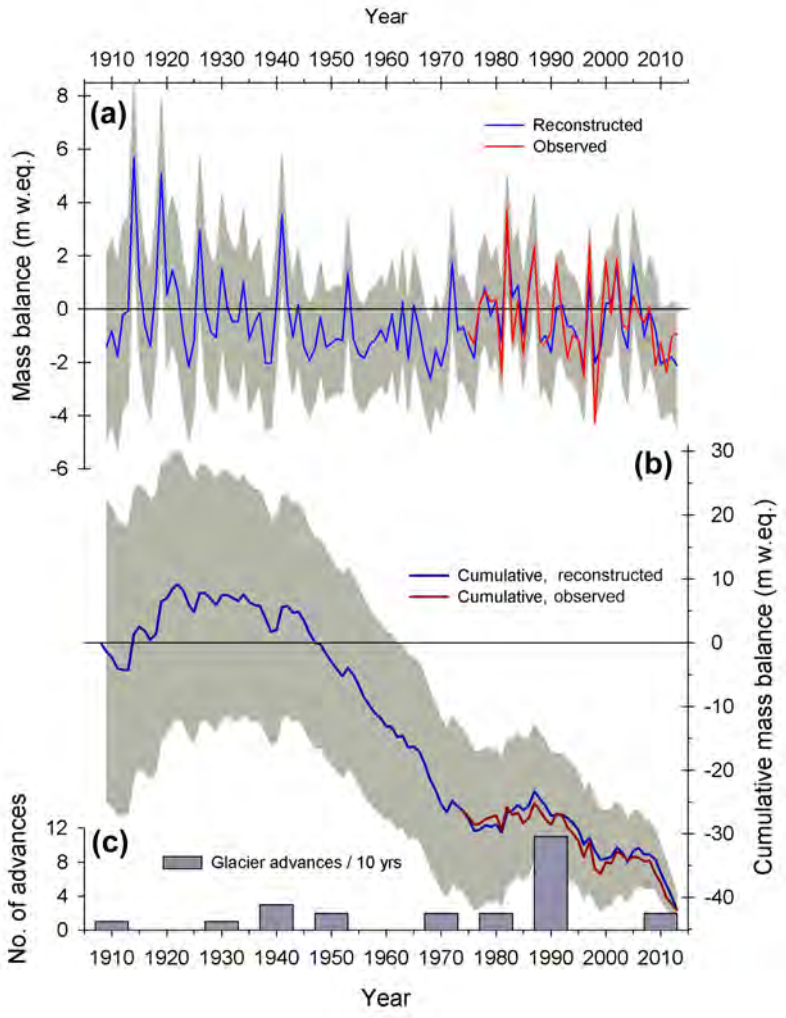

Figure 1.13: **(a)** Comparison between the annual mass balance record observed at the Echaurren Norte glacier (red line) and the reconstructed series derived from regionally averaged streamflow data (blue line). **(b)** Cumulative record of the observed and reconstructed Echaurren Norte mass balance series. **(c)** Glaciers advances identified in the Central Andes of Chile and Argentina during the past 100 years. Events are grouped in 10 years intervals, centred on the last year. Figure from Masiokas et al. (2016).

The scarcity of field observations in the Andes is also due to the fact that the majority of glaciers are located either at high elevations or in remote locations, making it difficult to implement field work. In Patagonia for example, field campaigns involve very complicated logistics and the extreme climate conditions may sometimes expose researchers to high risk. Moreover, the largest glaciers of the Andes are located in Patagonia, and calculating their mass balance with the glaciological method is very difficult or even impossible.

The last glacier change bulletin from the World Glacier Monitoring Service (WGMS, 2013) reports changes for 14 Andean glaciers (7 in the Tropical Andes, 6 in the Central Andes, and 1 in the Fueguian Andes). Only five of these mass balance series begin before the year 2000, the longest belonging to two glaciers located in the Central Andes, Echaurren Norte (Chile) and Piloto Este (Argentina). Only Echaurren Norte has a complete record spanning more than 35 years, standing as the only 'reference glacier'

for the Southern Hemisphere in the WGMS global assessments (WGMS, Masiokas et al., 2016). Masiokas et al. (2016) used the Echaurren Norte mass balance series and available well-correlated hydrological records to calibrate a simple mass balance model permitting to reconstruct the glacier annual mass balance since 1910 (Figure 1.13). This is the longest existing reconstruction in the Andes and provides crucial information about 20th century glacier changes in the Central Andes of Chile and Argentina. As seen in Figure 1.13, Echaurren Norte has followed successive periods of mass loss and mass gain throughout the last century, with a marked increase in mass loss after 2010.

The exploitation of historical photographs allowed to extend direct observations of glacier fluctuations further back in time and survey larger regions than possible with the glaciological method. This technique has been widely used in the Tropical Andes (e.g. Ramírez et al., 2001; Soruco et al., 2009a,b, 2015) and in Patagonia (e.g. Aniya, 1999; Bown and Rivera, 2007) to evaluate glacier volume fluctuations during the last decades of the 20th century (see Annexe 1, Tables A1 and A2).

Even though these few direct estimations remain very local and spatially spread, they are already able to reveal the accelerated shrinkage on different glaciers distributed along the Andes (Figures 1.11 and 1.12). Most of these observations correspond to small glaciers that are not necessarily representative of the glacier responses at larger regional scales, but provide vital information to understand glacier-climate relationships in the Andes.

1.4.2 Glacier change observations during the satellite era

Satellite imagery permitted the observation of glacier changes for larger glacierized areas that were not monitored before in the field or by airborne photographs. It permitted the creation of glacier inventories for extended regions, including the first complete Andes glacier inventory that permitted to approximate the Andes-wide glacierized area for the first time (Pfeffer et al., 2014). A series of studies employ satellite imagery to observe length and areal changes (e.g. Lopez et al., 2010; Meier et al., 2018; Reinthaler et al., 2019; Schneider et al., 2007) and volume fluctuations over local glacier or extended glacierized regions along the Andes (Figure 1.12). The combination of satellite derived DEMs with moraine dating techniques permitted to reconstruct past glacier extensions, and approximate past volume changes by reconstructing past glacier hypsometry. Glacier length, surface area and volume changes since the Little Ice Age maximum (between 1650 and 1700, Rabatel et al. (2006)) have been reconstructed in the Tropical Andes (e.g. Jomelli et al., 2008, 2009; Rabatel et al., 2005, 2006) and in Patagonia (e.g. Davies and Glasser, 2012; Glasser et al., 2011) contributing greatly to the knowledge on Andes glacier past evolution.

With the pioneering geodetic study of Rignot et al. (2003) over the NPI and SPI, satellite data started being used to estimate volume changes over larger glacierized regions of the Andes in a direct way (Moraine based studies calculate volume changes indirectly). The strong mass losses estimated for the NPI (-0.65 ± 0.08 m w.e. yr^{-1}) and SPI (-0.88 ± 0.05 m w.e. yr^{-1}) for the period 1975-2000, brought attention towards these fast shrinking glaciers. Many studies followed in the effort to constrain NPI and SPI mass loss for the post 2000 period, making use of a wide variety of satellite data (optical DEMs, radar DEMs, GRACE, altimetry, see Figure 1.12 and Annex 1, Table A2). These estimates, however, are not directly comparable because of the different methodologies, time periods and different icefield extents considered. Still, the high variability within them is noteworthy. Only the most recent studies using radar DEMs since year 2000 and for periods larger than a decade agree within each other (e.g. Abdel Jaber et al., 2018; Jaber et al., 2016; Braun et al., 2019; Malz et al., 2018). Jaber et al. (2016) and Abdel Jaber et al. (2018) estimate NPI mass losses of -1.02 ± 0.04 m w.e. yr^{-1} for 2000-2012 and -0.91 ± 0.04 m w.e. yr^{-1} for 2000-2014, respectively, in agreement with Willis et al. (2012a) estimate (-0.96 ± 0.04 m w.e. yr^{-1}) based on optical DEMs for 2001-2011. Slightly less negative NPI rates (-0.85 ± 0.07 m w.e. yr^{-1}) are estimated by Braun et al. (2019) for 2000-2011/15. For the SPI, the mass loss rates of -0.89 ± 0.24 m w.e. yr^{-1} from Malz et al. (2018) for 2000-20115/16 agree with those from Braun et al. (2019) for 2000-2011/15 (-0.86 ± 0.08 m w.e. yr^{-1}) and from Abdel Jaber et al. (2018) for 2000-2012 (-0.97 ± 0.03 m w.e. yr^{-1}). For this icefield, the mass loss calculated by Willis et al. (2012b) based on

optical DEMs for the period 2000-2012 is significantly more negative (-1.49 ± 0.09 m w.e. yr^{-1}).

It is noteworthy that all recently published studies using radar DEMs hold upon a demonstration performed during this PhD work (see Chapter 2) where we verified the negligible effect of SRTM C-band radar signal penetration on the NPI (due to low mean altitudes and the wet and temperate conditions of the glacier surface during the Austral summer, SRTM acquisition season). They also assume this is true for SRTM and TanDEM-X X-band derived DEMs, a reasonable assumption given that the X-band is known to have less penetration that the C-Band. A more detailed discussion about the differences within icefield-wide geodetic estimates is provided later in this manuscript, more precisely in Chapters 2 and 3. Outside the large icefields, mountain glaciers have received relatively less attention. Geodetic estimates exist only for Cordillera de Darwin (Melkonian et al., 2013), mountain glaciers near de SPI (Falaschi et al., 2016; Rivera et al., 2015; Ruiz et al., 2017) and some glaciers in the Central Andes (Burger et al., 2018; Farías-Barahona et al., 2019).

Glacier change observations in the Andes remains highly heterogeneous and spatially unresolved. Despite the recent advances, the existing studies are not able to reveal the specific patterns of glacier mass balance along the entire Cordillera. Initially, my thesis project was though-out with the objective to fill this gap and provide the first homogeneous Andes-wide geodetic estimate. Unfortunately a German research group got the lead and published in January 2019 a geodetic estimate at the Andes scale using radar TanDEM-X DEMs for the period 2000-2011/15 (Braun et al., 2019). Braun et al. (2019) results were not included in this section because they are going to be discussed later and compared in detail with our results. Notwithstanding, both the geodetic estimates from Braun et al. (2019), and those from this thesis, represent important contributions to constrain Andean glacier mass changes since 2000.

1.4.3 Andes-wide glacier change observations

It is only during the last decades (after year 2000), that the increased efforts on the exploitation of remote sensing data and modelling techniques have allowed to picture the global distribution of mountain glacier changes. The Andes are settled within the regions of higher mass loss rates and higher cumulative specific mass changes compared to other mountain glacierized regions of the world (Figure 1.14) (e.g. Zemp et al., 2019; Huss and Hock, 2015; Gardner et al., 2013).

Before and during the 3 years of my doctoral thesis (2016-2019) many new Andes-wide mass balance estimates where published using all existing methodologies (Figure 1.15). The most recent global mass loss assessment interpolates all available up to date glaciological and geodetic data from the WGMS, complemented with new and yet unpublished geodetic estimates for many glaciers over many regions of the world (Zemp et al., 2019). Noteworthy, the Andes is one of the only regions where no additional geodetic data was used with respect to the previous assessment from Zemp et al. (2015). Thus, even if this new estimate is better constrained with additional data for many mountain glacierized regions of the world since their last publication, assuming the same for the Andes is not so straightforward. As shown in Figures 1.12 and 1.11, existing in situ data in the Andes is sparse and geodetic estimates are highly concentrated in specific sites. The mass loss estimated by Zemp et al. (2019) for the Southern Andes (-29.1 ± 8.8 Gt yr^{-1}) during the period 2000-2016, is more negative than the -21 ± 11 Gt yr^{-1} estimated in Gardner et al. (2013) from interpolation of the updated Cogley (2009) in situ data for the period 2003-2009, but is in good agreement with the 'reconciled estimate' (-29 ± 11 Gt yr^{-1}) derived from GRACE in the same study (Figure 1.15). Zemp et al. (2019) estimate for the Southern Andes is also in good agreement with a more recent GRACE estimate of -30.3 ± 10 Gt yr^{-1} (2002-2016) from Wouters et al. (2019). But finally all together, GRACE and Zemp et al. (2019) estimates are considerably more negative than the recently published Southern Andes geodetic estimate by Braun et al. (2019) displaying mass losses of -17.8 ± 0.6 Gt yr^{-1} for 2000-2011/15.

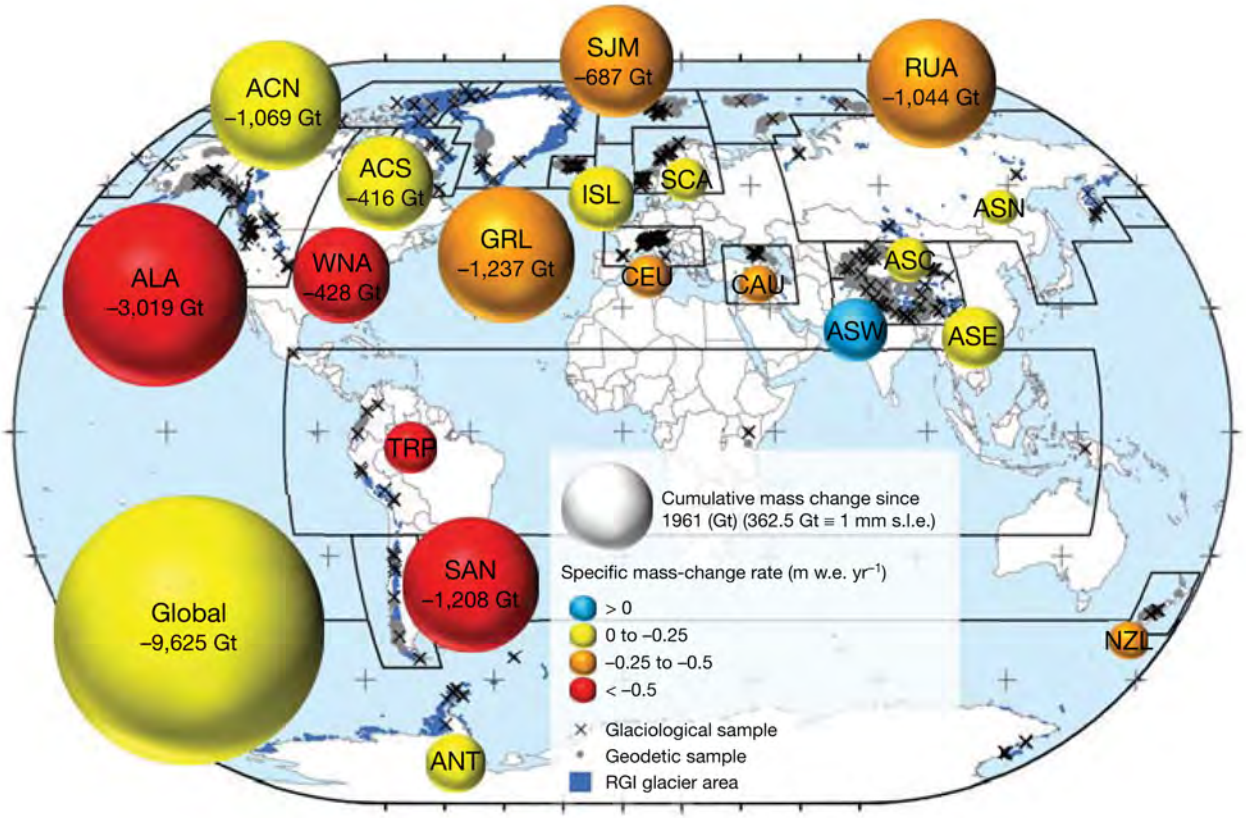

Figure 1.14: Regional glacier contributions to sea-level rise from 1961 to 2016. The cumulative regional and global mass changes (in Gt yr^{-1}) are represented by the volume of the bubbles, and the specific mass-change rates (m w.e. yr^{-1}) are indicated by the colour of the bubbles. Results are shown for the 19 RGI regions. From Zemp et al. (2019).

Despite the differences, each independent estimates holds its own uncertainties. First, substantial errors may arise from the interpolation of scarce glaciological and geodetic estimates (Gardner et al., 2013). Second, GRACE corrections to isolate the glacier change signal are not yet fully understood for the Andes. The hydrological signal correction used by Wouters et al. (2019) vary from -2 ± 1 Gt yr^{-1} to -9.5 ± 1.2 Gt yr^{-1} for the Southern Andes region depending on the model applied, and correction due to mass displacement since the LIA are largest for this region (9 ± 5 Gt yr^{-1}) compared to others (Ivins and James, 2004; Wouters et al., 2019). Surprisingly, the Southern Andes mass loss estimate obtained by Wouters et al. (2019) is in better agreement with the geodetic estimate from Braun et al. (2019) when no corrections are applied to the GRACE data (-21.8 ± 1.2 Gt yr^{-1}). Finally, the radar signal penetration on snow and ice of the SRTM and TanDEM-X DEMs used by Braun et al. (2019), has been proved negligible in the Southernmost regions, but no study has examined this aspect before for glaciers located in colder climates like those on the northern regions of the Andes.

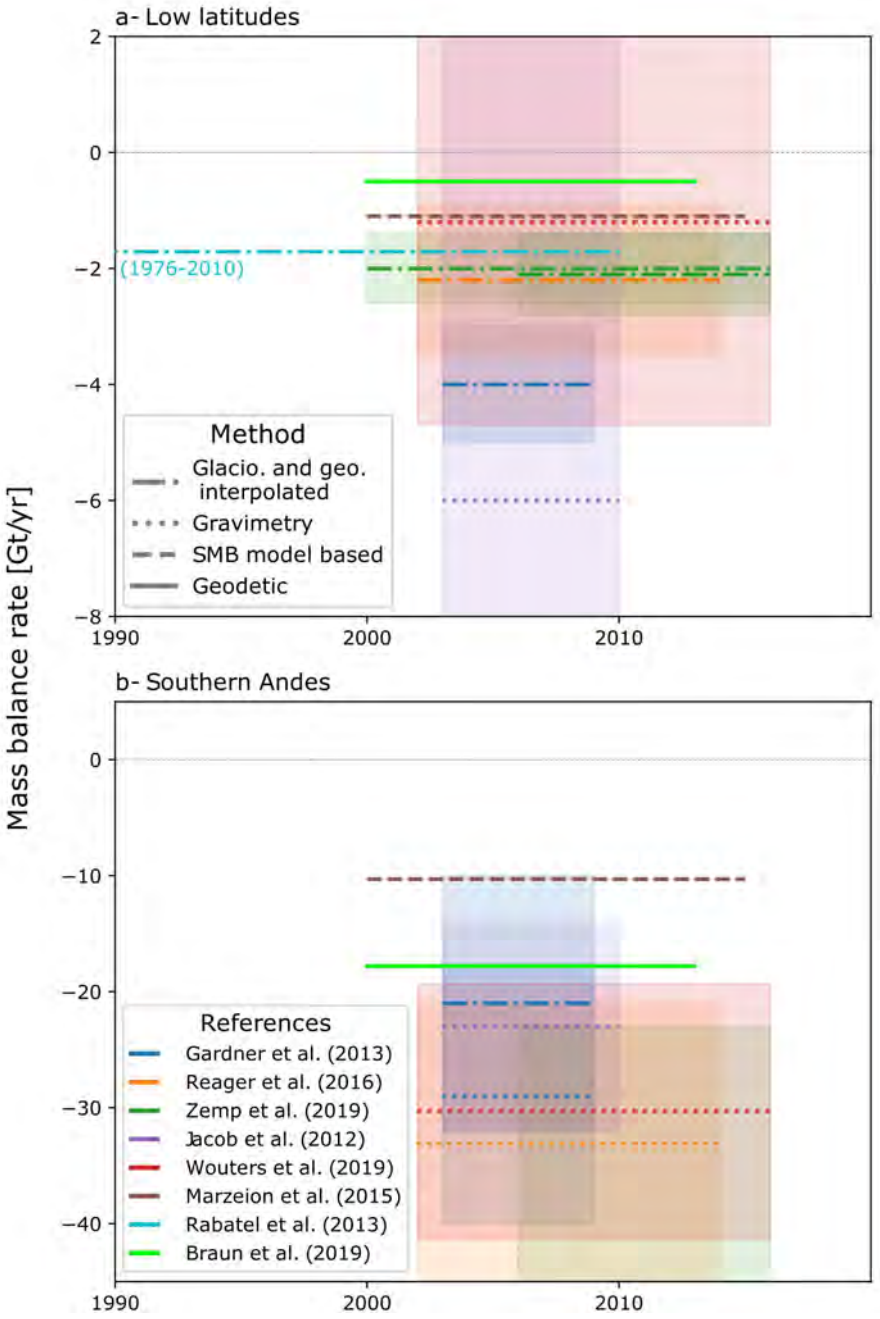

Figure 1.15: Summary of published Andes-wide glacier mass change rates for (a) Low Latitude (99% Andean glacier) and (b) Southern Andes regions from multiple methodologies. Estimates from Braun et al. (2019) and correspond to Andean Low latitude glaciers only. In bold, studies published during the development of this PhD work (2016 onwards). For more details please refer to Annex 1, Table A3.

1.5 An opportunity to constrain recent Andes-wide glacier changes

Despite the recent improvements in the knowledge about Andean glaciers, the Andes-wide glacier mass losses are still not clearly constrained. Reaching a consensus is crucial as this datasets are used for the calibration of glaciological and hydrological models aiming for future projections of glacier responses. Until that consensus is reached, the interpretation of model results might be biased by the arbitrary choice of the 'best' estimate within the existing ones.

At the regional Andes scale, the present Andes-wide datasets are not still able to resolve for the inter-decadal variability of regional glacier changes, as they consider fluctuations for one period only, most of them during the first decade of the 20th century. The study from Braun et al. (2019) is the only dataset

sufficiently resolved and homogeneous to reveal sub-regional patterns of glacier mass balance change, however, there is still the need to compare these results with non-radar geodetic estimates along the Andean sub-regions where the occurrence of radar signal penetration is still unknown. Moreover, none of these previous large-scale works has been able to assess glacier changes at a smaller scale, for individual glaciers or specific hydrological basins. A dataset with these characteristics would allow analysing the impact of decadal glacier changes on the 'imbalance glacier' contribution to river flow, estimate calving rates, and countless applications. More specifically, in my thesis, I want to address the following research questions.

Question 1: Can we accurately measure glacier changes in the Andes using multi-temporal optical ASTER DEMs?

Recent efforts have been deployed by our working team to automatize a work flow for massive ASTER DEM production and post-processing, with the goal to make it applicable for geodetic studies over large glacierized surfaces (Berthier et al., 2016, 2018; Brun et al., 2017; Menounos et al., 2019). This methodology is named ASTERiX , standing for 'ASTER monitoring of Ice toward eXtinction'. ASTERIX has been validated against independent geodetic estimates in several regions of the world, but at the beginning of this thesis (September 2016) it had never been used nor validated in the Andes. Thus, the first part of this work will focus on the validation of the ASTERIX methodology. We chose the NPI as validation site, because it presents two major challenges for optical DEMs: frequent clouds and vast homogeneous snow surfaces. The validation is performed through direct comparison with a second geodetic estimate using SPOT5 and SRTM DEMs (obtained by us) and inter-comparison with radar and optical geodetic published estimates. This work is presented in Chapter 2.

Question 2: What are the recent changes of Andean glaciers? Can we produce an homogeneous and spatially resolved dataset of glacier elevation changes during the last two decades? Can we obtain the sufficiently high spatial resolution that would allow analysing multiscale glacier changes and their respective impacts?

The aim of this part of the work is to contribute with a high resolution dataset of glacier elevation changes that will be readily available for exploitation at different scales. We explore the inter-decadal patterns of mass loss, we inquire on the hydrological impacts resulting from this mass loss and we explore the potentiality of the dataset to calculate calving rates. This work is presented in Chapter 3.

Question 3: Are NPI glaciers increasing their mass loss rates since 1975? Can we exploit a multiple archive of elevation data to measure sub-period elevation changes in the NPI from 2000 to 2016?

This question arises with the good results obtained while responding to Question 1. The availability of a multiple archive of elevation data on the NPI, motivated us to explore sub-period mass balance changes in the NPI and observe if individual glacier mass loss rates are actually increasing on the recent years or not. This question is presented on Chapter 4.

Chapter 2

Validation of the ASTERIX method over Andes glaciers: Geodetic mass balance of the Northern Patagonian Icefield from 2000 to 2012 using two independent methods

Note: This chapter is adapted from an article published in the journal Frontiers of Earth Sciences, Dussaillant et al. (2018). The methodology named here 'ASTER trend' is the same as ASTERIX. We implemented the ASTERIX name after this validation was performed.

2.1 Objectives and previous ASTERIX validation efforts

The first objective of my PhD work was to validate the ASTERIX method over Andean glaciers, a necessary step before applying the methodology to the entire Andes mountain range. At the time when I started, the methodology had already been validated over mountain glaciers in the Alps and over selected sites in High Mountain Asia (HMA) (Berthier et al., 2016; Brun et al., 2017).

Similar processing strategies using multi-temporal ASTER DEMs (i.e. ASTERIX) to extract glacier mass balance estimates had been used before over glaciers around the world (Melkonian et al., 2013; Nuimura et al., 2012; Wang and Kääb, 2015; Willis et al., 2012a,b) but these earlier studies lacked or relied on weak validation data. The vast amount of available accurate independent spaceborne (SPOT5 and Pleiades DEMs) and field measurements over the Mont Blanc massif allowed Berthier et al. (2016) to focus their efforts on the methodological uncertainty assessment. They contributed with a thorough evaluation of the multi-temporal ASTER technique over alpine glaciers, with an estimated elevation change error of 0.2 – 0.3 m yr^{-1} for areas larger than 1-2 km^2. Following this encouraging results, Brun et al. (2017) applied the ASTERIX methodology to the entire High Mountain Asia glaciers. Further validations were performed over specific glaciers and validation sites comparing with multiple accurate DEM differences (including Pleiades and SPOT5 DEMs) and available glaciological measurements. For 60 individual glaciers larger than 2 km^2, they obtain a standard deviation of the residual of 0.17 m w.e. yr^{-1} in agreement with errors in the Alps.

We could assume that the Tropical and Dry Andes mountain glacier characteristics are quite similar to those from the Alps or HMA, so previous validations would be enough to ensure ASTERIX performance in these regions. Yet, this is not the case of Patagonia were the geographic context is very different with large icefields mostly dominated by a maritime regime. Thus, an exhaustive validation in this region is needed, first, to ensure the validity of the methodology over large icefields where the variability

of glacier responses is much larger than in the Alps or HMA. And secondly because of the non negligible risk related to the use optical derived DEMs a region with an almost permanent occurrence of clouds.

We selected the North Patagonian Icefield (NPI) as validation zone for the Andes because it is one of the largest Patagonia Icefields and because we had in hand a high quality SPOT5 DEM for year 2012 (almost cloudless and covering the entire NPI) ideal to perform an accurate validation of ASTERIX.

During the progress of my ASTERIX validation effort on the NPI, a parallel icefield-wide validation was performed by Berthier et al. (2018) over two Alaskan Icefields, by comparing with repeat laser altimetry data. The standard deviation of the mass balance difference between ASTERIX and airborne Lidar obtained over 12 glaciers (0.18 m w.e. yr^{-1}) is in striking agreement with previous error estimates in the Alps and HMA, considering the extreme differences of geographical and climatological contexts.

In this work we additionally find a good performance of ASTERIX over the NPI glaciers with uncertainties comparable to previous validation efforts. Largest differences between SPOT5-SRTM and ASTERIX mass balance estimates over the largest NPI glaciers do not exceed 0.2 m w.e. yr^{-1}. In particular, this work provided me the green light needed before engaging on the analysis of glacier mass loss at the entire Andes scale.

I presented this work at the Gaby-Vasa, Fuego Patagonia Conference and workshop 2017 (Berlin) and published it afterwards in a Special Issue of Frontiers in Earth Sciences.

2.2 Abstract

We compare two independent estimates of the rate of elevation change and geodetic mass balance of the Northern Patagonian Icefield (NPI) between 2000 (3856 km^2) and 2012 (3740 km^2) from spaceborne data. The first is obtained by differencing the Shuttle Radar Topography Mission (SRTM) digital elevation model (DEM) from February 2000 and a Satellite pour l'Observation de la Terre 5 (SPOT5) DEM from March 2012. The second is deduced by fitting pixel-based linear elevation trends over 118 DEMs calculated from Advanced Spaceborne Thermal Emission and Reflection Radiometer (ASTER) stereo images acquired between 2000 and 2012. Both methods lead to similar and strongly negative icefield-wide mass balance rates of -1.02 ± 0.21 and -1.06 ± 0.14 m w.e. yr^{-1} respectively, which is in agreement with earlier studies. Contrasting glacier responses are observed, with individual glacier mass balance rates ranging from -0.15 to -2.30 m w.e. yr^{-1} (standard deviation = 0.49 m w.e. yr^{-1}; N = 38). For individual glaciers, the two methods agree within error bars, except for small glaciers poorly sampled in the SPOT5 DEM due to clouds. Importantly, our study confirms the lack of penetration of the C-band SRTM radar signal into the NPI snow and firn except for a region above 2900 m a.s.l. covering less than 1% of the total area. Ignoring penetration would bias the mass balance by only 0.005 m w.e. yr^{-1}. A strong advantage of the ASTER method is that it relies only on freely available data and can thus be extended to other glacierized areas.

2.3 Introduction

Patagonian glaciers and icefields, including the Northern Patagonian Icefield (NPI), are essential indicators of climate change in the southern hemisphere and also stand as one of the major contributors to recent sea level rise (Gardner et al., 2013; Mernild and Wilson, 2016). Direct glaciological observations in this remote region are still scarce, mainly due to the region's inaccessibility and its harsh climate (Buttstädt et al., 2009; Mernild et al., 2015; Schaefer et al., 2015). In recent decades, remote sensing techniques have enabled the spatial coverage of glaciological observations to be extended. They are particularly useful in remote and inaccessible areas like the NPI, making it possible to observe and measure glacier variations and to estimate mass balance at regional scales (Davies and Glasser, 2012; Dixon and Ambinakudige, 2015; Jaber et al., 2016; Lopez et al., 2010; Rignot et al., 2003; Rivera et al., 2007; Willis et al., 2012a,b). Among those studies, mass balance estimates are often based on the geodetic method,

which allows calculation of glacier volume changes by differentiation of two or more multi-temporal digital elevation models (DEMs) (e.g., Marzeion et al., 2017; Paul et al., 2015). In particular for the NPI, Willis et al. (2012a) measured mass balance using the Shuttle Radar Topography Mission (SRTM) DEM and a collection of freely available Advanced Spaceborne Thermal Emission and Reflection Radiometer (ASTER) DEMs from 2001 to 2011. Jaber et al. (2016) also provided a mass balance estimate for 2000–2014 by comparing two interferometric DEMs, SRTM and TanDEM-X.

The goal of our study is to produce two new and independent geodetic estimates of the NPI mass balance for the time period 2000-2012 using, on one hand, SRTM and SPOT5 and, on the other hand, ASTER DEMs. Although the NPI mass balance during this time period has already been estimated in two previous studies (Jaber et al., 2016; Willis et al., 2012a) our contribution is justified by:

(i) The use of ASTER DEMs calculated using the Ames Stereo Pipeline (ASP) (Shean et al., 2016). As shown in the supplement of our study, these DEMs have less artefacts than the 14DMO DEM available from LP-DAAC and used in many earlier studies including the one of Willis et al. (2012a) over the NPI.

(ii) The need to verify the lack of penetration of the February 2000 SRTM radar signal. Until now the effect of radar wave penetration into snow and ice has been assumed to be negligible in Patagonia due to the likely wet condition at the glacier surface in summer, favouring surface scattering of the signal (Jaber et al., 2013, 2016; Willis et al., 2012a). However, this assumption has not been verified yet.

(iii) The need to account for changes in ice-covered areas when calculating the glacier mass balance. None of the earlier studies considered these area changes, known to be large in Patagonia (Davies and Glasser, 2012)

2.3.1 The Northern Patagonian Icefield, Chile

The NPI is the second largest temperate ice mass in the southern hemisphere, after the Southern Patagonian Icefield. Located in Chile, it extends from 46°30'S to 47°30'S, stretching for almost 125 km north–south (Figure 2.1). It covers an area of approximately 3740 km^2 (measured in this study for year 2012) extending from sea level to altitudes higher than 4000 m a.s.l. at the summit of Mount San Valentin. It is composed of 38 glaciers larger than 0.5 km^2. San Quintin is the largest glacier, covering 790 km^2. San Rafael (714 km^2) is the only tidewater calving glacier of the icefield and the lowest-latitude tidewater glacier as well as one of the fastest-flowing glaciers in the world (Rignot et al., 1996). The largest proportion of glaciers present fresh-water calving fronts (66% of the total area), whilst a smaller proportion (16%) correspond to land-terminating fronts (Rivera et al., 2007).

The climate of the Northern Patagonian region is dominated by the southern hemisphere westerlies that bring moisture from the Pacific, and the equatorial Pacific sea surface temperature that regulates the El Niño Southern Oscillation (ENSO) and the Pacific Decadal Oscillation (Aravena and Luckman, 2009). This later two large scale modes of natural climate variability, together with the southern annular mode (SAM), are key modulators of temperature and precipitation in the southern Andes at inter-annual and inter-decadal timescales (Garreaud et al., 2009; Gillett et al., 2006). The north–south orientation and high altitude of the Andes chain at this latitude acts as a geographical barrier for the moisture, generating a föhn effect that creates a strong west-to-east gradient of precipitation, with considerably dryer conditions and higher temperatures on the eastern side of the icefield (Fujiyoshi et al., 1987). The average annual precipitation between 1975 and 2011 is 8.03 ± 0.37 m (Schaefer et al., 2013) with little seasonal variability. The 0°C isotherm altitude is at about 2000 m a.s.l. during the summer, dropping to 900 m a.s.l. during winter (Barcaza et al., 2009).

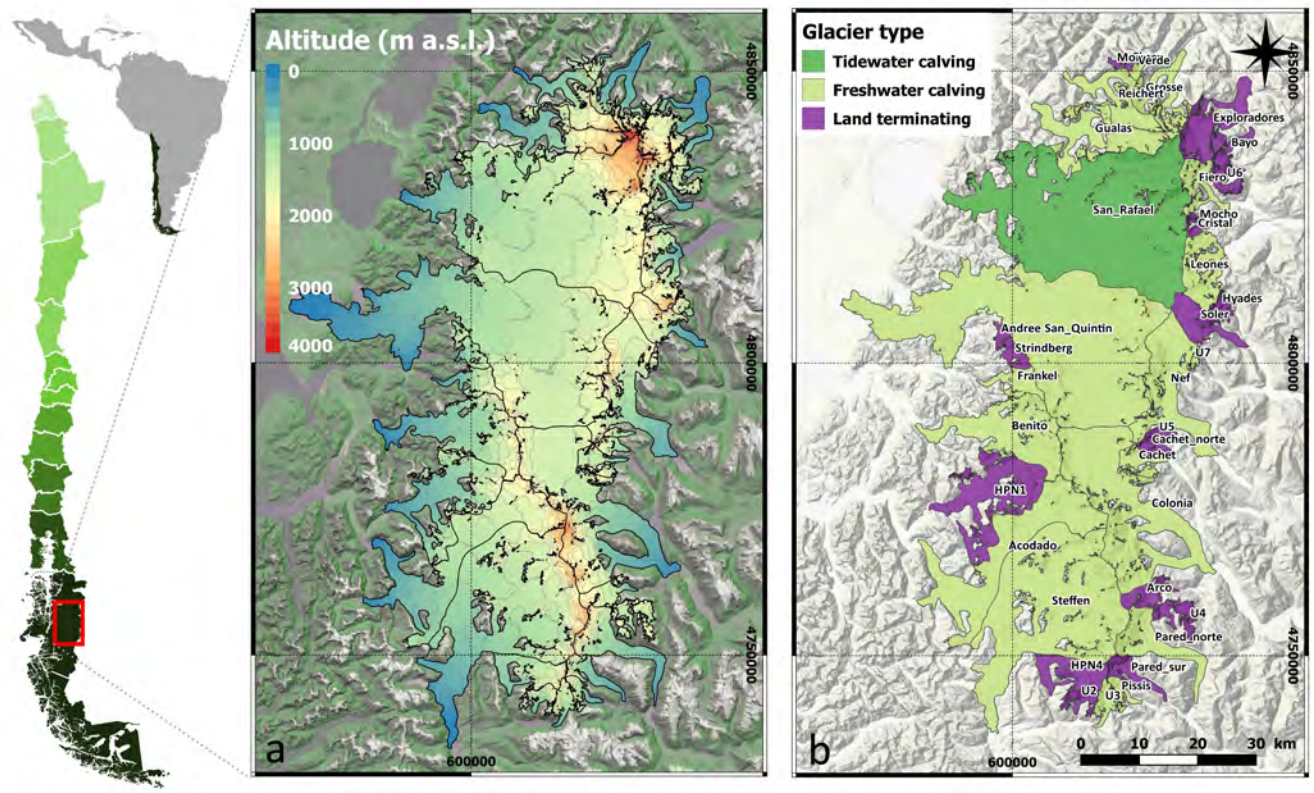

Figure 2.1: Location of the Northern Patagonian Icefield in Chile. (a) Elevation map of the NPI from the SRTM (void-filled version) on top of a cloud-free Landsat image acquired on 11 March 2001. Glacier outline corresponds to ice extents of year 2000. (b) 38 glaciers of the NPI are represented using the outline of year 2012 and ice divides from Mouginot and Rignot (2015) with the shaded relief from the SRTM void-filled DEM as background. Colours correspond to different glacier types: dark green is for the single tidewater calving glacier (San Rafael), light green for freshwater calving (i.e. lake terminating) glaciers and purple for land-terminating glaciers as defined by Rivera et al. (2007).

2.4 Data

2.4.1 DEMs and satellite stereo images

SRTM DEM: The SRTM acquired elevation data between 11 and 22 February 2000 using an interferometric aperture radar sensor (SAR) (Farr et al., 2007). We used the SRTM DEM processed by NASA from the raw C-band radar signal at 1 arcsecond resolution (about 30 m). Due to radar layover or loss of coherence over vegetation and steep terrain, the SRTM DEM may contain data voids that are sometimes filled by interpolation or using an external DEM. For the purposes of DEM comparison, we use the non-void-filled version in which data voids cover 13% of the total NPI glacierized area. By specific elevation bands the percentage of data voids is 3% below 1000 m a.s.l (total area 1163 km^2), 22% between 1000 and 2000 m a.s.l. (2323 km^2) and 13% above 2000 m a.s.l. (370 km^2). A second, void-filled SRTM DEM (version 4, 3 arcsec resolution) produced by the CGIAR-CSI (http://srtm.csi.cgiar.org) is also used to obtain a complete hypsometry of the icefield, necessary for the mass balance calculation.

SPOT5-HRS DEM: The SPIRIT project produced DEMs over glacierized zones from stereo-pairs acquired by the SPOT5 high-resolution stereoscopic (HRS) sensor (Korona et al., 2009). A 40 m DEM, acquired on 18 March 2012, provides a complete coverage of the NPI (see section 2.9 Figure 2.8). The DEM is delivered with a reliability mask and one ortho-image generated from the rear HRS image. Reliability mask values range from 0 to 255, with 0 indicating the least reliable elevations that are thus masked out in the SPOT5 DEM. Data voids cover 16% of the total NPI glacierized area. By specific elevation bands the percentage of data voids is 7% below 1000 m a.s.l, 22% between 1000 and 2000 m a.s.l. and 13% above 2000 m a.s.l.

TERRA–ASTER stereo images: Raw stereo images obtained by the ASTER sensor on board the TERRA satellite were ordered free of charge from the ECHO/REVERB website (https://reverb.echo.nasa.gov) from April 2000 to April 2012. After excluding all images with cloud cover fraction larger than 80%, a total of 118 ASTER Level 1A stereo images intersecting the NPI were selected. For the sake of concision, the list of ASTER images used in this study were not provided but is available upon request to the corresponding author.

LANDSAT images: Four late-summer nearly cloud-free LANDSAT L7 ETM+ orthoimages at 30 m spatial resolution acquired from the USGS Earth Explorer were used to improve glacier and water outlines for years 2000 and 2012 (8 March 2000 and 21 January, 22 February, 26 April 2012).

2.4.2 Glacier outlines, water bodies and ice divides

Initial outlines for glacier limits and water bodies over the NPI area were obtained from online datasets. The Global Land Ice Measurements from Space (GLIMS) database and the Randolph Glacier Inventory version 5.0 (RGI 5.0) offer access to glacier outlines from previous studies and inventories over the Southern Andes region (Davies and Glasser, 2012; Mouginot and Rignot, 2015; Pfeffer et al., 2014; Rivera et al., 2007). Following visual assessment, RGI5.0 was selected as the best existing outline, corresponding to the ice extent of year 2001 (RGI6.0 was not available at the time of our study). RGI5.0 was not used "as is" but was improved as explained in section 2.5.1. Water body outlines were acquired from the USGS Earth Explorer SRTM water body data (https://earthexplorer.usgs.gov/), and the ice divides derived from velocity fields (Mouginot and Rignot, 2015) were used to split the icefield into individual glaciers.

2.5 Methodology

2.5.1 Improvement of the glacier outlines

The RGI 5.0 glacier outline was corrected manually using late-summer and cloud-free LANDSAT, ASTER and SPOT5-HRS images as references to adjust the position of the ice for the years 2000 and 2012. RGI 5.0 ice divides were replaced by the ice divides from (Mouginot and Rignot, 2015). A visual comparison between our final outlines and best existing previous ones can be observed in section 2.9 Figure 2.9. Significant errors and gaps were found in the SRTM water body data, so manual corrections were also performed. Furthermore, a cloud mask was drawn manually to exclude the cloudy pixels over the SPOT5-HRS DEM. No cloud mask was created for ASTER DEMs because the lack of correlation over the clouds leads directly to data voids in the DEMs.

2.5.2 Glacier volume change and mass balance

As explained above, two different methods were applied to derive the map of the rate of elevation changes over the NPI: SRTM and SPOT5 DEM differencing (SPOT-SRTM hereafter) and linear trend analysis of multiple ASTER DEMs (ASTER trend hereafter).

Generation of ASTER DEMs

ASP is a NASA open source pipeline that allows for the mass production of DEMs out of high-resolution stereo images (Shean et al., 2016). We generated 118 ASTER-ASP DEMs with a grid spacing of 30 m from the raw ASTER L1A stereo images. ASP processing parameters are available upon request to the authors. Each ASTER DEM has a different footprint and, given the 60 km swath of ASTER, does not cover the entire NPI. The result is a spatially-varying number of ASTER DEMs available over the NPI (see section 2.9 Figure 2.8).

Adjustments of the DEMs

Horizontal adjustment of the DEMs The DEMs used in this study are produced independently using different methods and without ground control points such that a horizontal shift is expected to exist

between them. 2D coregistration (i.e. horizontal adjustment) should be performed on stable terrain and in regions where DEMs are most reliable (Paul et al., 2015). Stable terrain corresponds to all pixels with valid elevation values after excluding ice, snow, water bodies and clouds. The SRTM DEM was used as reference, and all other DEMs (SPOT5 and ASTER) were adjusted to it. For SPOT-SRTM, the horizontal shift is determined by an iterative minimization of the standard deviation of the elevation difference (dh) on stable terrain (Berthier et al., 2007). For ASTER trend, an approach based on terrain slope and aspect was used to calculate the horizontal shift (Kääb, 2005; Nuth and Kääb, 2011). Both coregistration methods lead to similar results. The Nuth and Kääb method is preferred to coregister ASTER DEMs as it is numerically faster and thus more suitable for managing large amounts of data (Paul et al., 2015).

Vertical adjustment of the DEMs Three different types of vertical biases are quantified on stable terrain and corrected in SPOT5 and ASTER DEMs. We first correct for a simple vertical shift, then biases along and across the satellite tracks and finally we account for elevation difference due to different DEM resolution. For SPOT5 and ASTER DEMs, the median of the altitude difference with the SRTM DEM over stable terrain is first substracted. To avoid anomalous values that are usually found over steep terrain, only pixels where the slope is less than 30° are considered to estimate this median vertical shift (Berthier et al., 2016). We recognize that this limit is somewhat arbitrary but further justified by the fact that over 90% of the NPI surface has a slope lower than 30°. For SPOT5 and ASTER DEMs, all derived from stereo imagery, the satellite acquisition geometry and its particular trajectory may induce biases in the DEMs along and across the satellite track direction (Berthier et al., 2007; Nuth and Kääb, 2011; Scherler et al., 2008). We rotate the original coordinate system of the SPOT5 and ASTER DEMs tracks to match their specific trajectory (Nuth and Kääb, 2011). The elevation difference (dh) is then computed over stable terrain along and across the satellite track, and corrected using a fifth-order polynomial fit. We applied a curvature-dependent correction to the SPOT5 and ASTER DEMs. This correction is calculated on the stable terrain by fitting a fifth-order polynomial to the elevation difference with the SRTM DEM plotted as a function of terrain maximum curvature (Gardelle et al., 2012). After all adjustments, pixels from the SPOT5 and ASTER DEMs which have an absolute elevation difference with SRTM greater than 150 m are considered as outliers and excluded from all subsequent analysis.

Rate of elevation change and mass balance calculation

The maps of elevation change rates (dh/dt) are obtained differently for the two methods. For SPOT-SRTM, a simple DEM difference is computed and divided by their time separation (12.1 yr) to calculate $\mathrm{dh/dt}_{SPOT-SRTM}$. In the case of ASTER trend, for each pixel, a first linear trend is fit through all the available elevation values (from all ASTER DEMs and the SRTM DEM) during 2000–2012. The final $\mathrm{dh/dt}_{ASTER\ trend}$ is calculated from a second fit considering only the ASTER DEMs within the 95% confidence interval of the first regression line and excluding the SRTM DEM to avoid possible bias due to signal penetration. For the majority of the NPI area, the first valid elevation measurements used in this second linear fit come from a DEM acquired in April 2000, and the last measurements from two DEMs acquired in March 2012 and April 2012 (see section 2.9 Figure 2.10). We did not observe any obvious temporal concentration of ASTER DEMs. Thus, the time-stamp of the dh/dt maps from the two methods is similar, i.e. 2000-2012.

In the conversion from dh/dt to mass balance, only reliable pixels from glacierized terrain are considered. For ASTER trend, we further exclude all pixels for which the uncertainty of the second linear fit is larger than 3 m yr^{-1} (at the 95% confidence level).

NPI individual glaciers have shown different volume change rates during recent years, with differential responses within glaciers and a strong contrast between the eastern and western margins (Rivera et al., 2007; Willis et al., 2012a). To take into account these local effects, separate calculations were made for each glacier, and then the overall volume change and mass balance of the NPI was calculated as the area-weighted sum of every glacier. Each individual glacier is divided into 50 m altitude bands using the void-filled version of the SRTM DEM. For each altitude band, we compute the mean dh/dt after excluding all values lying outside of ±3*NMAD (normalized median absolute deviation).This is an ef-

ficient way to exclude outliers (Berthier et al., 2004; Gardelle et al., 2013). The band average dh/dt is then weighted by its area to calculate the glacier-wide average dh/dt. In the rare cases where no measurement is available for an altitude band, the rate of elevation change is assumed to be 0.

Following Fischer et al. (2015), we considered the varying areas of each individual glacier between 2000 and 2012 to convert volume change to mass balance. We use a value of 850 ± 60 kg m^{-3} as the volume-to-mass conversion factor, which is reasonable regarding the duration of our study (>5 years) (Huss, 2013).

Penetration of the SRTM C-band radar signal over snow

The ASTER trend method allows rough estimation of the SRTM penetration depth (Berthier et al., 2016; Wang and Kääb, 2015). By extrapolating dh/dt to the date of acquisition of the SRTM DEM, a reconstructed SRTM DEM (called hereafter SRTMrec) can be obtained. The differencing of SRTMrec–SRTM maps the penetration depth of the C-band radar signal.

2.5.3 Error assessment

Formal uncertainties for mass balance estimates were calculated taking into account six main sources of error: errors on dh/dt, errors in glacier area, errors due to data voids, error on the density conversion factor, error due to departure from a linear trend and seasonal cycle sampling irregularities.

Uncertainty in rate of elevation change ($\sigma_{\frac{dh}{dt}}$): The uncertainty on the elevation change of a pixel is mainly given by the uncertainty inherent in the original DEMs, including the random and systematic errors produced during their coregistration. To assess this error we split the stable terrain dh/dt maps into 3 × 3 tiles as in Berthier et al. (2016). For each tile the median of dh/dt on stable ground is computed to visualize the spatial pattern of biases in dh/dt$_{ASTER\ trend}$ and dh/dt$_{SPOT-SRTM}$ maps (Figure 2.2). We then compute the error in dh/dt as the mean of the absolute difference of the median dh/dt for these 9 tiles. We obtained an error ($\sigma_{\frac{dh}{dt}}$) of 0.07 m yr^{-1} for SPOT-SRTM and 0.06 m yr^{-1} for ASTER trend.

Uncertainty in area(σ_A): Glacier outlines were improved manually and contain an error that is inherent to the individual that performed the work. The error in glacier area was assessed by drawing buffers around the glacier outline (Granshaw and Fountain, 2006). A one-pixel buffer is a reasonable error level for glacier outlines produced manually, except for debris-covered glaciers (Paul et al., 2015). As the NPI debris coverage is limited, a one-pixel buffer was applied to the NPI outline, leading to an error of about 5% of the measured area. This value is consistent with Paul et al. (2015) and Pfeffer et al. (2014).

Uncertainty in density factor (σ_{f_ρ}): For density the error of ±60 kg m^{-3} is obtained from Huss (2013).

Uncertainty in data gaps (g): A conservative multiplicative factor of 5 is used for the uncertainties in the unsurveyed areas (Berthier et al., 2014).

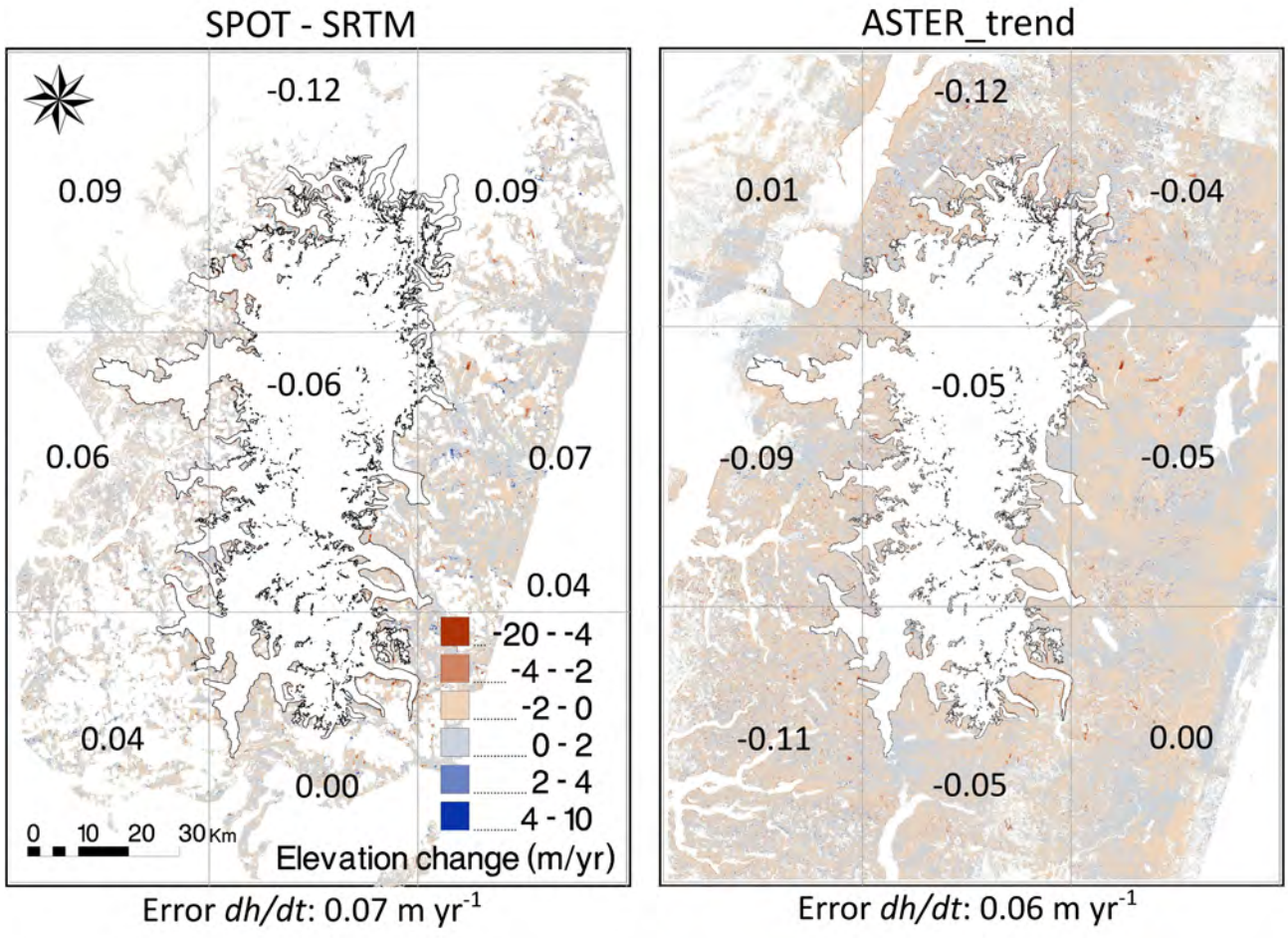

Figure 2.2: Rate of elevation change over stable terrain in the NPI region during 2000–2012, calculated by the SPOT-SRTM (left) and ASTER trend (right) methods. The study region is divided into 3×3 tiles. The values correspond to the median dh/dt on stable ground in each tile. For comparison, the colour scale is the same as for the maps of dh/dt over glaciers in 2.4.

Uncertainties due to the uneven sampling of the seasonal cycle: The dh/dt from ASTER trend could come from an irregular sampling of the seasonal elevation change cycle as the ASTER DEMs were acquired at different times of the year. For example, a large systematic error (i.e. too negative mass balance) could occur if ASTER DEMs were acquired mostly in winter at the beginning of the study period and mostly in summer toward the end of the study period. To quantify the magnitude of this potential error, we sample a hypothetical seasonal cycle at the time of acquisition of the ASTER DEMs. The amplitude of the seasonal cycle is poorly known for Patagonia and must be spatially variable, so we prefer to use a normalized value of 1 m, with a minimum at the end of April and a maximum at the end of October. As shown in Figure 2.3, the ASTER temporal sampling is sufficiently random that the regression slope is only -0.0013 m yr^{-1}. Even if the seasonal elevation change cycle was as large as 10 m (a high value but not unrealistic for the maritime NPI), the resulting systematic error would be 0.013 m yr^{-1}, well below other sources of uncertainties. This source of error is thus neglected.

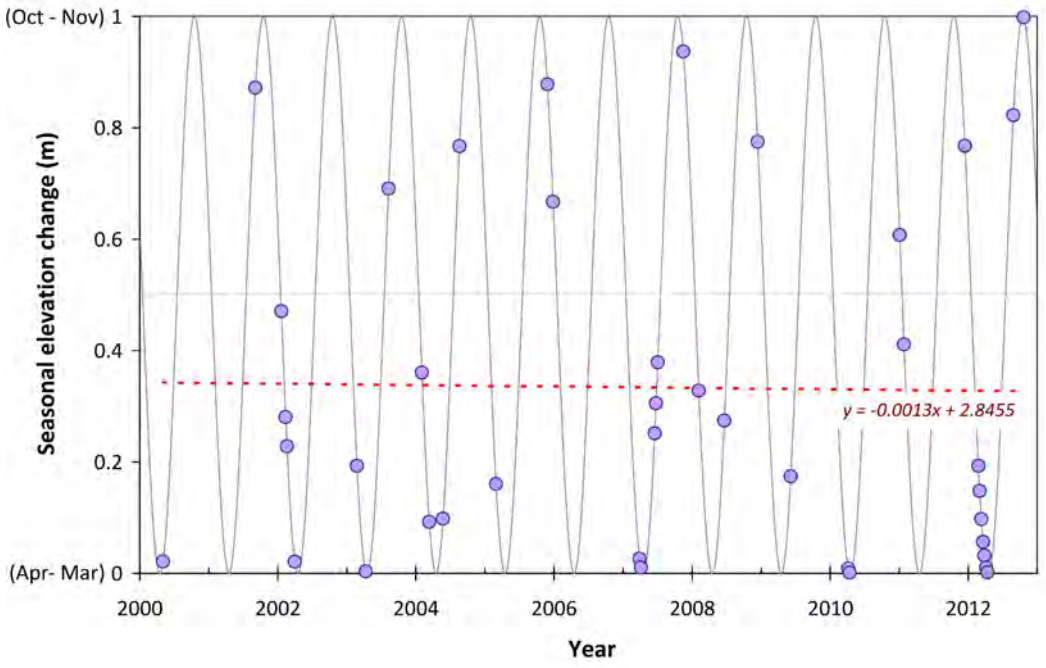

Figure 2.3: Temporal sampling of the 118 ASTER DEMs used in the ASTER trend method. The amplitude of the seasonal cycle is normalized to 1 m. Dots correspond to theoretical elevations at the time of acquisition of the ASTER DEM; the red line shows the linear fit to the elevation time series, with a slope of -0.0013 m yr^{-1}.

Uncertainties due to departure from a linear trend: The assumption of linearity is one of the weaknesses of our ASTER-based method, as in principle glacier elevation change do not follow a linear behaviour. To detect potential changes of the ASTER trends (and mass balances) over time, we divided 2000-2012 into two sub-periods: 2000 to March 2007 (2007.3) and 2007 to May 2012 (2012.5). We did not split the 12-year study period in two sub-periods of equal duration because there was no DEM for year 2006. Conversely, several useful ASTER DEMs were acquired in 2007 (late summer, no clouds, and good spatial coverage of the NPI), thus we decided to cut the period at 2007 and include summer 2007 DEMs in both trends. The NPI-wide mass balance from 2000 to 2007.3 was -1.06 ± 0.20 m w.e. yr^{-1}, and -0.99 ± 0.20 m w.e. yr^{-1} from 2007 to 2012.5. Given error bars, mass balances for both sub-periods are not different and agree with the estimate for the whole period 2000-2012 (-1.06 ± 0.15 m w.e. yr^{-1}). This result justifies the assumption of linearity and demonstrates that, within the error bars of our method, we are not able to detect a temporal change in the NPI mass balance.

We then consider all the significant sources of error to calculate our formal uncertainties on mass balance. First, the uncertainty in glacier rate of volume change ($\sigma_{\frac{dV}{dt}}$), assuming that the uncertainty on area is independent of the uncertainty on rate of elevation change, was calculated as:

$$\sigma_{\frac{dV}{dt}} = \sqrt{\left(\sigma_A \times \overline{\frac{dh}{dt}}\right)^2 + \left(\sigma_{\frac{dh}{dt}} \times (5g + (1-g))A\right)^2} \tag{2.1}$$

Where ($\overline{\frac{dh}{dt}}$) is the mean rate of elevation change, $\sigma_A = \frac{5}{100}A$) and g is the proportion of data gaps from the total area. Assuming that the uncertainty in rate of volume change is independent of the uncertainty of the density conversion factor, the uncertainty on geodetic mass balance (σ_{MB}), was calculated as:

$$\sigma_{MB} = \sqrt{\left(\sigma_{\frac{dV}{dt}} \times f_\rho\right)^2 + \left(\sigma_{f_\rho} \times \frac{dV}{dt}\right)^2} \tag{2.2}$$

where (f_ρ = 850 kg m^{-3}) is the density conversion factor and (σ_{f_ρ} = 60 kg m^{-3}) is the uncertainty on the density conversion factor (Huss, 2013).

2.6 Results

2.6.1 Area changes

The NPI had a total glacierized area of 3856 ± 211 km^2 in 2000, and 3740 ± 200 km^2 in 2012. The total area loss for the period 2000-2012 is 116 km^2 (3%), at a rate of -9.7 km^2 yr^{-1}. Areal changes are heterogeneous and do not follow any obvious spatial pattern. Largest areal changes are observed on glaciers U4 (19%) located in the south-east, and glaciers Circo (12%) and Grosse (10%) located in the north of the NPI. The largest frontal retreats were observed in the tongues of two glaciers in the south-west, Steffens (3.3 km frontal retreat) and HPN1 (2.5 km retreat over its main tongue and even 3.1 km retreat over one of its tributaries), and San Quintin in the north-west (2.5 km frontal retreat). Glaciers Gualas, Grosse and Reicher in the north and glacier Acodado in the south also showed significant frontal retreats of the order of 1 and 2 km between 2000 and 2012.

2.6.2 Elevation change rates and glacier mass balance

Entire NPI

Both methods (SPOT-SRTM and ASTER trend) resulted in a similar spatial distribution of dh/dt over the NPI (Figure 2.4), with maximum thinning rates localized at low elevations over the glacier tongues. Icefield-wide mass balances rates during 2000–2012 are also in excellent agreement: -1.02 ± 0.21 m w.e. yr^{-1} for SPOT-SRTM and -1.06 ± 0.15 m w.e. yr^{-1} for ASTER trend (Table 2.1).

Strongest thinning rates are observed over the outlet glaciers of the western margins of the icefield, with dh/dt rates as negative as -10 m yr^{-1} for the terminating tongues of Frankel, Benito, HPN1 and Acodado glaciers. The largest differences between the two dh/dt maps are observed over San Rafael glacier, where thinning rates are more negative for SPOT-SRTM, and over the north-east margins. Looking closely at the dh/dt vs altitude curves for the two methods, a strong thickening is observed above 2900 m a.s.l. for SPOT-SRTM, whereas a slight thinning is measured by ASTER trend (Figure 2.4c). The anomalously positive values in SPOT-SRTM dh/dt curves at high altitude will be discussed in section 2.7.2.

Spatial coverage of valid dh/dt rates is different for the two methods, with 68% of the total NPI area covered in SPOT-SRTM, and a better coverage of 82% in ASTER trend. Almost complete coverage was achieved below 1000 m a.s.l. in both cases. Higher concentrations of data gaps exist in the accumulation zone (> 1000 m a.s.l.) with 35% gaps for SPOT-SRTM vs. 22% for ASTER trend. Both the SPOT5 reliability mask and the ASTER error grid produced during the linear fit suggest larger errors in this region. The lack of image texture over the flat and homogeneous snow surface makes correlation of the stereo images either impossible or erroneous. Higher altitudes are better represented in ASTER trend, with only 10% of data gaps above 2000 m a.s.l. vs. 49% for SPOT-SRTM; the latter is mainly due to voids in the SRTM DEM.

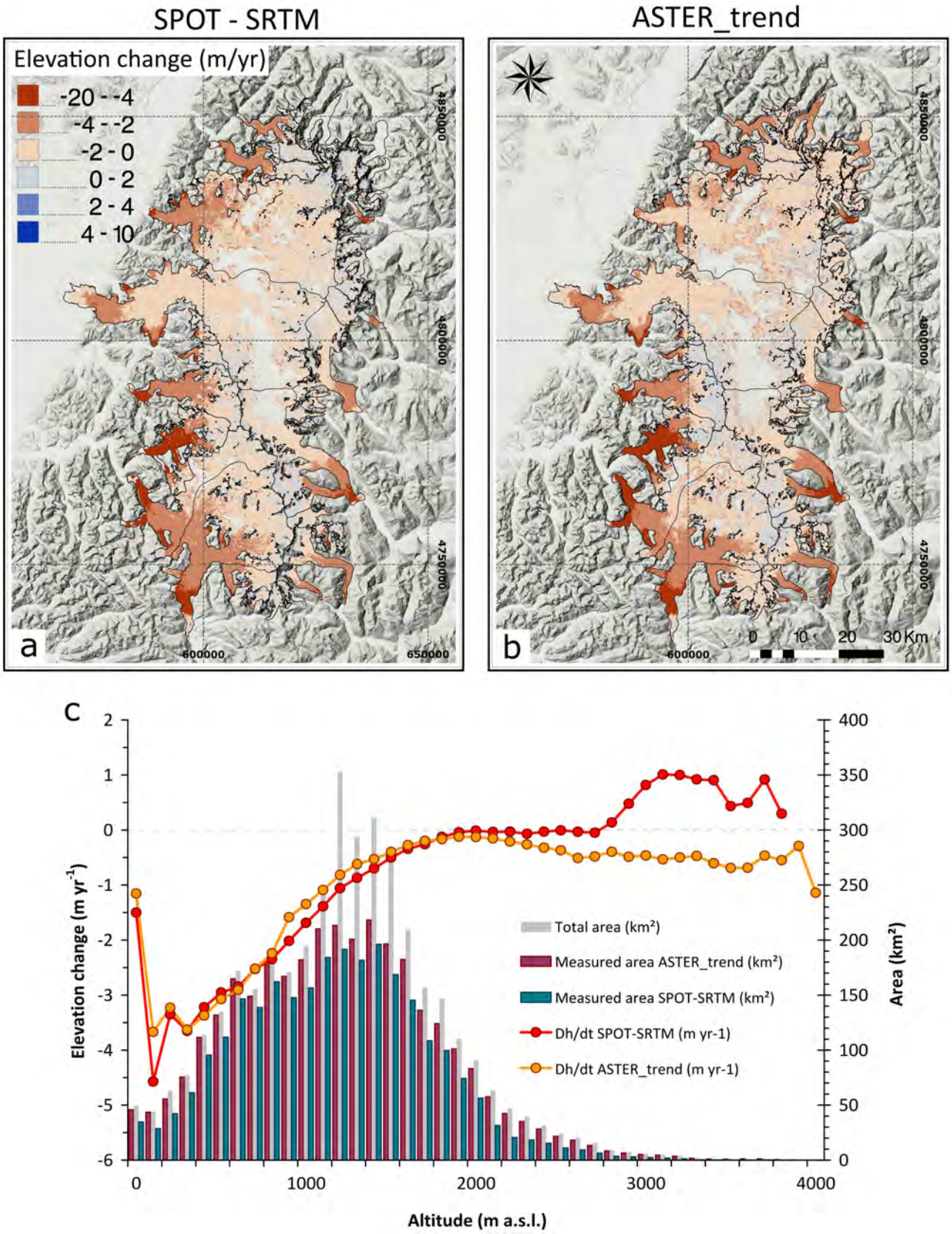

Figure 2.4: Rate of elevation change (m yr^{-1}) over the NPI for the time period 2000–2012. (a) Rate of elevation change from SPOT-SRTM; white blank corresponds to data gaps. (b) Rate of elevation change from ASTER trend; white blank corresponds to data gaps. (c) Distribution of the rate of elevation changes as function of altitude; red dots represent SPOT-SRTM and orange dots represent ASTER trend. The histograms show the hypsometry of the NPI by 100 m elevation bands (grey bars), and the corresponding measured area from SPOT-SRTM (blue bars) and ASTER trend (purple bars). (Note that hypsometry is shown here every 100 m bands. This is to help visualization although the entire processing was made using 50 m bands).

Table 2.1: NPI-wide volume change rate, thinning rate and mass balance rate estimates for the 2000–2012 time period for the two methods.

Method	dV/dt ($km^3\ yr^{-1}$)	dh/dt ($m\ yr^{-1}$)	Mass balance ($m\ w.e.\ yr^{-1}$)
SPOT-SRTM	-4.55 ± 0.41	-1.20 ± 0.11	-1.02 ± 0.21
ASTER trend	-4.72 ± 0.34	-1.25 ± 0.09	-1.06 ± 0.15

Individual glaciers

The coverage of individual glaciers with valid dh/dt measurements is much better for ASTER trend, where all glaciers show two-thirds (66%) of their total area with valid data. In the case of SPOT-SRTM, coverage is not as good. 14 out of 38 glaciers, corresponding to 77% of the total NPI area, show between one- and two-thirds of their area with valid measurements, while 11 glaciers (6% of the NPI area) show less than one-third (Figure 2.5a).

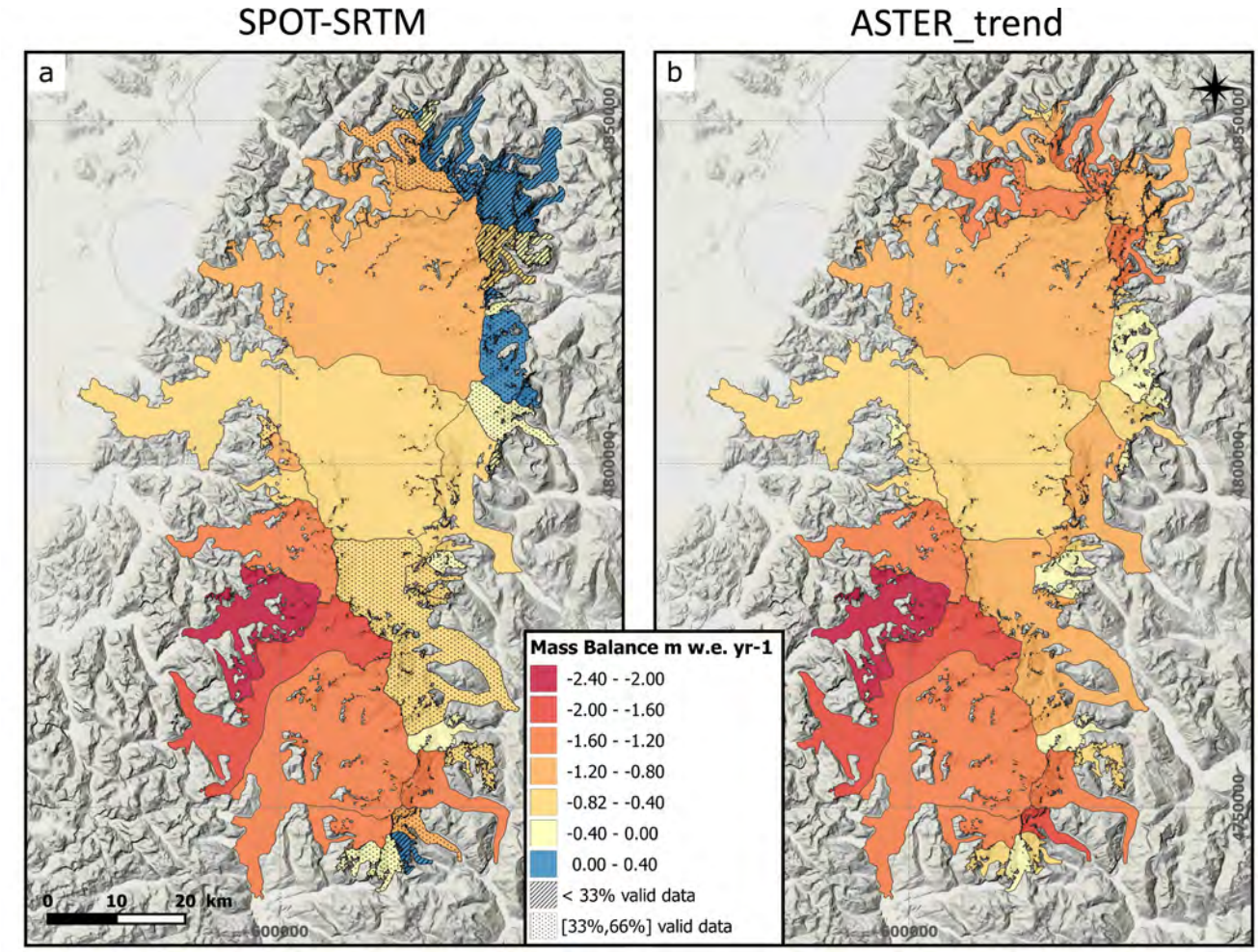

Figure 2.5: Mass balance rate of NPI individual glaciers from 2000 to 2012. (a) Mass balance rate obtained from method SPOT-SRTM. Hatched glaciers have less than 33% data coverage whereas pointed glaciers have between 33% and 66% coverage. (b) Mass balance rate obtained from method ASTER trend. All glaciers present more than 66% of their area with valid dh/dt values.

Individual glacier mass balance rates ($\dot{M}$) for the period 2000–2012 are shown in Figure 2.5 and Table 2.4 for both methods. All glaciers show negative $\dot{M}$ ASTER trend. Contrarily, $\dot{M}$ SPOT-SRTM for glaciers Grosse, Exploradores, Bayo and Leones in the north-east part of the NPI and glacier Pissis in the south are slightly positive. However, these five glaciers were poorly sampled due to gaps in the SPOT5 DEM. Both methods agree on highly negative mass balances for south-west glaciers. The most negative $\dot{M}$ coincide in glacier HPN1 with values of -2.38 ± 0.32 and -2.30 ± 0.24 m w.e. yr^{-1} for ASTER

trend and SPOT-SRTM respectively. The $\dot{M}$ for the three largest glaciers of the icefield, San Quintin, San Rafael and Steffens, accounting together for 51% of the total area, are strongly negative and in good agreement between methods.

For all glaciers larger than 100 km^2, $\dot{M}$ from both methods agree within error bars, and their absolute difference is smaller than 0.3 m w.e. yr^{-1} (Figure 2.6b). Conversely, smaller glaciers tend to show larger disagreement between methods, with $\dot{M}$ differences up to 1.6 m w.e. yr^{-1}. The largest differences are observed for glaciers poorly sampled in SPOT-SRTM (green and orange dots on Figure 2.6).

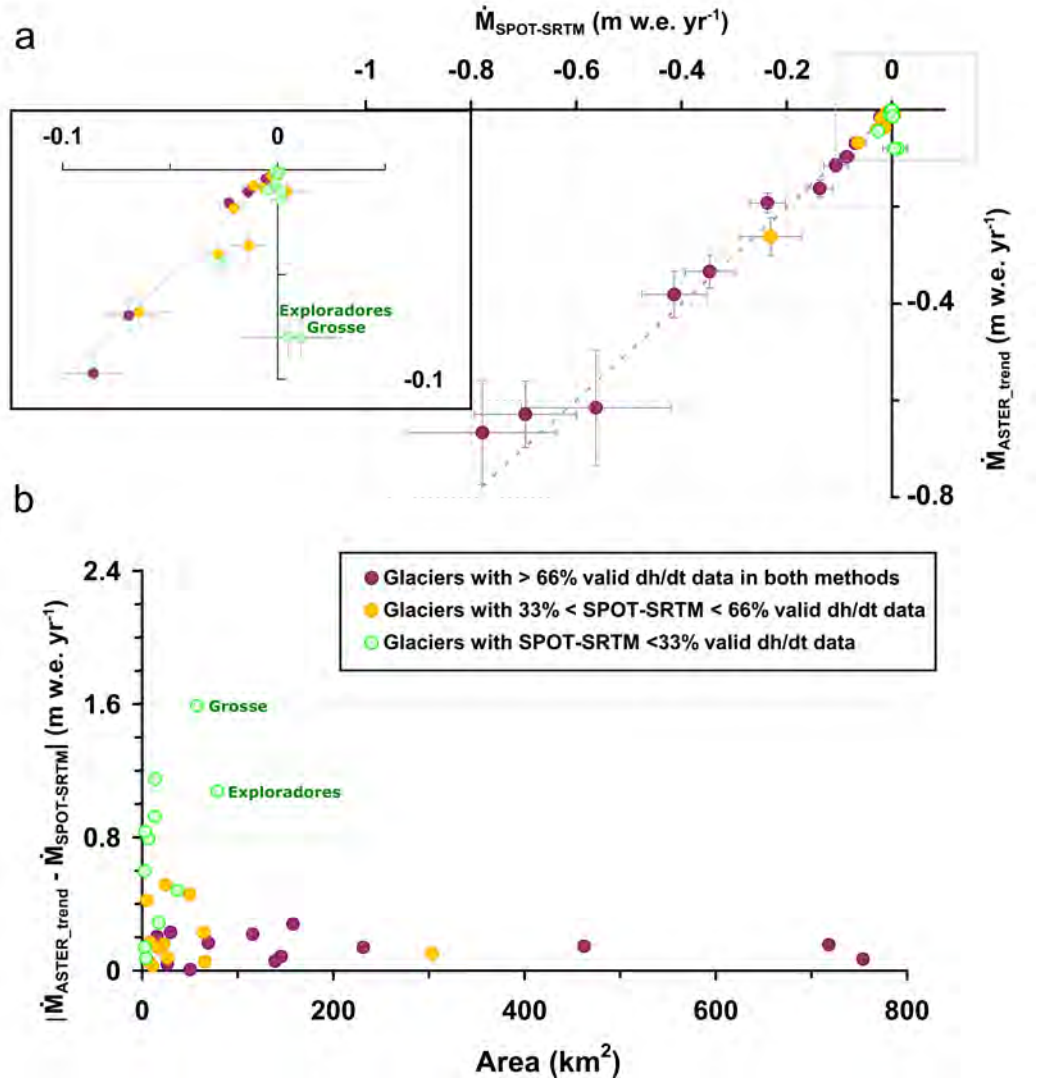

Figure 2.6: Comparison of individual glacier mass balances from the two methods. (a) Mass balance rates obtained from method ASTER trend as function of mass balance rates obtained from method SPOT-SRTM. The dashed line corresponds to the 1:1 line. (b) Absolute difference of $\dot{M}$ (m w.e. yr^{-1}) between the two methods as a function of glacier area.

2.7 Discussion

2.7.1 Area changes

Our area estimate for 2000 is in good agreement with previous studies, especially with Jaber et al. (2016), suggesting that our error bars are conservative (Table 2.2). Davies and Glasser (2012) obtained a slightly larger value for the NPI area in 2001 because they considered some of the rock nunataks as part of the icefield area. Similarly, Rivera et al. (2007) included adjacent small icy areas as part of the

icefield. To our knowledge, we provide the first estimate of NPI area for 2012.

Glacier areal changes are not homogeneous through the NPI. In general the largest frontal retreats were observed for glacier tongues situated in the south-west of the icefield (glaciers Steffens and HPN1), also in agreement with previous studies (Davies and Glasser, 2012; Lopez et al., 2010; Willis et al., 2012a; Rivera et al., 2007). No convincing relationship was observed between glacier-specific area loss and mass balance. This conclusion is in agreement with earlier findings for Alaskan glaciers (Arendt et al., 2002).

We accounted for these area changes in our mass balance rate estimates. At the scale of the entire icefield, the effect is minor as the NPI mass balance rate is changed by 0.01 m w.e. $yr^{-}1$ if only the 2000 inventory is available. Yet, the mass balance rate can vary by up to 10% for the fastest retreating glaciers.

Table 2.2: Comparison of the NPI total area in this and previous studies.

Reference	year	Area(km^2)
This study	2000	3856 ± 211
This study	2012	3740 ± 200
Jaber et al. (2016)	2000	3867
Davies and Glasser (2012)	2001	4070
Rivera et al. (2007)	2001	3953

2.7.2 Penetration of SRTM signal over NPI

Some positive dh values were found above 2900 m a.s.l. with the SPOT-SRTM method. These positive values are anomalous as, to our knowledge, no study documented thickening in the upper part of the NPI since 2000. Figure 2.7 shows the distribution with altitude of our estimate of the SRTM penetration depth (SRTMrec-SRTM), a side product of the ASTER trend method. Positive values are observed above 2900 m a.s.l. This is consistent with the apparent thickening observed above 2900 m a.s.l. in the SPOT-SRTM dh/dt and thus suggest possible penetration of the SRTM C-band signal on the NPI snow located above 2900 m a.s.l.

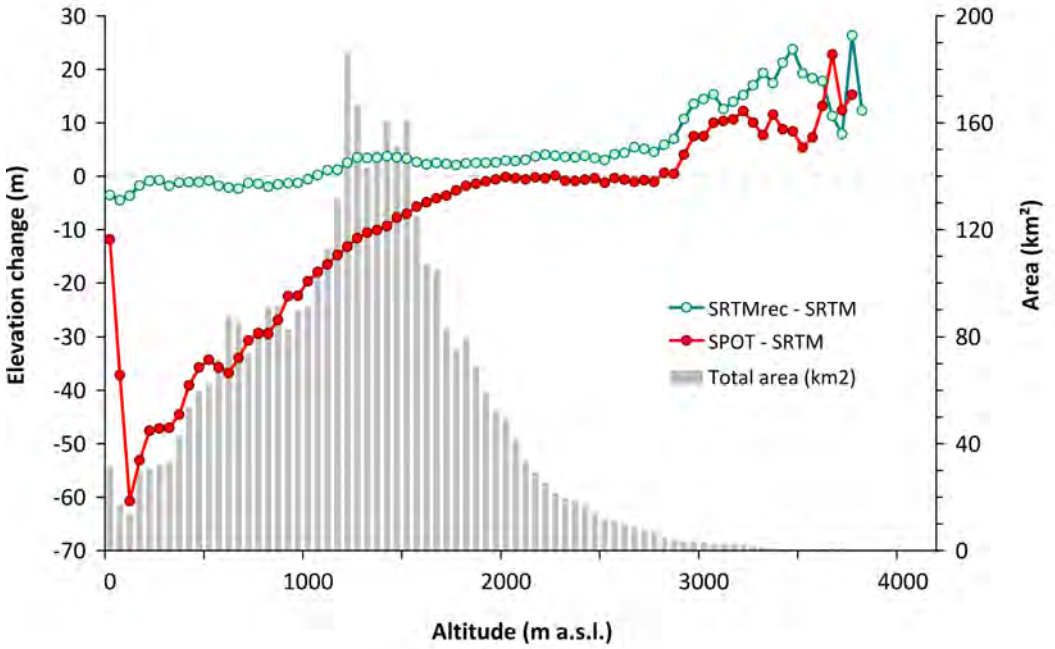

Figure 2.7: Penetration of the SRTM C-band radar signal as a function of altitude. Curves represent the total elevation difference from SPOT-SRTM (red curve) and SRTMrec–SRTM (green curve). Positive values in SRTMrec–SRTM represent penetration. The histogram shows the area/altitude distribution.

The SRTMrec–SRTM and the SPOT-SRTM curves in Figure 2.7 do not match perfectly over this high-altitude zone. Likewise, the SRTMrec–SRTM curve shows positive values between 1000 m a.s.l. and 2900 m a.s.l. However, these differences remain within the uncertainties of the SRTM penetration depth, assumed to be roughly ±3 m in Berthier et al. (2016), and cannot be further interpreted. We further confirmed that this ±3.1 m is conservative by extrapolating $dh/dt_{ASTER\ trend}$ to reconstruct two DEMs at the dates of acquisition of the SPOT5 2012 DEM and of an additional SPOT5 DEM acquired 18 May 2005 (not used in the study for measuring elevation changes but with similar specifications as the SPOT5 DEM 2012). Differencing between $SPOT5_{rec2012}$ - $SPOT5_{2012}$ and $SPOT5_{rec2005}$ - $SPOT5_{2005}$ yielded mean dh on the NPI of 1.03 m and 0.14 m, respectively, both values well below the 3.1 m assumed error.

If we consider the region above 2900 m a.s.l., the mean penetration depth is 10 m, a value similar to the 10 m C-band penetration depth found on the dry and cold firn of Greenland and Alaska (Rignot et al., 2001). Averaged over the whole icefield, the mean penetration depth is negligible (0.02 m), in agreement with a recent study in New Zealand (also in the southern hemisphere), where no penetration was found (Wang and Kääb, 2015).

Up to now, SRTM penetration depth has been considered negligible in Patagonia due to almost constant wet conditions at the glacier surface in February 2000 (Jaber et al., 2013). Here we show that penetration is actually occurring at the highest elevations, where temperatures are lower and firn is probably dry even in summer. Nevertheless, only 0.75% of the NPI area (29 km^2) is found above 2900 m a.s.l., a fraction small enough not to affect the overall mass balance rate of the icefield (the corresponding bias is less than 0.01 m w.e. yr^{-1}). Therefore, SRTM penetration can be assumed negligible over the NPI. Still, future geodetic mass balance studies in Patagonia using SRTM C-band DEM, should carefully consider the penetration depth, especially when a significant fraction of the glacier lies at high elevations.

The lack of SRTM penetration, except at the highest elevations, is in line with a backscattering analysis using the SRTM swath image data (SRTM-IMGR) in Jaber et al. (2016). They found low backscattering values over the plateau, indicating the presence of wet snow and consequent insignificant penetration

depth. Less negative backscattering values are also observed over the highest zones, suggesting dryer snow where the C-band signal can penetrate.

2.7.3 Comparison of the two geodetic methods

Both methods led to similar estimates of the NPI mass balance rate for the 2000–2012 period (Table 2.1). The SPOT-SRTM method has already been used in the southern Andes (Falaschi et al., 2016) but this method is all the more relevant now that we have verified the negligible penetration of the SRTM C-band signal at this latitude. Even though individual ASTER DEMs have a higher noise level than the SPOT5 DEM when subtracted from the SRTM DEM (mean standard deviation of the residual for ASTER DEMs: 14 m, vs 8 m for SPOT5 DEMs), their larger number led to final errors on stable ground very similar to those obtained with the SPOT-STRM method.

Icefield-wide mass balance error differs slightly between methods (±0.21 m w.e. yr^{-1} for SPOT-SRTM and ±0.15 m w.e yr^{-1} for ASTER trend). This difference is mainly related to the amount of data gaps, higher in SPOT-SRTM. The distribution of data gaps coincides over the NPI plateau (1200–1700 m a.s.l.) for both methods. Yet, over some glaciers in the north-east margins of the NPI, specifically Grosse, Bayo and Exploradores glaciers, less than one-third of their area is covered with the SPOT-SRTM method due to clouds in the SPOT5 images. Coverage is also restricted on small steep glaciers like glacier Pissis in the south, where a high percentage of data gaps exists over the SRTM DEM. These latter glaciers are those for which the mass balance rate differs most between the two methods. The redundancy of the acquisitions used in the ASTER trend method overcomes this issue.

The 2000–2012 $\dot{M}$ are in agreement within error bars between the two methods for all glaciers with coverage larger than 66%. Specific cases where $\dot{M}$ do not agree within error bars correspond to glaciers poorly sampled in the SPOT-SRTM method due to clouds or SRTM data gaps. The three largest glaciers of the icefield (51% of the total area) present $\dot{M}$ differences smaller than 0.2 m w.e. yr^{-1}. Availability of the data is also important to consider when comparing the two methods. A strong advantage of the ASTER trend method is that it is based on freely and nearly globally available ASTER L1A stereo images. SPOT5 stereo images were only acquired over specific areas and are not yet freely available. Thus, the ASTER trend has the potential to be extended to wider areas.

2.7.4 Comparison with previous estimates

Many studies already estimated the geodetic mass balance rates of the NPI for diverse time periods (Aniya, 2007; Glasser et al., 2011; Jaber et al., 2016; Rignot et al., 2003; Rivera et al., 2007; Willis et al., 2012a). However, only two of these studies examined the same time period as us and can therefore be directly compared with our results (Table 2.3). NPI-wide surface mass balances have also been estimated from atmospheric models (Mernild and Wilson, 2016; Schaefer et al., 2013), but these numbers cannot be compared with ours as they do not account for the mass loss by calving which is an important component of the mass loss for the NPI.

Generally, good agreement is found between our two estimates and previous geodetic estimates (Table 2.3). Although they used ASTER stereo images like us, Willis et al. (2012a) found a smaller mass loss. The difference may result either from the use of different ASTER DEMs, different co-registration methods, the amount of DEMs considered to extract dh/dt (55 in Willis et al. (2012a), 118 in our study) or the slight difference between time periods. We generated our own ASTER DEM using ASP, and they exhibit less artefacts than the DEMs from the 14DMO product used in Willis et al. (2012a) (see section 2.9, Figure 2.11).

Table 2.3: Global volume change rates estimates for the NPI from this and previous studies during similar time periods.

Reference	Time period	dV/dt (km^3 yr^{-1})
This study (SPOT-SRTM)	2000-2012	-4.55 ± 0.41
This study (ASTER trend)	2000-2012	-4.72 ± 0.34
Jaber et al. (2016)	2000-2014	-4.40 ± 0.13
Willis et al. (2012a)	2001-2011	-4.06 ± 0.11

Our mass loss estimates agree with Jaber et al. (2016) who compared the SRTM DEM with a TanDEM-X DEM mosaic. These two DEMs, derived from radar interferometry, are not affected by clouds and provide good coverage of the accumulation zone. Nevertheless, their coverage of the icefield was not complete, as northernmost NPI glaciers were not covered by TanDEM-X DEMs. Error estimates in Jaber et al. (2016) and Willis et al. (2012a) are three to four times smaller than ours. One reason for our larger errors could be the factor of five that we conservatively allocated to errors over data gaps. However, mass balance differences of typically 0.2 m w.e. yr^{-1} between our two methods for well-sampled glaciers (Figure 2.6, (see section 2.9, Table 2.4) suggest that our error bars are reasonable and not too conservative.

2.8 Conclusions

We compared two geodetic methods to obtain the region-wide and glacier-wide mass balance rates of the NPI. The first is based on the standard differencing of two DEMs (SRTM and SPOT5) whereas the second method extracts the rate of surface elevation change by fitting a linear trend to over 100 DEMs derived from ASTER stereo images.

For the entire NPI (about 3800 km^2), excellent agreement is found between the two methods. Following previous studies, our analysis confirms the strong mass loss, with an icefield-wide mass balance rate of -1.06 ± 0.15 m w.e. yr^{-1} (ASTER trend). The thinning rate reaches up to 10 m yr^{-1} for some low-elevation glacier tongues. Importantly, we also verify the lack of significant penetration of the SRTM C-band radar signal in the wet and temperate firn of the icefield except for the highest altitudes where dry snow was present in February 2000 (>2900 m a.s.l.; less than 1% of the icefield).

For individual glaciers, larger differences exist between the two methods, especially when the data coverage is more limited. By definition the SPOT5-SRTM estimate does not cover the area where clouds are present in the SPOT5 stereo images. The ASTER trend method is less prone to this effect because it relies on numerous (>100) ASTER DEMs. Both methods exhibit data gaps in the upper accumulation areas due to the lack of texture in the optical stereo images. This issue could be solved in the future by using images with higher spatial resolution and better radiometric depth.

Here we have provided insight into the effectiveness, advantages and disadvantages of two methods for estimating the geodetic mass balance rates of Patagonian glaciers and icefields. Both methods lead to coherent and satisfying results, though the free availability of the extensive archive of ASTER stereo images is a strong advantage.

2.9 Supplementary information

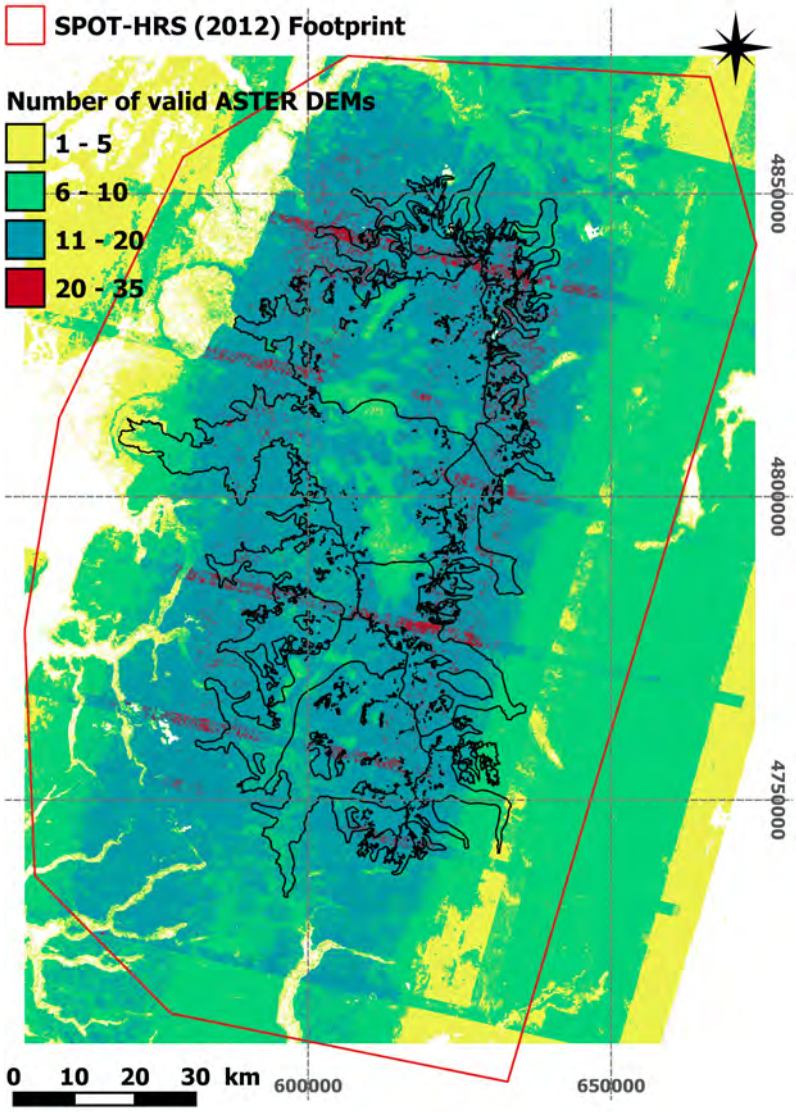

Figure 2.8: Spatial footprint of the SPOT5-HRS DEM for year 2012 (red line). The colour code corresponds to the number of **ASTER** elevation measurements available for every pixel from year 2000 to 2012 (after excluding elevation values outside the following accepted elevation range: within 150 m from the median of all DEMs on ice, and within 100 m off ice).

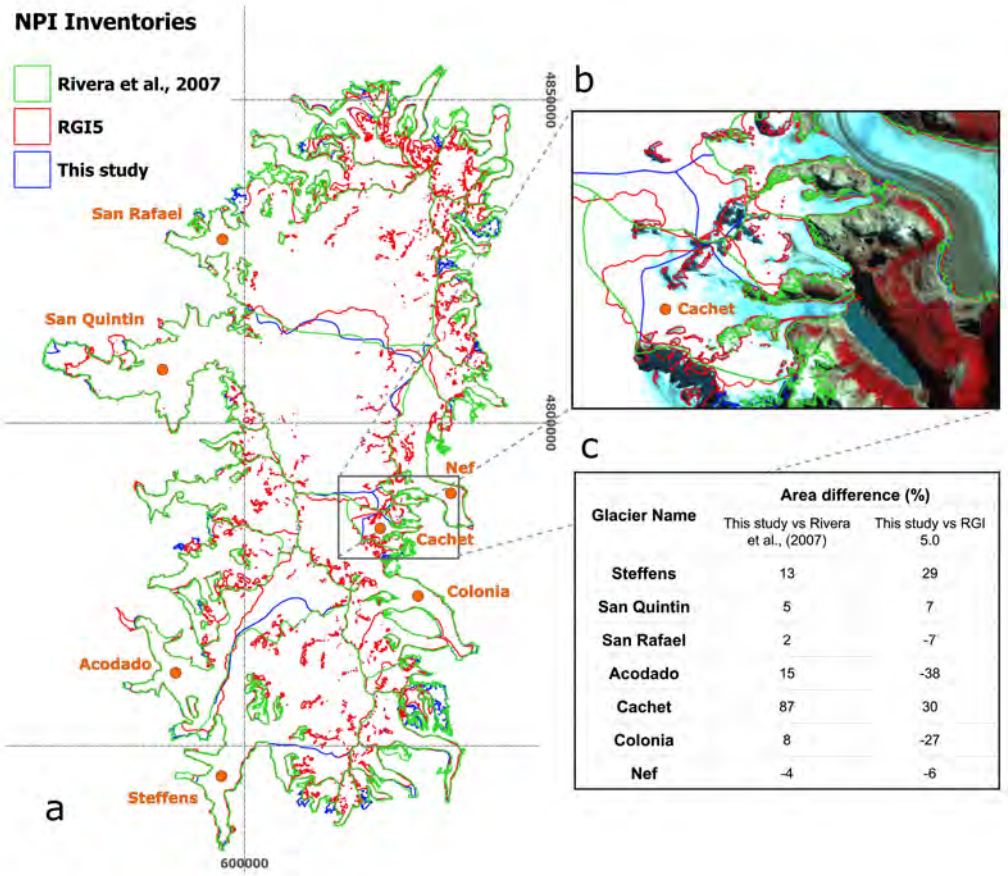

Glacier Name	Area difference (%)	
	This study vs Rivera et al., (2007)	This study vs RGI 5.0
Steffens	13	29
San Quintin	5	7
San Rafael	2	-7
Acodado	15	-38
Cachet	87	30
Colonia	8	-27
Nef	-4	-6

Figure 2.9: Comparison of three NPI glacier inventories. (a) The Blue line corresponds to the inventory created and used in this study for year 2000 (see section 3.2), ice divides are obtained from Mouginot and Rignot (2015). The red and green lines correspond to the RGI 5.0 and Rivera et al. (2007) inventories for year 2001 (recently incorporated in RGI 6.0), respectively. Named glaciers are those showing the largest area differences between inventories. (b) Zoom over the Cachet glacier area where inventories largely disagree on ice divides. Landsat Image for the 8 of mars 2000 as background. (c) Table shows the differences in glacier area between the inventories from Rivera et al. (2007) and the RGI 5.0 compared to the one used in this study, for the 7 glaciers that showed the largest differences. Note that the three largest glaciers of the NPI, San Quintin, San Rafael and Steffens, covering together 51% of the NPI area are included in this table.

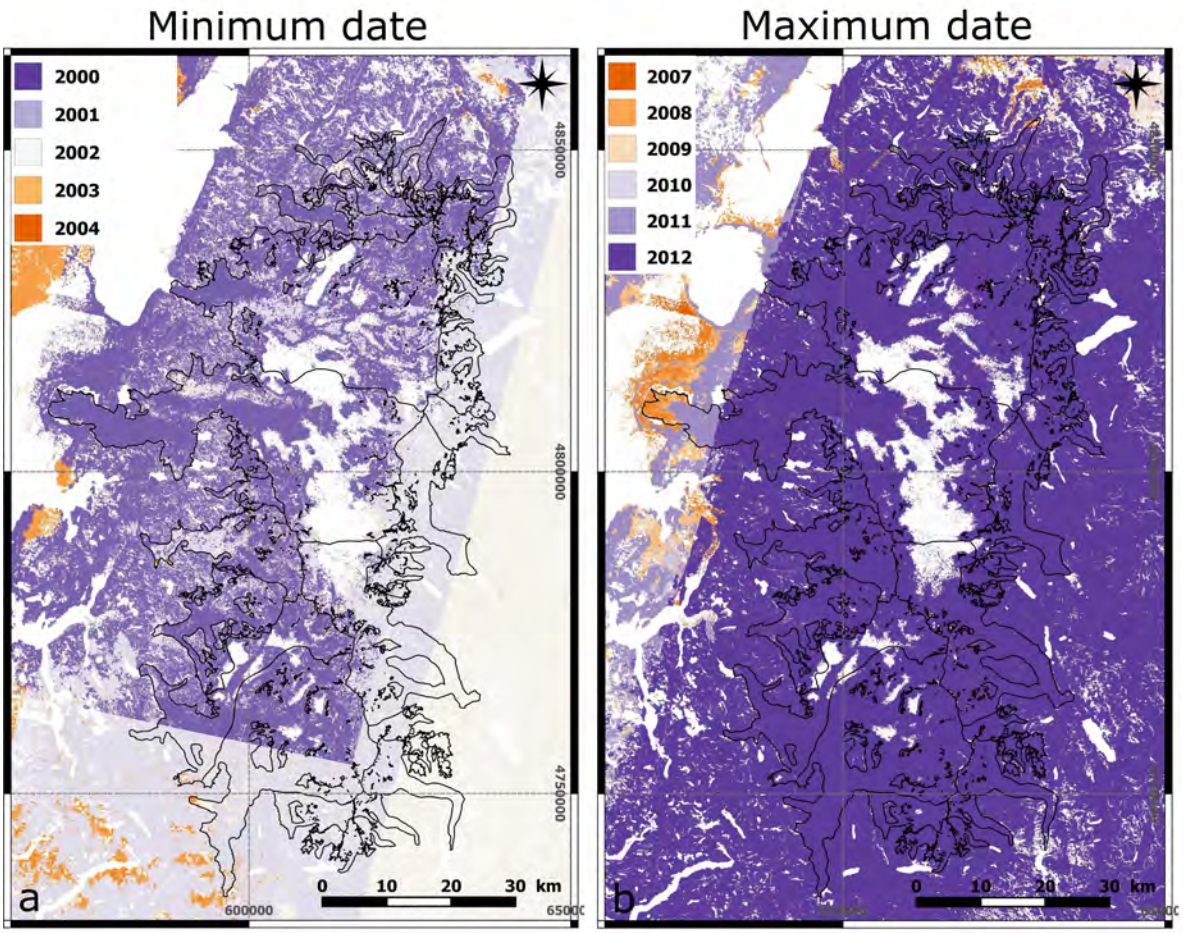

Figure 2.10: Spatial distribution of the minimum (a) and maximum (b) dates of ASTER DEMs used in our study. White gaps correspond to water bodies and locations where the uncertainty of $dh/dt_{ASTER\ trend}$ is larger than 3 m yr^{-1} (at the 95% confidence level).

Table 2.4: Mass balance of NPI individual glaciers from 2000 to 2012 and percentage area measured for SPOT-SRTM and ASTER trend methods. Glaciers are sorted in alphabetical order.

Glacier	Area year 2000 (km^2)	SPOT-SRTM $\dot{M}$ (m w.e. yr^{-1})	SPOT-SRTM Measured area (%)	ASTER trend $\dot{M}$ (m w.e. yr^{-1})	ASTER trend Measured area (%)
Acodado	237	-1.79 ± 0.26	73	-1.65 ± 0.21	81
Andree	7	-0.41 ± 0.23	46	-0.36 ± 0.06	97
Arco	26	-0.21 ± 0.14	75	-0.17 ± 0.06	94
Bayo	14	0.10 ± 0.32	7	-1.05 ± 0.12	92
Benito	161	-1.50 ± 0.21	79	-1.22 ± 0.13	95
Cachet	23	-0.49 ± 0.22	50	-0.33 ± 0.07	93
Cachet Norte	11	-0.25 ± 0.20	53	-0.28 ± 0.06	95
Circo	3	0.01 ± 0.34	2	-0.58 ± 0.09	92
Colonia	306	-0.76 ± 0.19	66	-0.86 ± 0.13	82
Cristal	5	-0.06 ± 0.19	57	-0.48 ± 0.07	96
Exploradores	80	0.06 ± 0.28	21	-1.01 ± 0.12	93
Fiero	38	-0.72 ± 0.29	31	-1.20 ± 0.14	89
Frankel	31	-0.76 ± 0.15	79	-0.53 ± 0.08	93
Grosse	60	0.19 ± 0.34	2	-1.40 ± 0.16	90
Gualas	119	-1.19 ± 0.22	69	-1.40 ± 0.15	91
HPN1	151	-2.38 ± 0.32	75	-2.30 ± 0.24	90
HPN4	51	-1.37 ± 0.23	72	-1.38 ± 0.15	90
Hyades	9	0.01 ± 0.23	40	-0.15 ± 0.07	92
Leones	65	0.07 ± 0.17	63	-0.16 ± 0.07	92
Mocho	3	0.40 ± 0.31	17	-0.43 ± 0.07	95
Mormex	3	-0.54 ± 0.33	12	-0.40 ± 0.07	94
Nef	140	-0.77 ± 0.17	75	-0.83 ± 0.10	92
Pared Norte	70	-1.24 ± 0.20	75	-1.40 ± 0.14	95
Pared Sur	25	-1.14 ± 0.25	59	-1.66 ± 0.17	93
Pissis	14	0.13 ± 0.27	26	-0.79 ± 0.09	95
Reichert	67	-0.98 ± 0.23	61	-1.04 ± 0.12	91
San Quintin	765	-0.75 ± 0.19	67	-0.82 ± 0.16	68
San Rafael	722	-1.08 ± 0.20	73	-0.93 ± 0.25	75
Soler	50	-0.27 ± 0.17	63	-0.73 ± 0.10	88
Steffens	468	-1.51 ± 0.21	80	-1.36 ± 0.15	91
Strindberg	16	-0.87 ± 0.19	69	-0.67 ± 0.08	95
U2	17	-0.37 ± 0.22	46	-0.51 ± 0.08	94
U3	17	-0.11 ± 0.18	58	-0.25 ± 0.07	94
U4	30	-0.76 ± 0.23	52	-0.69 ± 0.09	96
U5	5	-0.78 ± 0.18	71	-0.71 ± 0.09	94
U6	18	-0.27 ± 0.34	2	-0.56 ± 0.08	97
U7	4	-0.12 ± 0.31	13	-0.20 ± 0.07	93
Verde	7	-0.13 ± 0.29	20	-0.93 ± 0.12	88

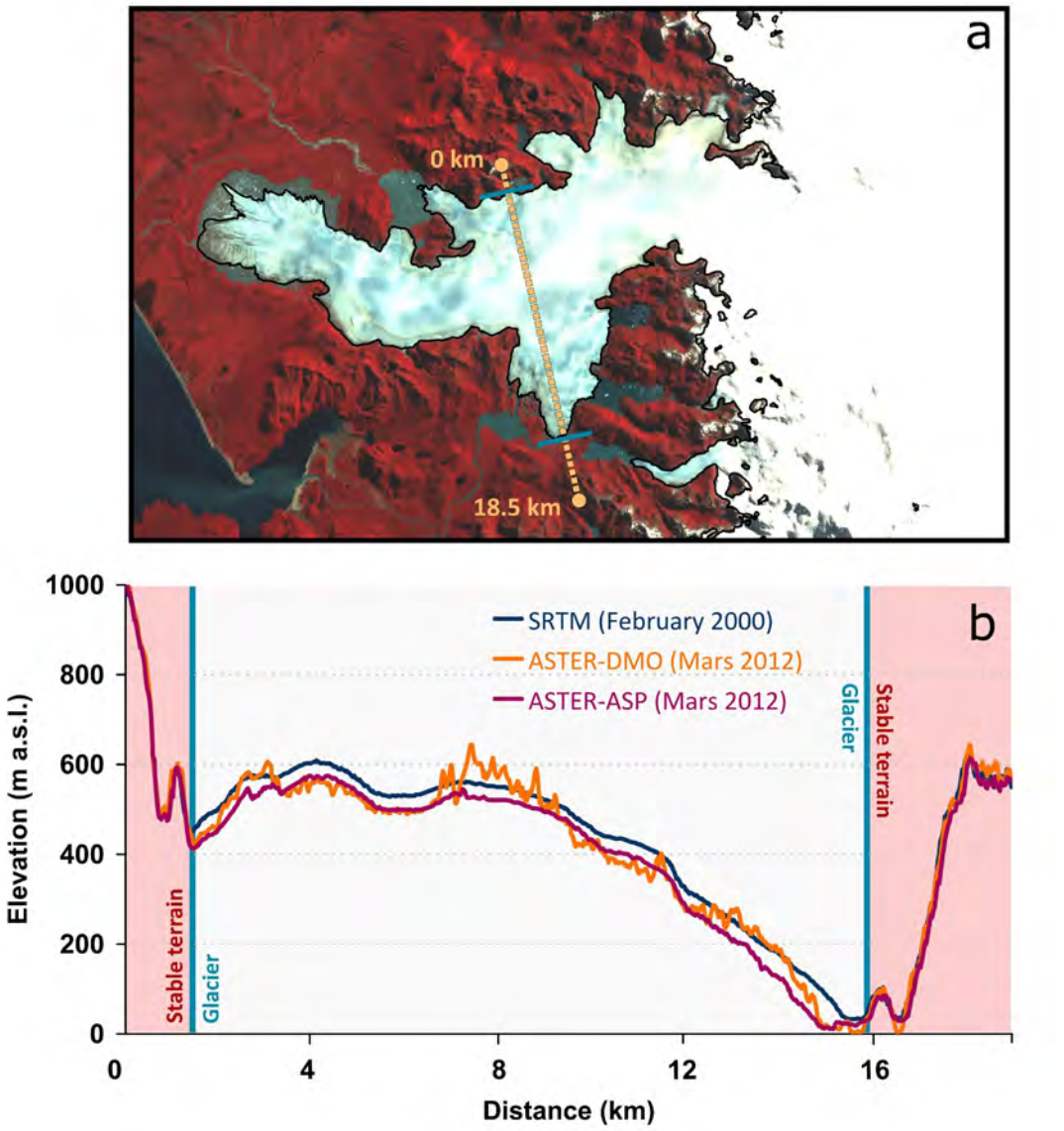

Figure 2.11: Comparison of SRTM, ASTER-14DMO and ASTER-ASP DEMs along a transverse profile of San Quintin glacier. (a) Location of the profile including glacier and stable terrain; transitions are presented as blue lines. (b) Elevation profiles extracted from the SRTM (February 2000) ASTER-14DMO and ASTER-ASP (18 March 2012) DEMs. Both ASTER DEMs are derived from the same Level 1A stereo pair. The ASTER-14DMO DEM (used in Willis et al., 2012a) was downloaded from LPDAAC. This profile illustrates the occurrence of numerous artefacts over the glacier surface in the ASTER-14DMO DEM. Conversely, the ASTER-ASP DEM is smoother and follows nicely the undulations of the SRTM DEM with an offset due to glacier thinning between 2000 and 2012. Hence, ASTER-ASP DEMs are more precise and should be preferred to ASTER-DMO DEMs to study glacier elevation changes.

Chapter 3

Two decades of glacier mass loss along the Andes

Note: This chapter is adapted from an article published in Nature Geo-Science, Dussaillant et al. (2019). Ongoing work beyond this article is described at the end of the chapter.

3.1 Brief introduction

The main objective of my PhD work was to assess the recent glacier mass change along the entire Andes based on the ASTERIX geodetic method. Our first motivation was to provide the scientific community with a first fully resolved and up to date assessment of mass changes in South American glaciers during the last two decades. This dataset, of unprecedented resolution, would permit to constrain Andes glacier contribution to sea level rise and the relative contribution of glacier decadal mass loss to regional hydrology, surpassing the large uncertainties associated to mass loss estimates obtained by previous strategies in this particular region (e.g. Gardner et al., 2013; Zemp et al., 2015).

The good performance of the ASTERIX methodology in the assessment of glacier mass balance rates for the entire High Mountain Asia (Brun et al., 2017), was the first step that gave us confidence to apply it at the entire Andes regional scale. This decision was further encouraged by the strong validation efforts over glacierized regions around the world, permitting to assure the robustness of the methodology. All validations agree on an error for individual glaciers of around 0.2 m w.e. yr^{-1}, including the one performed over the NPI, described Chapter 2 (Dussaillant et al., 2018), and all further validations performed before and during the progress of this work (Berthier et al., 2016, 2018; Brun et al., 2017; Menounos et al., 2019).

When I started this part of my PhD thesis, an homogeneous geodetic estimate of mass loss was still missing for the Andean region. However, in January 2019, a team of researchers led by Mathias Braun from the University of Nuremberg, Germany, published an article constraining glacier mass changes in South America using repeat TanDEM-X radar interferometry DEMs for the period 2000-2011/15 (Braun et al., 2019). Far from being a setback, this provided us with a directly comparable geodetic dataset at the entire Andes scale, helping to evaluate and even improve the ASTERIX methodology for the Andes. At the Andes-wide scale, ASTERIX and TanDEM-X geodetic estimates mostly agree, being considerably smaller than previous estimates, questioning the validity of previous strategies to estimate mass loss in the Andes (i.e. GRACE, Model based or interpolation of scarce existing glaciological and geodetic estimates). However, for individual regions excluding the Patagonian icefields, ASTERIX mass loss estimates where consistently more negative than those from Braun et al. (2019).

Three important findings were derived from the thorough comparison performed between ASTERIX and TanDEM-X data, described in more detail in this chapter. First, the high percentage of data gaps in the Patagonia region due to the limitations of ASTER DEMs derived from optical images (clouds,

lack of texture in the accumulations area) is an issue only for short periods of observations (usually less than 10 years, see section 3.8.4). Secondly, penetration of radar signal was verified to be negligible over South Patagonian glaciers due to the temperate conditions of the snow during the Austral summer and the low mean glacier altitude, but we demonstrate that it cannot be neglected over glaciers located at higher elevations and in colder environments further North in the Andes (section 3.8.3). And finally, in regions with a high variability of glacier mass loss like Patagonia and Tierra del Fuego, the 3NMAD filter widely used to exclude outliers when integrating elevation change trends at the regional scale (e.g. Braun et al., 2019; Brun et al., 2017), underestimates the mass loss if it is applied over regional elevation bands (including dh/dt values of all glaciers within the altitude range). Thus, this statistical filter should only be applied to individual glaciers (more information in section 3.8.5).

This last important finding (i.e. the mass balance bias induced by the 3NMAD filter at the regional scale) triggered a team effort, together with my colleagues Fanny Brun and Romain Hugonnet, to improve our processing technique, enabling an "in route" decision to change the ASTERIX processing from a regional approach to an individual glacier approach. We therefore computed mass balance rate estimates for all individual Andean glaciers for a complete period 2000 – 2018 and two sub-periods, 2000-2009 and 2009-2018. We were able to observe for the first time the temporal changes in mass balance rates along the entire Andes and its implications on regional hydrology, improving our understanding of both local and regional glacier variations in response to climate change. This is an aspect that could not be addressed by the Braun et al. (2019) geodetic estimates as they consider only one time period. We were also able to provide a first-order estimate of calving rates in the Andes for the period 2000-2015 (section 3.9).

I presented this work during two oral presentations at the European Geoscience Union meeting of 2019 (Vienna) and The POLAR2018 Open Science Conference of 2018 (Davos).

3.2 Abstract

Glaciers in the Andes are among the fastest shrinking and largest contributors to sea level rise in the world. They also represent crucial water resources in many tropical and semi-arid portions of this extense mountain range. Yet, the magnitude of the recent ice loss over the entire Andes cordillera is still debated. Here we present Andean glacier mass changes (from 10°N to 56°S) between 2000 and 2018 using time series of digital elevation models derived from ASTER stereo images. The total mass change over this period is -22.9 ± 5.9 Gt yr^{-1} (-0.72 ± 0.22 m w.e. yr^{-1}), with the most negative mass balances in the Patagonic Andes (-0.78 ± 0.25 m w.e. yr^{-1}) and the Tropical Andes (-0.42 ± 0.24 m w.e. yr^{-1}), and relatively moderate losses (-0.28 ± 0.18 m w.e. yr^{-1}) in the Dry Andes. Sub-period analysis (2000-2009 vs. 2009-2018) reveals steady mass loss in the Tropics and south of 45°S. Conversely, a shift from slightly positive to strongly negative mass balance is measured between 26° and 45°S. In this latter region, the rapid glacier loss in recent years coincides with extremely dry conditions since 2010 and partially helped to mitigate the negative hydrological impacts of this severe and sustained drought. These results provide a comprehensive, high resolution and multi-decadal dataset of recent Andes-wide glacier mass changes that constitutes a relevant basis for calibration and validation of hydrological and glaciological models intended to project future glacier changes and their hydrological impacts.

3.3 Introduction

The Andes, located along the western portion of South America between ca. 10°N and 56°S, contain a wide variety of topographic and climatic conditions resulting in a large diversity of ice masses (Clapperton, 1983; Garreaud, 2009). It hosts the largest glacierized area in the Southern Hemisphere outside Antarctica. Glaciers cover a wide range of altitudes from the highest peaks and volcanoes above 6000 m a.s.l. in the Tropical and Equatorial Andes to sea level in Patagonia and Tierra del Fuego. All recent global estimates of glacier contribution to sea level rise (SLR) place the Andean glaciers among the highest contributors (Bamber et al., 2018; Gardner et al., 2013; Glasser et al., 2011; Jacob et al., 2012;

Marzeion et al., 2015; Reager et al., 2016) . This region experienced the largest cumulative specific mass losses since 1961 (Zemp et al., 2019). Many Andean glaciers represent important water resources along an extensive portion of the Tropical and Dry Andes where glacier melt acts as a buffer during periods of drought (Buytaert et al., 2017; Huss and Hock, 2018; Kaser et al., 2010). Together with Central Asia, the Andes is a region where snow and ice melt contribution can reach 50% or more of the total runoff in some basins (Huss et al., 2017) and where the largest reductions in glacier runoff are projected for the end of the 21^{st} century (Huss and Hock, 2018). In many places along the Andes, glaciers also constitute important tourist attractions that generate significant revenue for local and regional economies (Vuille et al., 2018).

Although the recent shrinkage of Andean glaciers is relatively well documented, the magnitude of the total mass loss remains debated. Glacier mass change estimates have been obtained using four main strategies: (*i*) Extrapolation of the scarce glaciological (field) measurements (Cogley, 2009; Mernild et al., 2015; Rabatel et al., 2013a; Zemp et al., 2019, 2015); (*ii*) using geodetic estimates derived from digital elevation models (DEMs) for specific glacierized areas such as the North Patagonian Icefield (NPI, e.g. Jaber et al., 2016), South Patagonian Icefield (SPI, e.g. Malz et al., 2018) and Cordillera Darwin Icefield (CDI, e.g. Melkonian et al., 2013) and recently for the entire Andes (Braun et al., 2019); (*iii*) using low-resolution remote sensing methods (Gardner et al., 2013; Jacob et al., 2012; Reager et al., 2016; Wouters et al., 2019) that provide regional estimates but do not resolve individual glaciers nor regions with a small concentration of glaciers (ICESat-based estimates are restricted to 2003-2009, and GRACE-based estimates need to account for leakage of the hydrological signal and the strong signal from glacio-isostatic adjustment (Ivins et al., 2011; Richter et al., 2016); and (*iv*) using models of different complexity (Huss and Hock, 2015; Marzeion et al., 2015; Mernild and Wilson, 2016). Among others, uncertainties in these models arise from lack of measurements for calibrating both surface mass balance (accumulation is particularly uncertain over the Patagonian icefields (Collao-Barrios et al., 2018; Schaefer et al., 2015) and frontal ablation (calving) when included in the glacier model.

Despite these previous efforts, a comprehensive, high resolution and multi-periods assessment of recent changes in all South American glaciers is still lacking. In this study we provide an Andes-wide mass balance estimate extending from 10°N to 56°S based on the 'ASTER monitoring of Ice towards eXtinction' geodetic method (hereafter called ASTERIX). This method (see materials and methods and Brun et al. (2017) for more details) relies on the extensive and freely available archive of optical stereo images acquired by the Advanced Spaceborne Thermal Emission and Reflection Radiometer (ASTER) sensor, and was used in recent studies in Alaska, the high mountains of Asia, and the NPI (Berthier et al., 2018; Brun et al., 2017; Dussaillant et al., 2018). One of the strengths of the ASTERIX method is that it relies on optical imagery, avoiding the uncertainties associated with the signal penetration into snow and ice of radar-based DEMs (e.g. Berthier et al., 2018). Compared to earlier assessments, our mass loss estimates have a significantly higher resolution (down to individual glaciers) and they are almost exhaustive. They extend over nearly two decades (2000-2018) and can capture the shift in mass balance between two subperiods, 2000-2009 and 2009-2018. It is based on the processing of 90 1° by 1° (latitude–longitude) tiles altogether containing 99.6% (31505 km^2) of the Andes glacierized area, for which the overall ASTERIX coverage with valid elevation change data is close to three-quarters (Table 3.1).

3.4 Data and methodology

The data and methodology (ASTERIX) applied to the entire Andes was inspired by previous studies (Nuimura et al., 2012; Wang and Kääb, 2015; Willis et al., 2012a,b). Below we briefly summarize the processing steps and highlight the specificity for the application to the Andes. The reader is referred to (Brun et al., 2017) for further details.

The ASTER DEMs were processed based on 1° by 1° (latitude, longitude) tiles. The entire processing is done in UTM at a resolution of 30 m. Tiles containing less than 10 km^2 of glacier were not processed and their glacier change signal was substituted by their regional average (see section 3.7.5). We derived

about 30000 DEMs from raw ASTER level L1A (freely available from Earthdata) acquired from March 2000 to April 2018 using the open source Ames Stereo Pipeline routine (ASP, Shean et al., 2016). After co-registration of individual ASTER DEMs to the SRTM DEM (Nuth and Kääb, 2011) we fit a two-step linear regression through the time series of available ASTER DEMs to estimate the rate of elevation change for each pixel. These trends were extracted after excluding unrealistic outliers from the ASTER DEMs, i.e. pixels for which the absolute elevation difference is larger than 25 m plus 60 m per year since the last valid elevation (initialized by the elevation value of the SRTM DEM). The latter value was chosen based on the highest observed thinning rate in the Andes of approximately 50 m yr^{-1}. A first linear trend is fit to the elevation time series from ASTER DEMs and the SRTM DEM. Then, a second linear regression is fit excluding the SRTM DEM and all the data outside the 99% confidence interval of the first fit. Exclusion of the SRTM DEM is generally recommended to avoid the biases due to radar penetration into dry snow and ice (Berthier et al., 2018) (Berthier et al., 2018). Exceptionally for the 1° by 1° tiles south of 48°S (SPI to the South) we kept the SRTM DEM when computing the final trend. This choice is justified by the limited number of ASTER DEMs in these sub-regions due to a higher occurrence of clouds and reduced image acquisition and by the lack of measurable penetration of the SRTM C-band radar signal on the wet surface of Patagonian icefields in February 2000, the summer period in the southern hemisphere (Dussaillant et al., 2018; Jaber et al., 2013). The linear regression was computed for the entire period (January 2000–April 2018) and two 9 year sub-periods (January 2000–March 2009 and January 2009–April 2018).

We then integrated the rates of elevation change using the local hypsometric method (McNabb et al., 2019), using 100 m elevation bands. Data gaps are thus filled on an individual glacier basis using the mean rate of elevation change of the corresponding elevation bin, proved to be one of the most robust methods of void interpolation (McNabb et al., 2019). The mean elevation change rate was computed after excluding all values lying further than three normalized median absolute deviations (3 NMAD) from the median of the elevation bands. We also excluded pixels on slopes larger than 45°, pixels with uncertainties in the linear fit larger than 3.0 m yr^{-1} (at the 95% confidence level) and unrealistic absolute dh/dt values larger than 30 m yr^{-1}. Excluding glacier HPS12, the most negative elevation change rates (-28 m yr^{-1}) are observed on Upsala and Jorge Mont glaciers (SPI). Glacier HPS12 is the only glacier presenting stronger elevation change rates (up to -44 m yr^{-1}) and was processed separately. The total individual glacier volume change rate was then calculated as the sum of the mean elevation change rates multiplied by the area of the elevation band to which it corresponds. In the rare cases where no elevation change rates were available for an altitude band, we interpolated hypsometrically using a linear function forced to 0 for the highest band, corresponding to the glacier accumulation zone. Finally, mass balance rate was computed assuming a volume to mass conversion factor of 850 ± 60 kg m^{-3} (Huss, 2013). Mass balance rates for large regions (i.e. entire Andes, Andes sub-regions, river basins, 1° by 1° tile) were computed as the weighted sum of all individual glaciers. In the specific case of 1° by 1° tiles, all glaciers whose geometric centroid were located inside the tile limits were considered. Glaciers presenting mass balance errors higher than 1 m w.e. yr^{-1}, and a measured area lower than 20% of their total surface area where excluded and their mass balance rate replaced by the regional mean.

For DEM adjustment over stable terrain and mass balance calculations, we used a glacier mask derived from the Southern Andes and Low Latitudes regions of the Randolph Glacier Inventory (RGI v6.0) (excluding glaciers in Africa and Indonesia, less than 1% of the total glacierized area in the Low Latitudes region). Water-body outlines from the Global Lakes and Wetlands Database, level 1 and 2 (Lehner and Döll, 2004), and ocean water polygons(OpenStreetMap) were also used to define stable terrain. We selected the RGI inventory for three main reasons: RGI is available for the entire Andes (Pfeffer et al., 2014), it represents the glacier extent around 2000, the year of the earliest ASTER DEM and allows comparison to model results also based on RGI. Areal changes were not considered in our mass balance change estimates due to the lack of a more recent inventory for the entire Andes. Sensitivity of our mass balance change estimates to areal changes and to the imperfections inherent in the RGI are discussed in the section 3.7.7.

3.4.1 Uncertainty assessment

The total uncertainty of the mass balance rates for our seven sub-regions, the selected river basins and the large icefields was calculated as the quadratic sum of the random ($\sigma_{\dot{M}_{rdm}}$) and the triangulation error ($\sigma_{\dot{M}_{trg}}$) (Brun et al., 2017; Nuth and Kääb, 2011).

$$\sigma_{\dot{M}_{tot}} = \sqrt{\left(\sigma_{\dot{M}_{rdm}}\right)^2 + \left(\sigma_{\dot{M}_{trg}}\right)^2} \tag{3.1}$$

The random and triangulation errors where calculated considering sub-regions as a single ice body. The random error has three main sources, assumed to be independent of one another: the uncertainty in the rate of elevation change, the uncertainty in the volume to mass conversion factor and the uncertainty in the glacierized area. This calculation of the uncertainty in the rate of elevation change is derived from Fischer et al. (2015) Rolstad et al. (2009) and details can be found in Brun et al. (2017).

The triangulation error was assessed as the absolute value of the triangulation residual, r, between two equally long sub-periods.

$$r = \left| \frac{(\dot{M}_{2000-2009} + \dot{M}_{2009-2018}}{2} - \dot{M}_{2000-2018} \right| \tag{3.2}$$

Where $\dot{M}_{y_1-y_2}$ is the mass balance rate for the period between year y_1 and year y_2 expressed in m w.e. yr^{-1}. Similarly to Brun et al. (2017) and Menounos et al. (2019) the distribution of residuals showed dependence on the mean number of DEMs used to calculate $\dot{M}_{2000-2018}$, increasing when mass balances were calculated using fewer DEMs. Following the strategy used by Menounos et al. (2019) in North American glaciers, we derived the 68^{th} percentile of the residual distribution in a moving window of two DEMs. The triangulation error was then approximated as the linear relation of the observed trend of the 68^{th} percentile of residuals for each window (Figure 3.9). Our triangulation error varies from 0.27 m w.e. yr^{-1} when the trend is fitted on three DEMs, to 0.08 m w.e. yr^{-1} for 60 DEMs. Sub-regional triangulation error was then calculated using this relation and the mean number of DEMs for every sub-region.

The total uncertainty of our Andes-wide glacier mass change (in Gt yr^{-1}) was calculated as the quadratic sum of the total uncertainty on glacier mass change for each Andes sub-region. The total uncertainty on the specific mass balance (in m w.e. yr^{-1}) was then calculated by conserving the relative uncertainty.

3.5 Results and Discussion

3.5.1 Spatial variability of glacier elevation changes and mass balances

Results are reported as average mass balance rates over grid cells of 1° by 1° to help with their visualization and interpretation (Figure 3.1). Selected maps of the elevation change rates are shown in section 3.7.2 (Figures 3.6, 3.7 and 3.8) to illustrate the variety of patterns and the level of noise off-glacier. Region-wide thinning extends across the entire Andes for the period 2000-2018. A contrasted latitudinal pattern is also revealed with rapidly thinning small glaciers in the northernmost latitudes (10°N to 20°S) and over the largest glacierized area of the Patagonian Andes. An intermediate region from 26°S to 37°S exhibits comparatively smaller thinning rates (Figure 3.1).

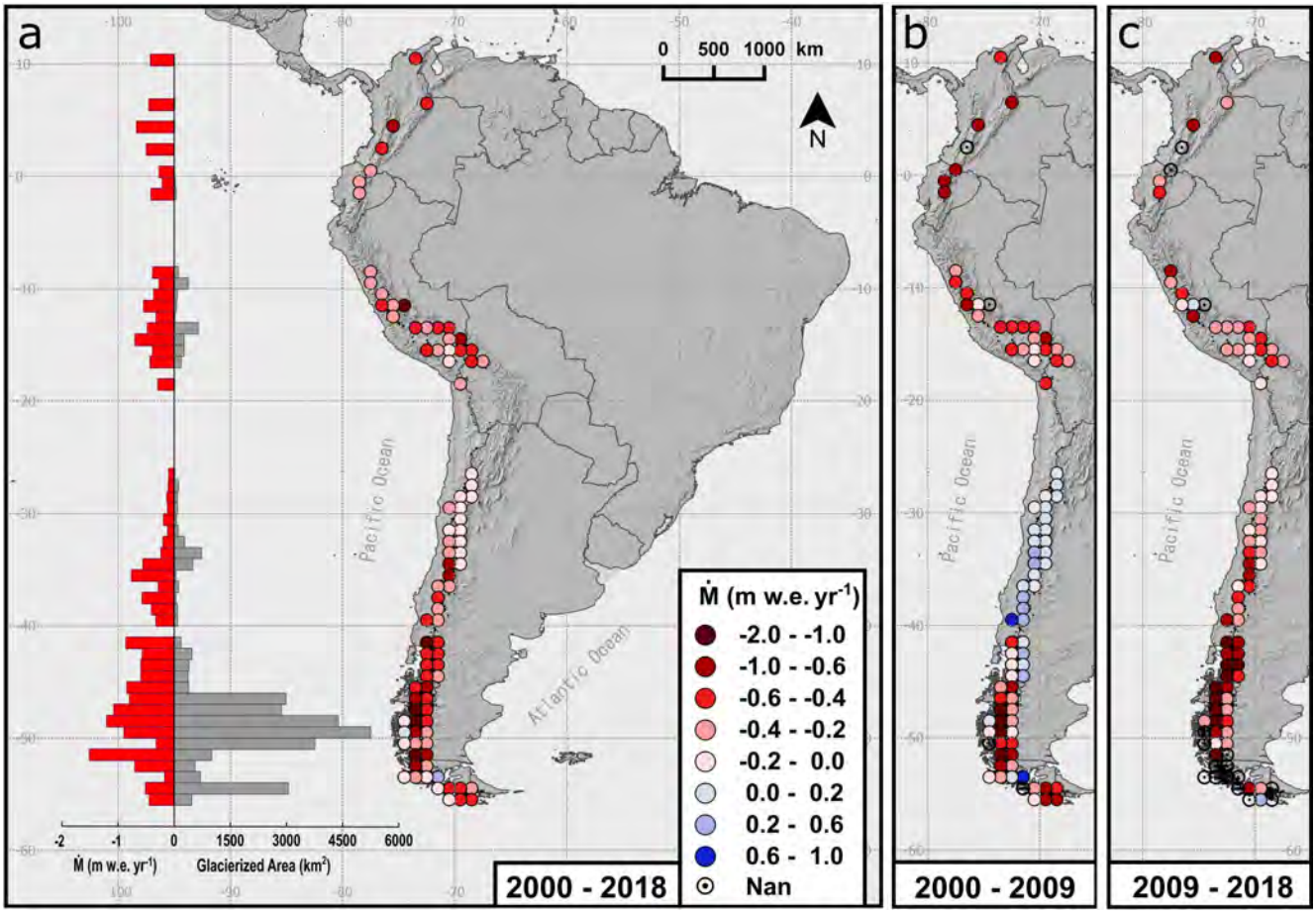

Figure 3.1: Andes-wide glacier mass balance rates averaged by 1° latitude and 1° longitude tiles from, (a) January 2000 to April 2018 (b) January 2000 to March 2009 and (c) January 2009 to April 2018. Histograms represent the glacierized area (grey bars) and the mean rate of elevation change (red bars) as a function of latitude. Empty values (Nan cells) correspond to tiles where the mean coverage with rate-of-elevation-change data is less than 20%, i.e. tiles situated in the Southern and Fuegian Andes, near to the Pacific coast, where cloud cover is persistent (see Figure 3.5). Note that color scale intervals are irregular to help visualization.

Mass balance estimates were computed for 17832 glaciers (out of 18799 in RGI v6.0). Regional mass balance rates were calculated for seven sub-regions, defined by latitude and climatology (modified from Sagredo and Lowell, 2012; Masiokas et al., 2009), as the area-weighted sum of all glaciers belonging to the sub-region (Figure 3.2, Table 3.1). Andes-wide mass loss rate (area weighted sum of sub-regional rates) totals -22.9 ± 5.9 Gt yr^{-1} (-0.72 ± 0.22 m w.e. yr^{-1}) from March 2000 to April 2018 (not considering sub-aqueous losses). These dates correspond to the first and last available DEMs in our time series, but the exact temporal sampling varies from one sub-region to another (Table 3.1).

Over the entire study period, the most negative mass balance rate is found in South Patagonia (-0.86 ± 0.27 m w.e. yr^{-1}), the sub-region that contains the two largest icefields (NPI and SPI) and is characterized by large calving outlet glaciers. In the surroundings of South Patagonia, the glaciers of North Patagonia and the Fuegian Andes also present negative mass balance rates of -0.57 ± 0.22 m w.e. yr^{-1} and -0.48 ± 0.27 m w.e. yr^{-1} respectivelly. The tropics, corresponding to rather small and spatially isolated glaciers in Ecuador and Colombia (Inner Tropics), and larger glaciers in Peru and Bolivia (Outer Tropics), also present negative mass balance rates of -0.37 ± 0.25 m w.e. yr^{-1} and -0.42 ± 0.23 m w.e. yr^{-1}, respectively. Slightly less negative mass balance rates of -0.31 ± 0.19 m w.e. yr^{-1} are detected in the Central Andes. The least negative value is measured in the Desert Andes, with -0.12 ± 0.17 m w.e. yr^{-1}. The ASTERIX coverage with valid glacier elevation change data exceeds 94% of the glacierized area in most sub-regions, with the exception of Inner Tropics (80%), South Patagonia (70%) and the Fuegian Andes (62%) (Table 3.1). In South Patagonia this is explained by the homogeneity of the snow surface on the flat NPI and SPI plateaus which prevents correlation of the stereo pairs and leads to

missing values in many of the DEMs at high elevations, and consequently in data gaps in the final maps of elevation changes (Figure 3.8). Despite these data gaps, our total mass losses for the SPI and NPI are in good agreement with recent state-of-the-art and independent estimates (Jaber et al., 2016; Malz et al., 2018). In the Fuegian Andes, the relatively poorer ASTERIX coverage is explained mostly by the high frequency of clouds. Nonetheless, the good agreement with radar-based estimates, together with the validation over Alaska icefields using airborne laser altimetry (Berthier et al., 2018), and a further sensitivity analysis to data gaps performed here (section 3.8.4) proves the relevance of our method, even in the featureless accumulation area of large icefields.

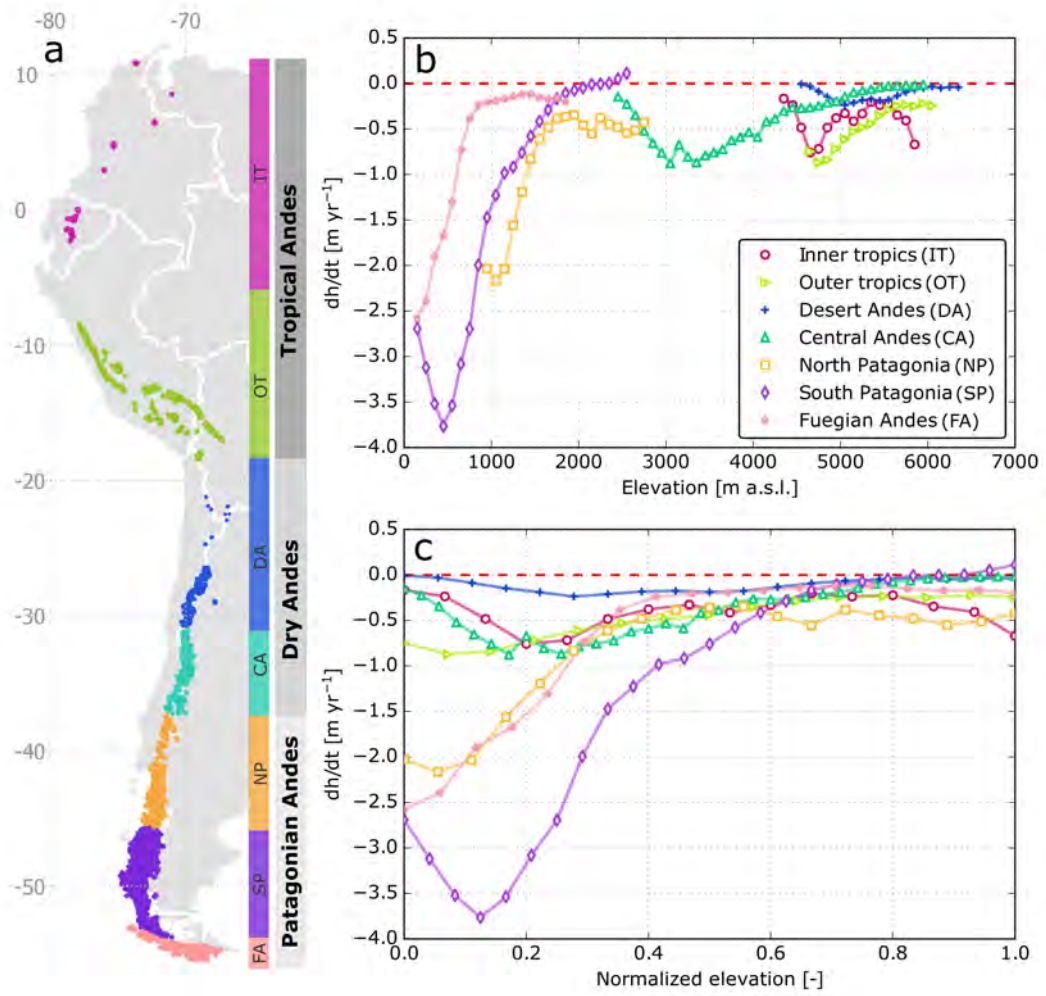

Figure 3.2: Delimitation of sub-regions and altitudinal distribution of glacier elevation change. (a) Seven sub-regions defined according to latitude and climate. The Patagonian and Dry Andes correspond to the RGI Southern Andes region. (b) Rate of elevation change of all Andes sub-regions for the period 2000–2018 as function of elevation. (c) Same as (b) expressed as normalized elevation defined as $(h - h_1) = (h_{99} - h_1)$, where h is the elevation and h_1 and h_{99} are the elevations of the 1st and 99th percentile of the glacierized area respectively.

Table 3.1: Region-wide mass balances for different sub-regions of the Andes from 2000 to 2018. (see Tables 3.4 and 3.5 for sub-periods).

Region	Total glacier area (km^2)	Glacier area measured (%)	Mean number of DEMs	Survey period (yyyy/mm)**	Mass balance	
					(m w.e. yr^{-1})	(Gt yr^{-1})
Inner Tropics	174	80	11.5	2001/08 – 2016/11	-0.37 ± 0.25	-0.1 ± 0.0
Outer Tropics	1967	94	17.3	2001/06 – 2017/03	-0.42 ± 0.23	-0.9 ± 0.5
Desert Andes	387	97	31.5	2000/11 – 2017/09	-0.12 ± 0.17	-0.1 ± 0.1
Central Andes	1795	97	28.3	2001/08 – 2017/11	-0.31 ± 0.19	-0.6 ± 0.3
North Patagonia	1753	96	18.2	2001/12 – 2017/07	-0.57 ± 0.22	-1.0 ± 0.4
South Patagonia*	21362	70	11.3	2000/10 – 2016/09	-0.86 ± 0.27	-18.3 ± 5.7
Fuegian Andes*	4053	62	6.9	2000/06 – 2016/03	-0.48 ± 0.27	-1.9 ± 1.1
TOTAL Andes	31631	74	12.8	2000/11 – 2016/10	-0.72 ± 0.22	-22.9 ± 5.9
Tropical Andes	2271	93	16.9	2001/06 – 2017/03	-0.42 ± 0.24	-1.0 ± 0.5
Southern Andes	29360	73	12.4	2000/11 – 2016/10	-0.75 ± 0.23	-21.9 ± 5.8

* SRTM DEM is included when computing the final trend

** For a specific region, the survey period varies because, for each pixel, the date of the first/last DEM can be different. The survey period is thus the interval from the mean first date to the mean last date of all DEMs used to extract rate of elevation change (Figures 3.10 and 3.11)

A consistent altitudinal distribution of elevation change rates is observed among the different sub-regions, with the highest thinning rates at the lowest elevations (Figure 3.2). The strongest thinning rates are observed at the lowest elevations of the Patagonian sub-regions (up to 4 m yr^{-1} in South Patagonia). The reduced thinning at the lowermost elevation is a signature of receding ice tongues (Schwitter and Raymond, 1993). A record-breaking thinning rate of 44 m yr^{-1} is observed at the tongue of glacier HPS12 (SPI). In the glacier upper reaches, rates of elevation change tend toward zero in most sub-regions. Exceptions to this are the glaciers in North Patagonia and the Inner Tropics, and to a lesser extent in the Outer Tropics, where negative rates of elevation change are observed even at their highest elevation bands. This suggests that glaciers in these sub-regions are in disequilibrium with the current climate and in advanced state of decline (Cook et al., 2016; Rabatel et al., 2017; Paul and Mölg, 2014; Vuille et al., 2018).

3.5.2 Decadal variability of glacier changes

To detect temporal variations in glacier mass change, we computed elevation change rates from January 2000 to March 2009 and January 2009 to April 2018 for the different sub-regions (Figure 3.1B and 3.1C; see also Tables 3.4 and 3.5). For most sub-regions, the glacier mass changes do not differ significantly from one period to the other. Conversely, a noticeable difference is observed for the Desert Andes, Central Andes and North Patagonia. In these sub-regions, the rates of elevation change during the first sub-period are close to zero or slightly positive. In contrast, strong negative elevation change rates were detected during the second sub-period (see section 3.7.6). The weighted-average mass balance rate for these three sub-regions decreased from 0.04 ± 0.18 m w.e. yr-1 (2000-2009) to -0.63 ± 0.18 m w.e. yr-1 (2009-2018). These estimates are robust, as these sub-regions present the largest percentage of valid data in the elevation change maps, with only 3% of data gaps for the 2000-2018 period (11% for 2000-2009 and 6% for 2009-2018). Moreover, the few available direct and local geodetic measurements support our findings of a shift from slightly positive to strongly negative mass balances after 2009 (Farías-Barahona et al., 2019; Burger et al., 2018; Masiokas et al., 2016).

3.5.3 Comparison with previous mass balance estimates

Previous studies provided mass balance estimates for the Southern Andes and Low Latitude glaciers (Figure 3.3, Table 3.2) but in most cases the comparison is not straightforward, due to differences in time periods and/or different geographic coverage. The annual mass change estimates reported here for the entire Andes (-22.9 ± 5.9 Gt yr^{-1}) is slightly more negative than the recent Andes-wide radar-

based geodetic estimate from Braun et al. (2019) (-18.4 ± 0.6 Gt yr^{-1}). Both studies agree over the large Patagonia icefields, where the coverage with radar DEMs is superior to ours. However, our ASTERIX estimates are consistently more negative than those from Braun et al. (2019) over all other Andean sub-regions (Table 3.7, Figure 3.14). The differences stem mostly from methodological aspects (i.e. the choice of the filtering technique applied to the elevation change maps leads to biases in the sub-region mass losses) and the differential penetration of the C-Band (SRTM) and X-band (Tandem-X) radar signals used in Braun et al. (2019). A comprehensive comparison between our results and Braun et al. (2019) is available in section 3.8.

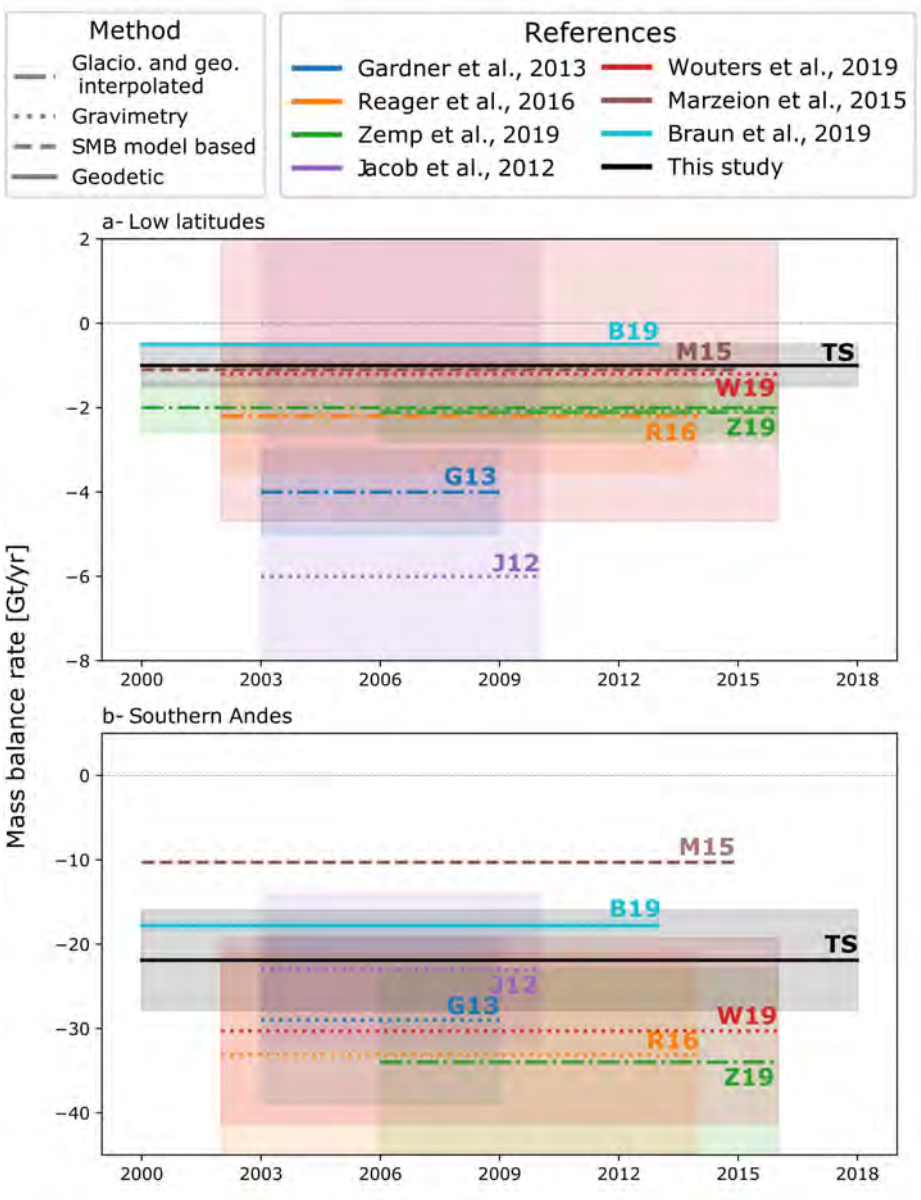

Figure 3.3: Glacier mass change rates estimates for (a) Low Latitude (10°N – 25°S, 99% Andean glaciers) and (b) Southern Andes (25°S – 56°S) regions from multiple methodologies. The results from this study do not account for subaqueous mass loss. In (a) the estimates from 3.8 and This study correspond to Andean Low latitude glaciers only.

For Low latitude Andean glaciers, the annual mass changes reported here (-1.0 ± 0.5 Gt yr-1 for 2000-2018 and -1.1 ± 0.5 Gt yr-1 for 2000-2009) are significantly less negative than those estimated Gardner et al. (2013), Reager et al. (2016) and Zemp et al. (2019) using interpolation of both glaciological and local geodetic measurements for 2003-2009 (-4 ± 1 Gt yr^{-1}), 2002-2014 (-2.2 ± 1.3 Gt yr^{-1}) and 2000-2016 (-2.0 ± 0.6 Gt yr^{-1}) respectively (Figure 3.3, Table 3.2). A better agreement is found with Wouters et al. (2019), based on GRACE (-1.2 ± 3.5 Gt yr^{-1}) for the period 2002-2016. For the Southern Andes,

our mass change of -21.9 ± 5.8 Gt yr^{-1} for 2000-2018 and -21.0 ± 6.6 Gt yr^{-1} for 2000-2009 are in good agreement with Jacob et al. (2012) GRACE estimates for 2003-2010 (-23 ± 9 Gt yr^{-1}) but are less negative than other GRACE estimates from Wouters et al. (2019) (-30 ± 11 Gt yr^{-1}), Gardner et al. (2013) (-29 ± 11 Gt yr^{-1}) and Reager et al. (2016) (-33 ± 12 Gt yr^{-1}) and with the glaciological and geodetic interpolated estimates from Zemp et al. (2019) (-34 ± 11 Gt yr^{-1}). Overall, these differences suggest a strong sensitivity of the region-wide values to very small number of glaciers with direct measurements in the Andes and their limited representability. Mass changes estimated by GRACE are generally the most negative ones in both RGI regions, suggesting an overestimation of the mass loss by this method. This overestimation is possibly due to the strong influence of the glacio-isostatic adjustment in Patagonia (Dietrich et al., 2010; Ivins et al., 2011; Richter et al., 2016). The magnitude of hydrological corrections also varies greatly depending on the model (Wouters et al., 2019). A detailed comparison of our ASTERIX results with published local glaciological and geodetic observations is presented in section 3.7.8.

Table 3.2: Comparison of mass balance change estimates for Low Latitude and Southern Andes glaciers.

RGI Region	Method	Period	$\dot{M}$ rate (Gt yr^{-1})	Reference
Low Latitudes	Glaciological and geodetic interpolated	2003 - 2009	-4 ± 1	Gardner et al. (2013) update of Cogley (2009)
	Glaciological and geodetic interpolated	2002 - 2014	-2.2 ± 1.3	Reager et al. (2016) update of Cogley (2009)
	Glaciological and geodetic interpolated	2006 - 2016	-2.1 ± 0.7	Zemp et al. (2019)
	Glaciological and geodetic interpolated	2000 - 2016	-2.0 ± 0.6	Zemp et al. (2019)
	Gravimetry (GRACE)	2003 - 2010	-6 ± 12	Jacob et al. (2012)
	Gravimetry (GRACE)	2002 - 2016	-1.2 ± 3.5	Wouters et al. (2019)
	Model based SMB reconstruction	2000 - 2013	-0.9	Marzeion et al. (2015)
	Model based SMB reconstruction	2000 - 2015	-1.1	Marzeion et al. (2015) updated in this study
	Geodetic (TanDEM-X)	2000 - 2011/15	-0.5 ± 0.0	Braun et al. (2019)
	Geodetic (ASTERiX)	2000 - 2018	-1.0 ± 0.5	This study
	Geodetic (ASTERiX)	2000 - 2009	-1.1 ± 0.5	This study
	Geodetic (ASTERiX)	2009 - 2018	-0.9 ± 0.5	This study
Southern Andes	Glaciological and geodetic interpolated	2003 - 2009	-21 ± 11	(Gardner et al. (2013) update of Cogley (2009)
	Glaciological and geodetic interpolated	2006 - 2016	-34 ± 11	Zemp et al. (2019)
	Gravimetry (GRACE)	2003 - 2010	-23 ± 9	Jacob et al. (2012)
	Gravimetry (GRACE)	2003 - 2009	-29 ± 11	Gardner et al. (2013)
	Gravimetry (GRACE)	2002 - 2014	-33.1 ± 12.1	Reager et al. (2016)
	Gravimetry (GRACE)	2002 - 2016	-30.3 ± 11	Wouters et al. (2019)
	Model based SMB reconstruction	2000 - 2013	-7.3	Marzeion et al. (2015)
	Model based SMB reconstruction	2000 - 2015	-10.3	Marzeion et al. (2015) updated in this study
	Geodetic (TanDEM-X)	2000 - 2011/15	-17.8 ± 0.6	Braun et al. (2019)
	Geodetic (ASTERiX)	2000 - 2018	-21.9 ± 5.9	This study
	Geodetic (ASTERiX)	2000 - 2009	-21.0 ± 6.6	This study
	Geodetic (ASTERiX)	2009 - 2018	-20.2 ± 6.2	This study

* Values are converted from mm w.e. yr^{-1} to Gt yr^{-1} using the same glacierized area as in our study.

The modeled surface mass balance (SMB) rate from Marzeion et al. (2015) is in good agreement with our mass balance rate for Low latitudes but is significantly less negative for the Southern Andes. This is probably because their model does not account for ice mass loss due to frontal ablation, an important component of mass loss in the Southern Andes. We separated calving and non-calving glaciers and compared the modeled SMB rates from Marzeion et al. (2015) (updated to 2000-2015) with ASTERIX mass loss rates for the same period. The ASTERIX (-5.5 ± 3.3 Gt yr^{-1}) and modeled (-4.8 Gt yr^{-1}) estimates agree for non-calving glaciers, which gives confidence in the modeling approach. For calving glaciers, the ASTERIX mass loss (-15.9 ± 4.8 Gt yr^{-1}) is considerably larger than the modelled one (-4.3 Gt yr^{-1}). Assuming that Marzeion et al. (2015) SMB rate estimates are also valid for calving glaciers, we can provide a first-order estimate of the frontal ablation of Andes calving glaciers by subtracting SMB

from our geodetic mass loss summed with the subaqueous mass loss (approximated to be -3.1 ± 1.2 Gt yr^{-1} in Patagonia for 2000-2016 by Braun et al. (2019)). Our first-order estimate of frontal ablation is therefore 14.7 ± 6.0 Gt yr^{-1} for 2000-2015, assuming that basal and internal processes are negligible.

3.5.4 Influence of glacier mass loss on river runoff

In order to estimate the contribution of glacier mass loss to surface runoff (e.g. Buytaert et al., 2017; Kaser et al., 2010), we selected seven major Andean river basins and compared the total discharge with the observed glacier changes for the sub-periods 2000-2009 and 2009-2018 (Figure 3.4 and Table 3.3). Glacier contribution to streamflow can be split into two terms: the seasonally-delayed component and the imbalance (or excess discharge) contribution (Radić and Hock, 2014; Pritchard, 2019). Our decadal mass loss estimates only provide an indication of the imbalance contribution, which is a lower bound of the glacier contribution to streamflow, in particular for winter accumulation regimes where the seasonally delayed fraction due to snow and ice melt is the dominant contribution.

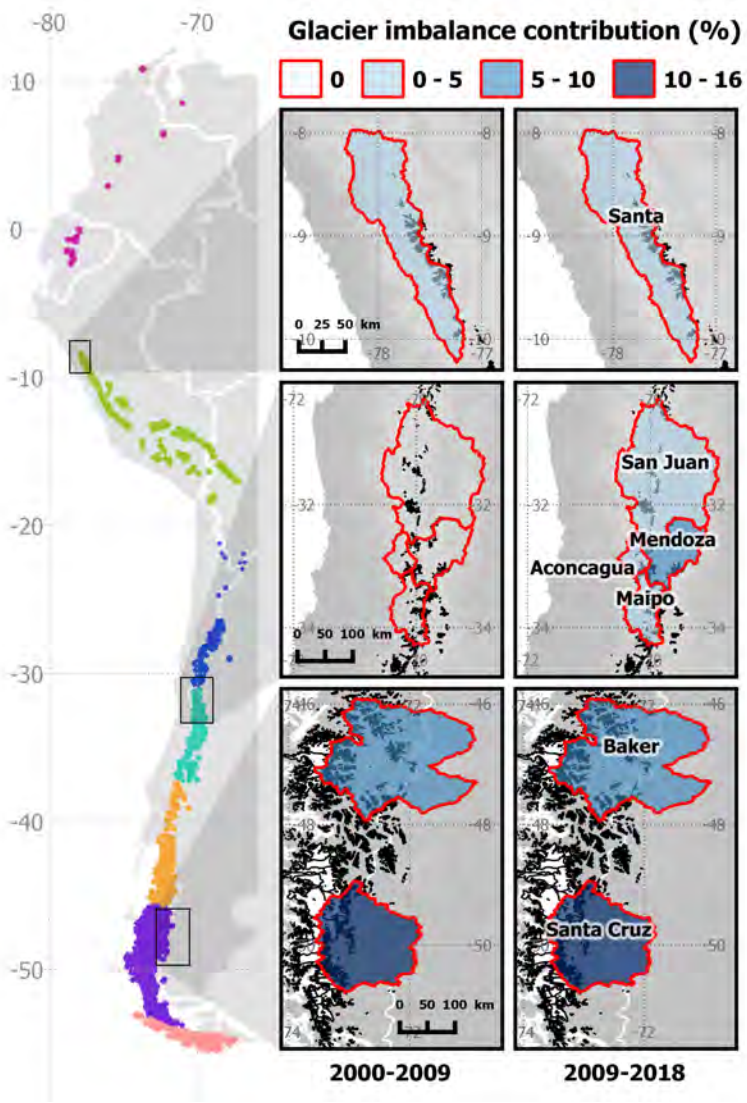

Figure 3.4: Seven main river basins used in the hydrological analyses: Santa basin (Peru); Aconcagua, Maipo and Baker basin (Chile); San Juan, Mendoza and Santa Cruz basins (Argentina). Color scale represents the relative decadal glacier imbalance contribution to river runoff for each decade.

Assuming that all measured glacier mass loss contributed to the discharge measured in the outlet gauging stations, glacier imbalance in the Santa River basin contributed to 5 m^3 s^{-1} of the measured streamflow in each decade (i.e. around 4% of the total annual discharge). For the four catchments analyzed in the Dry Andes of Chile and Argentina (the San Juan, Mendoza, Aconcagua and Maipo rivers), river discharge decreased markedly after 2009, with reductions ranging between 28% and 46%. This worri-

some river runoff reduction in these populated, semi-arid basins coincides with a substantial increase in glacier mass loss after 2009. These changes reflect the very dry conditions experienced in this region since 2010, which have collectively been termed the "megadrought" and can also be observed in terms of rainfall, snow accumulation, lake levels, water table depths and vegetation productivity, among other indicators (Garreaud et al., 2017; Rivera et al., 2017). Our results suggest that the decrease in perennial ice storage in these basins since 2009 effectively helped to mitigate the magnitude of this widespread dry period by contributing with 3% to 8% of the total discharge recorded in these rivers. As indicated in previous studies (Gascoin et al., 2011; Ragettli and Pellicciotti, 2012), the glacier contribution has likely been substantially larger during the warm months, and in particular during the several extremely dry late summers that have occurred in this region since 2010 (Garreaud et al., 2017; Rivera et al., 2017). The two Patagonian basins, show a slight increase on the decadal glacier imbalance contribution (from 3% to 5% in Baker river draining the NPI and from 14% to 16% in Santa Cruz river draining the SPI). These results reflect the more negative glacier mass balance rates observed during the most recent decade.

Table 3.3: Mass balance and glacier melt water contribution to river discharge in selected basins. Numbers in parentheses indicate the percentage of glacierized area of a river basin. All basins were delineated using the SRTM (resampled to 100 m) as a reference.

Basin name	Region	Glacier area (km2)	Survey period (yyyy/mm)	Glacier mass balance (m w.e. yr-1)	Annual excess discharge (m3 s-1)	Annual mean river runoff (m3 s-1)	Sub-period runoff change (%)	Glacier imbalance contribution (%)
Santa	Outer Tropics	361	2001/02 – 2007/12	-0.41 ± 0.25	4.7 ± 2.8	129.1	+10	4
	Peru	(3%)	2009/10 – 2017/10	-0.46 ± 0.25	5.0 ± 2.8	142.6		4
San Juan	Arid Andes	270	2000/11 – 2008/11	0.10 ± 0.23	0.0*	68.5	-43	0
	Argentina	(1%)	2009/04 – 2017/10	-0.24 ± 0.21	1.9 ± 1.9	38.9		5
Mendoza	Central Andes	304	2001/01 – 2008/11	0.14 ± 0.22	0.0*	53.0	-28	0
	Argentina	(4%)	2009/06 – 2017/12	-0.32 ± 0.21	3.2 ± 1.9	38.0		8
Aconcagua	Central Andes	36	2000/10 – 2008/11	0.28 ± 0.22	0.0*	38.4	-46	0
	Chile	(2%)	2009/04 – 2017/12	-0.55 ± 0.21	0.6 ± 0.3	20.6		3
Maipo	Central Andes	352	2001/03 – 2008/11	0.10 ± 0.22	0.0*	123.4	-32	0
	Chile	(7%)	2009/07 – 2017/12	-0.25 ± 0.20	2.8 ± 2.2	83.6		3
Baker	Southern Patagonia	1867	2001/10 – 2008/05	-0.31 ± 0.25	18.3 ± 14.8	649.2	-12	3
	Chile	(7%)	2010/02 – 2017/07	-0.48 ± 0.25	28.4 ± 14.5	568.7		5
Santa Cruz	Southern Patagonia	3010	2000/04 – 2007/09	-1.05 ± 0.32	99.7 ± 30.3	689.5	+16	14
	Argentina	(18%)	2009/12 – 2017/03	-1.37 ± 0.31	129.6 ± 29.3	799.3		16

* Following Radić and Hock (2014), Lambrecht and Mayer (2009) and Pritchard (2019) the excess discharge is set to 0 for periods when glaciers have zero or positive mass balance rates.

3.6 Conclusions

Contribution of Andean glaciers to sea level rise

The total Andes glacier mass loss of -22.9 ± 5.9 Gt yr^{-1} (-26.0 ± 6.0 Gt yr^{-1} including subaqueous loss estimated in Braun et al. (2019)) during 2000-2018 corresponds to 0.06 ± 0.02 mm yr^{-1} of SLR (subaqueous losses not taken into account), slightly more than 10% of the global glacier contribution (0.55 mm yr^{-1}) during 2002-2016 (Bamber et al., 2018). This value is 50% larger than the SLR contribution of all High Mountain Asia glaciers (Brun et al., 2017), although the latter cover an area three times larger. Our results also show that the total contribution of Andean glaciers to SLR has been relatively steady during the first two decades of the 21^{st} century, largely due to the unabated glacier mass loss observed in Southern Patagonia, where the largest glaciers are located. Nonetheless, within this large-scale pattern of unabated ice mass loss, we found an extensive region (between 26° and 45°S) where glaciers remained relatively stable or slightly gained mass from 2000 to 2009 (Figure 3.1). This behavior is similar to that observed in the West Kunlun and Karakoram regions of the high mountains of Asia (Brun et al., 2017; Kääb et al., 2015), and puts these regions among the few glacierized areas on Earth where glaciers were stable or slightly gained mass at the beginning of the 21^{st} century.

The new, multi-period and high-resolution dataset presented here provides original, up-to-date information on Andes-wide glacier changes for the first two decades of the 21^{st} century. These estimates have numerous potential applications for local, regional and larger-scale assessments, and will contribute to

better understand the response of Andean glaciers to climate change. They also have important implications for the management and conservation of Andean water resources, especially in the semi-arid regions. The highly resolved maps of glacier elevation changes for the entire Andes will also provide useful information to validate glaciological and hydrological models throughout South America.

3.7 Supplementary information

3.7.1 Spatial distribution of data gaps in the elevation change rate maps

The spatial distribution of data gaps in the elevation change rate maps for each 1° by 1° tile, for periods 2000-2018, 2000-2009 and 2009-2018 is shown in Figure 3.5. Values are expressed as percentage of data gaps on the rate-of-elevation-change maps relative to the total glacierized area in each tile. Every glacier whose centroid is located inside the 1° by 1° tile is considered to belong to the tile. The relatively poor ASTERIX coverage in the Fuegian Andes, especially during the 2009-2018 sub-period is clearly illustrated.

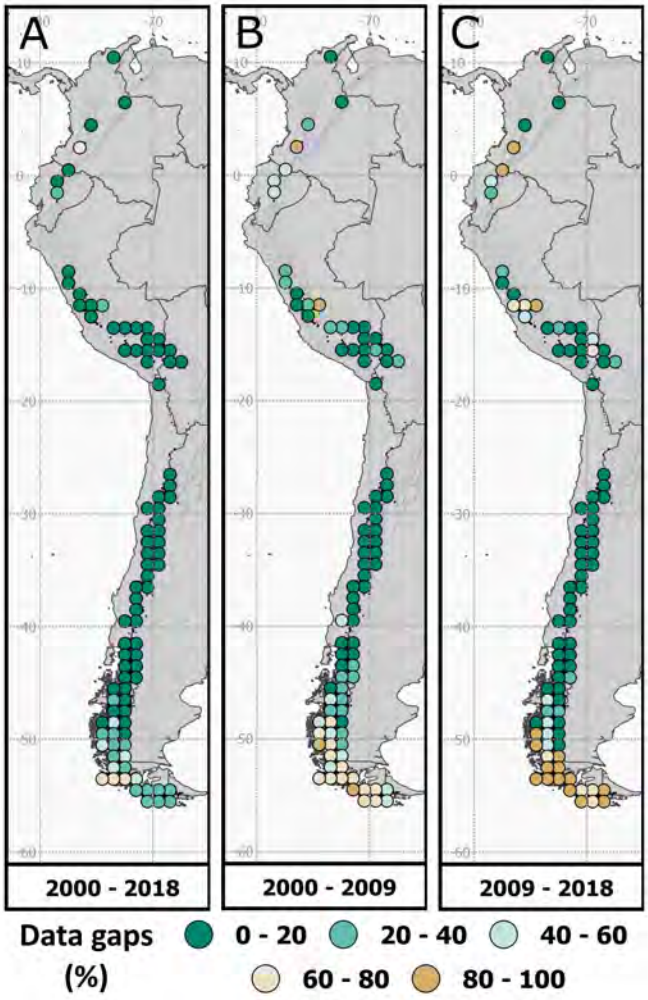

Figure 3.5: Spatial distribution of elevation change rate data gaps in the Andes for (A) 2000-2018 (B) 2000-2009 and (C) 2009-2018 periods. Colors circles represent the percentage data gaps on the rate-of-elevation-change maps for each 1° by 1° tile relative to the total glacierized area of the tiles. Green colors correspond to high ASTERIX coverage (i.e. less than 60% data gaps or more than 40% of the glacier area with valid dh/dt values).

3.7.2 Examples of ASTERIX elevation change maps from 2000 to 2018

Here we show examples of 2000-2018 elevation changes for 1° by 1° tiles in the Desert Andes (Figure 3.7), the Santa River basin in Cordillera Blanca (Outer Tropics sub-region, Figure 3.6) and over the

Southern Patagonian Icefield (SPI)(South Patagonia, Figure 3.8).

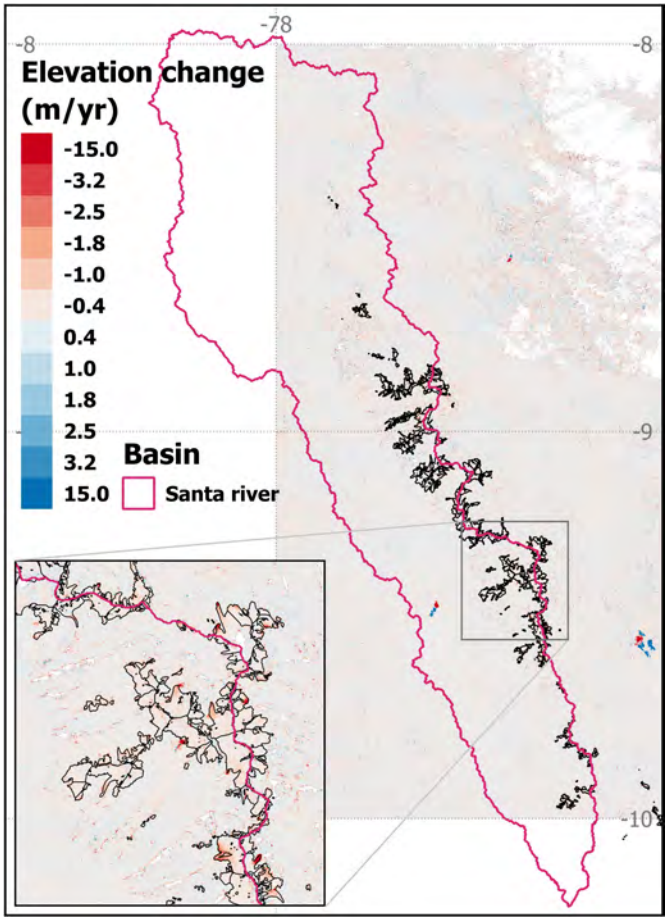

Figure 3.6: Elevation change rates for the Santa river basin in Peru from 2000 to 2018. The data gaps in the northeast corner corresponds to a non-glacierized region with a significantly lower number of ASTER stereo image acquisitions.

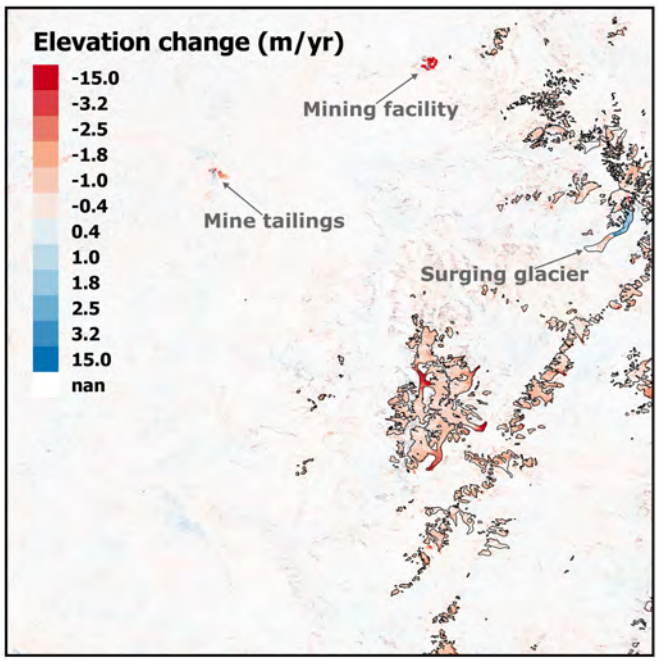

Figure 3.7: Elevation change rates for the tile located at 33-34°S, 70-71°W from 2000 to 2018. Note the limited noise on stable terrain off glacier. Glacier elevation changes (mostly thinning) are evident, but we can also detect the surging activity of the Piuquenes Glacier. Chilean mining activity is also detectable, with anomalous thinning and thickening outside the glacier outlines corresponding to the El Teniente mine.

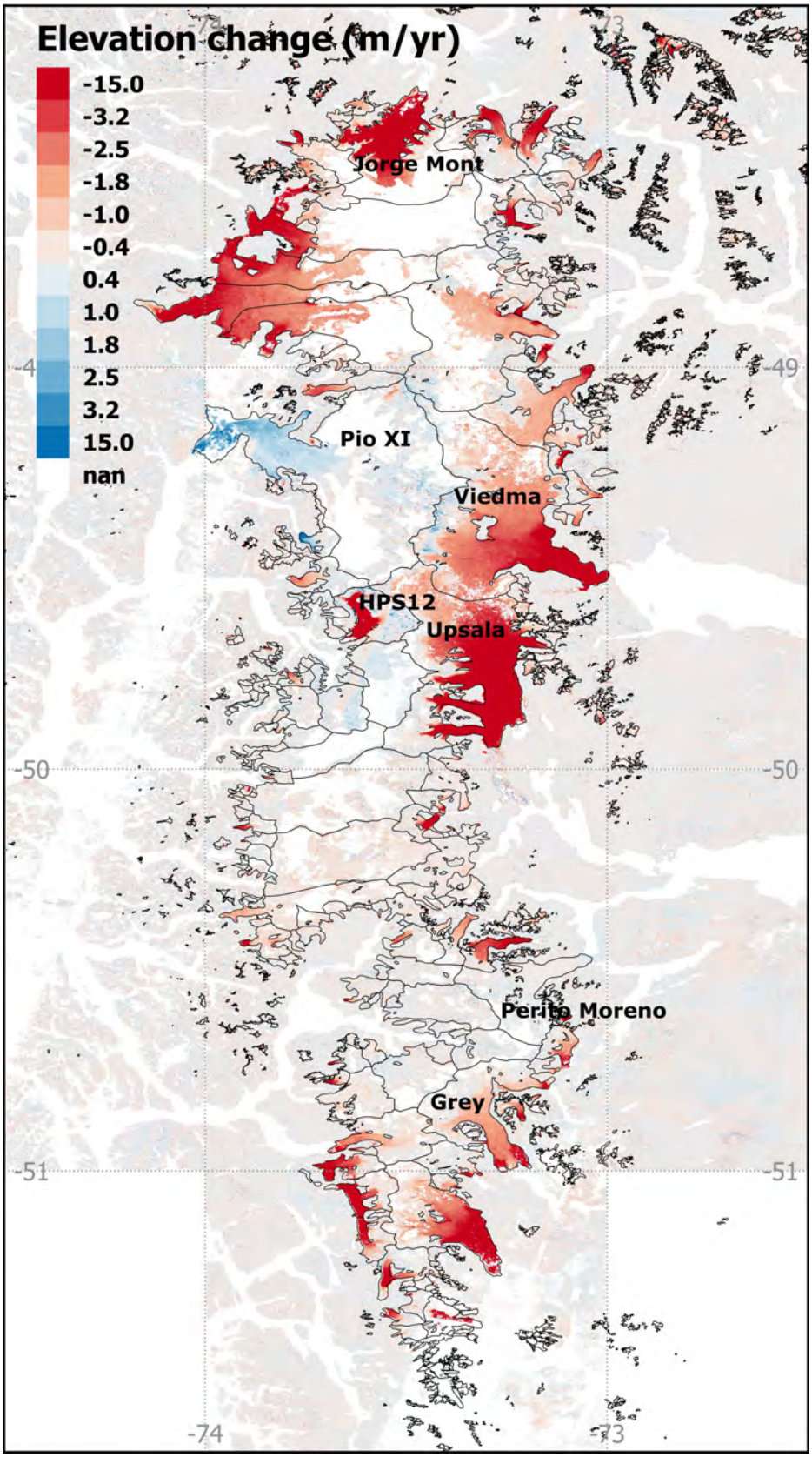

Figure 3.8: Elevation change rates for the Southern Patagonian Icefield from 2000 to 2018. The complex pattern of elevation changes can be observed, including the thickening and advance of Pio XI (Wilson et al., 2016) , the strong thinning rates of HPS12, Jorge Mont, Upsala, Viedma, and Grey glaciers (Malz et al., 2018; Foresta et al., 2018; Rivera et al., 2012; Sakakibara et al., 2013) and the rather stable conditions of Perito Moreno glacier (Minowa et al., 2015). Data gaps are shown in white.

3.7.3 Triangulation error calculation

To quantify departures from linear trends, we investigated the distribution of the triangulation residuals (see section 3.4, equation 3.2)) for each individual glacier as a function of the mean number of DEMs used in the 2000-2018 period. For that, only residuals from glaciers having more than 20% measured area and mass balance error smaller than 1 m w.e. yr^{-1} in all three periods where considered (corresponding to 59% of the total Andes glacierized area).

Similar to Brun et al. (2017) we found that the distribution of the residuals is related to the number of DEMs used to fit the trend. The number of DEMs varies greatly, from 3 DEMs in the southernmost regions to more than 60 in the Central Andes. We derived the 68th percentile of the residual distribution (corresponding to $\pm$ 1 σ) in a moving window of two DEMs, following the strategy used by Menounos et al. (2019). The triangulation error was then approximated as the linear relation of the observed trend of the 68th percentile of residuals for each window (Figure 3.9). Our triangulation error varies from 0.27 m w.e. yr^{-1} (three DEMs only), to 0.08 m w.e. yr^{-1} (60 DEMs).

This triangulation error is the largest source of uncertainties in our Andes sub-region geodetic mass balance estimates. The frequent ASTER acquisitions over the Arid, Central and North Patagonian regions, together with the lower probability of occurrence of clouds, ensures a sufficient number of DEMs to fit a realistic trend for the two sub-periods 2000-2009 and 2009-2018 (14 and 18 DEMs respectively, in average for these three regions). In the Tropics, elevation change rates are fit over a mean of 11 and 12 DEMs for the first and second periods, respectively. Conversely, in the cloudy southern regions (South Patagonia and Fuegian Andes), the mean number of DEMs varies between six and 10 and the triangulation error is thus larger. We also noticed that the ASTER sensor acquired fewer images in these southernmost latitudes, specially in the Fuegian Andes.

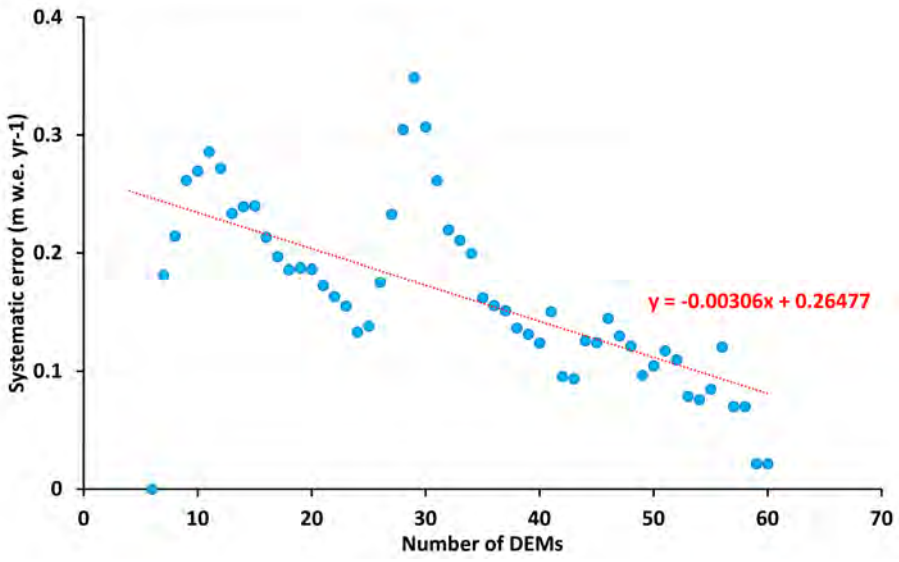

Figure 3.9: Triangulation error as a function of the number of DEMs considered to fit the final regression of the complete period 2000-2018. Dots correspond to the 68th percentile of residuals for each 2 DEM window.

3.7.4 Temporal coverage of mass balance estimates

Distribution of the first and last dates of the DEMs used to estimate the elevation change rates for each Andes sub-region and sub-period are presented in Figures 3.10 and 3.11 together with, as an example, a map showing the spatial distribution of first and last DEM dates for the three 1° by 1° tiles surrounding the North Patagonian Icefield (NPI).

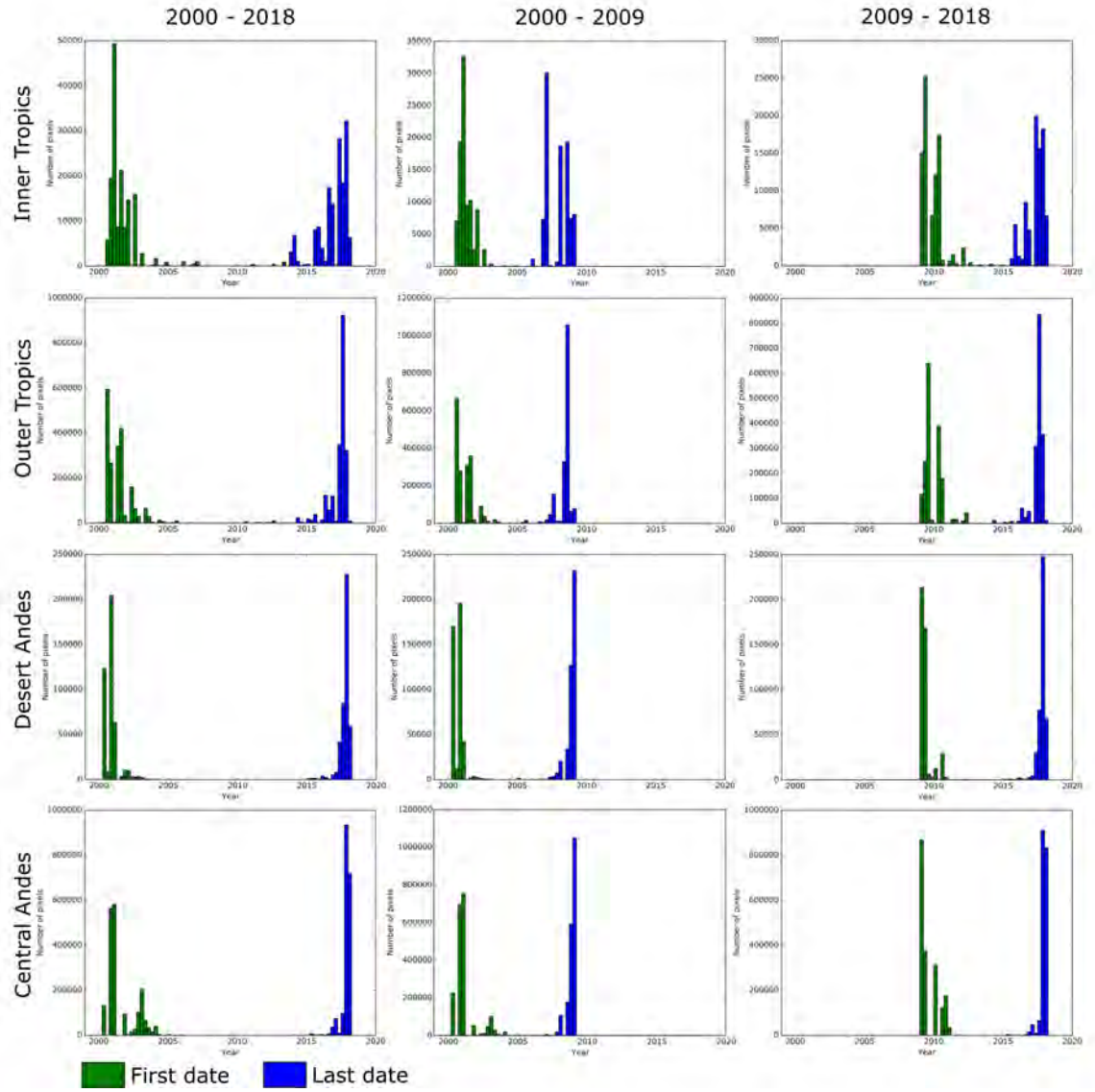

Figure 3.10: Histograms showing the first and last dates of the DEMs used to estimate the elevation change rate for the Tropic and Dry Andes sub-regions.

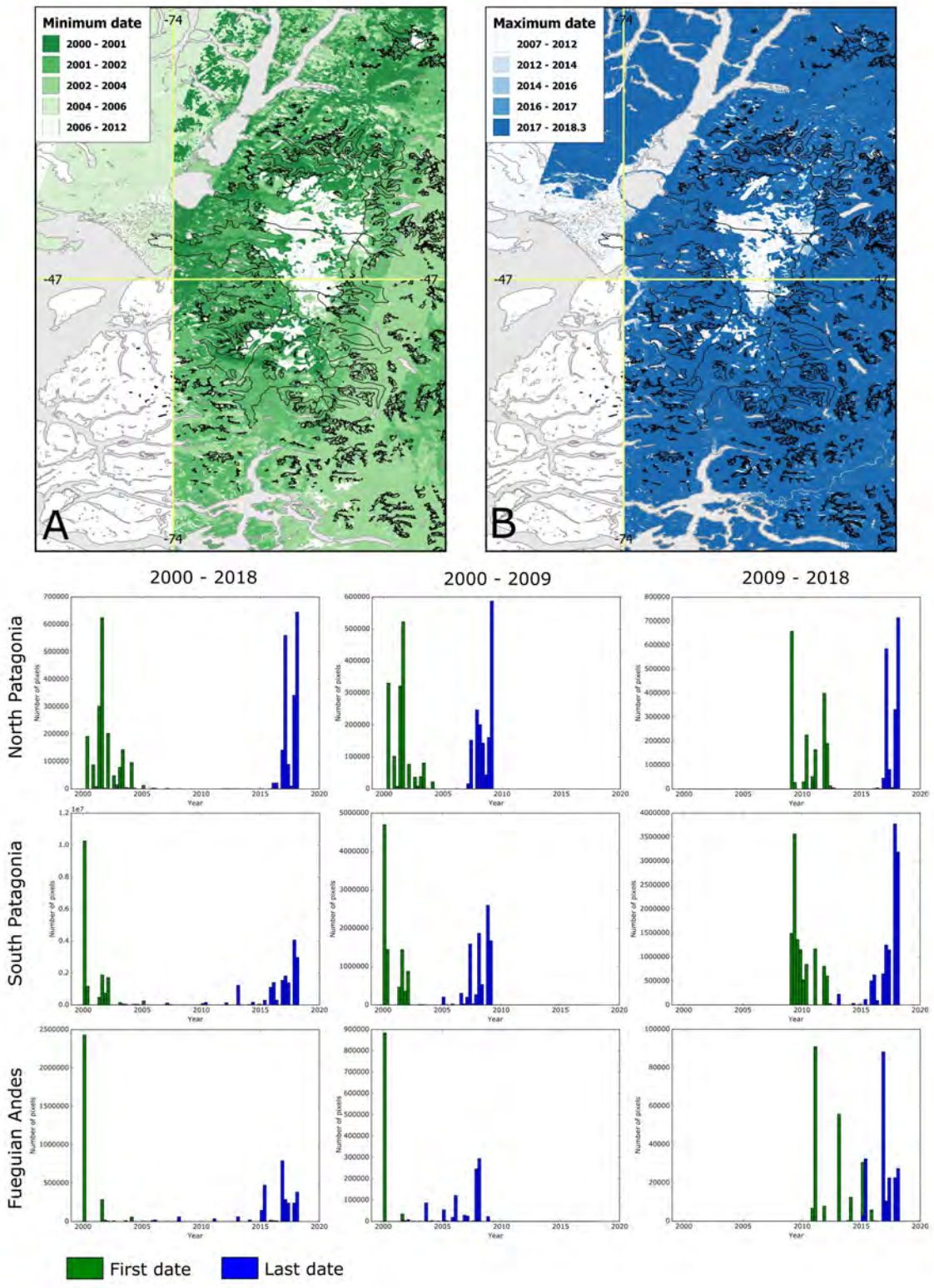

Figure 3.11: First and last dates of the DEMs used to estimate the elevation change rate. Maps showing the spatial distribution of first (A) and last (B) DEM dates for the three 1° by 1° tiles surrounding the NPI. Bellow, histograms showing the first and last dates of the DEMs used to estimate the elevation change rate in the Patagonian Andes sub-regions.

3.7.5 Selection of the 1° by 1° processing tiles

All Andes glaciers from RGI v6.0 are distributed in a total of 134 1° by 1° (latitude, longitude) tiles. After reprojection to their corresponding UTM zones, we observed that a large number of these tiles contained a very small glacierized surface area (a few km2). The processing of each tile was computationally expensive (typically 4 days on a 6-core computing cluster), implying the need for a compromise between the monitored area and optimization of the computing time. We computed the cumulative distribution of glacierized area as a function of the number of tiles (Figure 3.12), and calculated the elevation change maps over the 90 tiles containing more than 10 km^2 of glacier area. These 90 tiles account for 99.6% of the total Andes glacierized area.

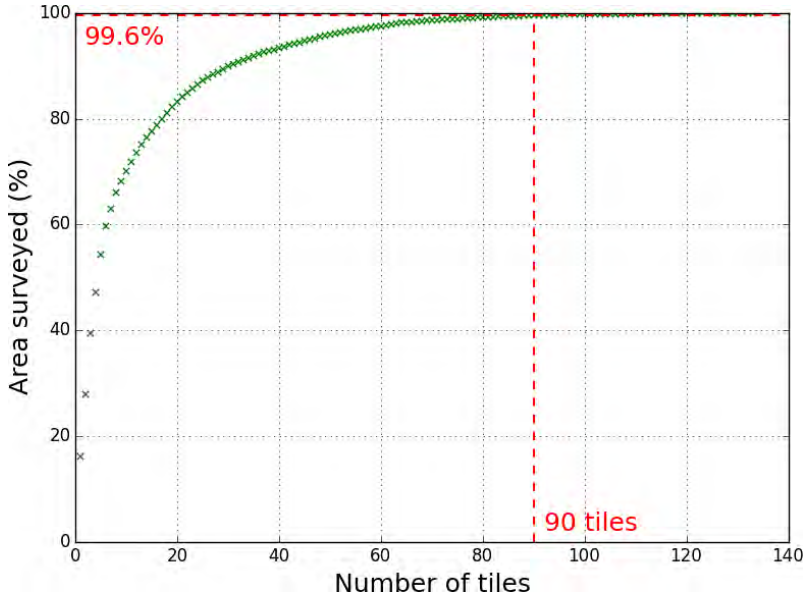

Figure 3.12: Cumulative distribution of glacierized area as a function of the number of tiles (sorted in descending order). The 90 most glacierized tiles cover 99.6% of the total Andes glacier area in RGI v6.0 (red lines).

3.7.6 Sub-period region-wide mass balance rates

The region-wide mass balance rates for different sub-regions of the Andes for 2000–2009 and 2009–2018 are listed in Tables 3.4 and 3.5 respectively. Sub-region inter-decadal mass balance rate changes are summarized in Figure 3.13.

Table 3.4: Region-wide mass balance rate changes for different sub-regions of the Andes from 2000 to 2009. Null and Positive values are highlighted in bold.

Region	Total glacier area (km^2)	Glacier area measured (%)	Mean number of DEMs	Survey period (yyyy/mm)*	Mass balance (m w.e. yr^{-1})	Mass balance (Gt yr^{-1})
Inner Tropics	174	49	8.1	2001/04 – 2007/12	-0.72 ± 0.30	-0.1 ± 0.1
Outer Tropics	2097	81	11.2	2001/04 – 2008/05	-0.44 ± 0.25	-0.9 ± 0.5
Desert Andes	397	96	18.2	2000/09 – 2008/11	0.00 ± 0.22	0.0 ± 0.1
Central Andes	1795	95	16.5	2001/02 – 2008/11	0.17 ± 0.23	0.3 ± 0.4
North Patagonia	1753	80	10.4	2001/06 – 2008/06	-0.08 ± 0.25	-0.1 ± 0.4
South Patagonia	21362	39	7.7	2000/09 – 2008/04	-0.85 ± 0.30	-18.1 ± 6.4
Fuegian Andes	4053	20	5.9	2000/03 – 2006/12	-0.76 ± 0.31	-3.1 ± 1.3
TOTAL Andes	31631	45	8.5	2000/10 – 2008/03	-0.70 ± 0.25	-22.1 ± 6.6
Tropical Andes	2271	78	11.0	2001/03 – 2008/05	-0.46 ± 0.27	-1.1 ± 0.5
Southern Andes	29360	43	8.3	2000/09 – 2008/02	-0.72 ± 0.26	-21.3 ± 6.6

Table 3.5: Region-wide mass balance changes for different sub-regions of the Andes from 2009 to 2018.

Region	Total glacier area (km^2)	Glacier area measured (%)	Mean number of DEMs	Survey period (yyyy/mm)*	Mass balance	
					(m w.e. yr^{-1})	(Gt yr^{-1})
Inner Tropics	174	43	9.7	2009/11 – 2017/04	-0.44 ± 0.29	0.1 ± 0.1
Outer Tropics	2097	76	12.0	2009/12 – 2017/06	-0.38 ± 0.24	-0.8 ± 0.5
Desert Andes	397	98	22.9	2009/05 – 2017/10	-0.11 ± 0.20	-0.0 ± 0.1
Central Andes	1795	97	21.1	2009/08 – 2017/12	-0.40 ± 0.21	-0.7 ± 0.4
North Patagonia	1753	92	14.3	2010/07 – 2017/09	-0.98 ± 0.25	-1.7 ± 0.4
South Patagonia	21361	48	10.0	2010/01 – 2017/06	-0.76 ± 0.28	-16.3 ± 6.0
Fuegian Andes	4053	5	5.8	2012/08 – 2016/12	-0.35 ± 0.37	-1.4 ± 1.5
TOTAL Andes	31631	50	10.6	2010/05 – 2017/05	-0.66 ± 0.23	-21.0 ± 6.2
Tropical Andes	2271	73	11.8	2009/12 – 2017/06	-0.38 ± 0.27	-0.9 ± 0.5
Southern Andes	29360	48	10.5	2010/06 – 2017/05	-0.69 ± 0.25	-20.2 ± 6.2

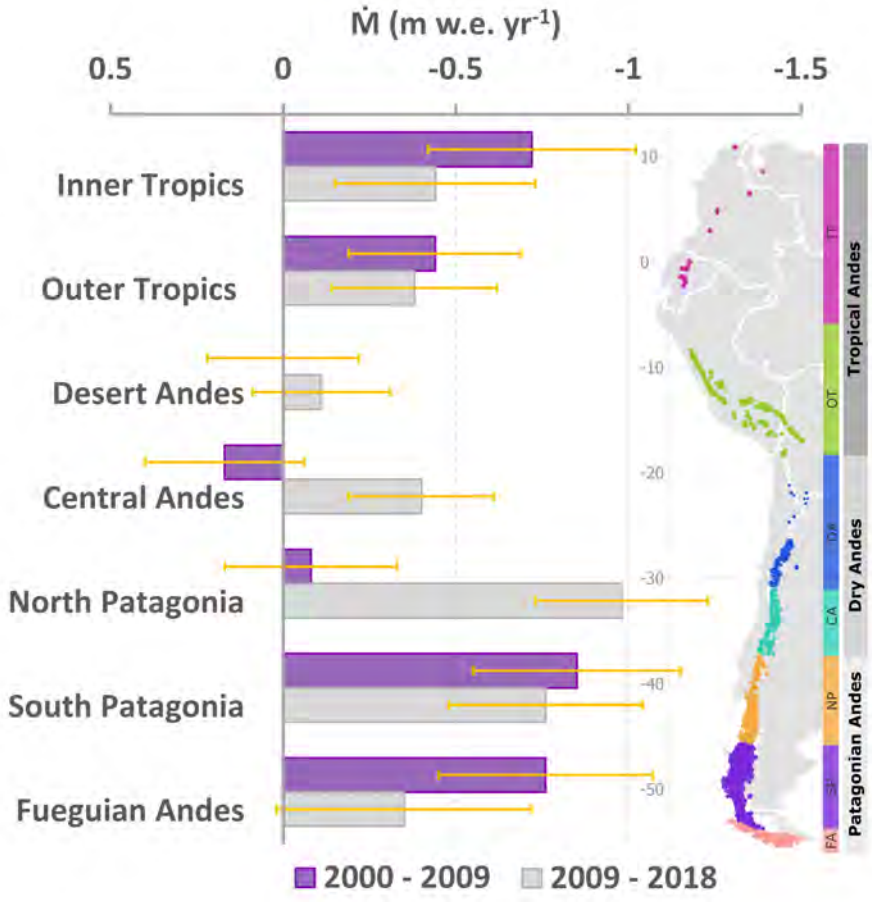

Figure 3.13: Interdecadal mass balance rate changes for the seven Andean subregions.

3.7.7 Sensitivity to the glacier inventory

Influence of glacier area change

Additional uncertainties can arise from changing glacierized areas during the study period. In regions where glaciers are shrinking, the use of only one inventory corresponding to the initial year does not affect the total mass change rate (in Gt yr^{-1}), but can influence the specific glacier mass balance rate (in m w.e. yr^{-1}), as one needs to divide the total mass change rate by the mean glacier area.

In a previous study (Dussaillant et al., 2018), we tested the sensitivity of our ASTERIX mass balance es-

timate for the NPI to the availability of a single inventory for year 2000 (as done here) and of temporally actualized inventories. In the first case, the mass balance rate is calculated dividing by the area for year 2000 only, while in the second case, we divide by the average area between both (Fischer et al., 2015). The effect was minor on the NPI, where the icefield-wide mass balance rate varied by only 0.01 m w.e. yr^{-1} (1%). However, it was larger for individual fast-retreating glaciers, with a mass balance rate difference of up to 10%. Falaschi et al. (2016) also tested the sensitivity of glacier mass balance to changing glacier inventories on mountain glaciers at the eastern margin of the SPI. They found changes of only 2 to 3% in mass balance estimates of glaciers larger than 3 km^2. Thus, neglecting the area changes of glaciers has limited impact on the region-wide mass balance rates (well within the other source of errors).

Influence of the quality of inventories

Errors in the glacier inventory can also lead to further uncertainties in our mass balance estimates. The RGI version 6.0 used in this study is the only glacier inventory currently available for the entire extent of the Andes cordillera. We calculated the sensitivity of ASTERIX mass balance rates to the choice of inventory in three particular zones of the Andes for which we accessed detailed high-quality inventories. The effect was minor in all regions.

- **NPI:** For the NPI, the ASTERIX mass balance for the period 2000-2018 was 0.02 m w.e. yr^{-1} (2%) more negative when using the outlines from Dussaillant et al. (2018). The later inventory reports an NPI area of 3841 km^2 (year 2000), while the RGI v6.0 reports 3917 km^2. The difference for the total NPI mass change (in Gt yr^{-1}) is even smaller, with less than 1% change (from -4.35 ± 1.05 Gt yr^{-1} to -4.34 ± 1.03 Gt yr^{-1} using RGI v6.0).
- **Mountain glaciers in Patagonia:** The same test was performed over the mountain glaciers close to the SPI (Falaschi et al., 2016), comparing the RGI 6.0 with the detail inventory from Falaschi et al. (2016). ASTERIX mass balance rates for the period 2000-2012, are 0.06 m w.e. yr^{-1} (or 14%) more negative when using the detail inventory. This difference is mostly because the RGI v6.0 inventory contains almost 180 km^2 (14%) more glacierized area. The difference in total mass loss in Gt yr^{-1} is smaller, only 0.02 Gt yr^{-1}, less than 3%.
- **Mendoza river basin:** Finally, we also calculated the ASTERIX mass balance rate of glaciers from the Mendoza river basin using the detailed inventory from the Inventario Nacional de Glaciares (ING, http://www.glaciaresargentinos.gob.ar/), corresponding to the glacier extent of year 2010. This improved inventory reports a glacierized area of 578 km^2, almost two times larger than the glacierized area reported by the RGI v6.0 for the same basin (304 km^2). The mass balance rates were 0.10 m w.e. yr^{-1} more negative when using the RGI v6.0 inventory (-0.24 ± 0.18 m w.e. yr^{-1} vs -0.14 ± 0.18 m w.e. yr^{-1} using ING). Similarly to previous cases, the total mass loss was less affected by the selection of inventory changing only 9%, the result being more negative for the detail inventory (-0.07 ± 0.05 Gt yr^{-1} for RGI v6.0 to -0.08 ± 0.10 Gt yr^{-1} for IGA).

These results suggest that using the RGI inventory probably results in slightly biased specific mass balance rates (expressed in m w.e. yr^{-1}), but does not affect significantly the total mass loss in Gt yr^{-1}. In any case, the impact is smaller than other sources of uncertainty.

3.7.8 Comparison of ASTERIX mass balance rates with previously published Andes-wide and local direct and geodetic observations

Comparison with published geodetic estimates in the Patagonian Andes

Geodetic estimates for similar time periods as observed here are only available for the NPI and SPI Icefields and mountain glaciers to the North-East (NE) of the SPI in Patagonia (Table S3). There is a good agreement with previous estimates except for one earlier study based on ASTER DEMs which found more negative mass balance rates for the SPI Willis et al. (2012b). These agreements and differences are discussed below case by case.

Northern Patagonian Icefield (NPI)

In a previous work, we compared the ASTERIX mass balance rates over the NPI for the period 2000-2012 with an independent estimate using the SRTM DEM from February 2000 and a SPOT5 DEM from March 2012 (Dussaillant et al., 2018)(Table 3.6). Both methodologies led to similar mass balance rates, also in agreement with an earlier estimate obtained by Jaber et al. (2016) using radar DEMs for the period 2000-2014 (SRTM and TanDEM-X). The ASTERIX 2000-2015 estimate obtained in this study is also in agreement with Jaber et al. (2016). Two new estimates using SRTM and TanDEM-X for similar time periods have recently been published for the NPI (Abdel Jaber et al., 2018; Braun et al., 2019), both of them in agreement with ASTERIX. The value from Braun et al. (2019) is slightly less negative because the authors considered some surrounding mountain glaciers (covering 700 km^2) as part of the NPI. These glaciers are not part of the icefield sensu stricto and are loosing mass at much lower rates than NPI glaciers(see section 3.8.1). This estimate is thus not comparable with other estimates that consider NPI sensu stricto.

Table 3.6: Mass balance estimates for the NPI, SPI and mountain glaciers from this and previous studies during similar time periods.

Region	Method	Time period	Mass balance (m w.e. yr^{-1})	Reference
NPI	ASTER 14DMO time series	2001 - 2011	-0.96 ± 0.04*	Willis et al. (2012a)
	SRTM – TanDEM-X	2000 - 2014	-1.02 ± 0.04	Jaber et al. (2016)
	SRTM – TanDEM-X	2000 – 2011/15	-0.88 ± 0.26	Braun et al. (2019)
	SRTM – TanDEM-X	2000 – 2012	-0.91 ± 0.04*	Abdel Jaber et al. (2018)
	SRTM – SPOT5	2000 - 2012	-1.02 ± 0.21	Dussaillant et al. (2018)
	ASTERIX	2000 - 2012	-1.06 ± 0.15	Dussaillant et al. (2018)
	ASTERIX	2000 - 2015	-0.98 ± 0.27	This study
SPI	ASTER 14DMO time series	2000 - 2012	-1.49 ± 0.09*	Willis et al. (2012b)
	SRTM – TanDEM-X	2000 – 2015/16	-0.89 ± 0.24*	Malz et al. (2018)
	SRTM – TanDEM-X	2000 – 2011/15	-0.90 ± 0.26	Braun et al. (2019)
	SRTM – TanDEM-X	2000 – 2012	-0.97 ± 0.03*	Abdel Jaber et al. (2018)
	ASTERIX	2000 - 2012	-0.92 ± 0.30	This study
	ASTERIX	2000 - 2015	-0.96 ± 0.29	This study
NE margin SPI	SRTM – SPOT5	2000 - 2012	-0.46 ± 0.37	Falaschi et al. (2016)
	ASTERIX	2000 - 2012	-0.38 ± 0.25	This study

*Estimates modified to correspond to our density conversion factor of 850 kg m^3 (Huss, 2013).

Southern Patagonian Icefield (SPI)

We calculated mass balance rates for the SPI of -0.92 ± 0.30 m w.e. yr^{-1} for the period 2000 – 2012 and -0.96 ± 0.29 m w.e. yr^{-1} for the period 2000–2015 (Table 3.6). Malz et al. (2018) recently provided a geodetic estimate for the period 2000 – 2015/16 using SRTM and TanDEM-X radar DEMs. Their mass balance rate of -0.94 ± 0.19 m w.e. yr^{-1} (0.89 ± 0.24 m w.e. yr^{-1} if we use the same density conversion factor of 850 kg m^{-3} (Huss, 2013)) is in good agreement with our estimate for the same period. Willis et al. (2012b) calculated a more negative SPI mass balance of -1.49 ± 0.09 m w.e. yr^{-1} for the period 2000–2012 also using ASTER DEM time series.

The more negative mass balance from Willis et al. (2012b) over the SPI compared to all other geodetic studies are possibly explained firstly by the use of different ASTER DEMs and secondly by methodological differences, especially the co-registration method and data filtering. We calculated DEMs from L1A ASTER stereo pairs using the Ames Stereo Pipeline (ASP) whereas Willis et al. (2012b) relied on ASTER DEMs available online (14DMO product, where data gaps are interpolated). ASTER DEMs derived using ASP have shown to exhibit less artefact and lower noise level than the 14DMO version over the NPI (see Figure 2.11 in Chapter 2). In terms of methodology, the use of asymmetric filters in Willis et al. (2012b) to exclude outliers could also have biased their elevation change rates and mass balance

estimates toward too negative values.

The good agreement of ASTERIX estimates with radar based estimates over both Patagonian Icefields, together with the agreement with airborne laser altimetry over Alaska icefields (Berthier et al., 2018) and the sensitivity to data gaps analysis performed here in section 3.8.4 demonstrate the robustness of ASTERIX method even in the featureless accumulation areas of large icefields.

Mountain glaciers at the North-East (NE) margins of the SPI

Falaschi et al. (2016) calculated the mass balance of glaciers (covering 1314 km^2) located NE margins of the SPI, using the SRTM DEM for February 2000, and a SPOT5 DEM for March 2012. They obtained a total geodetic mass balance of -0.46 ± 0.37 m w.e. yr^{-1}. We recalculated ASTERIX estimates for the same study region and period, using the RGI 6.0 glacier outlines. Our mass balance rate of -0.40 ± 0.15 m w.e. yr^{-1} is in agreement with theirs. If we use their refined glacier inventory, we find a mass balance rate of -0.44 ± 0.15 m w.e. yr^{-1}, in even better agreement with their study.

Comparison with published local glaciological and geodetic estimates in the Dry and Tropical Andes

In the Dry and Tropical Andes only a few glaciological mass balance measurements and geodetic estimates are available for comparison over glaciers smaller than 2 km^2 (Basantes-Serrano et al., 2016; Mölg et al., 2017; Rabatel et al., 2011, 2013a, 2017; Soruco et al., 2009b). In addition, published geodetic estimates in this region rarely cover the 2010s. This is problematic as the ASTERIX method, although efficient for region-wide estimates, may present large uncertainties for small glaciers (typically smaller than 2 km^2) due to the relatively high noise level in the rate-of-elevation-change maps. Thus, we can only perform a qualitative comparison of the overall glacier signal.

By combining the available information (mostly glaciological) from the few monitored small glaciers in the Tropical Andes, Rabatel et al. (2013a) provided an average surface mass balance rate value of about -0.75 ± 0.37 m w.e. yr^{-1} for the period 2000-2008. Our ASTERIX regional mass balance rate estimate for the period 2000–2009 is less negative (-0.46 ± 0.27 m w.e. yr^{-1}). The difference is largely explained by the fact that Rabatel et al. (2013a) estimates are based on the extrapolation of a limited sample of mostly small glaciers, whereas ASTERIX also includes large glaciers known to present almost twice less negative surface mass balance rates (Rabatel et al., 2013a). In the Dry Andes, the few available direct and geodetic measurements support our findings of a shift from slightly positive to strongly negative mass balances rates after 2009 (Rabatel et al., 2011; Masiokas et al., 2016; Burger et al., 2018; Farías-Barahona et al., 2019). In addition, the mass balance record from Echaurren Norte glacier (33°S), the longest in the Southern Hemisphere, shows slightly positive mean annual mass balances (0.2 m w.e. yr^{-1} on average) between 2000 and 2009, but a significant reduction to about -1.2 m w.e. yr^{-1} afterwards (WGMS, Masiokas et al., 2016) .

3.8 A detail comparison with Braun et al. (2019) mass balance rates in the Andes

Braun et al. (2019) recently published mass balance rate estimates for the entire Andes by comparing TanDEM-X and SRTM radar DEMs for the period 2000-2011/15. To compare their results to ours and discuss the strength and weakness of each method, we used ASTERIX elevation change trends (dh/dt) for the period 2000-2015 and aggregated our results for the sub-regions considered in their study. First, we compare region-wide mass balance rates using both methods (section 3.8.1) and the maps of dh/dt for selected glaciers in the Tropical, Desert and Central Andes (section 3.8.2). Then we discuss the influence of the radar signal penetration (section 3.8.3), and perform some sensitivity tests to assess the impact of data gaps (section 3.8.4) and the post-processing filters used to exclude outliers (section 3.8.5) on the regional mass balance rate.

3.8.1 Comparison of ASTERIX vs TanDEM-X estimates in the Andes

A summary of TanDEM-X 2000-2011/15 and ASTERIX 2000-2015 results is displayed in Table 3.7. We note that the outlines considered as "NPI only" and "SPI only" by Braun et al. (2019) (referred as NPI and SPI in this section) include in fact many surrounding glaciers that are not part of the icefields sensu stricto. These values are therefore not comparable to previous estimates that consider NPI or SPI sensu stricto. This is why we included in Table 3.7 the ASTERIX mass balance rates for the icefields sensu stricto and the icefields as defined by Braun et al. (2019).

Table 3.7: ASTERIX vs TanDEM-X mass balance rate estimates for the sub-regions defined by Braun et al. (2019). ASTERIX estimates correspond to the period 2000-2015 in order to match the TanDEM-X 2000-2011/15 period

ID	Region name	Glacier area (km^2)	ASTERIX $\dot{M}$ rate 2000-2015 (m w.e. y^{-1})	TanDEM-X $\dot{M}$ rate (m w.e. y^{-1})	Area measured ASTERIX (%)	Area measured TanDEM-X (%)
01	Inner tropics	174	-0.40 ± 0.26	-0.17 ± 0.11	70	75
02	Outer tropics (Peru)	685	-0.23 ± 0.23	-0.01 ± 0.14	90	42
03	Outer tropics (Peru-Bolivia)	1269	-0.54 ± 0.24	-0.34 ± 0.08	93	62
04	Outer tropics (Peru-Bolivia)	141	-0.28 ± 0.21	-0.20 ± 0.08	97	91
05	Desert Andes	397	-0.15 ± 0.19	0.02 ± 0.15	98	96
06	Central Andes	1656	-0.31 ± 0.20	-0.09 ± 0.11	97	87
07	Lake District	457	-0.33 ± 0.21	-0.05 ± 0.09	97	95
08	Patagonia North	6953	-0.73 ± 0.25	-0.65 ± 0.07	80	79
081	NPI	4649	-0.88 ± 0.26	-0.85 ± 0.07	74	85
	NPI sensu stricto *	3917	-0.98 ± 0.27	-	71	-
09	Patagonia South	15102	-0.84 ± 0.28	-0.79 ± 0.06	63	92
091	SPI	13230	-0.90 ± 0.29	-0.86 ± 0.08	60	94
	SPI sensu stricto *	12299	-0.96 ± 0.29	-	59	-
10	Gran Campo Nevado and Isla Riesco	1254	-0.55 ± 0.29	-0.23 ± 0.05	25	89
11	Tierra del Fuego	3538	-0.52 ± 0.27	-0.27 ± 0.03	58	82
Total Andes		31626	-0.69 ± 0.17	-0.58 ± 0.07	69	85

* Outline from RGI 6.0 for NPI and SPI considering the Icefields sensu stricto, i.e. excluding all surrounding mountain glaciers.

Even though regional mass balance rate estimates agree within error bars, the TanDEM-X estimates are systematically less negative than the ASTERIX estimates. The ASTERIX error bars are larger than the TanDEM-X ones. This is due to our conservative, but relatively well validated approach for the uncertainty calculation (e.g. Brun et al., 2017; Berthier et al., 2018). The resulting ASTERIX Andes-wide mass balance rate is -0.69 ± 0.17 m w.e. yr^{-1}, 0.11 m w.e. yr^{-1} more negative than for TanDEM-X. It converts to a 10 % larger contribution to sea level rise than in Braun et al. (2019) (considering both time periods to be 15 years).

In the Tropical Andes (regions 01-04), region 04 presents the smallest mass balance rate differences (0.08 m w.e. yr^{-1}), and presents similar hypsometric distribution of dh/dt (Figure 3.14). For regions 01, 02 and 03, ASTERIX mass balance rates are systematically more negative by at least 0.2 m w.e. yr^{-1}. In the Tropics in general, the percentage measured area is larger for ASTERIX. For example, our coverage reaches 90 % in region 02, versus 42 % in the TanDEM-X study.

In regions 05 to 07, the coverage is high for both methods, often over 90 % of the glacier area. Differences in dh/dt are observed at all elevation bands for all three regions with, notably, the presence of

positive values in the upper and lower elevation bands of TanDEM-X curves (Figure 3.14). In the Lake District (region 07), TanDEM-X dh/dt are almost zero for all elevation bands, while ASTERIX shows considerably lower values and a 0.28 m w.e. yr^{-1} more negative regional mass balance rate. The same happens in the Central Andes with dh/dt consistently less negative for the TanDEM-X case at lower elevations, and even positive dh/dt values above 5000 m.a.s.l. (see section 3.8.3).

Patagonia North and Patagonia South show good agreement of methods. Patagonia South mass balance rate estimate is 0.05 m w.e. yr^{-1} more negative for ASTERIX, mainly a results of the more negative dh/dt values in the lower altitude bands (see section 3.8.5). The mass balance rates for the NPI and SPI are 0.06 and 0.10 m w.e. yr^{-1} more negative when surrounding mountain glaciers are excluded from the outlines. This result illustrate the importance of using the exact same definition of the icefield when comparing different studies and show that the two largest icefields are thinning at considerably higher rate than the surrounding smaller glaciers.

For all regions south of NPI, the ASTERIX coverage is much lower. Region 10 presents the lowest coverage for our method with only 25 % of the glacierized area sampled, casting doubts about the robustness of our estimate (see Section 3.8.4). Finally, in Tierra del Fuego (region 11), ASTERIX mass balance rate is 0.25 m w.e. yr^{-1} more negative than the TanDEM-X estimate, with a coverage of nearly 60 % (vs. 80 % for the TanDEM-X study).

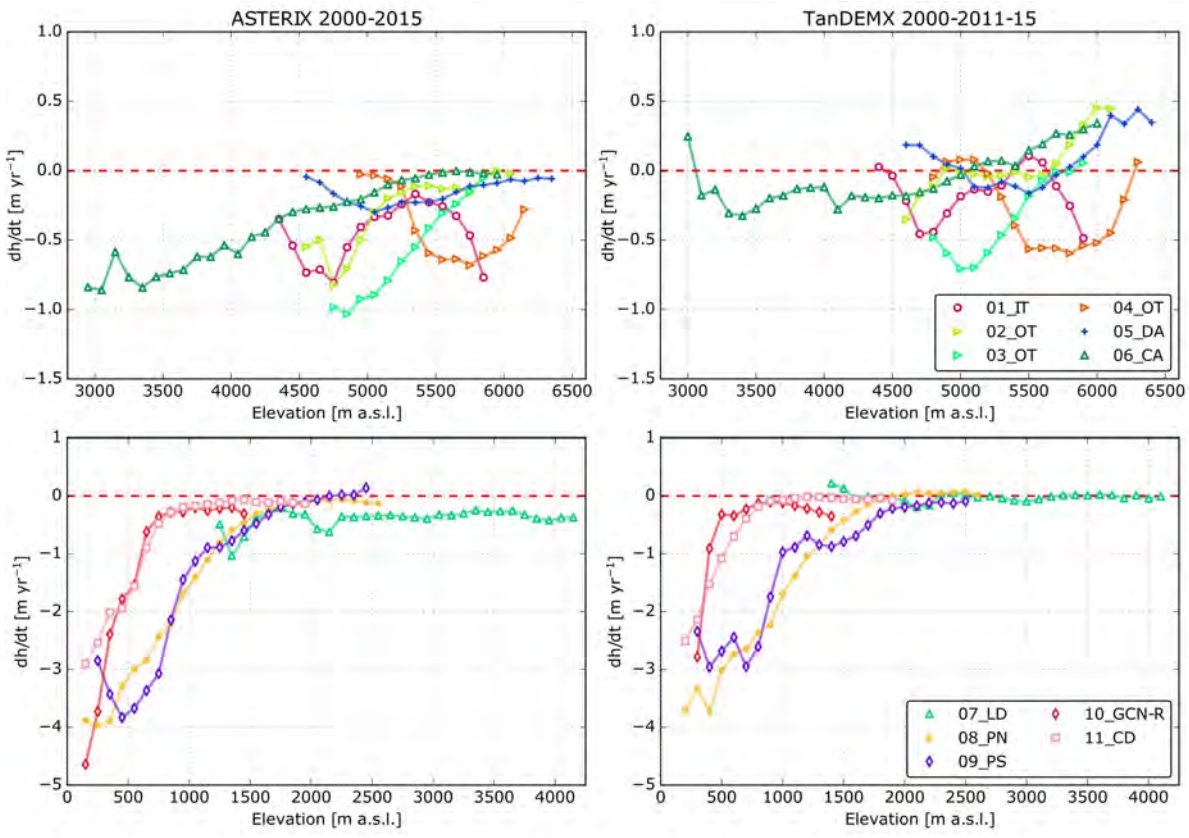

Figure 3.14: ASTERIX 2000-2015 vs TanDEM-X 2000-2011/15 elevation change trends as function of elevation for Andes sub-regions defined by Braun et al. (2019). All curves are filtered to the elevations of the 1st and 99th percentile of the glacierized area respectively. To help visualization of the different regions we separated the graph on two different elevation ranges, with the northern regions at higher altitudes in the top and southernmost regions with lower elevations below. Note different y-axis for the upper and lower panels.

3.8.2 Selected ASTERIX and TanDEM-X elevation change maps for the Tropical and Dry Andes

We selected specific glacier areas in the Inner Tropics, Outer Tropics, Desert Andes and Central Andes to compare side by side the ASTERIX vs. TanDEM-X dh/dt maps (Figures 3.15 and 3.16). These locations were chosen to include well-known glaciers, close to areas where glaciers are monitored. They are generally also representative of the noise level of the two methods for the Tropical, Desert and Central Andes regions.

In general TanDEM-X dh/dt maps tend to be noisier than ASTERIX dh/dt maps and/or show unexpected patterns in these regions, with some extreme examples for Illimani and Nevado Olivares (Figures 3.15A and 3.15B). In the TanDEM-X dh/dt maps, systematically positive dh/dt values can be observed over the accumulation zones of glaciers with extreme cases like Glacier Tortolas and Tupungato (Figures 3.16A and 3.16C). This apparent thickening is also observed at the regional scale, in the hypsometric curves of the Desert and Central Andes (regions 05 and 06, Figure 3.14). These positive values possibly result from the effect of a differential penetration of the SRTM C-band and TanDEM X-band radar signal over snow and firn surfaces (see section 3.8.3). The positive values of dh/dt in the upper reaches of the glaciers are also suspicious from a dynamical point of view. A dh/dt of 1 m yr^{-1} over 15 years implies an increase in surface elevation by 15 m. Dynamically, such an excess of mass should be balanced by an increase in the ice flux toward the lower part of the glacier resulting in a limited change in the elevation of the glacier surface (Span and Kuhn, 2003).

The dh/dt off-glacier are not provided by Braun et al. (2019) therefore, not allowing to assess the quality of their results in the stable terrains surrounding the glaciers.

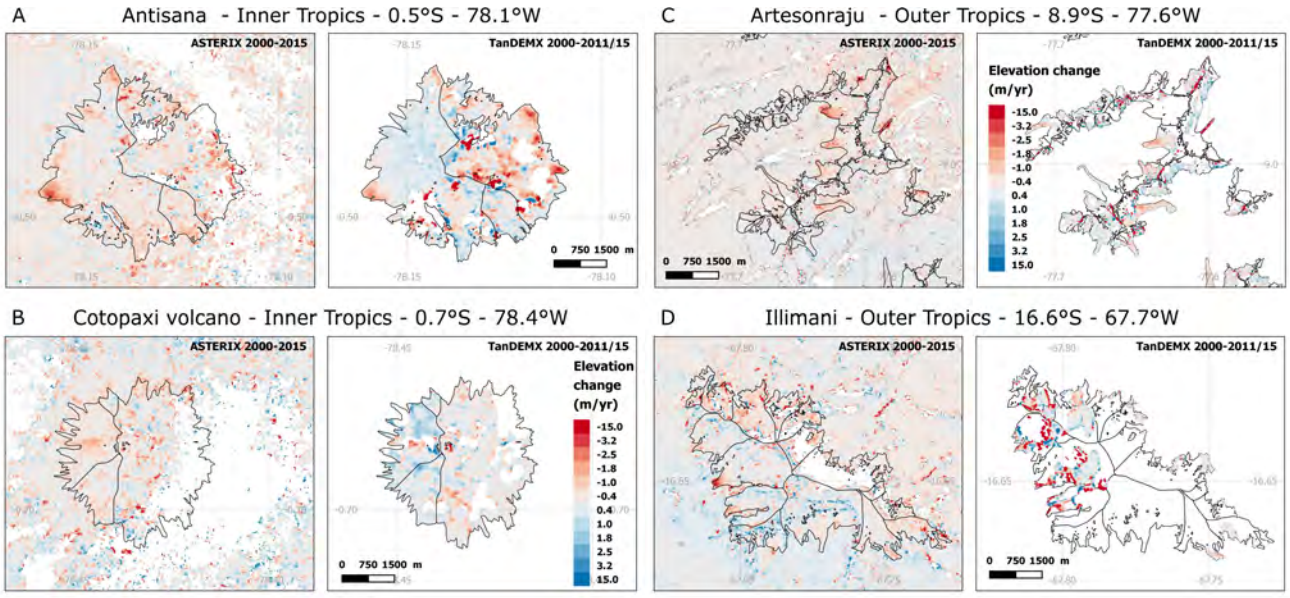

Figure 3.15: ASTERIX 2000-2015 vs Braun et al. (2019) TanDEM-X elevation change maps for (A) Antisana (Ecuador), (B) Cotopaxi Volcano (Ecuador) in the Inner Tropical Andes and (C) Artesonraju (Cordillera Blanca, Peru), (D) Illimani (Cordillera Real, Bolivia) in the Outer Tropical Andes.

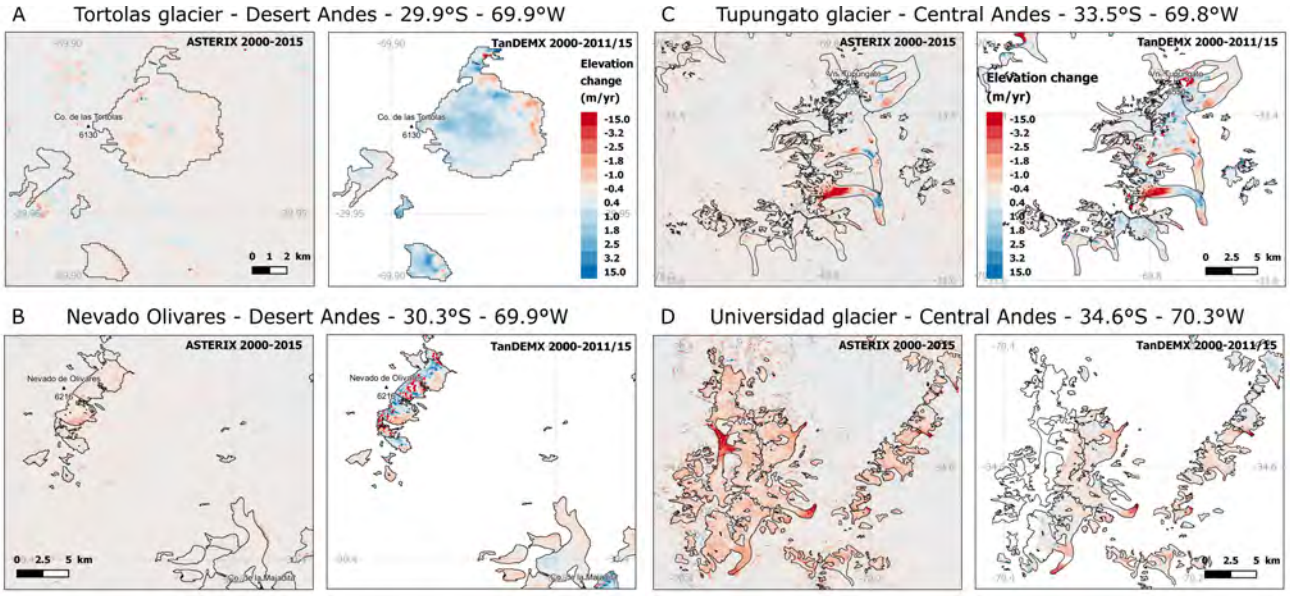

Figure 3.16: ASTERIX 2000-2015 vs Braun et al. (2019) TanDEM-X elevation change maps for (A) Tortolas glacier (Argentina), (B) Nevado Olivares (Chile-Argentina) in the Desert Andes and (C) Tupungato glacier (Argentina) and (D) Universidad glacier (Chile) in the Central Andes.

3.8.3 Penetration of the radar signal

Positive dh/dt values where found at different elevation bands in the TanDEM-X data, mainly in the Central and Desert Andes regions, but also in the Outer Tropics of Peru (region 02). These positive values are unexpected as, to our knowledge, no study has documented glacier thickening during 2000-2015 in these regions so far.

In addition, a paper currently in discussion for The Cryosphere by Braun team shows a strong surface area loss over this period (~27%) which is somehow incompatible with steady state surface mass balance conditions, even considering that the surface area loss over this period could be related to the response time of the glaciers and a former period of very strong mass loss. In line with the latter argument, several studies about tropical glaciers have shown that their response time is usually short (i.e. few years) due to the peculiar surface mass balance regime, with ablation occurring all year long in the lowermost part of the glacier tongues (e.g. Kaser, 2001; Francou et al., 2004, 2003; Rabatel et al., 2013a; Vuille et al., 2008)

Previous studies have shown that anomalous positive dh/dt values can occurs when the SRTM DEM is used as the initial glacier topography and penetration of the radar signal into snow and ice is not properly taken into account (Berthier et al., 2006, 2018; Dussaillant et al., 2018). Further, under similar (winter) cold firn conditions, the SRTM C-band penetration depth at high altitude (above 2500 m a.s.l.) has been shown to be almost twice as large as for TanDEM-X X-band over glaciers in the Alps, with mean values of 8.6 - 9.8 m (highest values of 12 m, Berthier et al., 2016) and 4 m (highest values of 7 m, Dehecq et al., 2016) respectively. The SRTM was acquired in the core of the summer (February) in the southern hemisphere, so liquid water can be expected in the snowpack and the amount of radar penetration should be limited. However, this assumption has only been verified in Patagonia so far (Dussaillant et al., 2018; Jaber et al., 2013, 2016), not elsewhere.

The ASTERIX method provides a first order estimate of the SRTM C-band penetration (Berthier et al., 2016; Dussaillant et al., 2018; Wang and Kääb, 2015). By extrapolating the ASTERIX dh/dt trends to the date of acquisition of the SRTM (February 2000) we can derive a reconstructed SRTM DEM (referred to as "SRTMrec"). Differencing SRTMrec with the original SRTM DEM allows estimating the C-band

radar signal penetration map. We performed this analysis in the Desert and Central Andes regions (regions 05 and 06 in Braun et al. (2019)). A similar analysis could not be performed for the TanDEM-X DEMs as they are not freely available, and the precise acquisition dates is not unique. The corresponding SRTMrec-SRTM dh curves, together with the regional hypsometric dh/dt for both ASTERIX and TanDEM-X methods, are shown in Figure 3.17.

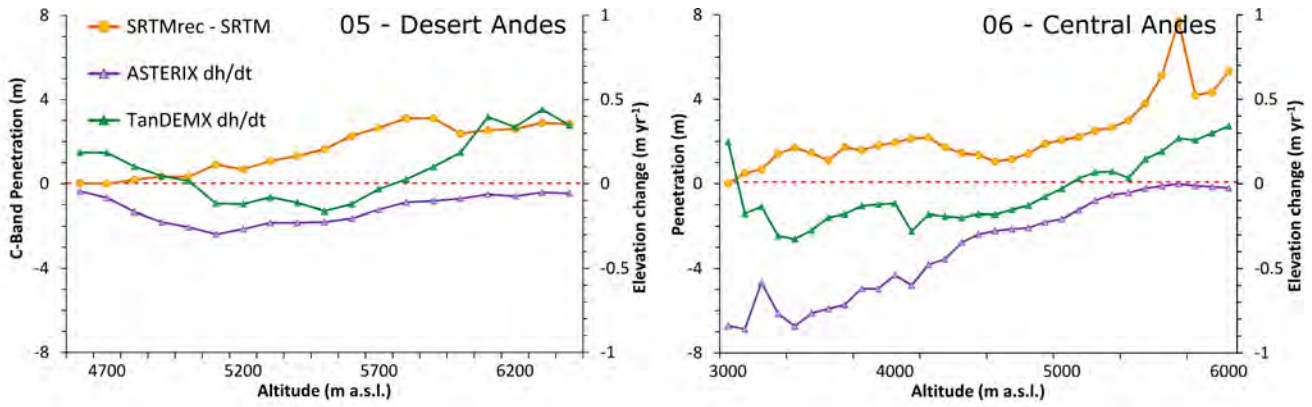

Figure 3.17: SRTM C-Band penetration depth analysis. Hypsometric distribution of ASTERIX (purple) and TanDEM-X (green) dh/dt curves (m yr^{-1}), and SRTMrec-SRTM (orange) dh curves (m), for the Desert Andes region 05 and Central Andes region 06.

When SRTMrec-SRTM curves are equal to zero, we interpret it has no or limited penetration of the C-band. Conversely, positive values indicate the penetration depth magnitude with an uncertainty assumed, conservatively, to be around 3 m (Berthier et al., 2016). The SRTMrec-SRTM curves present positive values along the entire elevation range of Central and Desert Andes glacierized surface (Figure 3.17). More specifically, in the Desert Andes penetration increases with altitude from ~0 m at 4800 m a.s.l. to up to 3 m above 6000 m a.s.l. with a regional mean of 1.6 m. In the Central Andes penetration is larger with a mean of 1.9 m, and a maximum of 4-8 m above 5500 m a.s.l.. Surprising penetration depths of up to 2 m are observed at lower elevations, below 4000 m a.s.l.

We have no mean to assess the penetration of the Tandem-X radar signal. If we assume the X-Band penetration to be half the one of the C-Band (Round et al., 2017), we deduce a differential penetration of about 0.8 m in the Desert Andes and 1 m in the Central Andes. Given the maximum time difference of 15 years between the SRTM and the TanDEM-X DEMs, it results in a possible systematic and positive bias on the dh/dt of 0.05 and 0.07 m a-1, explaining a fraction only of the dh/dt and mass balance rate differences observed in Figure 3.14 and Table 3.7 between the TanDEM-X and ASTERIX methods. The rest of the differences may come from the difference in time periods (15 years considered here for ASTERIX and something between 11 and 15 years for TanDEM-X) given that the mass balance rates as evolved towards more negative values after 2009.

More generally, regions 01 to 07 show consistently less negative TanDEM-X dh/dt and regional mass balance rate estimates than those obtained using ASTERIX. Glaciers through all these regions are distributed at high altitudes (always above 2500 m a.s.l., often above 5000 m a.s.l.) where the presence of dry and cold snow likely results in differential radar signal penetration. We suggest that radar penetration occurs in these regions, and is larger for the C-Band than for the X-Band, leading to a likely bias in the TanDEM-X estimates.

In Patagonia, penetration of the SRTM C-Band signal was shown to be negligible, except for the highermost altitudes, where the glacierized area is small and, thus, does not affect regional mass balance rate estimates (Dussaillant et al., 2018; Jaber et al., 2013). This is confirmed by the lack of systematic differences between TanDEM-X and ASTERIX dh/dt curves (Figure 3.14) in the accumulation areas of these glaciers.

3.8.4 sensitivity of ASTERIX mass balance rates to data gaps

One of the major weaknesses of using DEMs derived from optical images to observe glacier mass balance rates comes from the potentially high number of voids in the DEMs, due to the presence of clouds on images and the lack of correlation over textureless surfaces, such as areas covered by bright snow. These two issues are particularly prominent for the large Patagonian icefields, resulting in elevation change maps with high amount of unreliable elevation pixels considered as data gaps (e.g. 26 % and 40 % of the NPI and SPI surfaces, for ASTERIX 2000-2015 dh/dt maps, Table S5). Radar derived DEMs avoid both these problems, as radar signal is not affected neither by clouds nor by the homogeneity of the ice surface, being able to obtain almost full dh/dt maps.

The availability of an almost complete map of dh/dt from radar data (Braun et al., 2019) offers a unique opportunity to evaluate the influence of data gaps on the mass balance rates following the strategy of McNabb et al. (2019). We selected three relevant regions where the ASTERIX maps present a large percentage of data gaps: the NPI, the SPI and the Fuegian Andes. For the sake of comparison, we used the same NPI and SPI glacier outlines as Braun et al. (2019) and the glacier outlines from their region 11 (Tierra del Fuego).

Mass balance rate is calculated for every individual glacier using the local hypsometric approach (McNabb et al., 2019). The regional mass balance rate is the area-weighted sum of all glaciers in the region. We computed regional mass balance rates for four different cases: (A) TanDEM-X full dh/dt grid; (B) TanDEM-X dh/dt grid with ASTERIX 2000-2018 data gaps; (C) TanDEM-X dh/dt grid with ASTERIX 2000-2009 data gaps; (D) TanDEM-X dh/dt grid with ASTERIX 2009-2018 data gaps. An example of these four cases is shown in Figure 3.18 for SPI, and all results are shown in Table 3.8.

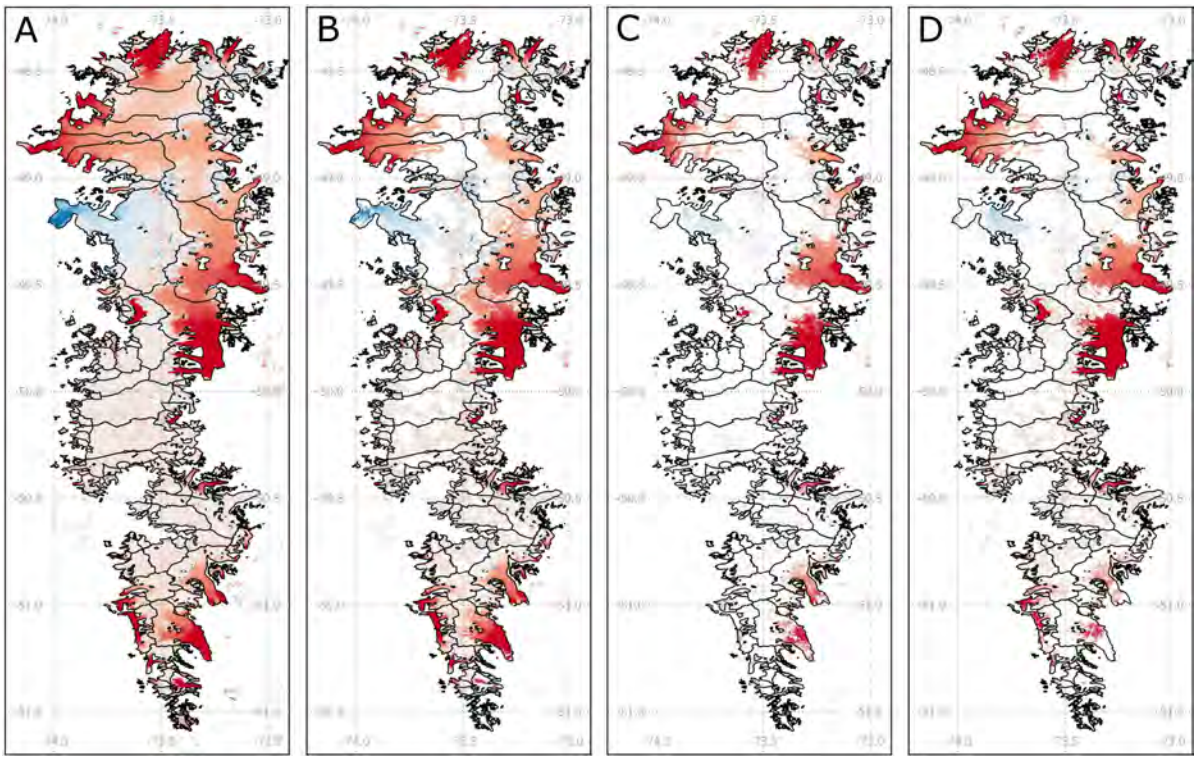

Figure 3.18: Example of the elevation change maps used for the SPI data gap sensitivity test. All maps correspond to the dh/dt trends obtained by Braun et al. (2019) using TanDEM-X DEMs for the period 2000-2011/15. Subfigures correspond to the different scenario tested, where (A) TanDEM-X full dh/dt grid; (B) TanDEM-X dh/dt grid with ASTERIX 2000-2018 data gaps; (C) TanDEM-X dh/dt grid with ASTERIX 2000-2009 data gaps; (D) TanDEM-X dh/dt grid with ASTERIX 2009-2018 data gaps.

Table 3.8: Mass balance rate and percentage of measured area for the NPI, SPI and Tierra del Fuego under four hypothetic cases of data gaps.

Region	Input data	$\dot{M}$ (m w.e. yr^{-1})	Measured area (%)
NPI*	TanDEM-X full trend	-0.85**	81
	TanDEM-X trend + ASTERIX 2000-2018 data gaps	-0.84	63
	TanDEM-X trend + ASTERIX 2000-2009 data gaps	-0.84	52
	TanDEM-X trend + ASTERIX 2009-2018 data gaps	-0.83	56
SPI*	TanDEM-X full trend	-1.02**	88
	TanDEM-X trend + ASTERIX 2000-2018 data gaps	-0.97	61
	TanDEM-X trend + ASTERIX 2000-2009 data gaps	-1.36	24
	TanDEM-X trend + ASTERIX 2009-2018 data gaps	-0.94	37
Tierra del Fuego	TanDEM-X full trend	-0.42**	76
	TanDEM-X trend + ASTERIX 2000-2018 data gaps	-0.41	57
	TanDEM-X trend + ASTERIX 2000-2009 data gaps	-0.40	20
	TanDEM-X trend + ASTERIX 2009-2018 data gaps	-0.11	4

* Outlines for NPI and SPI as used in Braun et al. (2019).

** Note that the mass balance rate listed here are not exactly the same as published in Braun et al. (2019). This is because here we calculate the mass balance rate for each individual glaciers first while Braun et al. (2019) compute directly the mass balance for the entire region. This issue is further considered in Section 3.8.5 below.

There is a good agreement on the NPI for all four cases. Even if half of the NPI area is not measured (period 2000-2009), the sampling of the different glaciers by the ASTERIX method is sufficient to compute the icefield mass balance rate with a difference lower than 0.02 m w.e. yr^{-1} compared to the full TanDEM-X grid. We can therefore assume that the uncertainty due to data gaps is negligible in the NPI for all time periods observed in this study (2000-2018, 2000-2009 and 2009-2018), validating our corresponding ASTERIX estimates on the NPI.

The SPI mass balance rates are in good agreement for cases (A), (B) and (D), but not for the (C) case corresponding to 2000-2009 (Figure 3.18C). In this period, only 24% of the SPI surface is covered in ASTERIX dh/dt map (76% data gaps), and only the lower glacier tongues, presenting strongly negative dh/dt trends, are well represented. As a result, the regional mass balance rate of the icefield is too negative (-1.36 m w.e. yr^{-1}) compared to the full TanDEM-X grid (-1.02 m w.e. yr^{-1}). We can be confident of our ASTERIX SPI mass balance rate estimate for the 2000-2018 period and 2009-2018 sub-period, but we anticipate larger errors in the 2000-2009 period, where the mass loss is likely overestimated due to the uneven distribution of the data gaps.

Similarly in Tierra del Fuego, case (D) where TanDEM-X dh/dt trends are masked with ASTERIX 2009-2018 data gaps (only 4% of the total ice surface is covered), does not agree with other cases, leading to a mass balance rate of -0.11 m w.e. a^{-1} compared with -0.42 m w.e. a^{-1} with the full TanDEM-X grid. Once again, we anticipate larger errors for this sub-period, while we can be confident in the ASTERIX 2000-2018 and 2000-2009 mass balance rates.

To conclude, the ASTERIX sampling is sufficient to compute confidently the mass balance rate for the complete study period (2000-2018) even in a region (Patagonia) where the issue of data gaps is important. Caution is required when observing shorter time periods (at least in the SPI and Tierra del Fuego), where the distribution of data gaps might probably either underestimate or overestimate the actual loss. Outside of Patagonia, the percentage of data gaps is much smaller (Table 3.7) and so we are confident that the effect is even smaller.

3.8.5 Post processing of the elevation change maps

Influence of the 3NMAD regional filter

The regional 3NMAD (normalized median absolute deviation) filter is a post processing technique to exclude outliers in elevation change maps (Braun et al., 2019; Brun et al., 2017). The principle of this filter is to exclude all values lying outside from three NMAD from the median dh/dt of a given elevation band. Data gaps (from the original map or created by the 3NMAD filter) are then filled using the mean dh/dt in each elevation band.

This technique can be applied locally (individual glacier) or regionally (considering all individual glaciers as a single body of ice). The 3NMAD filter is robust when the distribution of elevation changes is symmetrical. For the case of a normal distribution, it excludes less than 1% of the data. This assumption of symmetry generally holds for elevation bands on individual glaciers, or in regions where the variability of glacier response is small and glaciers vary similarly with elevation. However, this is not the case for Patagonian glaciers, where an extreme variability of glacier responses can be observed, with rapidly shrinking glaciers next to glaciers gaining mass, as seen in the SPI and Tierra del Fuego TanDEM-X dh/dt maps (Figures 3.18 and 3.21A).

To quantify the effect of applying the regional 3NMAD filter in Patagonia we use the TanDEM-X nearly complete dh/dt grids (Braun et al., 2019) over the two Patagonian icefields, NPI and SPI, and over the Tierra del Fuego region. These three regions contain altogether 67% of all Andes glaciers in area (considering Braun et al. (2019) outlines).

Starting from the TanDEM-X dh/dt maps we compared the rate of elevation changes within 100 m elevation bands and the region-wide mass balance rates using, (i) the regional mean dh/dt for every 100 m elevation band (hereafter referred as NO-3NMAD filter case); and (ii) the mean dh/dt for every 100 m elevation band applying a regional 3NMAD filter to exclude outliers (hereafter referred as 3NMAD filter case). Results are displayed in Figures 3.19, 3.20 and 3.21 for the NPI, SPI and Tierra del Fuego respectively and regional mass balance rates are listed in Table 3.9.

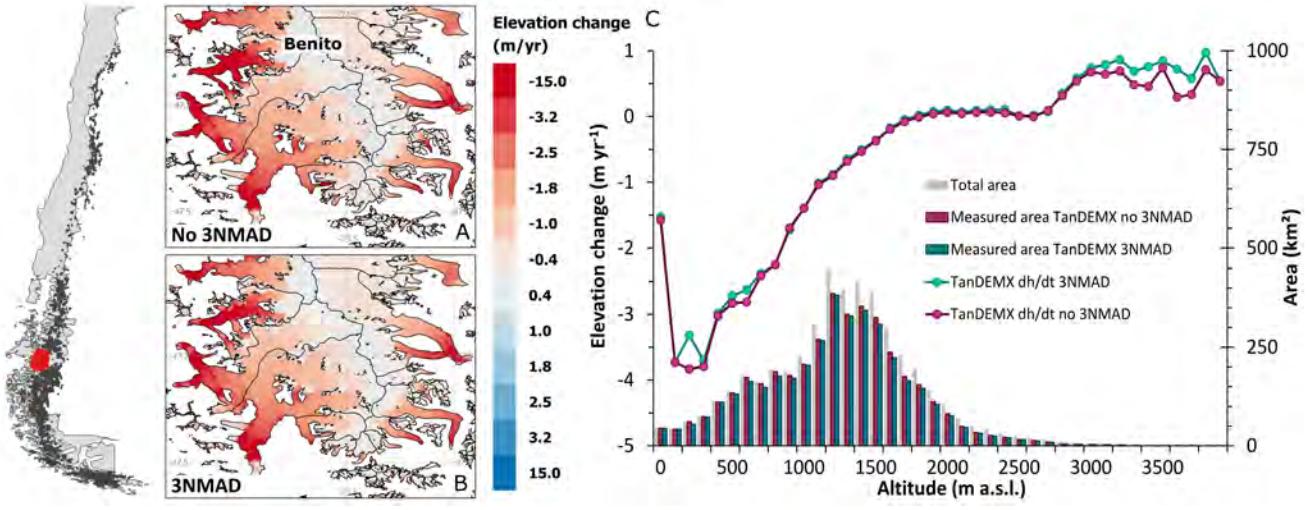

Figure 3.19: Influence of the 3NMAD regional filter on the NPI. (A) TanDEM-X dh/dt map for the southern part of the NPI, NO-3NMAD filter. (B) TanDEM-X dh/dt map for the southern part of the NPI, using the 3NMAD filter. (C) TanDEM-X hypsometric dh/dt (average of a 100 m elevation band) for the entire NPI, for NO-3NMAD filter (purple) and 3NMAD filter (blue).

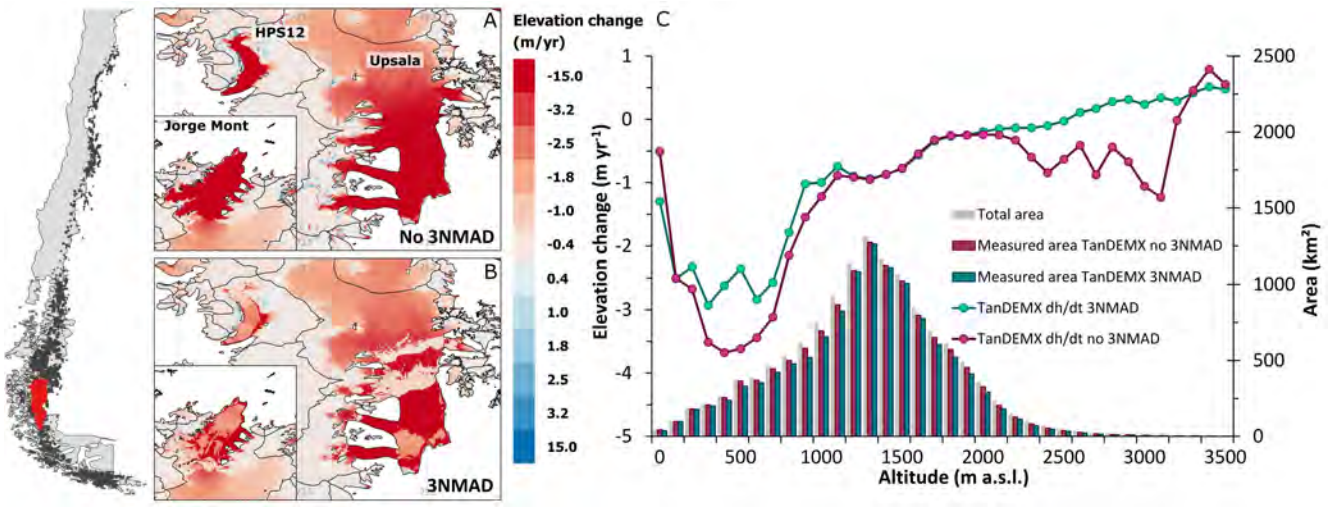

Figure 3.20: Influence of the 3NMAD regional filter on the SPI. (A) TanDEM-X dh/dt map for Jorge Mont, HPS12 and Upsala glaciers in the SPI, NO-3NMAD filter. (B) TanDEM-X dh/dt map for Jorge Mont, HPS12 and Upsala glaciers in the SPI, using 3NMAD filter. (C) TanDEM-X hypsometric dh/dt (average of a 100 m elevation band) for the entire SPI, for NO-3NMAD filter (purple) and 3NMAD filter (blue).

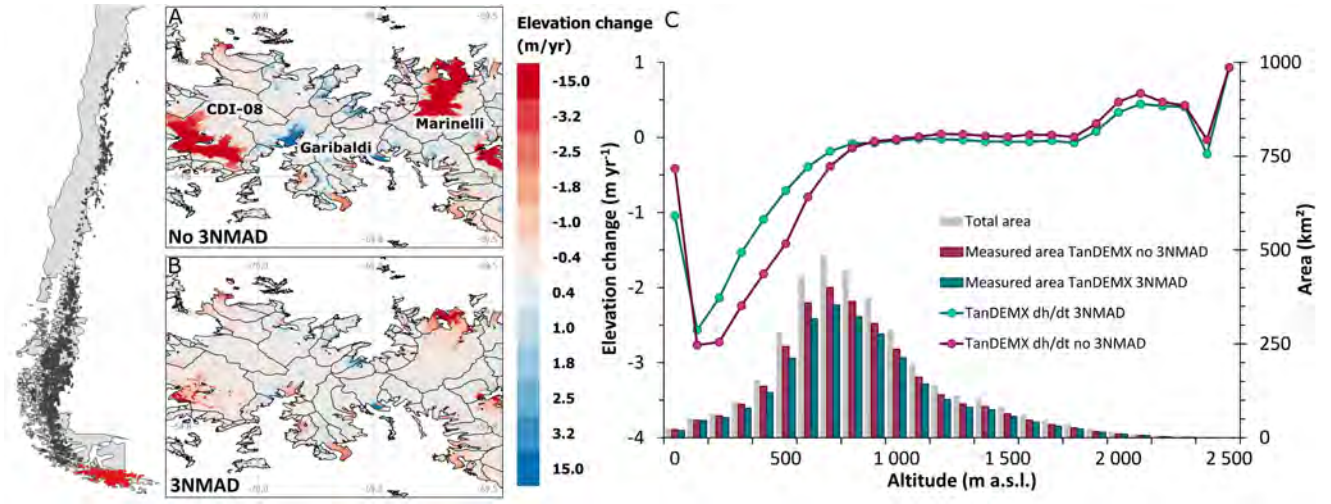

Figure 3.21: Influence of the 3NMAD regional filter on Tierra del Fuego. (A) TanDEM-X dh/dt map for Marinelli, Garibaldi and CDI-08 glaciers in Cordillera Darwin, NO-3NMAD filter. (B) TanDEM-X dh/dt map for Marinelli, Garibaldi and CDI-08 glaciers in Cordillera Darwin, using 3NMAD filter. (C) TanDEM-X hypsometric dh/dt (average of a 100 m elevation band) for the entire Tierra del Fuego region, for NO-3NMAD filter (purple) and 3NMAD filter (blue).

Table 3.9: Mass balance rates and measured areas for the NPI, SPI and Tierra del Fuego calculated from the TanDEM-X dh/dt using 3NMAD and NO-3NMAD regional filter. Results published in Braun et al. (2019) for this regions are also included for comparison.

Region	Input data	$\dot{M}$ (m w.e. yr^{-1})	Measured area (%)
NPI*	TanDEM-X no 3NMAD	-0.88	86
	TanDEM-X 3NMAD	-0.85	83
	Braun et al. (2019) 3NMAD	-0.85	85*
SPI*	TanDEM-X no 3NMAD	-1.02	94
	TanDEM-X 3NMAD	-0.86	90
	Braun et al. (2019) 3NMAD	-0.86	94*
Tierra del Fuego	TanDEM-X no 3NMAD	-0.43	83
	TanDEM-X 3NMAD	-0.28	74
	Braun et al. (2019) 3NMAD	-0.27	82*

* The percentage measured area from Braun et al. (2019) was calculated by those authors from the complete dh/dt grids, not taking into account the excluded pixels due to the 3NMAD filter. This is why there are almost identical to the case NO-3NMAD.

Generally, the 3NMAD filter is excluding pixels with extreme dh/dt values (positive or negative) with respect to the regional distribution of each given elevation band. The effect is thus strong over glaciers which are losing or gaining mass at faster rates than the region as a whole, for example Benito Glacier in NPI (Figure 3.19); HPS12, Jorge Mont and Upsala glaciers in SPI (Figure 3.20); and Marinelli and Garibaldi glaciers in Tierra del Fuego (Figure 3.21). Even though the TanDEM-X dh/dt are almost full over these glaciers, the filter is generating large data gaps, excluding areas of large elevation change, and replacing them with the regional mean. This effect can be clearly seen over these side to side maps (especially Figure 3.20 A and B and Figure 3.21 A and B), where a stripping effect resulting from the gap filling by erroneous values can be seen (e.g. Upsala, HPS12 and Marinelli Glaciers).

The effect is negligible on the NPI, where only Benito Glacier is affected. The distribution of the dh/dt trends in the NPI is relatively homogeneous. consequently, even though 3% of the measured area is excluded by the 3NMAD filter, the regional mass balance rate is only changed by 0.03 m w.e. yr^{-1} (-0.88 m w.e. yr^{-1} with NO-3NMAD filter to -0.85 m w.e. yr^{-1} with 3NMAD filter, Table 3.9).

As the variability of glacier responses is larger in the SPI and Tierra del Fuego, the effect of the 3NMAD filter is stronger. The hypsometric curves (Figures 3.20C and Fig 3.21C) in both regions suggest that the dh/dt are being strongly underestimated at lower elevation bands as a result of the regional 3NMAD filter applied to highly non-symmetrical distributions. These bands represent a considerable fraction of the glacier surface, so the corresponding regional mass balance rate is severely underestimated as well. In the SPI, the regional mass balance rate, originally at -1.02 m w.e. yr^{-1} in the NO-3NMAD filter case, is changed to -0.85 m w.e. yr^{-1} when the 3NMAD filter is applied. Similarly in the Tierra del Fuego, applying the 3NMAD regional filter leads to an underestimation of the regional mass balance rate by 0.15 m w.e. yr^{-1} (Table 3.9).

Overall, we conclude that the 3NMAD filter should not be applied at the regional scale, especially in regions where a large variability of glacier behavior is observed. A consequence is that the Braun et al. (2019) mass balance rate estimate are biased positively in these regions.

ASTERIX and TanDEM-X mass balance rates obtained with the same processing of dh/dt grids

Finally, we applied the local hypsometric approach to both ASTERIX and TanDEM-X dh/dt grids (the 3NMAD filter is applied locally to individual glacier elevation bands) and the resulting regional mass

balance rate corresponds to the area weighted sum of all glaciers. The TanDEM-X and ASTERIX 2000-2015 mass balance rates for NPI, SPI and Tierra del Fuego are in good agreement despite the data gaps in the ASTERIX dh/dt grids (Table 3.10). This is an encouraging result for a region, Patagonia, where the quality of optical DEMs does not match the one of radar derived DEMs like TanDEM-X.

Table 3.10: ASTERIX and TanDEM-X mass balance rates processed the same way, i.e. computing the mass balance for individual glaciers and not applying a 3NMAD regional filter.

Region name	$\dot{M}$ rate (m w.e. y^{-1})		Area measured (%)	
	ASTERIX 2000 - 2015	TanDEM-X 2000 – 2011/15	ASTERIX 2000 - 201	TanDEM-X 2000 – 2011/15
NPI	-0.88 ± 0.26	-0.85	74	81
SPI	-0.90 ± 0.29	-1.02	60	88
Tierra del Fuego	-0.52 ± 0.27	-0.42	58	73

3.9 Ongoing work: deriving frontal ablation in Patagonia

3.9.1 A method to calculate frontal ablation

Calving glaciers constitute a great majority of large glaciers in the Patagonian Andes (Warren and Aniya, 1999), accounting for most than half of the total Andes glacierized area. Frontal ablation is known to play an important role in the total mass budget of glaciers that terminate in deep lakes or the ocean (Sakakibara and Sugiyama, 2014; Truffer and Motyka, 2016). Still, due to the complexity of the processes involved, the components of frontal ablation are difficult to measure. Correctly quantifying calving rates on tidewater glaciers is still one of the key uncertainties in sea level rise projections (Luckman et al., 2015).

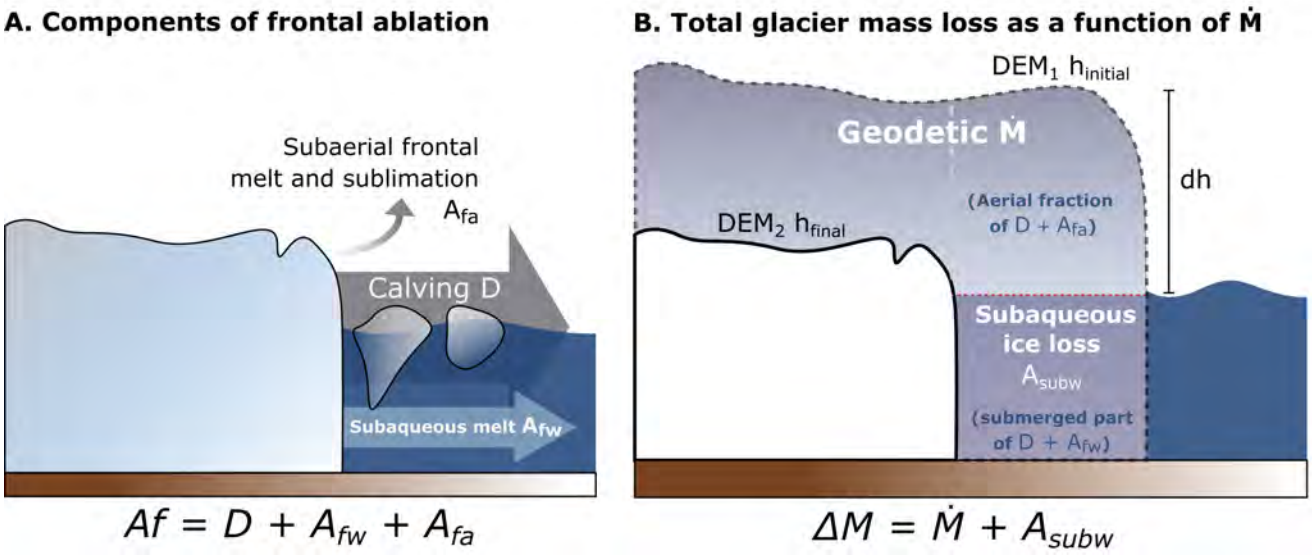

Figure 3.22: Conceptual diagrams presenting (A) the components of frontal Ablation, where Af is the frontal ablation and is equal to the sum of Calving (D), Subaqueous melt (Afw) and subaerial frontal melt and sublimation (Afa); **and (B) The total glacier mass loss as a function of** $\dot{M}$, where ΔM is the total mass loss and is equal to the sum of the geodetic mass balance and subaqueous mass loss (A_{subw}).

One advantage of the geodetic glacier mass balance estimate (here expressed as $\dot{M}$) is that it permits to calculate frontal ablation in a rather direct way. The total mass budget of glacier (ΔM) can be decomposed as the sum of two main components: the mass losses occurring at the glacier surface (surface

mass balance, SMB) and those occurring at the glacier front (Frontal ablation, Af) which depends on glacier dynamics (Figure 3.22A).

$$\Delta M = SMB + Af \tag{3.3}$$

ΔM can also be expressed as a function of the geodetic mass balance ($\dot{M}$), as shown in Figure 3.22B:

$$\Delta M = \dot{M} + A_{subw} \tag{3.4}$$

Where $\dot{M}$ includes the SMB and the aerial fraction of Frontal ablation (aerial fraction of D + A_{fa}) and the total subaqueous loss A_{subw} corresponds to all ice lost below the waterline (subaqueous fraction of D + Afw). We can therefore calculate Frontal ablation as the residual of the difference between ($\dot{M}$ + A_{subw}) and SMB:

$$Af = (\dot{M} + A_{subw}) - SMB \tag{3.5}$$

We used this relation to calculate frontal ablation for all Andean fresh-water (lake terminating) and tide-water (ocean terminating) calving glaciers using our ASTERIX Andes-wide geodetic estimate, together with a first order subaqueous mass loss estimates for Patagonian glaciers from Braun et al. (2019) and modelled SMB estimates by Marzeion et al. (2015) for the period 2000-2015. Due to the temperate climatic conditions in Patagonia, the contribution of A_{fa} to frontal ablation is very small and can be neglected. However, A_{fw} may become an important source of ablation depending on the temperature and circulation of the water at the pro-glacial water body (Truffer and Motyka, 2016). Here, we assume that regional A_{fw} is negligible compared with the regional calving rates in all Patagonian glaciers, so our estimate of frontal ablation is representing calving rates only. Nevertheless, for individual glaciers where A_{fw} could represent a substantial fraction of the mass loss, our estimate will most likely correspond to the sum of D and A_{fw}.

3.9.2 Choosing the right SMB Andes estimate

Several studies have estimated SMB in the Andes for different time periods (e.g. Lenaerts et al., 2014; Marzeion et al., 2015; Mernild and Wilson, 2016; Schaefer et al., 2015, 2013) , most of them covering only the large Patagonian icefields. Mernild and Wilson (2016) simulated the spatiotemporal distribution of SMB along the entire Andes for the period 1979-2014, validated with direct glaciological observations over 25 glaciers with variable observational time periods (only seven larger than 1 km^2). They obtain SMB of -1.13 ± 0.37 m w.e. yr^{-1} for their 35 years period, much more negative than our ASTERIX geodetic estimate for the first two decades of the 21st century (-0.72 ± 0.22 m w.e. yr^{-1}). This difference is unexpected as SMB does not account for mass losses due to frontal ablation and should always be less negative than geodetic estimates when calving glaciers are involved.

Marzeion et al. (2015) provides SMB estimates (hereafter referred as modelled SMB) simulated for almost all Andes individual glaciers, permitting a direct comparison with our ASTERIX estimates at an individual glacier level. In previous section 3.5.3 we compared briefly these estimates over all Andes calving and non-calving glaciers. We found a good agreement over all non-calving glaciers, which gives confidence in the modeling approach, and thus deduced a first order estimate for frontal ablation at 14.7 ± 6.0 Gt yr^{-1}, corresponding to both freshwater and tidewater calving glaciers located mostly in South Patagonia. The next section is based on unpublished work in progress where I decided to go deeper in the comparison between ASTERIX and the modeled SMB from Marzeion et al. (2015).

3.9.3 Comparing ASTERIX $\dot{M}$ and modelled SMB estimates

Results in Table 3.11 were obtained from 11461 glaciers covering 92% of the total Andes glacierized area. We excluded all glaciers glaciers for which less than 20% of the area was covered with dh/dt measurements and mass balance rate errors were higher than 1 m w.e. yr^{-1} for ASTERIX (corresponding to 5% of the total area). The remaining 3% correspond to glaciers with no valid ASTERIX or modelled SMB estimates. Here we discuss the similarity between $\dot{M}$ and SMB over non calving Andean glaciers, where there is no frontal ablation, as a direct measure of the reliability of the SMB estimate.

Table 3.11: Frontal ablation for Andes non-calving and calving glaciers calculated using ASTERIX $\dot{M}$ and modelled SMB for the period 2000-2015 and including subaqueous mass loss estimated by Braun et al. (2019). Non-calving glaciers correspond to land terminating glaciers. Calving glaciers may terminate in lakes (freshwater calving) or in the ocean (tidewater calving). Measured area here corresponds to the relative area covered by glaciers presenting valid values of $\dot{M}$ and SMB used to make the comparison.

Glacier type	Total area (km^2)	Measured area (%)	Number glaciers measured	ASTERIX $\dot{M}$ 2000 - 2015 (Gt yr^{-1})	Modelled SMB 2000 - 2015 (Gt yr^{-1})	A_{subw}** (Gt yr^{-1})	Frontal ablation ($\dot{M}$+A_{subw} - SMB) (Gt yr^{-1})
Non-calving glaciers	14809	86	11277	-5.5 ± 3.3	-4.8	0	-0.7 ± 3.3
Calving glaciers	16862	98	184	-15.9 ± 4.8	-4.3	-3.1 ± 1.2	-14.7 ± 6.0
Freshwater calving	9858	98	114	-11.5 ± 2.9	-2.6	-2.3 ± 0.9	-11.2 ± 3.8
Tidewater calving	7004	97	70	-4.4 ± 1.9	-1.9	-0.7 ± 0.3	-3.2 ± 2.2
TOTAL	31671	92	11461	-21.4 ± 5.8*	-9.1	-3.1 ± 1.2	-15.4 ± 7.0

* Only glaciers containing SMB and ASTERIX estimates considered. The value is thus slightly smaller than the real ASTERIX $\dot{M}$ for all glaciers from 2000 to 2015, -21.8 ± 5.4 Gt yr^{-1}.

** Calculated roughly by Braun et al. (2019) using frontal area changes from 2000 to 2016/17 and assuming an average lake and ocean depth of 250 ± 100 m at the glacier front obtained from few observations (e.g. Rivera et al., 2012; Sugiyama et al., 2016)

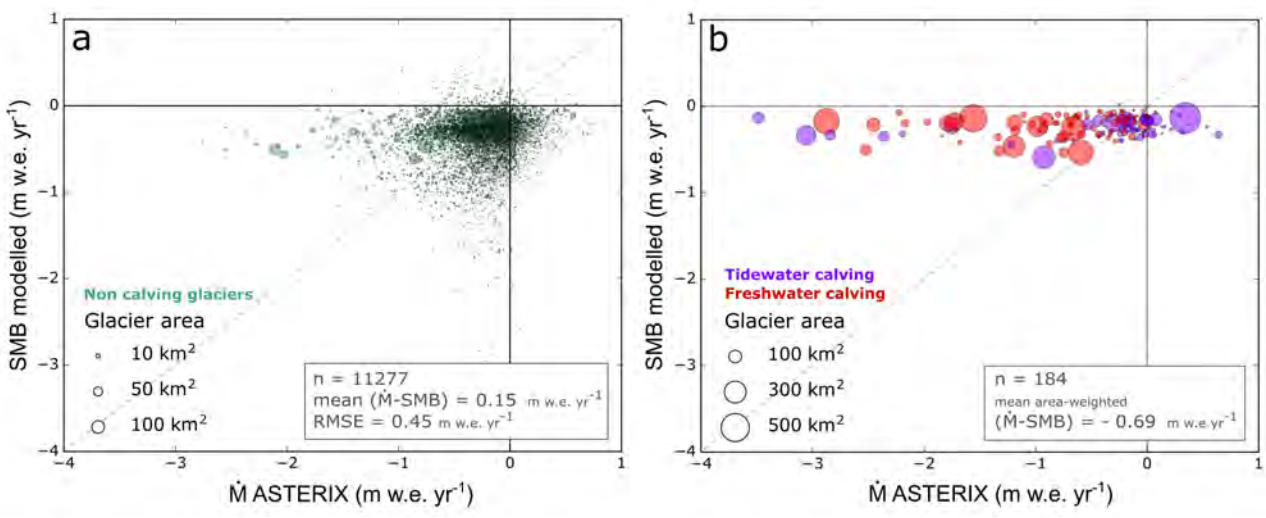

Figure 3.23: Modelled SMB rates as a function of geodetic mass balance rates for (a) non-calving glaciers (green) and (b) calving glaciers (purple and red). Each dot represents an individual glacier and the size of the dot represent glacier area.

In general, there is a good agreement between the regional ASTERIX $\dot{M}$ and the modelled SMB for non-calving glaciers, though for individual glaciers the spread is large, with a RMSE of 0.45 m w.e. yr^{-1} (Figure 3.23). The spread is similar if only glaciers larger than 2 km^2 are considered (RMSE 0.44 m w.e. yr^{-1}, n = 1466, not shown), implying that whatever the glacier size, the comparison of $\dot{M}$ and SMB estimates for individual glaciers must be regarded with great caution. For calving glaciers, the regional modelled SMB is less negative than the geodetic estimate, as expected. This behavior is also observed at the individual glacier scale over the majority of large calving glaciers.

ASTERIX $\dot{M}$, modelled SMB and the corresponding $\dot{M}$ – SMB rates are averaged over 1° by 1° grid

cells for the entire Andes non calving and calving glaciers and over individual glaciers for the SPI ((Figures 3.24, 3.25 and 3.26) respectively). In Patagonia (South of 40°S) and, particularly, in the SPI, modelled SMB rates are not able to reproduce the complex pattern of mass loss, specially when calving glaciers are involved. Also, despite the good agreement observed between $\dot{M}$ and SMB for non-calving glaciers for the entire Andes, when averaged over a 1° by 1° grid, SMB seems to be consistently more negative than $\dot{M}$ for non calving glaciers North of 40°S. Ideally $\dot{M}$ – SMB should be close to 0 m w.e. yr^{-1} when frontal ablation is minor, thus, the magnitude of this difference represents the limitations of the $\dot{M}$ and SMB estimation methodologies and recalls to be cautious on the interpretation of these results. It is important to note that the latitudinal differences observed between $\dot{M}$ and SMB estimates are not systematic. For example, modelled SMB estimates depends directly on the ability of ERA-interim reanalysis data to represent the real climatic conditions. The low resolution of reanalysis data (0.5° x 0.5°) is known to smooth precipitation fields in Patagonia, being unable to resolve the large East-West precipitation gradients observed through the Andes. They overestimate precipitation in the Pacific coast, underestimate orographic precipitation at the western slopes and simulates too much precipitation at the East Lenaerts et al. (2014).

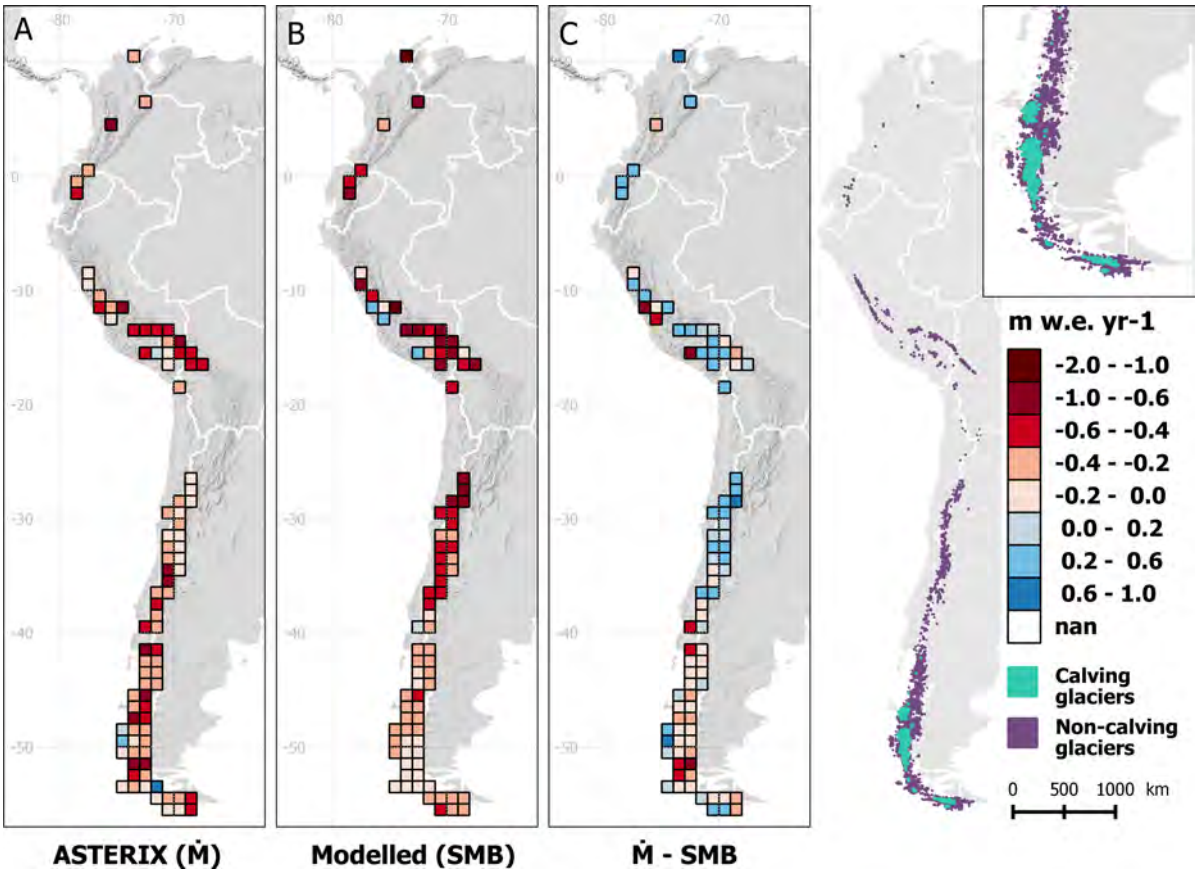

Figure 3.24: (A) ASTERIX $\dot{M}$ rates, (B) modelled SMB rates and (C) $\dot{M}$ – SMB rates averaged over 1° by 1° grid cells for grid cells for all Andes non calving glaciers during 2000-2015. The right panel represents the spatial distribution of calving (green) and non-calving (purple) glaciers along the Andes.

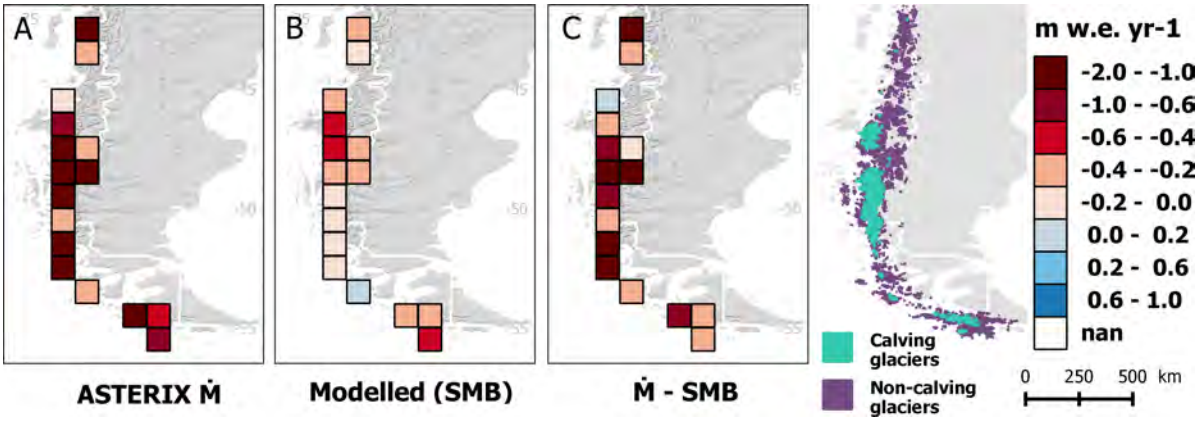

Figure 3.25: (A) ASTERIX $\dot{M}$ rates, (B) modelled SMB rates and (C) $\dot{M}$ – SMB rates averaged over 1° by 1° grid cells for grid cells for all Andes calving glaciers during 2000-2015. All calving glaciers are located south of 42°S. The right panel represents the spatial distribution of calving (green) and non-calving (purple).

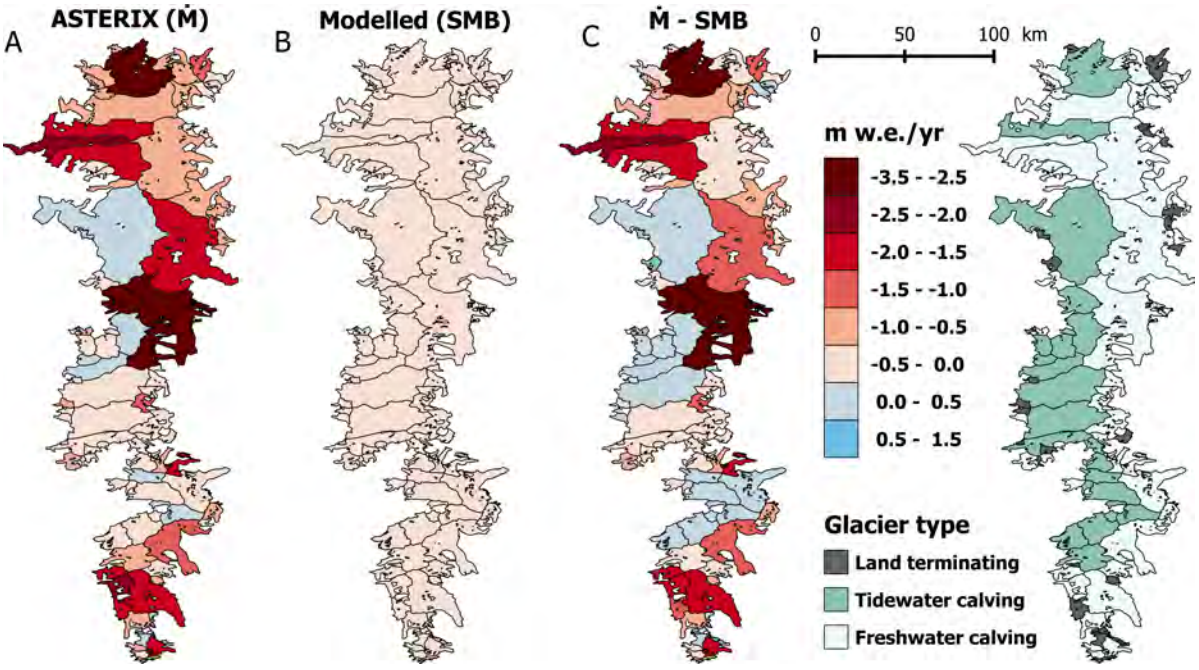

Figure 3.26: (A) ASTERIX $\dot{M}$ rates, (B) modelled SMB rates and (C) $\dot{M}$ – SMB rates for SPI glaciers during 2000-2015. The map to the right represents the spatial distribution of freshwater calving (light green), tidewater calving (green) and land terminating (grey) glaciers on the SPI.

3.9.4 Andes-wide frontal ablation

Considering the only existing rough estimation of A_{subw} provided by Braun et al. (2019), we calculated the first estimate of frontal ablation as expressed in equation 3.5 (Table 3.11). In general, frontal ablation amounts to almost two thirds of the total mass loss by all calving glaciers, and more than half of the total Andes mass loss, highlighting the important role of glacier dynamics in the Andes total glacier mass loss. Schaefer et al. (2015) had previously estimated calving rates for the SPI, by differencing their SMB estimates with Ṁ estimates from Willis et al. (2012b,a) and Rignot et al. (2003). Assuming no subaqueous mass loss they found calving rates of 17.5 Gt yr^{-1} for SPI glaciers during the period 2000-2011, much stronger than our estimate of 11.1 ± 2.3 Gt yr^{-1} for the same glaciers during the period 2000-2015 (also not including subaqueous mass loss for the sake of comparison). Calving results from Schaefer et al. (2015) were used to calibrate the Global Glacier Evolution Model (GloGEM) that aims to quantify glacier change and contribution to sea level rise at a global scale (Huss and Hock, 2018, 2015). At the time, this was the only previous estimation of frontal ablation available for the Southern Andes, however, here we present a second estimate that accounts for all Andes calving glaciers. The model

simulation and prediction for frontal ablation in the southern Andes is close to 0.7 m w.e. yr^{-1} for the period 1980-2000 and almost 0.2 m w.e. yr^{-1} for 2020-2040. We estimate a frontal ablation of 14.7 ± 6.0 Gt yr^{-1} , 0.74 ± 0.3 m w.e. yr^{-1} (or 11.6 ± 4.8 Gt yr^{-1} , 0.58 ± 0.2 m w.e. yr^{-1} without accounting for A_{subw}) for all Andes calving glaciers for the period 2000-2015. Fortunately, GloGEM modelled frontal ablation estimates are in line with ours, even though periods are not comparable. This is probably due to the different ice areas considered for our estimate and those from Schaefer et al. (2015), and the fact that we include A_{subw}, which makes our frontal ablation larger and in agreement with that from Schaefer et al. (2015) used to calibrate the model. However, the differences within estimates stresses the need to well constrain $\dot{M}$, SMB and frontal ablation estimates which have direct implications over modelling efforts use to predict future glacier changes.

In general, frontal ablation on lake calving glaciers accounted for 77% of the total frontal ablation during the period. This means that the ice lost towards lakes is almost four times larger than to the ocean, despite the similar ice surface of both glacier types. These contrasted $\dot{M}$ - SMB rates between freshwater and tidewater calving glaciers is also visually evident on SPI glaciers (Figure 3.26). Fast freshwater calving rates have already been reported on Jorge Mont, Perito Moreno and Upsala and Viedma glaciers (Rivera et al., 2012; Sakakibara et al., 2013; Skvarca et al., 2002; Sugiyama et al., 2016), the last three terminating in proglacial lakes. However, these estimations remain insufficient to compare this contrasted behavior.

The reason behind the contrasted response of freshwater and tidewater calving glaciers outline an interesting topic for future research. Recent studies have observed contrasting temperature trends along the subtropical west coast of South America since the second half of the 20^th century, with significant cooling trends in the pacific coast and warming trends inside the continent increasing with altitude in the Andes mountains (Falvey and Garreaud, 2009; Vuille et al., 2015). Gridded sea surface temperature data indicates coastal cooling trends that extend along the length of the entire Chilean coastlines. This suggest ocean cooling as a possible reason of the moderate calving rates observed over tidewater glaciers. In the other hand, Sugiyama et al. (2016) revealed the thermal structure of proglacial lakes near the glacier fronts of Viedma, Perito Moreno and Upsala glaciers, showing a clear stratification, with a warmer water layer at the surface and turbid cold water in the bottom. They suggest that the strong Patagonian wind enhances circulation and vertical mixing, which might be responsible for transporting heat to the ice-water interface, enhancing subaqueous melt (A_{fw}). This suggest an important role of A_{fw} on the total frontal ablation of lake terminating glaciers in Patagonia, implying that the stronger frontal ablation we found over lake terminating glaciers are not only due to calving but also to enhanced subaqueous melt.

These results suggest a possible influence of contrasted water and air temperatures between the Patagonian pacific coast and continental lakes located in the Andes on the contrasted glacier calving responses. It would be interesting to evaluate this hypothesis in the future with further observations over different Patagonian glaciers terminating at lakes and at the ocean at similar latitudes. Knowing thermal structure of the ocean at tidewater glacier fronts would allow to observe any differences with lakes. And, for example, having simultaneous air temperature measurements at freshwater and tidewater glacier fronts, would also help to validate if the conditions are really contrasted or not.

Chapter 4

Subperiod analysis of mass balance changes over the North Patagonian Icefield based on multiple archives of elevation data.

4.1 Introduction

The objective of the work presented in this chapter is to produce a time series of NPI glacier elevation changes for an extended period. An sufficiently long and multi-period dataset of glacier changes is useful to observe the patterns of past and recent glacier variation in the NPI, better understand glacier response to climate forcing and improve modelled projections of NPI glacier changes.

Following the good performance of the SPOT5-SRTM and ASTERIX methodologies over the NPI (Chapter 2) and the availability of a multi-temporal archive of elevation data for the NPI, we considered to extend the time period of mass balance observations from 1975 to 2016. In addition to the elevation data used before, SRTM (2000) and SPOT5-HRS (2012), we exploited additional satellite stereo images from SPOT5 (2005), SPOT6-7 (2016) and the topographic maps from the Instituto Geografico Militar (IGM, Chile) built from aerial photographs acquired in 1975.

This multiple elevation archive permitted us to analyse sub-period mass balance changes in the NPI, and observe specific patterns of glacier variations at an icefield-wide and individual glacier scale during four time-periods (1975-2000, 2000-2005, 2005-2012, 2012-2016). In this section I present our unpublished preliminary results.

4.2 Expanded dataset

As previously presented in Chapter 2, we use the SRTM DEM (year 2000) and a SPOT5 DEM (March 18, 2012) as basis for this analysis (see specifications in section 2.4). This dataset was expanded with:

- **SPOT5-HRS DEM (2005):** cloud free, 40 m resolution DEM acquired in May 18, 2005 providing an almost complete coverage of the NPI, missing only the southernmost glacier tongues (Steffens, HPN4, U2 and U3 glaciers, Figure 4.1). This 2005 SPOT5 DEM is delivered with a reliability mask and one ortho-image generated from the rear HRS image with the same characteristics described above for the 2012 SPOT5 DEM (section 2.4).
- **SPOT6-SPOT7 DEM (2016):** cloud free, 40 m resolution DEMs with their corresponding ortho-images, acquired over the NPI area March 9 and 10, 2016 (SPOT7 and SPOT6 respectively). The SPOT6-SPOT7 satellites were designed for a ten-year lifetime complementing SPOT5 since 2012.

They where launched in 2012 and 2013 respectively in order to maintain the continuity of the stereo capability provided by SPOT5-HRS. The NPI SPOT6 DEM covers almost all the NPI, with the exception of the San Quintin glacier tongue (Figure 4.1). Conversely, the SPOT7 DEM has a complete coverage of the western NPI (Including San Quintin Glacier).

- **IGM topographic maps (1975):** The IGM of Chile produced the first regular cartography of the NPI by photogrammetric restitution and analogue analysis of aerial photographs taken mostly during a campaign on the 15 March 1975. The maps for the NPI region consist in 25 m and 50 m contour lines, recently digitalized by the IGM. The NPI topography is not complete, presenting a lot of data gaps mostly in the accumulation zones (Figure 4.1).

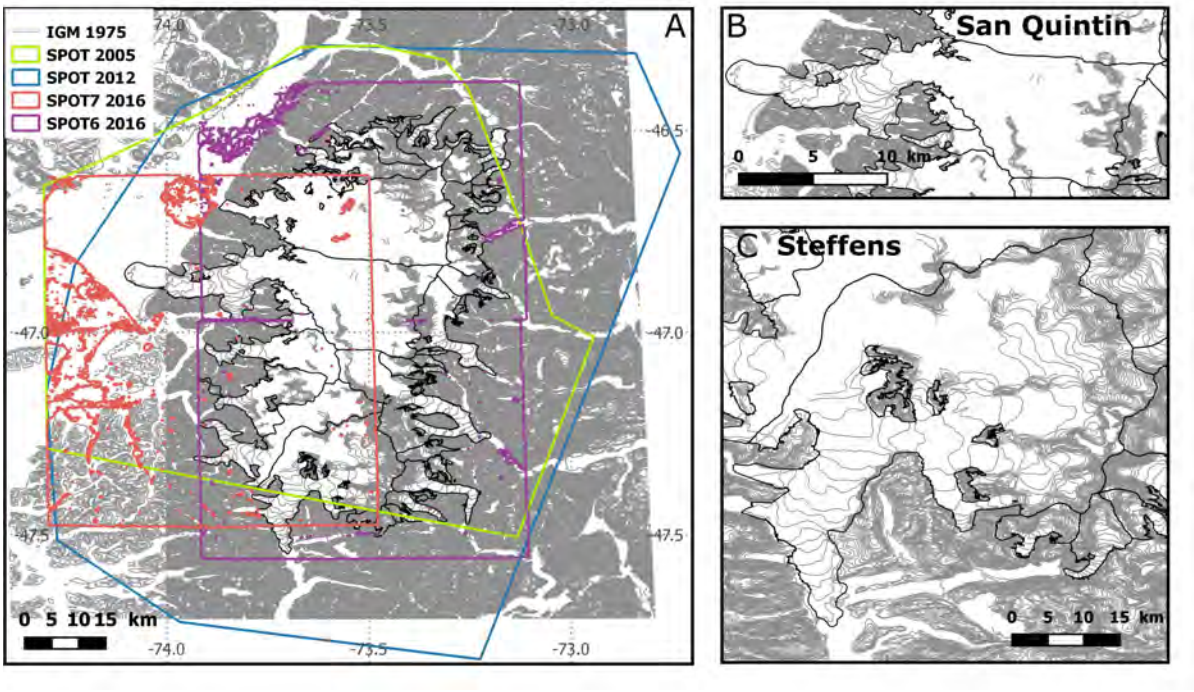

Figure 4.1: Spatial footprints of NPI data sets. (A) IGM 25 m contour lines over the NPI (west of -74W contours are every 50 m). Note that above ice the coverage is not complete with many data missing in the accumulation zones of the biggest glaciers and no data on San Rafael glacier tongue. Coloured polygons correspond to DEM footprints: SPOT5 2005 (green), SPOT5 2012 (blue), SPOT7 2016 (red) and SPOT6 2016 (purple). Selected subsets show the IGM contour lines over (B) San Quintin glacier and (C) Steffens glacier. IGM contour lines are rasterized to fit the 40 m SPOT DEM resolution, valid pixels correspond to the 7 % of the total icefield area.

4.3 Methodology

All data were processed using the simple DEM differentiation, following the SPOT5-SRTM methodology described in Chapter 2. The reader is referred to section 2.5 for more details. All DEMs, including the rasterized IGM contours lines (40 m resolution to fit SPOT DEM resolution) where adjusted horizontally and vertically using a reference DEM. For every sub-period the reference DEM was chosen either as the better quality DEM, or the one corresponding to the beginning of the period.

In the particular case of 2016 DEM, the SPOT6 and SPOT7 DEMs where adjusted individually. The tongue of glacier San Quintin (covered only in the SPOT7 DEM) was mosaicked to the SPOT6 DEM (the mosaicked glacier surface corresponds to 1% of the total NPI surface). We calculated four different DEM difference corresponding to each sub-period hereafter referred as SRTM-IGM (1975-2000), SPOT5-SRTM (2000-2005), SPOT5-SPOT5 (2005-2012) and SPOT6/7-SPOT5 (2012-2016)(The 2000-2012 period will be refered as SPOT-SRTM, as previously in Chapter 2). Elevation change rate (dh/dt) maps were then obtained by dividing by the respective time period. The NPI glacier outlines for year 1975, 2000 and 2012 where obtained from Davies and Glasser (2012) and Dussaillant et al. (2018). Outlines where adjusted manually to fit the glacier extents of year 2005 and 2016. For the 2000-2016 period

and sub-periods, volume change rates and mass balance rates were integrated by individual glacier hypsometry using 100 m elevation bands obtained from the SRTM DEM. As an exception, the SRTM-IGM rates where integrated using the icefield wide hypsometry by 100 m bands, i.e. considering the entire Icefield as a single ice mass. This decision is due to the high amount of data gaps on individual glaciers.

Volume change rates were computed considering the changing glacier areas, i.e. the mean elevation change rate was integrated to the mean area between the start and end dates of every sub period. Volume-to-mass conversion was computed using a density conversion factor of 850 ± 60 kg m^{-3} (Huss, 2013). The mass balance error was computed following the formal error assessment described in section 2.5.3. To check our formal error assessment, we additionally calculated a triangulation error as the absolute value of the triangulation residual, r, for the period 2000-2016.

$$r = \left| \left(\frac{(\dot{M}_{2000-2005} \times 5.3) + (\dot{M}_{2005-2012} \times 6.8) + (\dot{M}_{2012-2016} \times 4.0)}{16.1} \right) - \dot{M}_{2000-2005} \right| \tag{4.1}$$

Where $\dot{M}_{y1-y2}$ is the mass balance rate for the period between year $y1$ and year $y2$ expressed in m w.e. yr^{-1}. For Icefield-wide estimates, the triangulation residual is 0.17 m w.e. yr^{-1}, which is the same error obtained with the formal error assessment. At the individual glacier scale uncertainties are expected to be larger than for the entire icefield, due to the intensification of DEM co-registration biases. The mean residual for all NPI individual glaciers is 0.26 m w.e. yr^{-1}, slightly larger but similar to our formal error assessment of 0.24 m w.e. yr^{-1}. The similarity between the triangulation and formal errors support our methodological formal error assessment. .

4.4 IGM DEM processing

4.4.1 Suspicious values on 1975-2000 elevation change grids

Suspicious positive dh/dt above 1200 m a.s.l. were obtained when subtracting the IGM DEM from the SRTM DEM (Figure 4.2). If these values where correct, the accumulation zone of almost all NPI glaciers would have gained mass at rates of almost 2 m yr^{-1}, corresponding to almost 50 m during the 25 year period. To our knowledge, NPI glaciers have been shrinking since the Little Ice Age with accelerating trends during the last decades before 2000 (Davies and Glasser, 2012; Glasser et al., 2011; Lopez et al., 2010). In a previous publication, Rignot et al. (2003) differenced the IGM data with SRTM, calculating the NPI the volume change at -3.2 ± 0.4 km^3 yr^{-1} for 1975-2000 period. However, to calculate this rate, the authors considered only the dh/dt rates below 1200 m a.s.l., and assumed all elevation changes to be zero above this altitude (excepting Arco, U4 and Soler with the upper threshold set at 1400 m a.s.l., see table S1 on Rignot et al. (2003) supplementary material). We found no statement on their article justifying the exclusion of these unexpected high elevation data.

Here, we further analyse the IGM-SRTM dh/dt grids, to check the likelihood of the observed high altitude thickening. To do this, we compare a KH9-Hexagon USA spy satellite image acquired over the NPI the 6 April 1979 and a Landsat ETM-7 image acquired the 8 mars 2000 and observed the changes in the extent of nunataks located above 1200 m a.s.l. (Figure 4.3). If a thickening of almost 50 m did occur during this period, the extent of these nunataks would necessarily be reduced, or even some would have disappeared above 1200 m a.s.l. We did not observe such a situation. Contrarily, in Figure 4.3 we can clearly that the ice reaching the ridges of the selected nunataks experienced either thinning (at their lower ridges, around 1400 m a.s.l.) or no noticeable changes (at their higher ridges, above 1600 m a.s.l.) during the complete 1979-2000 period.

This qualitative comparison allows us to suggest that the NPI has more probably been loosing ice until altitudes of at least 1400 m a.s.l. between 1975 and 2000. Thus, the high altitude thickening expressed by the SRTM-IGM dh/dt grids is very likely an artefact resulting from the IGM data. Considering this,

we decided to exclude all dh/dt values above 1200 m.a.s.l. and replace them with 0 m yr^{-1} rates, as done previously by Rignot et al. (2003) .

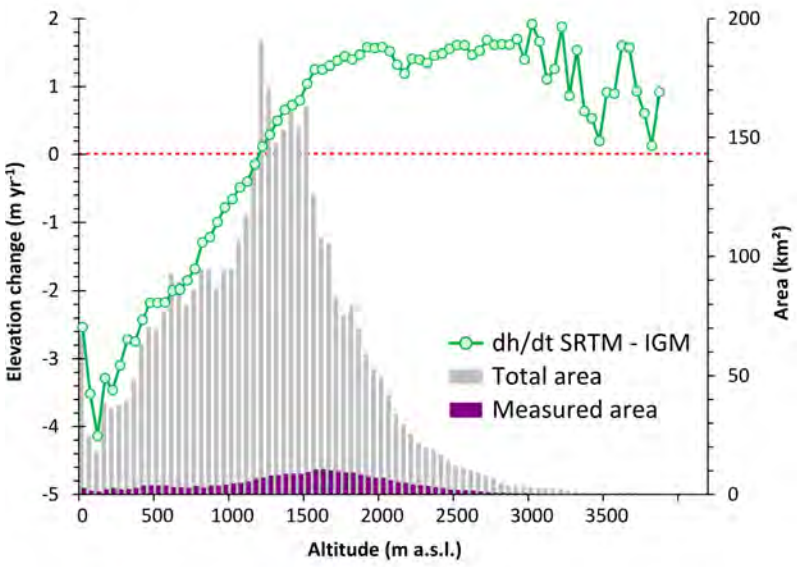

Figure 4.2: Hypsometric distribution of dh/dt rates by 100 m bands for SRTM–IGM.

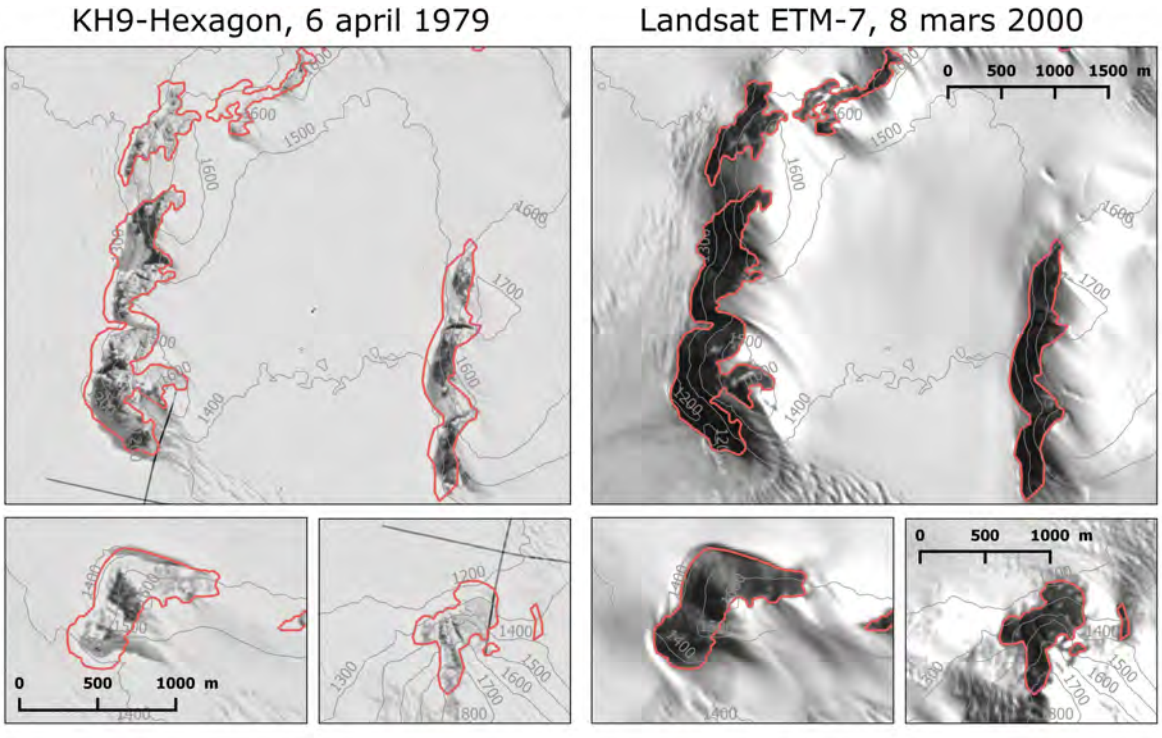

Figure 4.3: Comparison of NPI nunatak extents above 1200 m a.s.l. between 1979 and 2000. Left panels correspond to a KH9–Hexagon cloudless image from the 6 April 1979 covering the entire NPI. Right panels correspond to the same location on a Landsat ETM–7 also cloudless image acquired the 8 March 2000. Red contours correspond to the nunatak extents of year 2000. Grey elevation contours (SRTM 90 m void filled DEM) display the reference altitudes of year 2000.

4.4.2 Incomplete coverage of IGM data

The IGM-SRTM dh/dt grid contains elevation change values for only 7% of the total NPI glacierized area. This implies that the total mass loss calculation is calculated from a very small number of measurements. To analyse if these sparse data coverage is sufficient to to correctly assess the icefield-wide mass loss, we performed a sensitivity test to the spatial coverage of the IGM-SRTM dh/dt grids start-

ing from the more complete (84% coverage) and previously validated ASTERIX 2000-2012 dh/dt maps produced in chapter 2 (Figure 2.4b). The NPI region-wide mass balance rate obtained with the entire ASTERIX (i.e. ASTER trend) dh/dt grids is -1.03 ± 0.14 m w.e. yr^{-1} (containing 16 % data gaps). If we use this same dh/dt grids and calculate the mass balance rate considering only the pixels that present valid dh/dt values over the IGM-SRTM grids, we obtain a mass balance rate of -0.90 ± 0.34 m w.e. yr^{-1} in reasonable agreement with the first one (the higher uncertainty is explained by the 93% of data gaps in this grid). The difference is probably due to the slight overestimation of the dh/dt rates between 1000 to 1500 m a.s.l. observed in the hypsometric distribution of the dh/dt curves (Figure 4.4). Starting from this last ASTERIX grid, containing only valid IGM-SRTM values, we then assume all dh/dt values above 1200 m a.s.l. to be 0 m yr^{-1}. The resulting mass balance rate of -0.77 ± 0.35 m w.e. yr^{-1} is less negative but is still in agreement with the ASTERIX estimate obtained with the original grid (although the difference strats being considerable). This additional overestimation is explained by the replacement of the slightly negative dh/dt rates above 1200 m a.s.l. to 0 yr^{-1} (see Figure 4.4).

We conclude that the spatial distribution of the scarce IGM data is sufficient to accurately represent the NPI mass balance rates considering the uncertainties of our methodology. According to this sensitivity test, and assuming that the IGM-SRTM elevation values bellow 1200 m a.s.l. are not biased, our calculated estimate will most likely represent a lower bound of the actual NPI mass loss. There were no available direct glaciological measurements or geodetic estimate over NPI glaciers for this time period that allows us to support or contradict this assumption. We cannot ensure that the artefacts found on the IGM topographies above 1200 m a.s.l. are not existent also at lower elevations. For this reason, we insist in the fact that the IGM-SRTM estimate using the IGM maps as they are, should be considered with caution.

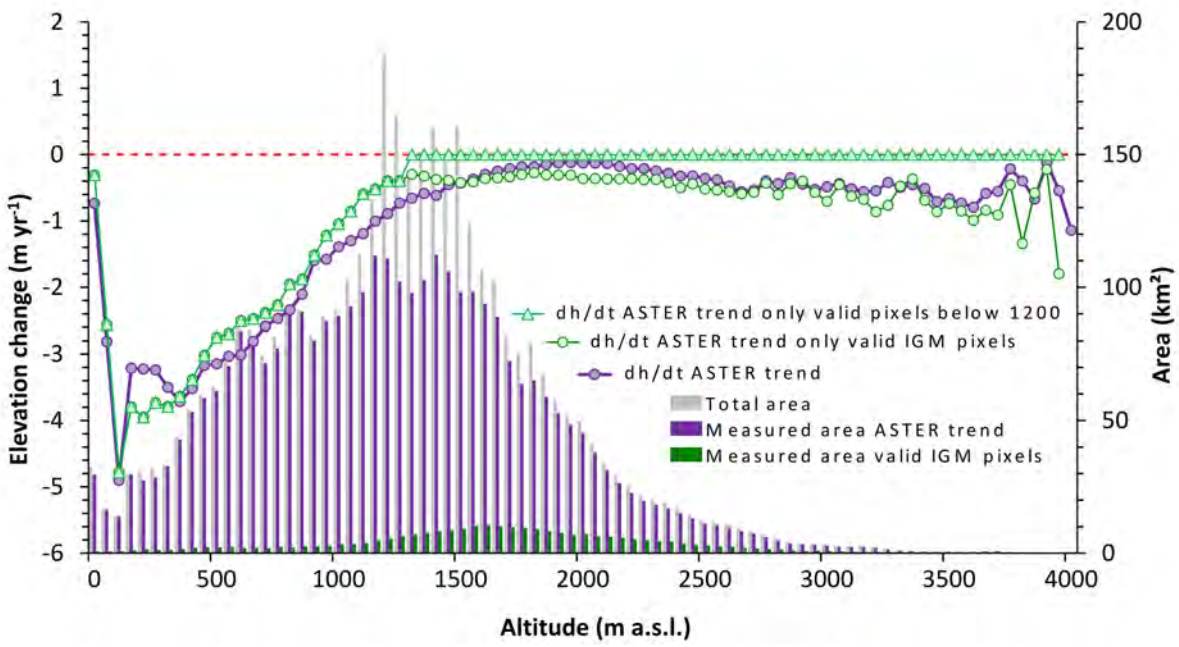

Figure 4.4: Hypsometric distribution of dh/dt rates for: ASTERIX (purple dots), ASTERIX considering only IGM valid pixels (green dots) and ASTERIX considering only IGM valid pixels below 1200 m a.s.l and assuming 0 m yr^{-1} for higher elevation bands. Histogram correspond to the NPI total area (grey bars), ASTERIX measured area (purple bars), and IGM measured area (green bars).

4.5 Results and discussion

We estimate NPI volume change rates and mass balance rates for the period 1975-2000 and for a more recent period 2000-2016, subdivided into three sub-periods 2000-2005, 2005-2012 and 2012-2016 (Table 4.1 and Figure 4.5). The NPI mass balance rates evolved from a moderate loss of -0.60 ± 0.73 m w.e.

yr^{-1} before year 2000 to a strongly negative -1.19 ± 0.24 m w.e. yr^{-1} from 2000 to 2016 (see also Figure 4.6). However, due to the high uncertainties of the 1975 – 2000 estimate, we cannot assure that the mass loss increased during the last decades. There is only one previous study assessing the NPI volume loss for the period 1975-2000 (Rignot et al., 2003) obtaining similar rates of -3.2 ± 0.4 km^3 yr^{-1} (or -0.65 ± 0.08 m w.e. yr^{-1} using a 850 kg m^3 density transformation factor). However, this estimate relies on the same IGM and SRTM data used here, and might be similarly biased by the low quality of the IGM, as discussed above. Considering our error bars, we cannot suggest a significant shift on NPI volume change rates from 1975-2000 compared to 2000-2016. However, the dh/dt rates are consistently less negative for almost all elevation bands during this period with respect to other sub-periods (Figure 4.5). Thus, we can suggest that the NPI glaciers mass loss rates have most likely been increased after 2000.

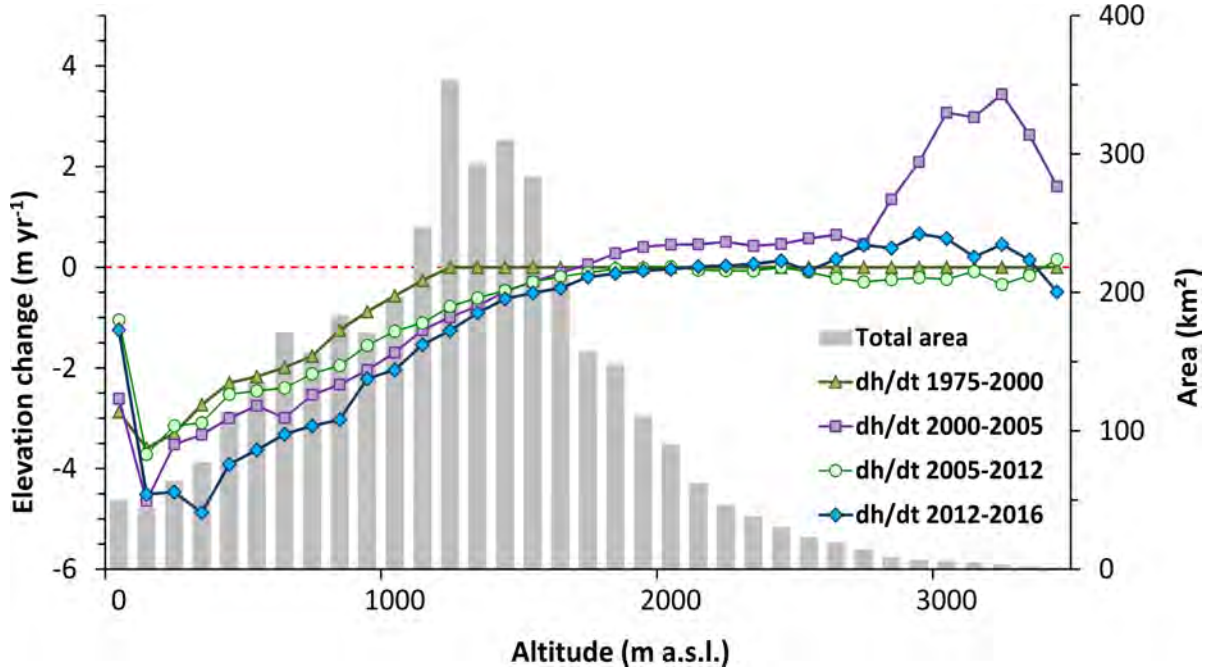

Figure 4.5: Hypsometric distribution of dh/dt rates for the NPI during four different time periods: 1975-2000 (dark green); 2000-2005 (purple); 2005-2012 (light green); and 2012-2016 (blue).

Table 4.1: NPI icefield-wide mean mass balance rates and volume change rates for different time periods. Reported areas correspond to the mean NPI area between the first and last years of the time period.

Time period	Mean area (km2)	Measured Area (%)	Mass balance rate (m w.e. yr^{-1})	Volume change rate (km^3 yr^{-1})
1975 - 2000	3937	2	-0.60 ± 0.73*	-2.80 ± 0.70
2000 - 2016	3771	86	-1.19 ± 0.24	-5.26 ± 0.39
2000 - 2005	3824	73	-0.88 ± 0.19	-3.97 ± 0.46
2005 - 2012	3766	56	-0.81 ± 0.23	-3.58 ± 0.44
2012 - 2016	3711	71	-1.20 ± 0.22	-5.23 ± 0.48

* Considering mean dh/dt rates of 0 m yr^{-1} for all elevation bands above 1200 m a.s.l.

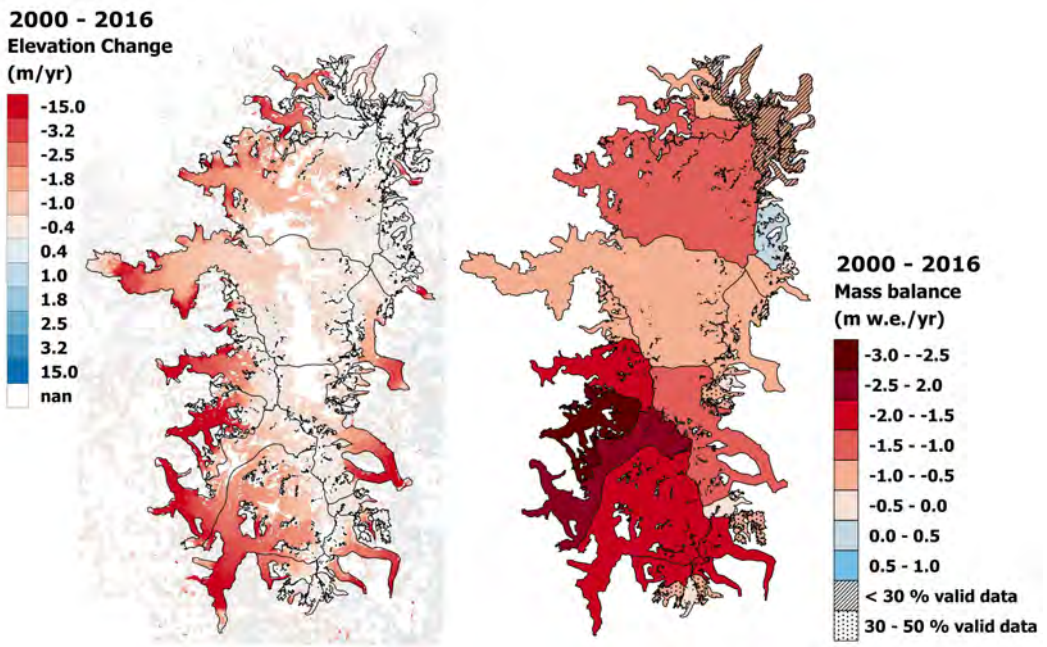

Figure 4.6: Maps of elevation change (m yr^{-1}) and individual glacier mass balance rate (m w.e. yr^{-1}).

After 2000, there is a clear signal of increased mass loss towards the last observed years. Mass balances rates are quite similar during the first two sub-periods with -0.88 ± 0.19 m w.e. yr^{-1} for 2000-2005 and -0.81 ± 0.23 m w.e. yr^{-1} for 2005-2012. Conversely, after 2012, the rate is significantly more negative, reaching -1.20 ± 0.22 m w.e. yr^{-1} (see also Figures 4.7 and 4.8). This shift can be noticed in the dh/dt curves for different sub-periods (Figure 4.5), where dh/dt rates are considerably more negative below 1800 m a.s.l. for the 2012-2016 period. This observation is even more pronounced at the lowest elevations (below 1000 m a.s.l.). The suspicious positive dh/dt above 2900 m a.s.l. for the period 2000-2005 are likely a result of the penetration of the SRTM C-band radar signal over the high altitude dry snow (see section 2.7.2).

The increased mass loss during the 2012-2016 years is consistent over most of the NPI glaciers but is mostly dominated by those located in the southern part of the NPI (Figures 4.7 and 4.8). There, the large glaciers like Steffens, Acodado, Benito, HPN1, HPN4, Pared sur, Pared Norte and Colonia, present all significant shifts toward strongly negative mass balance rates during the last period (Annexe 2, Tables A4 and A5). In the Northern NPI, large glaciers like San Quintin and Nef present a similar behaviour though their net mass balance rates are less negative. The San Rafael glacier, the second largest glacier in the NPI and the only tidewater calving glacier of the NPI, is an exception to this rule. This glacier showed a continued decrease of its mass balance along the three sub-periods within 2000-2016. This behaviour is in line with previous reporting stabilization of frontal retreat and a diminution of terminus velocities of the San Rafael glacier after 2000 (Collao-Barrios et al., 2018; Koppes et al., 2011).

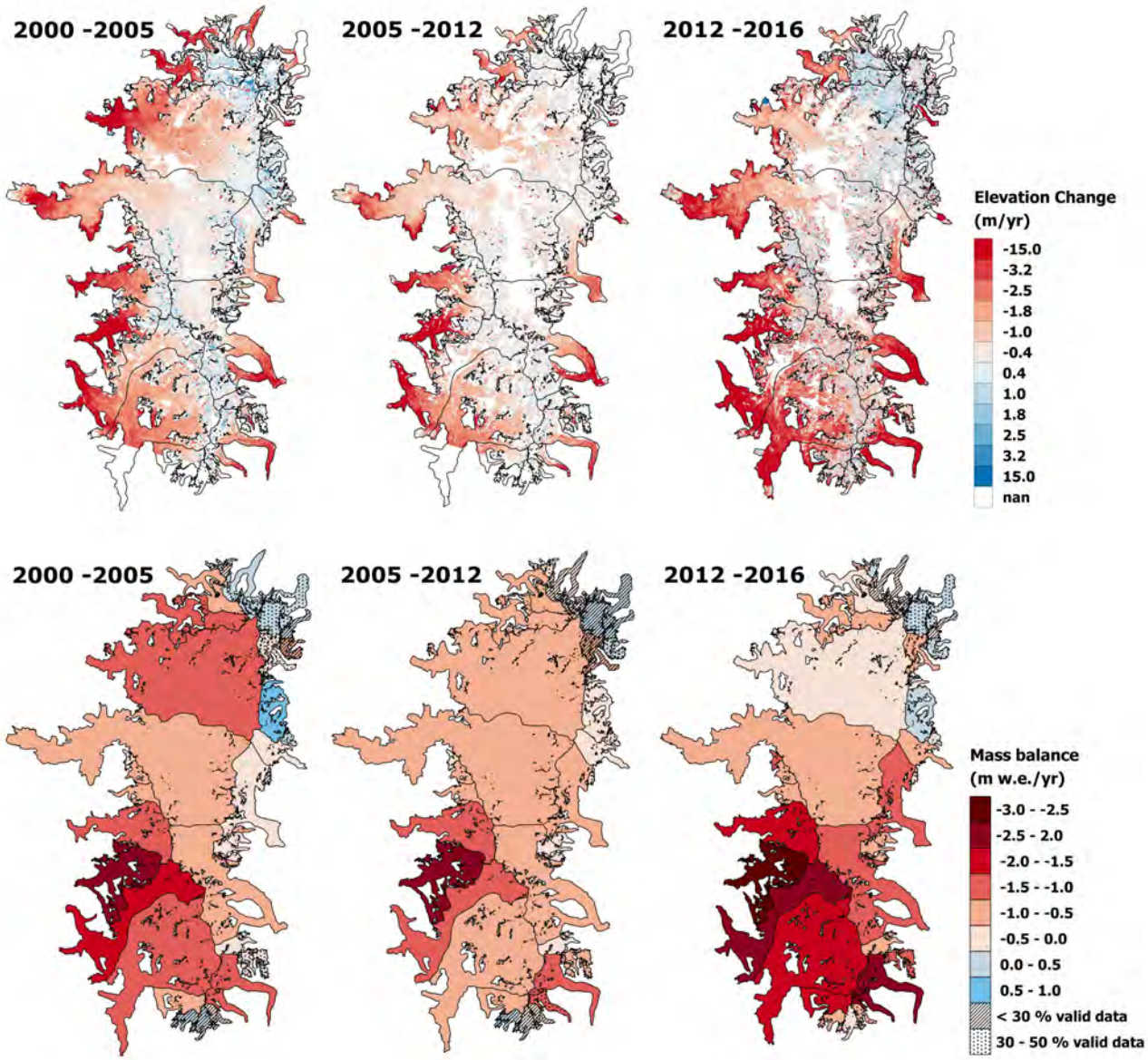

Figure 4.7: Maps of elevation change (m yr^{-1}) and individual glacier mass balance rate (m w.e. yr-1) over the NPI for the three sub-periods 2000-2005, 2005-2012 and 2012-2016.

Two previous studies have observed NPI volume change rates during similar sub-periods as done here (Table 4.1). Foresta et al. (2018) obtained strongly negative volume change rates of -6.79 ± 1.16 km^3 yr^{-1} between 2011 and 2017, by exploiting swath processed CryoSat-2 interferometric altimetry data (500m resolution) between 2011 and 2017. Abdel Jaber et al. (2018) observed NPI volume change rates during periods 2000-2012 (-4.26 ± 0.20 km^3 yr^{-1}) and 2012-2016 (-5.60 ± 0.20 km^3 yr^{-1}) using the SRTM DEM and two TanDEM-X DEMs for year 2012 and 2016. Their regional Icefield-wide volume changes agree with our results for both time periods (-4.55 ± 0.41 km^3 yr^{-1} and -5.23 ± 0.48 km^3 yr^{-1}, respectivelly).The strong agreement with TanDEM-X estimates allows us to suggest that Foresta et al. (2018) volume loss rates might be too negative. This may result from their data gap interpolation method, which relies on a reduced amount of dh/dt values, mostly on NPI glacier tongues.

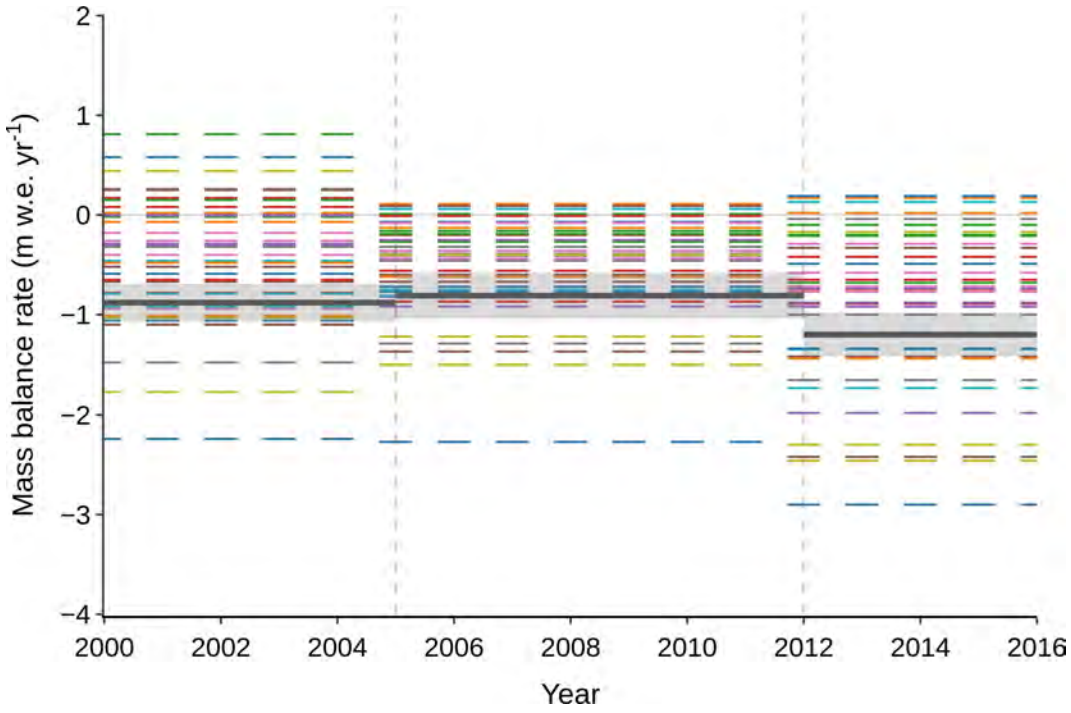

Figure 4.8: Changes in NPI mass balance rates during sub-periods 2000-2005, 2005-2012, and 2012-2016. Colored horizontal lines correspond to each NPI individual glacier (n=38), bold lines correspond to the area weighted mean mass balance rate for the entire Icefield. The uncertainties for each period are represented by the shaded intervals in grey. For details in subperiod mass balance rates for individual NPI glacier please refer to Annex 2 Table A4 and A5.

Table 4.2: Comparisson of available Icefield-wide volume change rates estimated for the NPI during similar sub-period.

Method	Period	Volume change rates ($km^3\ yr^{-1}$)	Reference
SPOT-SRTM	2000 - 2012	-4.55 ± 0.41	This study
TanDEM-X - SRTM	2000 - 2012	-4.26 ± 0.20	Abdel Jaber et al. (2018)
SPOT-SRTM	2012 - 2016	-5.23 ± 0.48	This study
TanDEM-X - TanDEM-X	2012 - 2016	-5.60 ± 0.20	Abdel Jaber et al. (2018)
CryoSat-2	2011 - 2017	-6.79 ± 1.16	Foresta et al. (2018)

At the individual glacier level, the differences with Abdel Jaber et al. (2018) become larger. Almost all glacier mass balance rates disagree within error bars with absolute differences up to 2.3 m w.e. yr^{-1} (RMSE = 0.89 m w.e. yr^{-1}) for the 2000-2012 period and 1.4 m w.e. yr^{-1} (RMSE = 0.63 m w.e. yr^{-1}) for 2012-2016 period (Figure 4.9). Differences are not dependent on glacier size, for example the large San Rafael glacier presents differences close to 1.5 m w.e. yr^{-1} (Figure 4.9C). Previously in this manuscript, we presented the good agreement of SPOT-SRTM with ASTERIX individual glacier mas balance estimates for the period 2000- 2012, (Figure 2.6, section 2.6.2) with absolute differences of 0.2 m w.e. yr^{-1} over glaciers larger than 100 km^2. However, determining which methodology is best for assessing individual glacier mas balance is out of the scope of this work. At this stage of my work, the icefield-wide agreement within the different available estimate is sufficient.

In general, a higher disagreement is expected over geodetic estimates at smaller spatial scales, because DEM co-registration biases and random elevation errors are increased with respect to regional scale assessments. To determine the causes of divergence of individual glacier rates, and separate the errors inherent to the dataset from those relative to the post-processing technique, we propose to compare directly the SPOT-SRTM and TanDEM-X grids. However, I leave this issue as an open question, which I will most probably inquire with more detail during my future work.

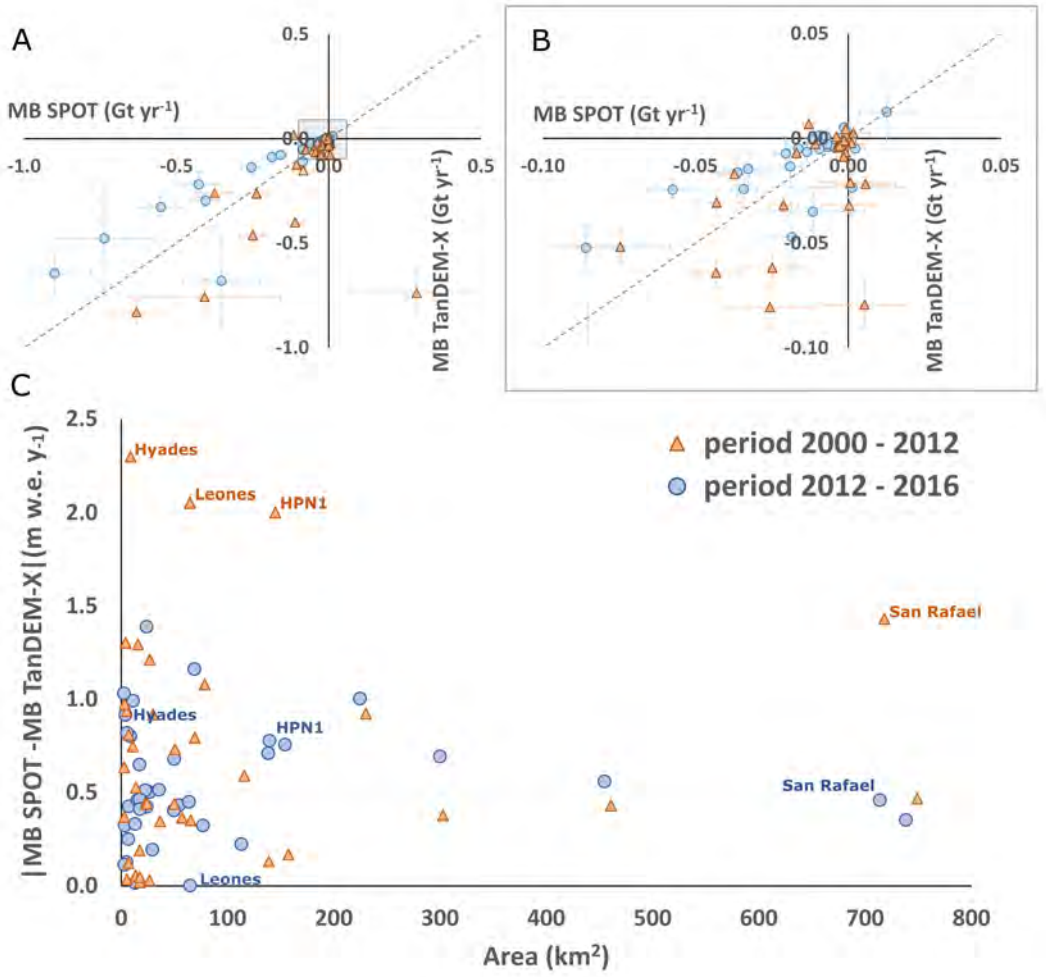

Figure 4.9: Comparison of individual glacier mass balance rates from TanDEM-X and SPOT grids (SPOT-SRTM and SPOT6/7-SPOT5 respectivelly) for sub-periods 2000-2012 (red triangles) and 2012-2016 (blue circle). (A) Mass balance rates (Gt yr^{-1}) obtained from methods using SPOT DEMs as function of mass balance rates obtained from TanDEM-X DEMs. The dashed line corresponds to the 1:1 line. (B) Is a zoomed panel of (A) and (C) Absolute difference of mass balance rates (m w.e. yr^{-1}) between the two methods as a function of glacier area.

4.6 Overlook and the pursue of future opportunities

We contribute here with unpublished results exhibiting a generalized temporal increase of NPI mass loss rates from 1975 to 2016. As a first result, we suggest a shift from moderately high Icefield-wide mass loss rates before 2000 (of the order of -0.6 m w.e. yr^{-1}), towards stronger mass loss rates during the first decades of the 21^{st} century (-1.2 ± 0.2 m w.e. yr^{-1}). However, this statement must be considered with caution accounting for the quality of the IGM data used to obtain the 1975-2000 NPI loss. After a detailed analysis of the elevation change grids, we suggest a possible bias due to artefacts over the IGM cartography resulting in unexpected positive elevation changes on the accumulation area. We suggest that the IGM cartography, as it is, is not sufficiently reliable to accurately calculate the NPI mass balance.

These biases may most likely come from the outdated techniques used to produce this cartography. The best solution to this problem would be to rebuild the 1975 topography from the original aerial photographs using state of the art photogrammetry techniques. The processing of optical stereo imagery has been improved during the last years due to advances in computer machines and image processing. New algorithms and tools are available to solve image orientation and correlation which are accessible to the community as open source software such as MicMac (Rupnik et al., 2017) and the Ames Stereo Pipeline from the NASA (Shean et al., 2016, used in this work to create ASTER DEMs). Recent studies have used and automatized these techniques to obtain digital elevation models over glacierized regions

out of historical photographs, obtaining better results than existing cartographies and allowing to extend the time period of glacier observations with a high level of statistical accuracy (Belart et al., 2019; Papasodoro et al., 2015).

Applying these techniques to the IGM aerial photographs over the NPI would allow to build a much more accurate elevation maps for year 1975, with probably less artefacts than the contour lines used here (and by Rignot et al. (2003)). Comparing them with more accurate DEMs like SPOT over stable terrain would also allow to measure biases and assure the good quality of the new data. The exploitation of these images would definitely give value to the work presented here, but stays now beyond the scope of this PhD. However, it would be a good starting point for my future work and necessary for a possible publication of these results.

As a second result, and considering only the period after 2000, we observed a marked pattern on NPI Icefield-wide thinning rates, with moderately high but constant thinning rates until 2012, shifting towards intense thinning rates during the last 4 years before 2016. These results are robust due to the good quality of the SPOT DEMs used as input data and to the strong agreement observed with recently published icefield-wide estimates for similar sub-periods (Abdel Jaber et al., 2018).

I propose two directions for future work: first, to recalculate the 1975-2000 thinning rates with improved IGM maps, and secondly, try to understand the reasons behind the temporal changes in glacier response observed in the NPI. An analysis of the climatic forcing on temperature and precipitation using the reanalysis data available since 1979 together with the recent advances in climactic modelling of the Patagonian region, would also be a promising objective. For this task, I leave an open door to collaborate with a climatological expert willing to offer new insight and information to into this problematic.

Conclusions and perspectives

Summary of the results

The objective of this Thesis was to analyse recent Andes-wide glacier changes and their decadal imbalance contribution to water resources and sea level rise. Here I summarize the main results, conclusions and contributions of each one of the three research questions addressed in this work, specified at the end of Chapter 1.

Question 1: Can we accurately measure glacier changes in the Andes using multi-temporal optical ASTER DEMs?

In Chapter 2, we validated the performance of the ASTERIX methodology to calculate glacier mass changes over Andean glaciers. We chose the NPI as validation site, because it permitted us to test the two major challenges for optical DEMs: frequent clouds and vast homogeneous snow surfaces. At the moment when I started this work (year 2016), ASTERIX had never been validated under this conditions elsewhere. Our first contribution is an improved NPI glacier inventory.

Following previous studies, our analysis confirms the strong NPI glacier mass loss for the period 2000 to 2012. For the entire NPI (about 3800 km^2), we found strongly negative ASTERIX mass balance rates of -1.06 ± 0.14 m w.e. yr^{-1}, in excellent agreement with the -1.02 ± 0.21 m w.e. yr^{-1} obtained by differencing two better resolved DEMs (SRTM and SPOT5). We confirm the NPI-wide mass loss estimated by two previously studies in the region (Jaber et al., 2016; Willis et al., 2012a). The good agreement of ASTERIX NPI mass loss with the -1.02 ± 0.04 m w.e. yr^{-1} estimated by Jaber et al. (2016) obtained by radar DEMs (which are not affected by clouds and provide good coverage of the accumulation zone), proves the relevance of our method, even in the featureless accumulation area of large icefields. The elevation change grids produced here for the NPI have been used to model surface mass balance on the San Rafael glacier (Collao-Barrios et al., 2018).

Importantly, we contribute with a detailed analysis of SRTM C-band radar signal penetration over NPI snow. We confirm the lack of significant penetration of the SRTM C-band radar signal in the wet and temperate snow and firn of the icefield, except for a small high altitude region where dry snow was present in February 2000 (>2900 m a.s.l.; less than 1% of the icefield), with negligible effect on the NPI-wide mass balance. With this work we validated the ASTERIX method as an accurate method to measure glacier changes in the Andes, obtaining uncertainties for individual glaciers of the order of 0.2 m w.e. yr^{-1}, comparable to previous validation efforts in different parts of the world (Berthier et al., 2016, 2018; Brun et al., 2017; Menounos et al., 2019) . This work opens the doors for the application of the ASTERIX methodology to the entire Andes (Question 2). It also provided the basis to address Question 3, where we analyse NPI mass balance changes during different sub-periods since 1975.

Question 2: What are the recent changes of Andean glaciers? Can we produce an homogeneous and spatially resolved dataset of glacier elevation changes during the last two decades? Can we obtain the sufficiently high spatial resolution that would allow analysing multiscale glacier changes and their respective impacts?

When this PhD work started, the main objective was to calculate glacier mass changes for the Southern Andes only (RGI region 17). However, the efforts deployed to automatize a work flow for massive ASTER DEM production and post-processing, permitted me to add the Tropical Andes (Andes only Low latitude RGI region 16, neglecting tropical glaciers in Africa and Indonesia) to my study area, and analyse the entire Andes. Fanny Brun, partially automatized the ASTERIX method to calculate glacier changes for the entire High Mountain Asia (Brun et al., 2017), followed by Romain Huggonet who completed this automation. My contribution consisted in cross validation tests, making sure everything was working correctly for the Andes. We also applied further modifications for the post processing technique of the elevation change grids, to make it suitable for the large variability of glacier responses in the Andes (much larger than in HMA for example).

In Chapter 3, we processed more than 30000 ASTER DEMs to generate a high resolution (30 m) dataset of Andes-wide glacier elevation change rates for a period of two decades (2000–2018) and for each decade within (2000–2009 and 2009–2018). We also provide individual glacier mass balance rates for 17832 glaciers (out of 18799 from RGI v6.0) for the three time periods. This homogeneous and spatially resolved dataset permitted us to analyse Andean glacier changes at diverse spatio-temporal scales. We estimated an Andes-wide total mass change amounting to -22.9 ± 5.9 Gt yr^{-1} during the past two decades (-26.0 ± 6.0 Gt yr^{-1} including subaqueous losses estimated by Braun et al. (2019)) for Patagonian glaciers). This loss corresponds to 0.06 ± 0.02 mm yr^{-1} of SLR (subaqueous losses not taken into account), slightly more than 10% of the global glacier contribution (0.55 mm yr^{-1}) during 2002-2016 (Bamber et al., 2018). Glacier wastage is consistent over all Andes sub-regions during the last 18 years, with the most negative mass balance rates found in the Patagonian Andes (-0.78 ± 0.25 m w.e. yr^{-1}) and Tropical Andes (-0.42 ± 0.24 m w.e. yr^{-1}) and relatively moderate loss in the intermediate regions of the Dry Andes (-0.28 ± 0.18 m w.e. yr^{-1}).

The analysis of the inter-decadal patterns of glacier mass loss at an Andes-wide scale is an important contribution and an original aspect of this work, which could not be assessed by previous estimates considering glacier mass changes for one period only (most of them during the first decade of the 21^{st} century). This analysis revealed steady glacier wastage during the first two decades of the 21^{st} century, largely due to the unabated glacier mass loss observed in Southern Patagonia, where most of the Andes glacier area is found. However, within this large-scale pattern of ice mass loss, we found an intermediate region (between 26°S and 45°S) where glaciers remained relatively stable from 2000 to 2009, shifting to drastic thinning rates during the 2010s. This marked shift coincides with conditions of sustained drought, already defined as the 'megadrought', affecting the Dry Andes since 2010 (Garreaud et al., 2017; Rivera et al., 2017). The evaluation of the imbalanced glacier contribution to river discharge during these two decades for four river basin located in the semi-arid Andes, revealed that glaciers partially helped to mitigate the negative impacts of this sustained drought. This results support previous studies already stating the importance of glaciers as water resources in this semi-arid Andes region (Buytaert et al., 2017; Huss et al., 2017; Huss and Hock, 2018; Kaser et al., 2010; Vuille et al., 2018; Soruco et al., 2015; Burger et al., 2018; Gascoin et al., 2011) .

As further application of our dataset, we provide a detailed analysis comparing our geodetic estimates with the surface mass balance provided by Marzeion et al. (2015), which allowed us to propose a first order estimate of the mass of ice lost by frontal ablation from lake and ocean calving glaciers in Patagonia. Losses by frontal ablation amount to 14.7 ± 6.0 Gt yr^{-1} for the period 2000-2015, corresponding to almost two thirds of the total mass losses for this time period (-24.9 ± 6.6 Gt yr^{-1} including the subaquatic mass loss calculated by Braun et al. (2019)). This illustrates the important role of calving dynamics in Patagonian glaciers.

The publication of the radar based geodetic estimates by (Braun et al., 2019) during the development of this work provided an opportunity to validate and improve the ASTERIX methodology for the Andes. Three important findings were obtained from a comprehensive comparison performed between ASTERIX elevation change grids and those from Braun et al. (2019). First, a sensitivity analysis of ASTERIX mass balance rates to data gaps (something possible only because the Braun et al. (2019) elevation change grids are almost complete over the large icefields), permitted us to confirm the relevance of our sampling, even in the featureless accumulation area of large icefields. Secondly, we showed a likely penetration of the radar signal over glaciers located at higher elevations and in colder environments. And finally, we discovered that the 3NMAD filter, widely used to exclude outliers when integrating elevation change trends at the regional scale (e.g. Braun et al., 2019; Brun et al., 2017; Menounos et al., 2019), can lead to biased mass balance estimates in regions with a high variability of glacier mass loss like Patagonia and Tierra del Fuego and thus should be applied to individual glaciers not entire regions.

This work is very close to publication (accepted "in principle"), so our Andes-wide datasets have not yet been used by other working groups which are waiting for their availability. Our highly resolved maps of glacier elevation changes have numerous potential applications for local, regional and larger-scale assessments of glacier mass changes in the Andes and will also provide useful calibration basis for glaciological and hydrological models intended to project future glacier changes and to improve water resource management throughout the Andes.

It is important to note that even if the performance of ASTERIX has proved to be accurate enough to measure glacier mass changes over many climatic contexts and glacier forms, the methodology still presents various limitations that could and need to be further improved. There are three main sources of uncertainties in our ASTERIX method that are not yet fully understood: (i) The assumption of linearity: we assume a linear evolution of glacier elevation changes when in principle glacier behaviour is far from being linear. (ii) The irregular sampling of seasonal surface elevation changes: large errors could occur if the ASTER DEMs were acquired mostly in one season (e.g. in winter) at the beginning of the study period and mostly in another season (e.g. in summer) towards the end of the study period (see section 2.5.3 and Berthier et al., 2016). This bias is difficult to quantify at the scale of the entire Andes, where glacier responses are highly variable and where the sampling of ASTER DEMs also varies from region to region. And (iii) Unknown sources of error inherent to our co-registration methodology: for example, we are not still able to correct the high frequency jitter effect of the ASTER sensor.

Our conservative error assessment aims at quantifying these three sources of error within the triangulation error. However, this triangulation error assessment is not yet fully understood for the Andes: we observe large triangulation residuals in regions with good ASTER coverage and large amount of DEMs. We suspect this could be linked to the large shift observed in the elevation change trends from one sub-period to the other in the Dry Andes (i.e. linearity issue), but they could also result from a possible seasonal effect. The efforts of our working team and other collaborators are now directed towards a new error assessment. They are exploring the possibility to apply a Gaussian regression over the available elevation values instead of the linear fit used in this work, allowing to account for non-linearity and seasonality biases at the same time. They are also exploring new methods to correct the high frequency jitter.

Question 3: Are NPI glaciers increasing their mass loss rates since 1975? Can we exploit a multiple archive of elevation data to measure sub-period elevation changes in the NPI from 2000 to 2016?

In Chapter 4, we exploited a multiple elevation archive to observe specific patterns of glacier changes in the NPI during four different time-periods (1975-2000, 2000-2005, 2005-2012, 2012-2016). Preliminary results show a generalized increase of NPI mass loss rates from 1975 to 2016. We suggest a significant shift from moderately high Icefield-wide mass loss rates before 2000 (of the order of -0.6 m w.e. yr^{-1}), towards stronger mass loss rates during the last years until 2016 (-1.2 ± 0.2 m w.e. yr^{-1}). Our estimation of the mass loss for the period 1975-2000 was not novel. We followed a similar strategy and used the same datasets (SRTM and digitalized Chilean IGM cartography) as previously published

by Rignot et al. (2003), obtaining the same estimate with larger uncertainties. After a detailed analysis of the elevation change grids, we suggest a possible bias due to artefacts over the IGM cartography resulting in unexpected positive elevation changes on the accumulation area. These biases may come from the outdated techniques used to produce this cartography in the first place. We suggest that the IGM cartography, as it is, is not sufficiently reliable to calculate accurately the NPI mass balance. To overcome this problem, a solution would be to reprocess the 1975 topography from the original historical aerial photographs using state of the art photogrammetry techniques that assure a high level of statistical accuracy (Belart et al., 2019; Papasodoro et al., 2015).

Our results for the three sub-periods after 2000 show a further acceleration of the NPI mass loss from high but constant thinning rates until 2012 (of the order of -0.8 m w.e. yr^{-1}), shifting towards intense thinning rates during the last observed years until 2016 (-1.2 ± 0.22 m w.e. yr^{-1}). This increased mass loss is significant also for the majority of NPI individual glaciers. We are confident in these results due to the good quality of the SPOT DEMs used as input data and the strong agreement observed with recently published icefield-wide geodetic estimates for similar sub-periods (Abdel Jaber et al., 2018). I would like to pursue this work in the future with recalculated elevation data for 1975. NPI mass loss rates have been estimated at -0.12 ± 0.02 m w.e. yr^{-1} since the last Lia maximum in 1870 (Glasser et al., 2011, , using a 850 kg m^{-3} density transformation). This centennial assessment, compared with an accurate assessment of recent NPI mass changes since 1975, is interesting to better understand glacier responses to past and present climate forcings in the Patagonian region and to improve modelled projections of NPI glacier changes.

Perspectives for future research

Below I present some future research directions regarding local and global applications of the datasets presented in this Thesis, and research questions that arise from the obtained results. Points 1 and 2 correspond to ongoing collaborations where our ASTERIX dataset is being applied to observe glacier changes at local scales (i.e. individual glacier or specific glacierized regions). Points 3 and 4 proposes further work on specific research directions. Points 5 and 6 address Andes-wide and global research directions.

Ongoing collaborations

1. Observing local glacier mass balance changes

The ASTERIX glacier elevation change dataset is a useful validation basis for direct glaciological measurements in the Andes. My thesis work had a close collaboration with the scientists from the IANIGLA (Mendoza). This institution is in charge of the national mass balance network presently including four glaciers since 2013, one for each of the major regions of the Southern Andes. During my thesis, I participated in the collection of mass balance data for these four glaciers. Pierre Pitte is now working on the publication of the observed changes over the Azufre Glacier (Central Andes, 35°S) and the Agua Negra glacier (Desert Andes, 30°S). The ASTERIX dataset produced here, together with other better-resolved geodetic estimates using SPOT and Pleiades DEMs will serve as calibration of the observed glaciological measurements. They will also provide a regional perspective of the changes experienced by these glaciers since the beginning of the 20th century. This interesting work will also allow to assess the reliability of ASTERIX over these two small glaciers (uncertainties in ASTERIX mass balance rates is high on glaciers smaller than 2 km2). This analysis can also be applied over other monitored Andean glaciers outside from Argentina and certainly opens the door for new collaborations.

Also in the frame of the collaboration with Argentinian glaciologists, Lidia Ferri is working on the analysis of ASTERIX individual glacier mass balance in the Central Andes (from 31°S-35°S) obtained using the National Glacier Inventory of Argentina (NGI). This complete and updated inventory gives unprecedented information about area, number and distribution of glaciers in the Argentine Andes and also includes detailed information on rock glaciers and debris-covered ice. Lidia's work is interesting in two ways: first, it will provide further insight on the sensitivity of the ASTERIX mass balance estimates

to the quality of the inventory (comparing the detailed NGI inventory with the RGI v6.0 used in this study). Secondly, Lidia will perform a first order analysis of the relation between glacier mass balance rates and the percentage of debris cover on the ice surfaces. Preliminary results show total glacier mass changes of -0.18 ± 0.17 m w.e. yr^{-1} in the entire study region for the period 2000-2018, ranging from -0.35 ± 0.08 m w.e. yr^{-1} in partly debris-covered glaciers to -0.02 ± 0.30 m w.e. yr^{-1} in rock glaciers.

2. Applying the albedo method to gain insight about annual glacier mass balance variability

The glacier snowline at the end of the summer, used as a proxy to retrieve the glacier ELA, has been successfully used to study glacier relationships with climate (Chinn et al., 2005; Rabatel et al., 2013b). A similar promising approach is the albedo method, which tracks the glacier mean albedo to find its annual minimum and link it with the glacier wide mass balance, because this minimum surface albedo is directly related to the equilibrium-line altitude (Brun et al., 2015; Dumont et al., 2012; Davaze et al., 2018). These methods permit to obtain annual mass balance variability in regions with scarce glacier mass balance observations, but need to be constrained with geodetic glacier mass balances estimates (Barandun et al., 2018; Davaze et al., 2018). During his PhD project, Lucas Davaze (IGE, Grenoble) developed a semi-automatic and reliable procedure to retrieve the end of summer snowlines from archives of high resolution satellite optical images. The algorithm was successfully applied in the Alps (Davaze et al., 2018), and was recently also successfully tested in the Inner Tropics during the Master's Thesis of Léna Gurriaran. In this last work, Léna was able to obtain the ELA and the annual mass balance for 82 glaciers in the Cordillera Blanca (Peru) and Cordillera Real (Bolivia). The algorithm was calibrated using the ASTERIX glacier elevation changes obtained during this PhD work for the period 2000-2018. The encouraging results already obtained in the Tropical regions open the possibility to apply the albedo method in other regions of the Andes. Its application in the Desert and Central Andes is certainly very interesting. We observed with this thesis work that these regions are presently undergoing an extended period of intense drought and present high future hydrological risks. Also, the latitudinal location and the infrequent cloud cover over this regions permit for an abundant satellite image acquisition, needed to assure the reliable observation and interpretation of the snowlines and albedo. The availability of annual mass balance observations over presently unmonitored glaciers, will allow a better understanding of the variability of annual glacier contribution in many vulnerable river basins in the Dry Andes, and will represent important information for future governmental decision.

Specific research directions

3. Constraining and understanding NPI sub-period mass balance changes

After a detailed analysis of the NPI IGM cartography (built from aerial photographs acquired in 1975, see Chapter 4), we suggest that this topography is not sufficiently reliable to calculate accurate NPI mass balance rates since 1975. This is an important finding, as important published studies have already relied on this NPI topography, and other topographies for different years (Aniya, 1999; Rignot et al., 2003; Rivera et al., 2007). All of these cartographies have been produced with outdated image processing techniques, which is most probably the source of the biases we found over the 1975 digitalized IGM contour lines at the high elevation ranges of the NPI. Rather than performing further analysis on this existing 'outdated' cartography, I propose to reprocess the 1975 topography from the original historical aerial photographs, directly obtaining better quality elevation maps. The use of state of the art photogrammetry techniques has proved to produce more accurate cartographies than the ones produced with outdated techniques, and assure a high level of statistical accuracy (e.g. Belart et al., 2019). This is possible for the NPI, as the original aerial images are available from the database of the IGM, Chile upon command. The availability of improved 1975-2000 NPI glacier elevation change rates, together with the results obtained in this work for more recent periods, will allow to observe accurate patterns on NPI Icefield-wide and individual glacier changes since 1975 (and even since the Last LIA maximum, considering the assessment from Glasser et al., 2011). A multi-temporal and resolved dataset like this is decisive to move forward in the understanding of the drivers of the temporal changes of glacier responses in Patagonia. However, direct climatic data available for this region is scarce, spatially isolated (e.g. there are no meteorological station recording data on the Western margins of the NPI) and in most

cases represent short or interrupted time periods. One promising objective is to exploit reanalysis climatic data available since 1979. Recent advances in climactic modelling have been able to better resolve the complex climatic patterns of the Patagonian region (Lenaerts et al., 2014). Gabriela Collao (PhD at IGE and now postdoc at NSIDC) is now working on the application of a regional atmospheric model (Modèle Athmosphérique Regional, MAR, Gallée and Schayes (1994)) to the NPI region (Collao Barrios, 2018). She aims on understanding the relation of NPI surface mass balance with atmospheric variables and large scale climatic modes like ENSO and SAM. Her results, together with the proposed ameliorations to the multi-period NPI mass balance estimations, would permit to analyse in more detail the climatic forcing on temperature and precipitation behind the observed glacier changes, at least since 1979.

4. The reason behind the contrasting response of freshwater and tidewater calving glaciers

When comparing our ASTERIX Andes-wide estimates with the surface mass balances modelled by Marzeion et al. (2015), we observed larger frontal ablations over freshwater calving glaciers than tidewater calving glaciers. These results suggest a possible influence of contrasted water and air temperatures between the Patagonian pacific coast and continental lakes located in the Andes (Falvey and Garreaud, 2009; Sugiyama et al., 2016; Vuille et al., 2015). To evaluate this hypothesis I propose to perform further data collection over selected Patagonian glaciers terminating at lakes and at the ocean at similar latitudes. Sugiyama et al. (2016) already revealed the thermal structure of proglacial lakes near the glacier fronts for several lake terminating glaciers. A good starting point would be to create a similar dataset showing the ocean thermal structure at tidewater glacier fronts. This, together with simultaneous air temperature measurements at freshwater and tidewater glacier fronts, would help validating if conditions are really contrasted or not for this Patagonian glaciers.

Global research directions

5. Using the ASTERIX glacier mass balance rates for model calibrations

The ASTERIX method is now highly automated: it has been successfully applied over the entire HMA (Brun et al., 2017) and the Andes (this PhD work) regions and has the potential to be applied at the global scale (ongoing PhD project of Romain Hugonnet). As suggested previously in the conclusions, there is still room for methodological improvements, mostly regarding the linearity assumption of glacier changes and the error assessment. The implementation of new DEM generation software like MicMac (Girod et al., 2015) could potentially improve the quality of ASTER DEMs with respect to the ASP DEMs used here (Shean et al., 2016). For future model calibration at the Andes-wide scale, our dataset is interesting. For example, Huss and Hock (2015) calibrated their GloGEM model with the glacier mass changes from Gardner et al. (2013). For the Andes, Gardner et al. (2013) mass loss is almost 30% larger for the period 2003-2009 than the ASTERIX mass loss estimated in this work (2000-2018). Moreover, this calibration is performed applying the same mass balance to all. This is not true for the Andes where we showed the important glacier to glacier variability. In this case, the error is much more than 30% for many glaciers. Consecutively, Huss and Hock (2018) use the glacier mass changes estimated by GloGEM to predict the global future hydrological response to glacier mass loss, where the Andes result as one of the regions where the largest changes are expected by the end of the century. It would be interesting to observe the difference of this model predictions (at least for the Andes) if the ASTERIX data is used as calibration. Pritchard (2019), applied the HMA ASTERIX data from Brun et al. (2017) in a recent assessment of the relative role of glaciers in river runoff at the scale of the entire HMA. He separates the three principal components contributing to river runoff: precipitation, the glacier balanced melt (seasonal component) and the glacier imbalance melt, showing that both components regarding glaciers are increased during a year of drought. An assessment like this is still lacking for the Andes, that has received relatively less attention than the HMA glaciers.

6. Using the ASTERIX glacier mass balance rates for Andes-wide applications

We hope our ASTERIX Andes-wide mass balance dataset will be as welcomed by the scientific community as it has been the case for HMA (Brun et al., 2017). Among other applications, the ASTERIX data

for the Asian region has been included as the reference for the HMA glacier contribution to sea level rise (Bamber et al., 2018). It has also been used to show that the 21st century slowdown of glaciers in the HMA is driven by the reduction of driving gravitational stress induced by the glacier thinning (Dehecq et al., 2019). We hope that Andes glaciers will get the interest of the scientific community they deserve. Our Andes-wide dataset will be freely available and will help to advance our understanding of ongoing and future Andean glacier response to climate change.

Conclusions Français

Résumé des résultats

Les objectifs de cette thèse étaient d'analyser les changements récents des glaciers andins ainsi que leur contribution décennale à la hausse du niveau des mers et à l'impact sur les ressources en eaux. Je résume ici les principaux résultats, les conclusions et nos réponses à de chacune des trois questions de recherche associée à ce travail, qui ont été introduites à la fin du Chapitre 1.

Question 1: Peut-on mesurer précisément les changements glaciaires dans les Andes en utilisant les DEMs multi temporelles optiques ASTER ?

Dans le Chapitre 2, nous avons validé la performance de la méthode ASTERIX en calculant les changements de masse des glaciers Andins. Le NPI a été choisi comme zone de validation car cela nous a permis d'appréhender les deux problématiques principales inhérent aux DEMs construits à partir d'images optiques : une couverture nuageuse fréquente et de vaste étendue enneigée. Au moment où j'ai commencé ce travail, en 2016, ASTERIX n'avait jamais été validé dans ces conditions sur un lieu différent. Au passage, une première contribution a été l'amélioration de l'inventaire du NPI.

En accord avec les précédentes études, notre analyse confirme la forte perte de masse des glaciers du NPI pour la période 2000-2012. Pour la totalité du NPI (environ 3800 km^2), nous avons trouvé un bilan de masse ATERIX fortement négatif de -1.06 ± 0.14 m w.e. a^{-1}, en très bon accord avec les -1.02 ± 0.21 m w.e. a^{-1} obtenu en comparant les DEMs SRTM et SPOT5. Nous confirmons la perte de masse à l'échelle globale du NPI estimé précédemment par deux études (Jaber et al., 2016; Willis et al., 2012a). La similarité de la perte de masse du NPI obtenu par ASTERIX avec les -1.02 ± 0.04 m w.e. a^{-1} estimé par Jaber et al. (2016) obtenue par DEMs à partir d'images radar (qui ne sont pas affectées par les nuages et qui couvrent bien la zone d'accumulation), prouve la pertinence de notre méthode, même pour les zones d'accumulation manquant de texture des grands champs de glace. La carte des changements d'élévation produite ici pour le NPI a ensuite été utilisée afin de contraindre le bilan de masse de surface du glacier San Rafael (Collao-Barrios et al., 2018).

Nous avons effectué une analyse détaillée de la pénétration du signal radar SRTM dans la bande C sur la neige du NPI. Nous confirmons le manque de pénétration significative sur la neige humide et le névé du champ de glace, sauf pour une petite région de haute altitude. En effet, de la neige sèche était présente en février 2000 au-dessus de 2900 m a.s.l (moins de 1% de la surface totale du NPI), avec des effets négligeables sur le bilan de mass du NPI. Nous avons ainsi validé la précision et cohérence de la méthode ASTERIX pour mesurer les changements glaciaires à l'échelle des Andes. Les incertitudes associées sont de l'ordre de 0.2 m w.e a^{-1}, comparable aux précédentes validations effectuées dans différents endroits du monde (Berthier et al., 2016, 2018; Brun et al., 2017; Menounos et al., 2019). Ce travail a constitué un tremplin vers une application globale de la méthode ASERIX à l'échelle des Andes (Question 2). Il constitue aussi la base pour répondre à la question 3, où nous analysons les variations du bilan de masse pendant différente sous-périodes depuis 1975.

Question 2: Quels sont les changements récents des glaciers Andins ? Pouvons-nous produire un jeu de données homogène et spatialement distribué des changements topographiques glaciaires des deux dernières décennies ? Pouvons-nous obtenir une résolution suffisamment bonne permettant d'analyser les changements glaciaires à différentes échelles et leur impact respectifs?

Au tout début de ce travail doctoral, l'objectif principale était de calculer les changements de masse des glaciers situé dans la partie sud des Andes seulement (région RGI 17). Cependant, les efforts fournis afin d'automatiser le protocole permettant la production et le post-traitement massif des DEMs ASTER m'ont permis d'ajouter les Andes Tropicales à ma zone d'étude (région RGI 16 seulement pour les Andes à faible latitude, excluant les glaciers tropicaux en Afrique et Indonésie). Ainsi j'ai pu analyser la totalité des Andes. Fanny Brun a en partie automatisé la méthode ASTERIX pour calculer les changements de masse pour les Hautes Montagne d'Asie (Brun et al., 2017), suivi par Romain Hugonnet qui compléta cette automatisation. J'ai ensuite effectué des validations croisées, pour s'assurer du bon fonctionnement sur la totalité des Andes. Nous avons aussi appliqué des modifications supplémentaires pour les techniques de post-traitement des grilles de changement d'élévation, afin de les rendre compatible face à la forte variabilité des réponses glaciaires dans les Andes (qui est bien plus grande qu'en Himalaya par exemple).

Dans le Chapitre 3, nous avons compilé plus de 30000 DEMs ASTER dans le but de générer des cartes des changements d'élévation de haute résolution (30m) à travers les Andes, pour une deux décennies (2000-2018) et pour chaque décennie également (2000-2009 et 2009-2018). Nous fournissons aussi les taux de bilans de masse individuels pour 17832 glaciers (parmi les 18799 du RGI v6.0) pour les 3 différentes périodes. Ce jeu de données homogène et spatialement résolu nous a permis d'analyser les changements des glaciers Andins à différentes échelles spatio-temporelles. Nous estimons ainsi une perte de masse de glace de -22.9 ± 5.9 Gt a^{-1} durant les deux dernières décennies (-26.0 ± 6.0 Gt a^{-1} en incluant les pertes subaquatiques estimées par Braun et al., (2019) pour les glaciers patagons). Cette perte correspond à 0.06 ± 0.02 mm a^{-1} de hausse du niveau des mers (les pertes subaquatiques ne sont pas prises en compte car cette glace "déplaçait" déjà l'eau de mer). Cela représente un peu plus de 10% de la contribution globales des glaciers dans le monde (0.55 mm a^{-1}) durant 2002-2016 (Bamber et al., 2018). La décroissance glaciaire concerne tous les sous-régions Andines, avec le taux de bilan de masse le plus négatif dans les Andes Patagoniennes (-0.78 ± 0.25 m w.e. a^{-1}) et les Andes Tropicales (-0.42 ± 0.24 m w.e. a^{-1}), et un bilan moins négatif pour la région intermédiaire des Andes arides (-0.28 ± 0.18 m w.e. a^{-1}).

L'analyse des des pertes de masses glaciaires par décennie est une contribution importante et un aspect original de ce travail, alors que les estimations précédentes ne concernaient qu'une seule période (pour la plupart d'entre elles la première décennie du 21^{me} siècle). Cette analyse révèle des pertes glaciaires relativement stables d'une décennie à l'autre, reflétant principalement le comportement similaire des champs de glaces Patagons qui représentent la majorité des glaciers Andins. Cependant, nous avons mis en évidence une région intermédiaire (entre 26° et 45°S) où les glaciers ont été relativement stables de 2000 à 2009, puis ont connu un taux d'amincissement drastique depuis 2010. Ce brutal changement coïncide avec la période de sécheresse intense, appelé aussi 'megadrought', sévissant dans les Andes arides depuis 2010 (Garreaud et al., 2017; Rivera et al., 2017). L'évaluation des contributions aux débit des rivières de ces pertes de masse des glaciers sur quatre bassins versants situés dans les Andes semi-arides révèle que les glaciers ont en partie aidé à minimiser les impacts négatifs de cette sécheresse sur les ressources en eau. Cette étude vient renforcer les travaux précédents indiquant l'importance des glaciers comme ressources en eau dans les région semi arides (Buytaert et al., 2017; Huss et al., 2017; Huss and Hock, 2018; Kaser et al., 2010; Vuille et al., 2018; Soruco et al., 2015; Burger et al., 2018; Gascoin et al., 2011) .

Nous proposons aussi une comparaison détaillée de notre estimation géodésique avec le bilan de masse de surface obtenu par Marzeion et al. (2015). Ceci nous a permis de proposer une estimation au premier ordre des pertes de glace par ablation frontale, issue du vêlage de la langue terminale des glaciers se

terminant dans les lacs ou l'océan en Patagonie. Les pertes par ablation frontale atteignent ainsi 14.7 ± 6.0 Gt a^{-1} pour la période 2000-2015, correspondant à presque deux tiers de la perte de glace totale pour la même période (-24.9 ± 6.6 Gt a^{-1} en considérant les pertes subaquatiques calculés par Braun et al. (2019)). Ceci met en évidence le rôle majeur de la dynamique de vêlage pour les glaciers Patagons.

La publication des estimations géodésiques basées sur les images radar par Braun et al. (2019) pendant le développement de ce travail a permis de valider et améliorer la méthode ASTERIX pour les Andes. Trois conclusions importantes sont ressorties de la comparaison détaillée entre nos cartes de changement d'élévation ASTERIX et celles de Braun et al. (2019). Premièrement, une étude de la sensitibité des données manquante concernant les bilans de masse ASTERIX nous a permis de confirmer la bonne représentativité de notre échantillonnage, même pour la zone d'accumulation peu texturée des champs de glace (ceci a été possible seulement parceque la grille des changements d'élévation obtenu par Braun et al. (2019) est presque complète pour les vastes champs de glace). Deuxièmement nous avons montré une pénétration probable du signal radar pour les glaciers de haute altitude et des parties les plus froides des Andes. Et finalement, nous avons découvert que le filtre 3NMAD, souvent utilisé afin d'exclure les valeurs aberrantes et ainsi intégrer les tendances de changement d'élévation à l'échelle régionale (e.g. Braun et al., 2019; Brun et al., 2017; Menounos et al., 2019), peut entraîner des erreurs dans les estimations des bilans de masse. Ceci concerne les régions avec une forte variabilité de perte de glace, comme en Patagonie et en Terre de Feu. Ce filtre doit donc être appliqué individuellement pour chaque glacier et non pour des régions entières.

Ce travail est très proche de la publication (accepté "en principe"), par conséquent notre jeu de données n'a pas encore été utilisé par d'autres groupe de recherche attendant sa disponibilité. Notre carte des changements d'élévations à haute résolution a de nombreuses applications. Elle permet l'évaluation des changements glaciaires à une échelle locale, régionale et globale dans les Andes. Elle procure aussi des informations supplémentaires afin de mieux calibrer les modèles glaciologiques et hydrologiques permettant de projeter le futur des glaciers et d'améliorer la gestion des ressources en eau dans les Andes.

Il est toutefois important de noter que même si la performance de la méthode ASTERIX a été bien démontré dans diférentes régions, certaines limitations sont encore présentes et devront être améliorer par la suite. L'une d'entre elle est le fait d'assumer un comportement linéaire des pertes de masse dans le temps. Les glaciers sont loin d'avoir ce comportement linéaire et nous suspectons, au sein de notre méthode ASTERIX, quelques problèmes issus de la saisonnalité des changements glaciaires. Pour cette même raison, l'origine des erreurs de triangulation n'est pas encore complètement comprise. En effet nous avons observé des résidus importants de triangulation pour des régions présentant une bonne couverture ASTER et un grand nombre de DEMs. Et cela est probablement inhérent aux variations saisonnière des glaciers. Les efforts de notre groupe de recherche et de nos collaborateurs sont directement dirigé vers une résolution de ces effets saisonnier et une meilleure évaluation des erreurs afin de poursuivre l'amélioration ASTERIX.

Question 3: Le taux de perte de masse des glaciers du NPI a-t-il augmenté depuis 1975 ? Pouvons-nous exploiter des archives multiples de données topographiques afin de mesurer les changements d'élévation du NPI selon des sous périodes, de 2000 à 2016 ?

Dans le Chapitre 4, nous avons exploité plusieurs DEMs dans le but de révéler les changements glaciaires du NPI pour quatre périodes distinctes (1975-2000, 2000-2005, 2005-2012, 2012-2016). Les résultats préliminaires indiquent une croissance générale du taux de perte de masse du NPI de 1975 à 2016. La période 1975-2000 est marqué par un taux de perte modéré (de l'ordre de -0.6 m w.e. a^{-1}) suivi d'un basculement notable vers un fort taux de perte depuis 2012 (1.2 ± 0.2 m w.e. a^{-1}). Notre estimation du taux d'amincissement depuis 1975 n'est pas pionnière. Nous avons suivi une stratégie similaire et utiliser le même jeu de données précédemment publié par Rignot et al. (2003), (SRTM et cartes topographiques IGM chiliennes digitalisées), en obtenant la même estimation avec des incertitudes plus grandes. Après une analyse exhaustive de la grille des changements d'élévation, nous mettons en évidence un biais

possible due aux artefacts des cartes IGM suggérant à un épaississement fort (et inattendu) en zone d'accumulation. Ces biais pourraient être liées aux techniques désuètes pour produire ces cartes et le manque de point de contrôle. Nous suggérons ainsi que les cartes IGN, en tant que-t-elle, sont inappropriées pour calculer précisément le bilan de masse du NPI. Afin de palier à ce problème, une solution serait de construire à nouveau les cartes de 1975 à partir des images aériennes d'origine en utilisant les techniques de photogrammétrie modernes, assurant un meilleur niveau de précision (Belart et al., 2019; Papasodoro et al., 2015).

Nos résultats issus des trois sous-périodes après 2000 montrent une accélération des pertes de masse du NPI, passant de taux fort mais constant d'amincissement (de l'ordre de -0.8 m w.e. a^{-1}), à des valeurs très forte dans les dernières années jusqu'en 2016 (-1.2 ± 0.22 m w.e. a^{-1}). Cette augmentation des pertes de masse est aussi observée pour la majorité des glaciers du NPI, pris individuellement. Nous avons confiance en ces résultats grâce à la bonne qualité des DEMs SPOT utilisé comme données d'entré et grâce au bon accord avec une étude récente du bilan de masse géodésique par (Abdel Jaber et al., 2018) pour les même sous-périodes. J'aimerais accorder une attention particulière à poursuivre ce travail dans le futur en recalculant les données d'élévation pour 1975. Le taux de perte de masse a été estimé à -0.12 ± 0.02 m w.e. a^{-1} depuis le dernier maximum du Petit Age de Glace en 1870 (Glasser et al., 2011, , en utilisant la valeur de 850 kg m^{-3} pour convertir en densité). Cette évaluation centenaire, comparée avec une évaluation précise des changements récent du NPI, est intéressante pour mieux comprendre les réponses des glaciers aux forçages climatiques passé, présent et future en Patagonie, et pour améliorer les projections modélisées des variations glaciaires du NPI.

Annexes

Annex 1: Summary of published mass balance estimates along the Andes

Table A1: Summary of the published mass balance estimates for local glaciers and specific glacierized regions of the RGI region 16 Low latitudes (Andes only, neglecting tropical glaciers in Africa and Indonesia) obtained by diverse methodologies. In bold, studies published during the development of this PhD work (2016 onwards).

Region	Source	Glacier name	Area (km^2)	MB (m w.e. yr^{-1})	Start date	End date	Method
Inner Tropics	**Basantes-Serrano et al. (2016)**	Antizana 15 alpha	0.28	-0.12 ± 0.16	1998	2009	Glaciological adjusted with Geodetic Aerial photographs
	Mölg et al. (2017)	Conejeras	0.2	-3.00 ± 0.20	2006	2015	Glaciological
	Rabatel et al. (2017)	Conejeras	0.2	-2.40	2005	2014	Geodetic Aerial photographs - LIDAR
	Rabatel et al. (2017)	Santa Isabel Icecap	12	-2.40	1987	2014	Geodetic Aerial photographs - LIDAR
	Rabatel et al. (2017)	Santa Isabel Icecap	12	-2.60	1987	2005	Geodetic Aerial photographs - LIDAR
Outer Tropics	Soruco et al. (2009b)	Zongo	1.96	-0.75	1956	2006	Glaciological and Geodetic Aerial photographs
	Soruco et al. (2015)	Hampaturi	2.5	-0.70	1963	2006	Geodetic Aerial photographs
	Soruco et al. (2015)	Hampaturi	1.6	-1.20	1997	2006	Geodetic Aerial photographs
	Soruco et al. (2015)	Incachaca	1.4	-0.60	1963	2006	Geodetic Aerial photographs
	Soruco et al. (2015)	Incachaca	0.9	-1.10	1997	2006	Geodetic Aerial photographs
	Soruco et al. (2015)	Milluni	2.5	-0.43	1963	2006	Geodetic Aerial photographs
	Soruco et al. (2015)	Milluni	1.6	-0.93	1997	2006	Geodetic Aerial photographs
	Soruco et al. (2015)	Tuni-Condoriri	7	-0.59	1963	2006	Geodetic Aerial photographs
	Soruco et al. (2015)	Tuni-Condoriri	4.6	-1.09	1997	2006	Geodetic Aerial photographs
	Soruco et al. (2009a)	Cordilera Real (21 glaciers)	8.4	0.70 ± 0.11	1963	1975	Geodetic Aerial photographs
	Soruco et al. (2009a)	Cordilera Real (21 glaciers)	8.4	-0.50 ± 0.27	1975	1983	Geodetic Aerial photographs
	Soruco et al. (2009a)	Cordilera Real (21 glaciers)	8.4	0.00 ± 0.23	1983	1997	Geodetic Aerial photographs
	Soruco et al. (2009a)	Cordilera Real (21 glaciers)	8.4	-0.40 ± 0.37	1997	2006	Geodetic Aerial photographs
	Ramírez et al. (2001)	Chacaltaya	0.06	-0.51	1940	1998	Glaciological and Geodetic Aerial photographs
	Ramírez et al. (2001)	Chacaltaya	0.06	-0.89	1983	1998	Glaciological and Geodetic Aerial photographs
	Rabatel et al. (2006)	Charquini	0.5	-0.10	1700	1870	Reconstruction since last LIA
	Rabatel et al. (2006)	Charquini	0.5	-0.40	1870	1910	Reconstruction since last LIA
	Rabatel et al. (2006)	Charquini	0.5	-0.25	1910	1983	Reconstruction since last LIA
	Rabatel et al. (2006)	Charquini	0.5	-1.36	1983	1997	Reconstruction since last LIA

*Estimates modified to correspond to the density conversion factor of 850 kg m^3 (Huss, 2013).

Table A2: Summary of the published mass balance estimates for local glaciers and specific glacierized regions of the RGI region 17 Southern Andes obtained by diverse methodologies. In bold, studies published during the development of this PhD work (2016 onwards).

Region	Source	Glacier name	Area (km^2)	MB (m w.e. yr^{-1})	Start date	End date	Method
Desert Andes	Gascoin et al. (2011)	Toro1, Toro 2, Guanaco, Esperanza	4.3	-0.84	2003	2008	Hydrological
	Rabatel et al. (2011)	Toro1, Toro 2, Guanaco, Esperanza	4.3	-0.97 ± 0.70	2003	2009	Glaciological
	Rabatel et al. (2011)	Guanaco	1.8	-0.41 ± 0.43	2003	2009	Glaciological
Central Andes	Leiva et al. (2007)	Piloto Este	1.4	-0.44	1979	2003	Glaciological
	Masiokas et al. (2016)	Echaurren Norte	0.17	-0.35	1977	2012	Model based reconstruction and glaciological records
	Farías-Barahona et al. (2019)	Echaurren Norte	0.17	-0.68 ± 0.09	1955	2015	Geodetic SRTM-TanDEM-X
	Farías-Barahona et al. (2019)	Echaurren Norte	0.17	0.54 ± 0.40	2000	2009	Geodetic SRTM-TanDEM-X
	Farías-Barahona et al. (2019)	Echaurren Norte	0.17	-1.20 ± 0.09	2010	2015	Geodetic SRTM-TanDEM-X
	Burger et al. (2018)	Yeso	2.2	-0.03 ± 0.08	2000	2013	Geodetic SRTM-TanDEM-X
	Burger et al. (2018)	Yeso	2.2	-0.92 ± 0.13	2012	2015	Geodetic LIDAR-LIDAR
	Burger et al. (2018)	Bello	4.6	-0.01 ± 0.08	2000	2013	Geodetic SRTM-TanDEM-X
	Burger et al. (2018)	Bello	4.6	-0.98 ± 0.13	2012	2015	Geodetic LIDAR-LIDAR
	Burger et al. (2018)	Piramide	4.7	-0.12 ± 0.08	2000	2013	Geodetic SRTM-TanDEM-X
	Burger et al. (2018)	Piramide	4.7	-0.64 ± 0.12	2012	2015	Geodetic LIDAR-LIDAR
North Patagonia	**Schaefer et al. (2017)**	Volcan Mocho Choshuenco	16.9	-1.05	2006	2015	Model based reconstruction
	Schaefer et al. (2017)	Volcan Mocho Choshuenco	16.9	-0.90 ± 0.36	2009	2013	Glaciological
	Rivera et al. (2006)	Volcan Mocho Choshuenco	16.9	-0.18 ± 0.46*	1961	2000	Geodetic Aerial photographs - SRTM
	Rivera et al. (2006)	Volcan Villarrica	30.1	-0.59 ± 0.46*	1961	2000	Geodetic Aerial photographs - SRTM
	Rivera et al. (2015)	Volcan Villarrica	30.1	-0.81*	1961	2012	Geodetic Aerial photographs - LIDAR
	Rivera et al. (2015)	Volcan Villarrica	30.1	-0.53*	2000	2012	Geodetic SRTM-LIDAR
	Bown and Rivera (2007)	Casa Pangue	6	-1.96 ± 0.51*	1961	1998	Geodetic Aerial photographs
	Bown and Rivera (2007)	Casa Pangue	6	-1.02 ± 0.94*	1961	1981	Geodetic Aerial photographs
	Bown and Rivera (2007)	Casa Pangue	6	-3.06 ± 0.51*	1981	1998	Geodetic Aerial photographs
	Ruiz et al. (2017)	Volcan Tronador	57	-0.17	2000	2012	Geodetic SRTM-Pleiades
South Patagonia	**Braun et al. (2019)**	NPI	4653	-0.85 ± 0.07	2000	2012/15	Geodetic SRTM-TanDEM-X
	Rignot et al. (2003)	NPI	4200	-0.65 ± 0.08*	1975	2000	Geodetic Aerial photographs - SRTM
	Rivera et al. (2007)	NPI	3953	-0.86 ± 0.25*	1975	2001	Geodetic Aerial photographs - ASTER
	Willis et al. (2012a)	NPI	3953	-0.96 ± 0.04*	2001	2011	Geodetic ASTER time series
	Jaber et al. (2016)	NPI	3867	-1.02 ± 0.04	2000	2014	Geodetic SRTM-TanDEM-X
	Abdel Jaber et al. (2018)	NPI	3975	-0.91 ± 0.04*	2000	2012	Geodetic SRTM-TanDEM-X
	Abdel Jaber et al. (2018)	NPI	3975	-1.20 ± 0.15*	2012	2016	Geodetic TanDEM-X-TanDEM-X
	Foresta et al. (2018)	NPI	4046	-1.43 ± 0.24*	2011	2017	Geodetic Cryosat 2
	Falaschi et al. (2016)	Mountain glaciers	1314	-0.46 ± 0.37	2000	2012	Geodetic SRTM-SPOT5
	Rignot et al. (2003)	SPI	13000	-0.88 ± 0.05*	1975	2000	Geodetic Aerial photographs - SRTM
	Braun et al. (2019)	SPI	13231	-0.86 ± 0.08	2000	2012/14	Geodetic SRTM-TanDEM-X
	Foresta et al. (2018)	SPI	12637	-0.98 ± 0.11*	2011	2017	Geodetic Cryosat 2
	Willis et al. (2012b)	SPI	12118	-1.49 ± 0.09*	2000	2012	Geodetic ASTER time series
	Abdel Jaber et al. (2018)	SPI	12999	-0.97 ± 0.03*	2000	2012	Geodetic SRTM-TanDEM-X
	Abdel Jaber et al. (2018)	SPI	12999	-0.78 ± 0.12*	2012	2016	Geodetic SRTM-TanDEM-X
	Malz et al. (2018)	SPI	12573	-0.89 ± 0.24*	2000	2015/16	Geodetic SRTM-TanDEM-X
	Schaefer et al. (2015)	SPI	13000	1.81	1975	2000	Model based SMB reconstruction
	Schaefer et al. (2015)	SPI	12100	1.49	2000	2011	Model based SMB reconstruction
	Glasser et al. (2011)	NPI & SPI	14000	-0.04 ± 0.01	1870	2010	Reconstruction since last LIA
	Aniya (1999)	NPI & SPI	17200	-0.80 ± 0.31	1945	1996	Aerial photographs
	Chen et al. (2007)	NPI & SPI	17200	-1.38 ± 0.54*	2002	2006	Gravimetry (GRACE)
	Ivins et al. (2011)	NPI & SPI	17200	-1.28 ± 0.30	2003	2009	Gravimetry (GRACE)
	Moller and Schneider (2010)	GCN	253	-0.35 ± 0.16	1984	2000	Model based reconstruction
Fueguian Andes	Buttstädt et al. (2009)	Martial Este	0.09	-0.77	1960	2006	Model based reconstruction
	Buttstädt et al. (2009)	Martial Este	0.09	-0.53	2000	2006	Model based reconstruction
	Melkonian et al. (2013)	Cordillera Darwin	2605	-1.42 ± 0.57*	2000	2011	Geodetic SRTM - ASTER time series

*Estimates modified to correspond to the density conversion factor of 850 kg m^3 (Huss, 2013).

Table A3: Comparison of mass balance change estimates for the entire Low Latitude and Southern Andes regions. In bold, studies published during the development of this PhD work (2016 onwards).

RGI Region	Method	Period	$\dot{M}$ rate (Gt yr^{-1})	Reference
Low Latitudes	Glaciological and geodetic interpolated	2003 - 2009	-4 ± 1	Gardner et al. (2013) update of Cogley (2009)
	Glaciological and geodetic interpolated	2002 - 2014	-2.2 ± 1.3	**Reager et al. (2016) update of Cogley (2009)**
	Glaciological and geodetic interpolated	2006 - 2016	-2.1 ± 0.7	**Zemp et al. (2019)**
	Glaciological and geodetic interpolated	2000 - 2016	-2.0 ± 0.6	**Zemp et al. (2019)**
	Gravimetry (GRACE)	2003 - 2010	-6 ± 12	Jacob et al. (2012)
	Gravimetry (GRACE)	2002 - 2016	-1.2 ± 3.5	**Wouters et al. (2019)**
	Model based SMB reconstruction	2000 - 2015	-1.1	Marzeion et al. (2015) updated in this study
	Geodetic (TanDEM-X)	2000 - 2011/15	-0.5 ± 0.0	**Braun et al. (2019)**
Southern Andes	Glaciological and geodetic interpolated	2003 - 2009	-21 ± 11	Gardner et al. (2013) update of Cogley (2009)
	Glaciological and geodetic interpolated	2006 - 2016	-34 ± 11	**Zemp et al. (2019)**
	Gravimetry (GRACE)	2003 - 2010	-23 ± 9	Jacob et al. (2012)
	Gravimetry (GRACE)	2003 - 2009	-29 ± 11	Gardner et al. (2013)
	Gravimetry (GRACE)	2002 - 2014	-33.1 ± 12.1	**Reager et al. (2016)**
	Gravimetry (GRACE)	2002 - 2016	-30.3 ± 11	**Wouters et al. (2019)**
	Model based SMB reconstruction	2000 - 2015	-10.3	Marzeion et al. (2015) updated in this study
	Geodetic (TanDEM-X)	2000 - 2011/15	-17.8 ± 0.6	**Braun et al. (2019)**

* Values are converted from mm w.e. yr^{-1} to Gt yr^{-1} using the same glacierized area as in our study.

Annex 2: Sub-period mass balance rates for NPI individual glaciers

Table A4: Mass balance rates of NPI individual glaciers for the sub-periods 2000-2005 and 2005-2012. Reported areas correspond to the mean glacier area between the first and last years of the time period. Glaciers are sorted in alphabetical order.

Glacier name	2000 - 2005			2005 - 2012		
	Mean Area (km^2)	Measured Area (%)	Mass balance (m w.e. yr^{-1})	Mean Area (km^2)	Measured Area (%)	Mass balance (m w.e. yr^{-1})
Acodado	235	80	-1.77 ± 0.24	230	62	-1.50 ± 0.27
Andree	7	43	-0.32 ± 0.23	7	71	-0.46 ± 0.16
Arco	26	73	-0.18 ± 0.14	26	62	-0.08 ± 0.17
Bayo	14	21	0.25 ± 0.29	14	16	0.09 ± 0.30
Benito	160	79	-1.48 ± 0.21	157	70	-1.29 ± 0.22
Cachet	23	51	-0.26 ± 0.20	23	50	-0.36 ± 0.21
Cachet Norte	11	52	0.00 ± 0.20	11	55	-0.25 ± 0.20
Circo	3	12	0.08 ± 0.31	3	33	-0.01 ± 0.25
Colonia	306	74	-0.52 ± 0.15	303	55	-0.67 ± 0.22
Cristal	5	60	0.81 ± 0.21	5	38	-0.19 ± 0.24
Exploradores	80	33	0.02 ± 0.25	79	19	0.11 ± 0.29
Fiero	38	30	-0.29 ± 0.26	37	27	-0.82 ± 0.32
Frankel	30	77	-0.78 ± 0.16	30	74	-0.56 ± 0.15
Grosse	59	52	0.15 ± 0.20	56	3	-0.16 ± 0.33
Gualas	117	64	-1.01 ± 0.22	114	56	-0.87 ± 0.23
HPN1	151	77	-2.24 ± 0.30	145	69	-2.27 ± 0.34
HPN4	51	57	-0.92 ± 0.23	50	55	-0.81 ± 0.23
Hyades	9	41	0.44 ± 0.24	9	42	-0.40 ± 0.24
Leones	65	61	0.58 ± 0.19	65	53	-0.07 ± 0.20
Mocho	3	22	0.26 ± 0.29	3	50	-0.39 ± 0.21
Mormex	3	12	-0.40 ± 0.32	3	46	-0.44 ± 0.23
Nef	140	78	-0.46 ± 0.14	139	65	-0.75 ± 0.19
Pared Norte	70	71	-1.03 ± 0.20	70	64	-1.22 ± 0.24
Pared Sur	25	57	-1.10 ± 0.25	24	45	-1.37 ± 0.33
Pissis	14	27	-0.01 ± 0.27	13	26	-0.32 ± 0.28
Reichert	66	60	-0.94 ± 0.23	65	57	-0.62 ± 0.21
San Quintin	760	80	-0.67 ± 0.14	749	57	-0.60 ± 0.21
San Rafael	721	81	-1.06 ± 0.17	717	54	-0.77 ± 0.23
Soler	50	67	-0.30 ± 0.16	50	54	-0.41 ± 0.20
Steffens	467	70	-1.10 ± 0.21	461	57	-0.92 ± 0.23
Strindberg	16	69	-0.65 ± 0.17	16	73	-0.87 ± 0.18
U2	17	1	0.00 ± 0.34	17	0	0.01 ± 0.34
U3	17	6	0.17 ± 0.33	17	5	-0.20 ± 0.33
U4	30	50	-0.48 ± 0.22	27	58	-0.62 ± 0.21
U5	5	72	-0.59 ± 0.16	5	59	-0.72 ± 0.21
U6	18	17	-0.79 ± 0.34	17	35	0.06 ± 0.25
U7	4	12	-0.02 ± 0.31	4	32	-0.27 ± 0.26
Verde	7	30	-0.07 ± 0.26	7	36	-0.13 ± 0.24

Table A5: Mass balance rates of NPI individual glaciers for the sub-period 2012-2016 and the complete period 2000-2016. Reported areas correspond to the mean glacier area between the first and last years of the time period. Glaciers are sorted in alphabetical order.

Glacier name	2000 - 2005			2005 - 2012		
	Mean Area (km^2)	Measured Area (%)	Mass balance (m w.e. yr^{-1})	Mean Area (km^2)	Measured Area (%)	Mass balance (m w.e. yr^{-1})
Acodado	224	72	-2.46 ± 0.35	230	69	-2.08 ± 0.31
Andree	7	89	-1.00 ± 0.14	7	43	-0.65 ± 0.25
Arco	26	81	-0.77 ± 0.15	26	69	-0.40 ± 0.16
Bayo	13	27	-0.33 ± 0.28	14	16	-0.74 ± 0.34
Benito	154	85	-1.65 ± 0.21	157	73	-1.63 ± 0.25
Cachet	23	70	-0.72 ± 0.18	23	47	-0.66 ± 0.24
Cachet Norte	11	79	-0.88 ± 0.16	11	52	-0.49 ± 0.21
Circo	2	43	-1.00 ± 0.29	3	5	-0.14 ± 0.33
Colonia	300	67	-1.42 ± 0.25	303	62	-1.03 ± 0.23
Cristal	5	77	-0.20 ± 0.13	5	58	-0.36 ± 0.19
Exploradores	77	38	0.02 ± 0.24	78	29	-0.56 ± 0.28
Fiero	36	63	-0.92 ± 0.21	36	27	-0.94 ± 0.33
Frankel	29	88	-0.65 ± 0.12	30	75	-0.80± 0.17
Grosse	54	11	-0.21 ± 0.32	57	19	-0.84 ± 0.34
Gualas	113	79	-0.76 ± 0.15	116	62	-1.14 ± 0.24
HPN1	139	83	-2.90 ± 0.34	145	74	-2.68 ± 0.36
HPN4	50	84	-1.73 ± 0.22	50	70	-1.57 ± 0.26
Hyades	8	62	-0.17 ± 0.17	9	40	-0.17 ± 0.23
Leones	65	76	0.19 ± 0.14	65	61	0.00 ± 0.18
Mocho	3	73	-0.04 ± 0.14	3	18	-0.17 ± 0.29
Mormex	3	84	-0.58 ± 0.13	3	12	-0.62 ± 0.34
Nef	138	76	-1.35 ± 0.21	139	70	-1.00 ± 0.20
Pared Norte	69	83	-2.30 ± 0.28	69	70	-1.52 ± 0.25
Pared Sur	24	72	-2.42 ± 0.34	24	54	-1.63 ± 0.32
Pissis	13	49	-0.72 ± 0.24	13	33	-0.71 ± 0.29
Reichert	64	74	-0.29 ± 0.14	65	59	-0.90 ± 0.23
San Quintin	738	63	-1.00 ± 0.22	749	66	-0.87 ± 0.20
San Rafael	714	65	-0.49 ± 0.18	718	68	-1.00 ± 0.20
Soler	49	71	-0.74 ± 0.17	50	59	-0.68 ± 0.20
Steffens	454	79	-1.98 ± 0.26	461	75	-1.74 ± 0.25
Strindberg	15	87	-0.89 ± 0.14	16	69	-0.97 ± 0.20
U2	17	77	-0.68 ± 0.15	17	46	-0.53 ± 0.23
U3	17	74	-0.42 ± 0.15	17	61	-0.23 ± 0.18
U4	24	87	-1.44 ± 0.18	27	49	-0.97 ± 0.26
U5	5	74	-1.34 ± 0.21	5	68	-0.98 ± 0.20
U6	17	57	0.13 ± 0.19	17	8	-0.57 ± 0.35
U7	4	64	-0.10 ± 0.17	4	12	-0.20 ± 0.31
Verde	7	54	0.17 ± 0.20	7	26	-0.29 ± 0.28

Bibliography

Abdel Jaber, W., Rott, H., Floricioiu, D., Wuite, J., and Miranda, N. (2018). Heterogeneous spatial and temporal pattern of surface elevation change and mass balance of the Patagonian icefields between 2000 and 2016. *The Cryosphere Discussions*, pages 1–39.

Andreassen, L. M., Elvehøy, H., Kjøllmoen, B., and Engeset, R. V. (2016). Reanalysis of long-term series of glaciological and geodetic mass balance for 10 Norwegian glaciers. *The Cryosphere*, 10(2):535–552.

Andreoli, R. V. and Kayano, M. T. (2005). ENSO-related rainfall anomalies in South America and associated circulation features during warm and cold Pacific decadal oscillation regimes. *International Journal of Climatology*, 25(15):2017–2030.

Aniya, M. (1999). Recent Glacier Variations of the Hielos Patagónicos, South America, and Their Contribution to Sea-Level Change. *Arctic, Antarctic, and Alpine Research*, 31(2):165–173.

Aniya, M. (2007). Glacier variations of Hielo Patagónico Norte, Chile, for 1944/45-2004/05. *Bulletin of glaciological research*, 24:59–70.

Aniya, M. and Enomoto, H. (1986). Glacier Variations and Their Causes in the Northern Patagonia Icefield, Chile, since 1944. *Arctic and Alpine Research*, 18(3):307–316.

Aniya, M., Sato, H., Naruse, R., Skvarca, P., and Casassa, G. (1997). Recent Glacier Variations in the Southern Patagonia Icefield, South America. *Arctic and Alpine Research*, 29(1):1–12.

Aravena, J.-C. and Luckman, B. H. (2009). Spatio-temporal rainfall patterns in Southern South America. *International Journal of Climatology*, 29(14):2106–2120.

Arendt, A. A., Echelmeyer, K. A., Harrison, W. D., Lingle, C. S., and Valentine, V. B. (2002). Rapid Wastage of Alaska Glaciers and Their Contribution to Rising Sea Level. *Science*, 297(5580):382–386.

Ayala, A., Pellicciotti, F., MacDonell, S., McPhee, J., Vivero, S., Campos, C., and Egli, P. (2016). Modelling the hydrological response of debris-free and debris-covered glaciers to present climatic conditions in the semiarid Andes of central Chile. *Hydrological Processes*, 30(22):4036–4058.

Bamber, J. L., Westaway, R. M., Marzeion, B., and Wouters, B. (2018). The land ice contribution to sea level during the satellite era. *Environmental Research Letters*, 13(6):063008.

Barandun, M., Huss, M., Usubaliev, R., Azisov, E., Berthier, E., Kääb, A., Bolch, T., and Hoelzle, M. (2018). Multi-decadal mass balance series of three Kyrgyz glaciers inferred from modelling constrained with repeated snow line observations.

Barcaza, G., Aniya, M., Matsumoto, T., and Aoki, T. (2009). Satellite-Derived Equilibrium Lines in Northern Patagonia Icefield, Chile, and Their Implications to Glacier Variations. *Arctic, Antarctic, and Alpine Research*, 41(2):174–182.

Basantes-Serrano, R., Rabatel, A., Francou, B., Vincent, C., Maisincho, L., Cáceres, B., Galarraga, R., and Alvarez, D. (2016). Slight mass loss revealed by reanalyzing glacier mass-balance observations on Glaciar Antisana 15 (inner tropics) during the 1995–2012 period. *Journal of Glaciology*, 62(231):124–136.

Belart, J. M. C., Magnússon, E., Berthier, E., Pálsson, F., Aðalgeirsdóttir, G., and Jóhannesson, T. (2019). The geodetic mass balance of Eyjafjallajökull ice cap for 1945–2014: processing guidelines and relation to climate. *Journal of Glaciology*, pages 1–15.

Berthier, E., Arnaud, Y., Baratoux, D., Vincent, C., and Rémy, F. (2004). Recent rapid thinning of the "Mer de Glace" glacier derived from satellite optical images. *Geophysical Research Letters*, 31(17):L17401.

Berthier, E., Arnaud, Y., Kumar, R., Ahmad, S., Wagnon, P., and Chevallier, P. (2007). Remote sensing estimates of glacier mass balances in the Himachal Pradesh (Western Himalaya, India). *Remote Sensing of Environment*, 108(3):327–338.

Berthier, E., Arnaud, Y., Vincent, C., and Remy, F. (2006). Biases of SRTM in high-mountain areas: Implications for the monitoring of glacier volume changes - art. no. L08502. *Geophysical Research Letters*, 33(8):NIL_19–NIL_23.

Berthier, E., Cabot, V., Vincent, C., and Six, D. (2016). Decadal region-wide and glacier-wide mass balances derived from multi-temporal ASTER satellite digital elevation models. Validation over the Mont-Blanc area. *Cryospheric Sciences*, 4:63.

Berthier, E., Larsen, C., Durkin, W. J., Willis, M. J., and Pritchard, M. E. (2018). Brief communication: Unabated wastage of the Juneau and Stikine icefields (southeast Alaska) in the early 21st century. *The Cryosphere*, 12(4):1523–1530.

Berthier, E., Schiefer, E., Clarke, G. K. C., Menounos, B., and Rémy, F. (2010). Contribution of Alaskan glaciers to sea-level rise derived from satellite imagery. *Nature Geoscience*, 3(2):92–95.

Berthier, E., Vincent, C., Magnússon, E., Gunnlaugsson, . ., Pitte, P., Le Meur, E., Masiokas, M., Ruiz, L., Pálsson, F., Belart, J. M. C., and Wagnon, P. (2014). Glacier topography and elevation changes derived from Pléiades sub-meter stereo images. *The Cryosphere*, 8(6):2275–2291.

Bown, F. and Rivera, A. (2007). Climate changes and recent glacier behaviour in the Chilean Lake District. *Global and Planetary Change*, 59(1–4):79–86.

Bradley, R. S., Vuille, M., Diaz, H. F., and Vergara, W. (2006). Threats to Water Supplies in the Tropical Andes. *Science*, 312(5781):1755–1756.

Braun, M. H., Malz, P., Sommer, C., Farías-Barahona, D., Sauter, T., Casassa, G., Soruco, A., Skvarca, P., and Seehaus, T. C. (2019). Constraining glacier elevation and mass changes in South America. *Nature Climate Change*, 9(2):130.

Bravo, C., Loriaux, T., Rivera, A., and Brock, B. (2017). Assessing glacier melt contribution to streamflow at Universidad Glacier, central Andes of Chile. *Hydrology and Earth System Sciences*, 21:3249–3266.

Bürgmann, R., Rosen, P. A., and Fielding, E. J. (2000). Synthetic Aperture Radar Interferometry to Measure Earth's Surface Topography and Its Deformation. *Annual Review of Earth and Planetary Sciences*, 28(1):169–209.

Brun, F., Berthier, E., Wagnon, P., Kääb, A., and Treichler, D. (2017). A spatially resolved estimate of High Mountain Asia glacier mass balances from 2000 to 2016. *Nature Geoscience*, 10(9):668–673.

Brun, F., Dumont, M., Wagnon, P., Berthier, E., Azam, M. F., Shea, J. M., Sirguey, P., Rabatel, A., and Ramanathan, A. (2015). Seasonal changes in surface albedo of Himalayan glaciers from MODIS data and links with the annual mass balance. *The Cryosphere*, 9(1):341–355.

Burger, F., Ayala, A., MacDonell, S., Shaw, T., Farias, D., Brock, B., McPhee, J., and Pellicciotti, F. (2018). Interannual and decadal variability in glacier contribution to runoff from high-elevation Andean catchments: understanding the role of debris cover in glacier hydrology. volume 20, page 18382.

Buttstädt, M., Möller, M., Iturraspe, R., and Schneider, C. (2009). Mass balance evolution of Martial Este Glacier, Tierra del Fuego (Argentina) for the period 1960–2099. *Adv. Geosci.*, 22:117–124.

Buytaert, W., Moulds, S., Acosta, L., Bièvre, B. D., Olmos, C., Villacis, M., Carolina Tovar, and Verbist, K. M. J. (2017). Glacial melt content of water use in the tropical Andes. *Environmental Research Letters*, 12(11):114014.

Casassa, G., Haeberli, W., Jones, G., Kaser, G., Ribstein, P., Rivera, A., and Schneider, C. (2007). Current status of Andean glaciers. *Global and Planetary Change*, 59:1–9.

Chen, J. L., Wilson C. R., Tapley B. D., Blankenship D. D., and Ivins E. R. (2007). Patagonia Icefield melting observed by Gravity Recovery and Climate Experiment (GRACE). *Geophysical Research Letters*, 34(22).

Chinn, T. J., Heydenrych, C., and Salinger, M. J. (2005). Use of the ELA as a practical method of monitoring glacier response to climate in New Zealand's Southern Alps. *Journal of Glaciology*, 51(172):85–95.

Church, J. A., Clark, P. U., Cazenave, A., Gregory, J. M., Jevrejeva, S., Levermann, A., Merrifield, M. A., Milne, G. A., Nerem, R. S., Nunn, P. D., Payne, A. J., Pfeffer, W. T., Stammer, D., and Unnikrishnan, A. S. (2013). Sea level change. Technical Report, P.M.Cambridge University Press.

Clapperton, C. M. (1983). The glaciation of the Andes. *Quaternary Science Reviews*, 2(2):83–155.

Cogley, J. G. (2009). Geodetic and direct mass-balance measurements: comparison and joint analysis. *Annals of Glaciology*, 50(50):96–100.

Cogley, J. G., Hock, R., Rasmussen, L. A., Arendt, A., Bauder, A., Braithwaite, R., Jansson, P., Kaser, G., Möller, M., Nicholson, L., and Zemp, M. (2011). *Glossary of Glacier Mass Balance and Related Terms*, volume No. 86 of *IHP-VII Technical Documents in Hydrology*. IACS Contribution No. 2 UNESCO-IHP, Paris, ihp-vii technical documents in hydrilogy no. 86 edition.

Collao Barrios, G. (2018). *Estimation du bilan masse de surface du Glacier San Rafael et du Champ du Glace Nord de Patagonie par diverses approches*. thesis, Grenoble Alpes.

Collao-Barrios, G., Gillet-Chaulet, F., Favier, V., Casassa, G., Berthier, E., Dussaillant, I., Mouginot, J., and Rignot, E. (2018). Ice flow modelling to constrain the surface mass balance and ice discharge of San Rafael Glacier, Northern Patagonia Icefield. *Journal of Glaciology*, pages 1–15.

Condom, T., Escobar, M., Purkey, D., Pouget, J. C., Suarez, W., Ramos, C., Apaestegui, J., Tacsi, A., and Gomez, J. (2012). Simulating the implications of glaciers' retreat for water management: a case study in the Rio Santa basin, Peru. *Water International*, 37(4):442–459.

Cook, S. J., Kougkoulos, I., Edwards, L. A., Dortch, J., and Hoffmann, D. (2016). Glacier change and glacial lake outburst flood risk in the Bolivian Andes. *The Cryosphere*, 10(5):2399–2413.

Cuffey, K. and Paterson, W. (2010). *The Physics of Glaciers*. Fourth edition edition.

Davaze, L., Rabatel, A., Arnaud, Y., Sirguey, P., Six, D., Letreguilly, A., and Dumont, M. (2018). Monitoring glacier albedo as a proxy to derive summer and annual surface mass balances from optical remote-sensing data. *The Cryosphere*, 12(1):271–286.

Davies, B. and Glasser, N. (2012). Accelerating shrinkage of Patagonian glaciers from the Little Ice Age (∼AD 1870) to 2011. *Journal of Glaciology*, 58(212):1063–1084.

Dehecq, A., Gourmelen, N., Gardner, A. S., Brun, F., Goldberg, D., Nienow, P. W., Berthier, E., Vincent, C., Wagnon, P., and Trouvé, E. (2019). Twenty-first century glacier slowdown driven by mass loss in High Mountain Asia. *Nature Geoscience*, 12(1):22.

Dehecq, A., Millan, R., Berthier, E., Gourmelen, N., Trouve, E., and Vionnet, V. (2016). Elevation Changes Inferred From TanDEM-X Data Over the Mont-Blanc Area: Impact of the X-Band Interferometric Bias. *IEEE Journal of Selected Topics in Applied Earth Observations and Remote Sensing*, pages 1–13.

DIAZ, H. F. A. (1992). *El Niño: Historical and Paleoclimatic Aspects of the Southern Oscillation*. Cambridge University Press. Google-Books-ID: maROAAAAIAAJ.

Dietrich, R., Ivins, E. R., Casassa, G., Lange, H., Wendt, J., and Fritsche, M. (2010). Rapid crustal uplift in Patagonia due to enhanced ice loss. *Earth and Planetary Science Letters*, 289:22–29.

Dixon, L. and Ambinakudige, S. (2015). Remote Sensing Study of Glacial Change in the Northern Patagonian Icefield. *Advances in Remote Sensing*, 04(04):270.

Dumont, M., Gardelle, J., Sirguey, P., Guillot, A., Six, D., Rabatel, A., and Arnaud, Y. (2012). Linking glacier annual mass balance and glacier albedo retrieved from MODIS data. *The Cryosphere*, 6:1527–1539.

Dussaillant, I., Berthier, E., and Brun, F. (2018). Geodetic Mass Balance of the Northern Patagonian Icefield from 2000 to 2012 Using Two Independent Methods. *Frontiers in Earth Science*, 6.

Dussaillant, I., Berthier, E., Brun, F., Masiokas, M., Hugonnet, R., Favier, V., Rabatel, A., Pitte, P., and Ruiz, L. (2019). Two decades of glacier mass loss along the Andes. *Nature Geoscience*, 12(10):802–808.

Falaschi, D., Bolch, T., Rastner, P., Lenzano, M. G., Lenzano, L., Vecchio, A. L., and Moragues, S. (2016). Mass changes of alpine glaciers at the eastern margin of the Northern and Southern Patagonian Icefields between 2000 and 2012. *Journal of Glaciology*, pages 1–15.

Falvey, M. and Garreaud, R. D. (2009). Regional cooling in a warming world: Recent temperature trends in the southeast Pacific and along the west coast of subtropical South America (1979–2006). *Journal of Geophysical Research: Atmospheres*, 114(D4).

Farías-Barahona, D., Vivero, S., Casassa, G., Schaefer, M., Burger, F., Seehaus, T., Iribarren-Anacona, P., Escobar, F., and Braun, M. H. (2019). Geodetic Mass Balances and Area Changes of Echaurren Norte Glacier (Central Andes, Chile) between 1955 and 2015. *Remote Sensing*, 11(3):260.

Farinotti, D., Huss, M., Fürst, J. J., Landmann, J., Machguth, H., Maussion, F., and Pandit, A. (2019). A consensus estimate for the ice thickness distribution of all glaciers on Earth. *Nature Geoscience*, 12(3):168.

Farr, T. G., Rosen, P. A., Caro, E., Crippen, R., Duren, R., Hensley, S., Kobrick, M., Paller, M., Rodriguez, E., Roth, L., Seal, D., Shaffer, S., Shimada, J., Umland, J., Werner, M., Oskin, M., Burbank, D., and Alsdorf, D. (2007). The Shuttle Radar Topography Mission. *Reviews of Geophysics*, 45(2):RG2004.

Favier, V., Wagnon, P., and Ribstein, P. (2004). Glaciers of the outer and inner tropics: A different behaviour but a common response to climatic forcing. *Geophysical Research Letters*, 31(16).

Fischer, M., Huss, M., and Hoelzle, M. (2015). Surface elevation and mass changes of all Swiss glaciers 1980–2010. *The Cryosphere*, 9(2):525–540.

Foresta, L., Gourmelen, N., Weissgerber, F., Nienow, P., Williams, J. J., Shepherd, A., Drinkwater, M. R., and Plummer, S. (2018). Heterogeneous and rapid ice loss over the Patagonian Ice Fields revealed by CryoSat-2 swath radar altimetry. *Remote Sensing of Environment*, 211:441–455.

Fountain, A. G., Jansson, P., Kaser, G., and Dyurgerov, M. (1999). Summary of the workshop on methods of mass balance measurements and modelling, tarfala, sweden august 10–12, 1998. *Geografiska Annaler: Series A, Physical Geography*, 81(4):461–465.

Francou, B., Vuille, M., Favier, V., and Cáceres, B. (2004). New evidence for an ENSO impact on low-latitude glaciers: Antizana 15, Andes of Ecuador, 0°28′S. *Journal of Geophysical Research: Atmospheres*, 109(D18).

Francou, B., Vuille, M., Wagnon, P., Mendoza, J., and Sicart, J.-E. (2003). Tropical climate change recorded by a glacier in the central Andes during the last decades of the twentieth century: Chacaltaya, Bolivia, 16°S. *Journal of Geophysical Research: Atmospheres*, 108(D5).

Fujita, K. (2008). Effect of precipitation seasonality on climatic sensitivity of glacier mass balance. *Earth and Planetary Science Letters*, 276(1):14–19.

Fujiyoshi, Y., Kondo, H., Inoue, J., and Yamada, T. (1987). Characteristics of precipitation and vertical structure of air temperature in the northern Patagonia. *Bulletin of glacier research*, (4):15–23.

Gallée, H. and Schayes, G. (1994). Development of a Three-Dimensional Meso-gamma Primitive Equation Model: Katabatic Winds Simulation in the Area of Terra Nova Bay, Antarctica. *Monthly Weather Review*, 122(4):671–685.

Gardelle, J., Berthier, E., and Arnaud, Y. (2012). Impact of resolution and radar penetration on glacier elevation changes computed from DEM differencing. *Journal of Glaciology*, 58(208):419–422.

Gardelle, J., Berthier, E., Arnaud, Y., and Kääb, A. (2013). Region-wide glacier mass balances over the Pamir-Karakoram-Himalaya during 1999–2011. *The Cryosphere*, 7(4):1263–1286.

Gardner, A. S., Moholdt, G., Cogley, J. G., Wouters, B., Arendt, A. A., Wahr, J., Berthier, E., Hock, R., Pfeffer, W. T., Kaser, G., Ligtenberg, S. R. M., Bolch, T., Sharp, M. J., Hagen, J. O., Broeke, M. R. v. d., and Paul, F. (2013). A Reconciled Estimate of Glacier Contributions to Sea Level Rise: 2003 to 2009. *Science*, 340(6134):852–857.

Garreaud, R., Vuille, M., and Clement, A. C. (2003). The climate of the Altiplano: observed current conditions and mechanisms of past changes. *Palaeogeography, Palaeoclimatology, Palaeoecology*, 194(1):5–22.

Garreaud, R. D. (2009). The Andes climate and weather. In *Advances in Geosciences*, volume 22, pages 3–11. Copernicus GmbH.

Garreaud, R. D., Alvarez-Garreton, C., Barichivich, J., Boisier, J. P., Christie, D., Galleguillos, M., LeQuesne, C., McPhee, J., and Zambrano-Bigiarini, M. (2017). The 2010–2015 megadrought in central Chile: impacts on regional hydroclimate and vegetation. *Hydrol. Earth Syst. Sci.*, 21(12):6307–6327.

Garreaud, R. D., Vuille, M., Compagnucci, R., and Marengo, J. (2009). Present-day South American climate. *Palaeogeography, Palaeoclimatology, Palaeoecology*, 281(3):180–195.

Gascoin, S., Kinnard, C., Ponce, R., Lhermitte, S., MacDonell, S., and Rabatel, A. (2011). Glacier contribution to streamflow in two headwaters of the Huasco River, Dry Andes of Chile. *The Cryosphere*, 5(4):1099–1113.

Gascoin, S., Lhermitte, S., Kinnard, C., Bortels, K., and Liston, G. E. (2013). Wind effects on snow cover in Pascua-Lama, Dry Andes of Chile. *Advances in Water Resources*, 55:25–39.

Gillett, N. P., Kell, T. D., and Jones, P. D. (2006). Regional climate impacts of the Southern Annular Mode. *Geophysical Research Letters*, 33(23):L23704.

Ginot, P., Kull, C., Schotterer, U., Schwikowski, M., and Gäggeler, H. W. (2006). Glacier mass balance reconstruction by sublimation induced enrichment of chemical species on Cerro Tapado (Chilean Andes). *Climate of the Past*, 2(1):21–30.

Girod, L., Nuth, C., and Kääb, A. (2015). Improvement of DEM generation from ASTER images using satellite jitter estimation and open source implementation. In *ISPRS - International Archives of the Photogrammetry, Remote Sensing and Spatial Information Sciences*, volume XL-1-W5, pages 249–253. Copernicus GmbH.

Glasser, N. F., Harrison, S., Jansson, K. N., Anderson, K., and Cowley, A. (2011). Global sea-level contribution from the Patagonian Icefields since the Little Ice Age maximum. *Nature Geoscience*, 4(5):303–307.

Granshaw, F. D. and Fountain, A. G. (2006). Glacier change (1958–1998) in the North Cascades National Park Complex, Washington, USA. *Journal of Glaciology*, 52(177):251–256.

Hagg, W. J., Braun, L. N., Uvarov, V. N., and Makarevich, K. G. (2004). A comparison of three methods of mass-balance determination in the Tuyuksu glacier region, Tien Shan, Central Asia. *Journal of Glaciology*, 50(171):505–510.

Helm, V., Humbert, A., and Miller, H. (2014). Elevation and elevation change of Greenland and Antarctica derived from CryoSat-2. *The Cryosphere Discussions*, 8:1673–1721.

Hock, R. (2003). Temperature index melt modelling in mountain areas. *Journal of Hydrology*, 282(1):104–115.

Houston, J. and Hartley, A. J. (2003). The central Andean west-slope rainshadow and its potential contribution to the origin of hyper-aridity in the Atacama Desert. *International Journal of Climatology*, 23:1453–1464.

Huss, M. (2011). Present and future contribution of glacier storage change to runoff from macroscale drainage basins in Europe. *Water Resources Research*, 47:W07511.

Huss, M. (2013). Density assumptions for converting geodetic glacier volume change to mass change. *The Cryosphere*, 7(3):877–887.

Huss, M., Bookhagen, B., Huggel, C., Jacobsen, D., Bradley, R. S., Clague, J. J., Vuille, M., Buytaert, W., Cayan, D. R., Greenwood, G., Mark, B. G., Milner, A. M., Weingartner, R., and Winder, M. (2017). Toward mountains without permanent snow and ice. *Earth's Future*, 5(5):418–435.

Huss, M. and Farinotti, D. (2012). Distributed ice thickness and volume of all glaciers around the globe. *Journal of Geophysical Research: Earth Surface*, 117(F4).

Huss, M. and Hock, R. (2015). A new model for global glacier change and sea-level rise. *Frontiers in Earth Science*, 3.

Huss, M. and Hock, R. (2018). Global-scale hydrological response to future glacier mass loss. *Nature Climate Change*, 8(2):135–140.

Ivins, E. R. and James, T. S. (2004). Bedrock response to Llanquihue Holocene and present-day glaciation in southernmost South America. *Geophysical Research Letters*, 31(24).

Ivins, E. R., Watkins, M. M., Yuan, D.-N., Dietrich, R., Casassa, G., and Rülke, A. (2011). On-land ice loss and glacial isostatic adjustment at the Drake Passage: 2003–2009. *Journal of Geophysical Research: Solid Earth*, 116(B2):B02403.

Jaber, W. A., Floricioiu, D., and Rott, H. (2016). Geodetic mass balance of the Patagonian Icefields derived from SRTM and TanDEM-X data. In *2016 IEEE International Geoscience and Remote Sensing Symposium (IGARSS)*, pages 342–345.

Jaber, W. A., Floricioiu, D., Rott, H., and Eineder, M. (2013). Surface elevation changes of glaciers derived from SRTM and TanDEM-X DEM differences. In *2013 IEEE International Geoscience and Remote Sensing Symposium - IGARSS*, pages 1893–1896.

Jacob, T., Wahr, J., Pfeffer, W. T., and Swenson, S. (2012). Recent contributions of glaciers and ice caps to sea level rise. *Nature*, 482(7386):514–518.

Jomelli, V., Favier, V., Rabatel, A., Brunstein, D., Hoffmann, G., and Francou, B. (2009). Fluctuations of glaciers in the tropical Andes over the last millennium and palaeoclimatic implications: A review. *Palaeogeography, Palaeoclimatology, Palaeoecology*, 281(3):269–282.

Jomelli, V., Grancher, D., Brunstein, D., and Solomina, O. (2008). Recalibration of the yellow Rhizocarpon growth curve in the Cordillera Blanca (Peru) and implications for LIA chronology. *Geomorphology*, 93(3):201–212.

Kaser, G. (2001). Glacier-climate interaction at low latitudes. *Journal of Glaciology*, 47(157):195–204.

Kaser, G. and Georges, C. (1999). On the Mass Balance of Low Latitude Glaciers with Particular Consideration of the Peruvian Cordillera Blanca. *Geografiska Annaler: Series A, Physical Geography*, 81(4):643–651.

Kaser, G., Gro˜hauser, M., and Marzeion, B. (2010). Contribution potential of glaciers to water availability in different climate regimes. *Proceedings of the National Academy of Sciences*, 107(47):20223–20227.

Kääb, A. (2005). Combination of SRTM3 and repeat ASTER data for deriving alpine glacier flow velocities in the Bhutan Himalaya. *Remote Sensing of Environment*, 94(4):463–474.

Kääb, A., Berthier, E., Nuth, C., Gardelle, J., and Arnaud, Y. (2012). Contrasting patterns of early twenty-first-century glacier mass change in the Himalayas. *Nature*, 488(7412):495–498.

Kääb, A., Treichler, D., Nuth, C., and Berthier, E. (2015). Brief Communication: Contending estimates of 2003–2008 glacier mass balance over the Pamir–Karakoram–Himalaya. *The Cryosphere*, 9(2):557–564.

Kerr, A. and Sugden, D. (1994). The sensitivity of the south chilean snowline to climatic change. *Climatic Change*, 28(3):255–272.

Koppes, M., Conway, H., Rasmussen, L. A., and Chernos, M. (2011). Deriving mass balance and calving variations from reanalysis data and sparse observations, Glaciar San Rafael, northern Patagonia, 1950–2005. *The Cryosphere*, 5(3):791–808.

Korona, J., Berthier, E., Bernard, M., Rémy, F., and Thouvenot, E. (2009). SPIRIT. SPOT 5 stereoscopic survey of Polar Ice: Reference Images and Topographies during the fourth International Polar Year (2007–2009). *ISPRS Journal of Photogrammetry and Remote Sensing*, 64(2):204–212.

Lambrecht, A. and Mayer, C. (2009). Temporal variability of the non-steady contribution from glaciers to water discharge in western Austria. *Journal of Hydrology*, 376:353–361.

Lehner, B. and Döll, P. (2004). Development and validation of a global database of lakes, reservoirs and wetlands. *Journal of Hydrology*, 296(1):1–22.

Leiva, J. C., Cabrera, G. A., and Lenzano, L. E. (2007). 20 years of mass balances on the Piloto glacier, Las Cuevas river basin, Mendoza, Argentina. *Global and Planetary Change*, 59(1):10–16.

Lenaerts, J. T. M., van den Broeke, M. R., van Wessem, J. M., van de Berg, W. J., van Meijgaard, E., van Ulft, L. H., and Schaefer, M. (2014). Extreme Precipitation and Climate Gradients in Patagonia Revealed by High-Resolution Regional Atmospheric Climate Modeling. *Journal of Climate*, 27:4607–4621.

Lliboutry, L. (1956). *Nieves y glaciares de Chile. Fundamentos en glaciologia.* Ediciones de la Universidad de Chile, Santiago.

Lopez, P., Chevallier, P., Favier, V., Pouyaud, B., Ordenes, F., and Oerlemans, J. (2010). A regional view of fluctuations in glacier length in southern South America. *Global and Planetary Change*, 71(1–2):85–108.

Luckman, A., Benn, D. I., Cottier, F., Bevan, S., Nilsen, F., and Inall, M. (2015). Calving rates at tidewater glaciers vary strongly with ocean temperature. *Nature Communications*, 6:8566.

MacDonell, S., Kinnard, C., Mölg, T., Nicholson, L., and Abermann, J. (2013). Meteorological drivers of ablation processes on a cold glacier in the semi-arid Andes of Chile. *The Cryosphere*, 7(5):1513–1526.

Malz, P., Meier, W., Casassa, G., Jaña, R., Skvarca, P., and Braun, M. H. (2018). Elevation and Mass Changes of the Southern Patagonia Icefield Derived from TanDEM-X and SRTM Data. *Remote Sensing*, 10(2):188.

Mantua, N. J. and Hare, S. R. (2002). The Pacific Decadal Oscillation. *Journal of Oceanography*, 58(1):35–44.

Marzeion, B., Champollion, N., Haeberli, W., Langley, K., Leclercq, P., and Paul, F. (2017). Observation-Based Estimates of Global Glacier Mass Change and Its Contribution to Sea-Level Change. *Surveys in Geophysics*, 38(1):105–130.

Marzeion, B., Cogley, J. G., Richter, K., and Parkes, D. (2014). Attribution of global glacier mass loss to anthropogenic and natural causes. *Science*, 345(6199):919–921.

Marzeion, B., Jarosch, A. H., and Hofer, M. (2012). Past and future sea-level change from the surface mass balance of glaciers. *The Cryosphere*, 6(6):1295–1322.

Marzeion, B., Leclercq, P. W., Cogley, J. G., and Jarosch, A. H. (2015). Brief Communication: Global reconstructions of glacier mass change during the 20th century are consistent. *The Cryosphere*, 9(6):2399–2404.

Masiokas, M. H., Christie, D. A., Le Quesne, C., Pitte, P., Ruiz, L., Villalba, R., Luckman, B. H., Berthier, E., Nussbaumer, S. U., González-Reyes, ., McPhee, J., and Barcaza, G. (2016). Reconstructing the annual mass balance of the Echaurren Norte glacier (Central Andes, 33.5°S) using local and regional hydroclimatic data. *The Cryosphere*, 10(2):927–940.

Masiokas, M. H., Rivera, A., Espizua, L. E., Villalba, R., Delgado, S., and Aravena, J. C. (2009). Glacier fluctuations in extratropical South America during the past 1000years. *Palaeogeography, Palaeoclimatology, Palaeoecology*, 281(3):242–268.

Masiokas, M. H., Villalba, R., Luckman, B. H., and Mauget, S. (2010). Intra- to Multidecadal Variations of Snowpack and Streamflow Records in the Andes of Chile and Argentina between 30° and 37°S. *Journal of Hydrometeorology*, 11(3):822–831.

McNabb, R., Nuth, C., Kääb, A., and Girod, L. (2019). Sensitivity of glacier volume change estimation to DEM void interpolation. *The Cryosphere*, 13(3):895–910.

Meier, M. F. (1984). Contribution of Small Glaciers to Global Sea Level. *Science*, 226(4681):1418–1421.

Meier, W. J.-H., Grie˜inger, J., Hochreuther, P., and Braun, M. H. (2018). An Updated Multi-Temporal Glacier Inventory for the Patagonian Andes With Changes Between the Little Ice Age and 2016. *Frontiers in Earth Science*, 6.

Melkonian, A. K., Willis, M. J., Pritchard, M. E., Rivera, A., Bown, F., and Bernstein, S. A. (2013). Satellite-derived volume loss rates and glacier speeds for the Cordillera Darwin Icefield, Chile. *The Cryosphere*, 7(3):823–839.

Menounos, B., Hugonnet, R., Shean, D., Gardner, A., Howat, I., Berthier, E., Pelto, B., Tennant, C., Shea, J., Noh, M.-J., Brun, F., and Dehecq, A. (2019). Heterogeneous Changes in Western North American Glaciers Linked to Decadal Variability in Zonal Wind Strength. *Geophysical Research Letters*, 46(1):200–209.

Mernild, S. and Wilson, R. (2016). The Andes Cordillera. Part III: Glacier surface mass balance and contribution to sea level rise (1979-2014). *International Journal of Climatology*.

Mernild, S. H., Beckerman, A. P., Yde, J. C., Hanna, E., Malmros, J. K., Wilson, R., and Zemp, M. (2015). Mass loss and imbalance of glaciers along the Andes Cordillera to the sub-Antarctic islands. *Global and Planetary Change*, 133:109–119.

Messerli, B., Ammann, B., Geyh, M., Grosjean, M., Jenny, B., Kammer, K., and Vuille, M. (1998). The problem of the "Andean dry diagonal": current precipitation, Lae Pleistocene snow line, and lake level changes in the Atacama Altiplano (18s-28s/29s). *Bamberger Geographische Schriften*, 15:17–34.

Minowa, M., Sugiyama, S., Sakakibara, D., and Sawagaki, T. (2015). Contrasting glacier variations of Glaciar Perito Moreno and Glaciar Ameghino, Southern Patagonia Icefield. *Annals of Glaciology*, 56(70):26–32.

Mölg, N., Ceballos, J. L., Huggel, C., Micheletti, N., Rabatel, A., and Zemp, M. (2017). Ten years of monthly mass balance of Conejeras glacier, Colombia, and their evaluation using different interpolation methods. *Geografiska Annaler: Series A, Physical Geography*, 99(2):155–176.

Moller, M. and Schneider, C. (2010). Volume change at Gran Campo Nevado, Patagonia, 1984-2000: a reassessment based on new findings. *Journal of Glaciology*, 56:363–365.

Mouginot, J. and Rignot, E. (2015). Ice motion of the Patagonian Icefields of South America: 1984–2014. *Geophysical Research Letters*, 42(5):2014GL062661.

New, M., Lister, D., Hulme, M., and Makin, I. (2002). A high-resolution data set of surface climate over global land areas. *Climate Research*, 21(1):1–25.

Nuimura, T., Fujita, K., Yamaguchi, S., and Sharma, R. R. (2012). Elevation changes of glaciers revealed by multitemporal digital elevation models calibrated by GPS survey in the Khumbu region, Nepal Himalaya, 1992-2008. *Journal of Glaciology*, 58(210):648–656.

Nuth, C. and Kääb, A. (2011). Co-registration and bias corrections of satellite elevation data sets for quantifying glacier thickness change. *The Cryosphere*, 5(1):271–290.

Oerlemans, J. (2001). *Glaciers and Climate Change*. CRC Press. Google-Books-ID: OJHXK91Ci1AC.

Oerlemans, J. and Reichert, B. K. (2000). Relating glacier mass balance to meteorological data by using a seasonal sensitivity characteristic. *Journal of Glaciology*, 46(152):1–6.

Papasodoro, C., Berthier, E., Royer, A., Zdanowicz, C., and Langlois, A. (2015). Area, elevation and mass changes of the two southernmost ice caps of the Canadian Arctic Archipelago between 1952 and 2014. *The Cryosphere*, 9(4):1535–1550.

Paul, F., Barrand, N. E., Baumann, S., Berthier, E., Bolch, T., Casey, K., Frey, H., Joshi, S. P., Konovalov, V., Bris, R. L., Mölg, N., Nosenko, G., Nuth, C., Pope, A., Racoviteanu, A., Rastner, P., Raup, B., Scharrer, K., Steffen, S., and Winsvold, S. (2013). On the accuracy of glacier outlines derived from remote-sensing data. *Annals of Glaciology*, 54(63):171–182.

Paul, F., Bolch, T., Kääb, A., Nagler, T., Nuth, C., Scharrer, K., Shepherd, A., Strozzi, T., Ticconi, F., Bhambri, R., Berthier, E., Bevan, S., Gourmelen, N., Heid, T., Jeong, S., Kunz, M., Lauknes, T. R., Luckman, A., Merryman Boncori, J. P., Moholdt, G., Muir, A., Neelmeijer, J., Rankl, M., VanLooy, J., and Van Niel, T. (2015). The glaciers climate change initiative: Methods for creating glacier area, elevation change and velocity products. *Remote Sensing of Environment*, 162:408–426.

Paul, F. and Mölg, N. (2014). Hasty retreat of glaciers in northern Patagonia from 1985 to 2011. *Journal of Glaciology*, 60(224):1033–1043.

Pellicciotti, F., Ragettli, S., Carenzo, M., and McPhee, J. (2014). Changes of glaciers in the Andes of Chile and priorities for future work. *The Science of the total environment*, 493:1197–1210.

Pfeffer, W. T., Arendt, A. A., Bliss, A., Bolch, T., Cogley, J. G., Gardner, A. S., Hagen, J.-O., Hock, R., Kaser, G., Kienholz, C., Miles, E. S., Moholdt, G., Mölg, N., Paul, F., Radić, V., Rastner, P., Raup, B. H., Rich, J., and Sharp, M. J. (2014). The Randolph Glacier Inventory: a globally complete inventory of glaciers. *Journal of Glaciology*, 60(221):537–552.

Pritchard, H. D. (2019). Asia's shrinking glaciers protect large populations from drought stress. *Nature*, 569(7758):649.

Pritchard, H. D., Ligtenberg, S. R. M., Fricker, H. A., Vaughan, D. G., van den Broeke, M. R., and Padman, L. (2012). Antarctic ice-sheet loss driven by basal melting of ice shelves. *Nature*, 484(7395):502–505.

Rabatel, A., Castebrunet, H., Favier, V., Nicholson, L., and Kinnard, C. (2011). Glacier changes in the Pascua-Lama region, Chilean Andes (29° S): recent mass balance and 50 yr surface area variations. *The Cryosphere*, 5(4):1029–1041.

Rabatel, A., Ceballos, J. L., Micheletti, N., Jordan, E., Braitmeier, M., González, J., Mölg, N., Ménégoz, M., Huggel, C., and Zemp, M. (2017). Toward an imminent extinction of Colombian glaciers? *Geografiska Annaler: Series A, Physical Geography*, 100(1):75–95.

Rabatel, A., Francou, B., Soruco, A., Gomez, J., Cáceres, B., Ceballos, J. L., Basantes, R., Vuille, M., Sicart, J.-E., Huggel, C., Scheel, M., Lejeune, Y., Arnaud, Y., Collet, M., Condom, T., Consoli, G., Favier, V., Jomelli, V., Galarraga, R., Ginot, P., Maisincho, L., Mendoza, J., Ménégoz, M., Ramirez, E., Ribstein, P., Suarez, W., Villacis, M., and Wagnon, P. (2013a). Current state of glaciers in the tropical Andes: a multi-century perspective on glacier evolution and climate change. *The Cryosphere*, 7(1):81–102.

Rabatel, A., Jomelli, V., Naveau, P., Francou, B., and Grancher, D. (2005). Dating of Little Ice Age glacier fluctuations in the tropical Andes: Charquini glaciers, Bolivia, 16°S. *Comptes Rendus Geoscience*, 337(15):1311–1322.

Rabatel, A., Letréguilly, A., Dedieu, J., and Eckert, N. (2013b). Changes in glacier equilibrium-line altitude in the western Alps from 1984 to 2010: evaluation by remote sensing and modeling of the morpho-topographic and climate controls. *The Cryosphere*, 7(5):p. 1455 – p. 1471.

Rabatel, A., Machaca, A., Francou, B., and Jomelli, V. (2006). Glacier recession on Cerro Charquini (16° S), Bolivia, since the maximum of the Little Ice Age (17th century). *Journal of Glaciology*, 52(176):110–118.

Racoviteanu, A. E., Paul, F., Raup, B., Khalsa, S. J. S., and Armstrong, R. (2009). Challenges and recommendations in mapping of glacier parameters from space: results of the 2008 Global Land Ice Measurements from Space (GLIMS) workshop, Boulder, Colorado, USA. *Annals of Glaciology*, 50(53):53–69.

Radić, V. and Hock, R. (2014). Glaciers in the Earth's Hydrological Cycle: Assessments of Glacier Mass and Runoff Changes on Global and Regional Scales. *Surveys in Geophysics*, 35(3):813–837.

Ragettli, S. and Pellicciotti, F. (2012). Calibration of a physically based, spatially distributed hydrological model in a glacierized basin: On the use of knowledge from glaciometeorological processes to constrain model parameters. *Water Resources Research*, 48(3).

Ramírez, E., Francou, B., Ribstein, P., Descloitres, M., Guérin, R., Mendoza, J., Gallaire, R., Pouyaud, B., and Jordan, E. (2001). Small glaciers disappearing in the tropical Andes: a case-study in Bolivia: Glaciar Chacaltaya (16o S). *Journal of Glaciology*, 47(157):187–194.

Reager, J. T., Gardner, A. S., Famiglietti, J. S., Wiese, D. N., Eicker, A., and Lo, M.-H. (2016). A decade of sea level rise slowed by climate-driven hydrology. *Science*, 351(6274):699–703.

Reinthaler, J., Paul, F., Granados, H. D., Rivera, A., and Huggel, C. (2019). Area changes of glaciers on active volcanoes in Latin America between 1986 and 2015 observed from multi-temporal satellite imagery. *Journal of Glaciology*, pages 1–15.

Richter, A., Ivins, E., Lange, H., Mendoza, L., Schröder, L., Hormaechea, J. L., Casassa, G., Marderwald, E., Fritsche, M., Perdomo, R., Horwath, M., and Dietrich, R. (2016). Crustal deformation across the Southern Patagonian Icefield observed by GNSS. *Earth and Planetary Science Letters*, 452:206–215.

Rignot, E., Echelmeyer, K., and Krabill, W. (2001). Penetration depth of interferometric synthetic-aperture radar signal in snow and ice. *Geophysical Research Letters*, 28(18).

Rignot, E., Forster, R., and Isacks, B. (1996). Mapping of glacial motion and surface topography of Hielo Patagónico Norte, Chile, using satellite SAR L-band interferometry data. *Annals of Glaciology*, 23(1):209–216.

Rignot, E., Rivera, A., and Casassa, G. (2003). Contribution of the Patagonia Icefields of South America to sea level rise. *Science (New York, N.Y.)*, 302(5644):434–437.

Rivera, A., Benham, T., Casassa, G., Bamber, J., and Dowdeswell, J. A. (2007). Ice elevation and areal changes of glaciers from the Northern Patagonia Icefield, Chile. *Global and Planetary Change*, 59(1–4):126–137.

Rivera, A., Bown, F., Mella, R., Wendt, J., Casassa, G., Acuña, C., Rignot, E., Clavero, J., and Brock, B. (2006). Ice volumetric changes on active volcanoes in southern Chile. *Annals of Glaciology*, 43:111–122.

Rivera, A., Corripio, J., Bravo, C., and Cisternas, S. (2012). Glaciar Jorge Montt (Chilean Patagonia) dynamics derived from photos obtained by fixed cameras and satellite image feature tracking. *Annals of Glaciology*, 53(60):147–155.

Rivera, A., Zamora, R., Uribe, J., Wendt, A., Oberreuter, J., Cisternas, S., Gimeno, F., and Clavero, J. (2015). Recent changes in total ice volume on Volcán Villarrica, Southern Chile. *Natural Hazards*, 75(1):33–55.

Rivera, J. A., Penalba, O. C., Villalba, R., and Araneo, D. C. (2017). Spatio-Temporal Patterns of the 2010–2015 Extreme Hydrological Drought across the Central Andes, Argentina. *Water*, 9(9):652.

Rodriguez, M., Ohlanders, N., Pellicciotti, F., Williams, M. W., and McPhee, J. (2016). Estimating runoff from a glacierized catchment using natural tracers in the semi-arid Andes cordillera. *Hydrological Processes*, 30(20):3609–3626.

Rolstad, C., Haug, T., and Denby, B. (2009). Spatially integrated geodetic glacier mass balance and its uncertainty based on geostatistical analysis: application to the western Svartisen ice cap, Norway. *Journal of Glaciology*, 55(192):666–680.

Round, V., Leinss, S., Huss, M., Haemmig, C., and Hajnsek, I. (2017). Surge dynamics and lake outbursts of Kyagar Glacier, Karakoram. *The Cryosphere*, 11(2):723–739.

Ruiz, L., Berthier, E., Viale, M., Pitte, P., and Masiokas, M. H. (2017). Recent geodetic mass balance of Monte Tronador glaciers, northern Patagonian Andes. *The Cryosphere*, 11(1):619–634.

Rupnik, E., Daakir, M., and Pierrot Deseilligny, M. (2017). MicMac – a free, open-source solution for photogrammetry. *Open Geospatial Data, Software and Standards*, 2(1):14.

Rupper, S. and Roe, G. (2008). Glacier Changes and Regional Climate: A Mass and Energy Balance Approach. *Journal of Climate*, 21(20):5384–5401.

Rutllant, J. A., Fuenzalida, H., and Aceituno, P. (2003). Climate dynamics along the arid northern coast of Chile: The 1997–1998 Dinámica del Clima de la Región de Antofagasta (DICLIMA) experiment. *Journal of Geophysical Research: Atmospheres*, 108(D17).

Réveillet, M., Vincent, C., Six, D., and Rabatel, A. (2017). Which empirical model is best suited to simulate glacier mass balances? *Journal of Glaciology*, 63(237):39–54.

Sagredo, E. A. and Lowell, T. V. (2012). Climatology of Andean glaciers: A framework to understand glacier response to climate change. *Global and Planetary Change*, 86:101–109.

Sagredo, E. A., Rupper, S., and Lowell, T. V. (2014). Sensitivities of the equilibrium line altitude to temperature and precipitation changes along the Andes. *Quaternary Research*, 81(2):355–366.

Sakakibara, D. and Sugiyama, S. (2014). Ice-front variations and speed changes of calving glaciers in the Southern Patagonia Icefield from 1984 to 2011. *Journal of Geophysical Research: Earth Surface*, 119(11):2541–2554.

Sakakibara, D., Sugiyama, S., Sawagaki, T., Marinsek, S., and Skvarca, P. (2013). Rapid retreat, acceleration and thinning of Glaciar Upsala, Southern Patagonia Icefield, initiated in 2008. *Annals of Glaciology*, 54(63):131–138.

Schaefer, M., Machguth, H., Falvey, M., and Casassa, G. (2013). Modeling past and future surface mass balance of the Northern Patagonia Icefield. *Journal of Geophysical Research: Earth Surface*, 118(2):571–588.

Schaefer, M., Machguth, H., Falvey, M., Casassa, G., and Rignot, E. (2015). Quantifying mass balance processes on the Southern Patagonia Icefield. *The Cryosphere*, 9(1):25–35.

Schaefer, M., Rodriguez, J. L., Scheiter, M., and Casassa, G. (2017). Climate and surface mass balance of Mocho Glacier, Chilean Lake District, 40°S. *Journal of Glaciology*, 63(238):218–228.

Scherler, D., Leprince, S., and Strecker, M. R. (2008). Glacier-surface velocities in alpine terrain from optical satellite imagery—Accuracy improvement and quality assessment. *Remote Sensing of Environment*, 112(10):3806–3819.

Schneider, C., Schnirch, M., Acuña, C., Casassa, G., and Kilian, R. (2007). Glacier inventory of the Gran Campo Nevado Ice Cap in the Southern Andes and glacier changes observed during recent decades. *Global and Planetary Change*, 59(1):87–100.

Schoolmeester, T., Johansen, K., Alfthan, B., Baker, E., Hesping, M., and Verblst, K. (2018). *The Andean Glacier and Water Atlas: The Impact of Glacier Retreat on Water Resources.* UNESCO and GRID-Arendal.

Schwitter, M. P. and Raymond, C. F. (1993). Changes in the longitudinal profiles of glaciers during advance and retreat. *Journal of Glaciology*, 39(133):582–590.

Shean, D. E., Alexandrov, O., Moratto, Z. M., Smith, B. E., Joughin, I. R., Porter, C., and Morin, P. (2016). An automated, open-source pipeline for mass production of digital elevation models (DEMs) from very-high-resolution commercial stereo satellite imagery. *ISPRS Journal of Photogrammetry and Remote Sensing*, 116:101–117.

Sicart, J. E., Hock, R., Ribstein, P., Litt, M., and Ramirez, E. (2011). Analysis of seasonal variations in mass balance and meltwater discharge of the tropical Zongo Glacier by application of a distributed energy balance model. *Journal of Geophysical Research: Atmospheres*, 116(D13).

Sicart, J. E., Ribstein, P., Francou, B., Pouyaud, B., and Condom, T. (2007). Glacier mass balance of tropical Zongo glacier, Bolivia, comparing hydrological and glaciological methods. *Global and Planetary Change*, 59(1):27–36.

Skvarca, P., Angelis, H. D., Naruse, R., Warren, C. R., and Aniya, M. (2002). Calving rates in fresh water: new data from southern Patagonia. *Annals of Glaciology*, 34:379–384.

Smith, R. B. and Evans, J. P. (2007). Orographic Precipitation and Water Vapor Fractionation over the Southern Andes. *Journal of Hydrometeorology*, 8(1):3–19.

Soruco, A., Vincent, C., Francou, B., and Gonzalez, J. F. (2009a). Glacier decline between 1963 and 2006 in the Cordillera Real, Bolivia. *Geophysical Research Letters*, 36(3).

Soruco, A., Vincent, C., Francou, B., Ribstein, P., Berger, T., Sicart, J. E., Wagnon, P., Arnaud, Y., Favier, V., and Lejeune, Y. (2009b). Mass balance of Glaciar Zongo, Bolivia, between 1956 and 2006, using glaciological, hydrological and geodetic methods. *Annals of Glaciology*, 50(50):1–8.

Soruco, A., Vincent, C., Rabatel, A., Francou, B., Thibert, E., Sicart, J. E., and Condom, T. (2015). Contribution of glacier runoff to water resources of La Paz city, Bolivia (16° S). *Annals of Glaciology*, 56(70):147–154.

Span, N. and Kuhn, M. (2003). Simulating annual glacier flow with a linear reservoir model. *Journal of Geophysical Research: Atmospheres*, 108(D10).

Sugiyama, S., Minowa, M., Sakakibara, D., Skvarca, P., Sawagaki, T., Ohashi, Y., Naito, N., and Chikita, K. (2016). Thermal structure of proglacial lakes in Patagonia. *Journal of Geophysical Research: Earth Surface*, 121(12):2270–2286.

Thibert, E., Blanc, R., Vincent, C., and Eckert, N. (2008). Glaciological and volumetric mass-balance measurements: error analysis over 51 years for Glacier de Sarennes, French Alps. *Journal of Glaciology*, 54(186):522–532.

Thibert, E. and Vincent, C. (2009). Best possible estimation of mass balance combining glaciological and geodetic methods. *Annals of Glaciology*, 50(50):112–118.

Thompson, D. W. J. and Solomon, S. (2002). Interpretation of Recent Southern Hemisphere Climate Change. *Science*, 296(5569):895–899.

Thompson, D. W. J. and Wallace, J. M. (2000). Annular Modes in the Extratropical Circulation. Part I: Month-to-Month Variability. *Journal of Climate*, 13(5):1000–1016.

Toutin, T. (2001). Elevation modelling from satellite visible and infrared (VIR) data. *International Journal of Remote Sensing*, 22(6):1097–1125.

Truffer, M. and Motyka, R. J. (2016). Where glaciers meet water: Subaqueous melt and its relevance to glaciers in various settings. *Reviews of Geophysics*, 54:220–239.

Vergara, W., Deeb, A., Valencia, A., Bradley, R., Francou, B., Zarzar, A., Grünwaldt, A., and Haeussling, S. (2007). Economic impacts of rapid glacier retreat in the Andes. *Eos, Transactions American Geophysical Union*, 88(25):261–264.

Villalba, R., Lara, A., Boninsegna, J. A., Masiokas, M., Delgado, S., Aravena, J. C., Roig, F. A., Schmelter, A., Wolodarsky, A., and Ripalta, A. (2003). Large-Scale Temperature Changes across the Southern Andes: 20th-Century Variations in the Context of the Past 400 Years. *Climatic Change*, 1-2(59):177–232.

Villalba, R., Lara, A., Masiokas, M. H., Urrutia, R., Luckman, B. H., Marshall, G. J., Mundo, I. A., Christie, D. A., Cook, E. R., Neukom, R., Allen, K., Fenwick, P., Boninsegna, J. A., Srur, A. M., Morales, M. S., Araneo, D., Palmer, J. G., Cuq, E., Aravena, J. C., Holz, A., and LeQuesne, C. (2012). Unusual Southern Hemisphere tree growth patterns induced by changes in the Southern Annular Mode. *Nature Geoscience*, 5(11):793–798.

Vuille, M., Bradley, R. S., and Keimig, F. (2000a). Climate Variability in the Andes of Ecuador and Its Relation to Tropical Pacific and Atlantic Sea Surface Temperature Anomalies. *Journal of Climate*, 13(14):2520–2535.

Vuille, M., Bradley, R. S., and Keimig, F. (2000b). Interannual climate variability in the Central Andes and its relation to tropical Pacific and Atlantic forcing. *Journal of Geophysical Research: Atmospheres*, 105(D10):12447–12460.

Vuille, M., Carey, M., Huggel, C., Buytaert, W., Rabatel, A., Jacobsen, D., Soruco, A., Villacis, M., Yarleque, C., Elison Timm, O., Condom, T., Salzmann, N., and Sicart, J.-E. (2018). Rapid decline of snow and ice in the tropical Andes – Impacts, uncertainties and challenges ahead. *Earth-Science Reviews*, 176:195–213.

Vuille, M., Francou, B., Wagnon, P., Juen, I., Kaser, G., Mark, B. G., and Bradley, R. S. (2008). Climate change and tropical Andean glaciers: Past, present and future. *Earth-Science Reviews*, 89(3):79–96.

Vuille, M., Franquist, E., Garreaud, R., Casimiro, W. S. L., and Cáceres, B. (2015). Impact of the global warming hiatus on Andean temperature. *Journal of Geophysical Research: Atmospheres*, 120(9):3745–3757.

Wagnon, P., Ribstein, P., Francou, B., and Pouyaud, B. (1999). Annual cycle of energy balance of Zongo glacier, Cordillera Real, Bolivia. *Journal of Geophysical Research*, 104(D4):3907–3923.

Wagnon, P., Ribstein, P., Francou, B., and Sicart, J. E. (2001). Anomalous heat and mass budget of Glaciar Zongo, Bolivia, during the 1997/98 El Niño year. *Journal of Glaciology*, 47(156):21–28.

Wang, D. and Kääb, A. (2015). Modeling Glacier Elevation Change from DEM Time Series. *Remote Sensing*, 7(8):10117–10142.

Warren, C. and Aniya, M. (1999). The calving glaciers of southern South America. *Global and Planetary Change*, 22(1):59–77.

Willis, M. J., Melkonian, A. K., Pritchard, M. E., and Ramage, J. M. (2012a). Ice loss rates at the Northern Patagonian Icefield derived using a decade of satellite remote sensing. *Remote Sensing of Environment*, 117:184–198.

Willis, M. J., Melkonian, A. K., Pritchard, M. E., and Rivera, A. (2012b). Ice loss from the Southern Patagonian Ice Field, South America, between 2000 and 2012. *Geophysical Research Letters*, 39(17):L17501.

Wilson, R., Carrión, D., and Rivera, A. (2016). Detailed dynamic, geometric and supraglacial moraine data for Glaciar Pio XI, the only surge-type glacier of the Southern Patagonia Icefield. *Annals of Glaciology*, 57(73):119–130.

Wouters, B., Gardner, A. S., and Moholdt, G. (2019). Global Glacier Mass Loss During the GRACE Satellite Mission (2002-2016). *Frontiers in Earth Science*, 7.

Zemp, M., Frey, H., Gärtner-Roer, I., Nussbaumer, S. U., Hoelzle, M., Paul, F., Haeberli, W., Denzinger, F., Ahlstrøm, A. P., Anderson, B., Bajracharya, S., Baroni, C., Braun, L. N., Cáceres, B. E., Casassa, G., Cobos, G., Dávila, L. R., Granados, H. D., Demuth, M. N., Espizua, L., Fischer, A., Fujita, K., Gadek, B., Ghazanfar, A., Hagen, J. O., Holmlund, P., Karimi, N., Li, Z., Pelto, M., Pitte, P., Popovnin, V. V., Portocarrero, C. A., Prinz, R., Sangewar, C. V., Severskiy, I., Sigurđsson, O., Soruco, A., Usubaliev, R., and Vincent, C. (2015). Historically unprecedented global glacier decline in the early 21st century. *Journal of Glaciology*, 61(228):745–762.

Zemp, M., Huss, M., Thibert, E., Eckert, N., McNabb, R., Huber, J., Barandun, M., Machguth, H., Nussbaumer, S. U., Gärtner-Roer, I., Thomson, L., Paul, F., Maussion, F., Kutuzov, S., and Cogley, J. G. (2019). Global glacier mass changes and their contributions to sea-level rise from 1961 to 2016. *Nature*, 568(7752):382.

Zemp, M., Thibert, E., Huss, M., Stumm, D., Rolstad Denby, C., Nuth, C., Nussbaumer, S., Moholdt, G., Mercer, A., Mayer, C., Joerg, P., Jansson, P., Hynek, B., Fischer, A., Escher-Vetter, H., Elvehoy, H., and Andreassen, L. (2013). Reanalysing glacier mass balance measurement series. *The Cryosphere*, 7(4):p. 1227 – p. 1245.

Zhou, J. and Lau, K.-M. (1998). Does a Monsoon Climate Exist over South America? *Journal of Climate*, 11(5):1020–1040.